Iron oxide driven methanogenesis and methanotrophy in methanic sediments of Helgoland Mud Area, North Sea

DISSERTATION

Zur

Erlangung des Grades eines

Doktors der Naturwissenschaften

(Dr. rer. nat.)

dem Fachbereich Biologie/Chemie der

Universität Bremen vorgelegt von

Adeyemi David Aromokeye

aus Kwara State, Nigeria

Bremen, October 2018

1. Gutachter: Prof. Dr. Michael W. Friedrich (Universität Bremen)

2. Gutachter: Prof. Dr. Jens Harder (Universität Bremen)

In loving memory of my mother (Mary Aromokeye)

whom I knew for only 10 years.

Time spent with her was short but sufficient enough

for her to teach me to value education

as a tool to change my life and the world around me positively.

Those early life lessons motivated the series of decisions

that brought me this far.

Preface

This doctoral thesis project was funded primarily by the Cluster of Excellence 209 grant "The Ocean in the Earth System - MARUM - Center for Marine Environmental Sciences". Additional funding and support was given by the University of Bremen. With this project, my goal was to investigate potential microbial activity driven mechanisms that drive concurrent reduction of iron oxides in sediments from the methanic zone of Helgoland Mud Area, North Sea. Primary supervision was given by Prof. Dr. Michael W. Friedrich and the main results compiled in this thesis are submitted as a dissertation to obtain a doctoral degree (Dr. rer. Nat.) in Marine Microbiology from the University of Bremen, Bremen, Germany.

Experiments and analyses yielding the presented results were carried out at the Microbial Ecophysiology Group, University of Bremen (Bremen, Germany), MARUM-Center for Marine Environmental Sciences (University of Bremen), Alfred Wegener Institute for Polar and Marine Research (Bremerhaven, Germany) and the Max Planck Institute for Marine Microbiology (Bremen, Germany).

The project was divided into three work packages and the thesis is presented in a format where methods used and results generated from each work package are written as independent chapters. Chapter one (Introduction) gives a general overview about anaerobic food chain in marine sediments and the questions my dissertation aimed to address. Chapters two, three and four present each work package as manuscripts that are either accepted, in preparation or submitted as at the time of thesis submission. Chapter five harmonises the main findings from each work package and presents my perspective of the research questions addressed based on data generated from my thesis.

Table of Contents

Summary

Elevated dissolved iron concentrations (Fe^{2+}), as signpost for on-going iron oxide reduction in the methanic zone, are currently being detected in a wide range of marine environments. The various mechanisms that result in Fe^{2+} release into porewater are a subject of intense debate amongst sediment geo-microbiologists. While abiotic cryptic sulfur cycling is suggested for some sites, biotic mechanisms potentially mediate iron reduction in many other sites, including the Helgoland Mud Area, North Sea. Iron oxide dependent anaerobic oxidation of methane (Fe-AOM) is primarily hypothesised as the biotic mechanism driving iron reduction in the methanic zone but organic matter degradation linked iron reduction could also play a role. Beyond geochemical data however, physiological evidence demonstrating that these processes occur and the microorganisms involved is rather scarce.

In chapter two, a short-term radiotracer based experiment revealed that Fe-AOM is indeed feasible in the methanic zone of Helgoland Mud Area, albeit at very low rates under close to *in situ* conditions (0.095 ± 0.03 nmol cm^{-3} d^{-1}). Despite the low rates, these estimates represent the first demonstration of Fe-AOM in a marine environment bearing geochemical preconditions for Fe-AOM to occur *in situ*. Additionally in long-term incubations, various iron oxides (lepidocrocite, hematite and magnetite) stimulated Fe-AOM in sediments from the methanic zone. Especially with crystalline magnetite, ANME-2a were highly enriched after 250 days showing clearly, and for the first time, that ANME-2a are involved in Fe-AOM.

Previous studies from the Helgoland Mud Area revealed that aromatic hydrocarbons are likely the preferred fermentation substrate in the methanic zone. This may have led to the strong correlations between fermentative bacteria, methanogenic archaea (which use fermentation products) and Fe^{2+} concentrations. Chapter three investigated this possibility further, initially in sediment incubations and subsequently in highly enriched cultures. With

benzoate as the only carbon substrate, enrichment efforts with crystalline iron oxides (magnetite and hematite) led to concurrent iron reduction and methanogenesis from benzoate degradation. In contrast, with poorly crystalline lepidocrocite, benzoate degradation and methanogenesis was slower. Thus, concurrent reduction of crystalline iron oxides facilitates organic matter degradation while poorly crystalline lepidocrocite inhibits the process. Therefore, a likely scenario might be in play in Helgoland Mud Area, whereby buried crystalline iron oxide phases which make up to 1.6 weight % of sediment volume could be advantageous to the microbial communities. These crystalline iron oxides likely facilitate methanogenic organic matter degradation while being reduced concurrently, thereby contributing to the Fe^{2+} pool detected in porewater. Additionally, we uncovered the clostridial family Halobacteroidaceae as previously unknown benzoate degraders from marine sediments.

In chapter four, sediment incubations with an easily fermentable substrate (glucose) revealed that crystalline iron oxides could act as conduits for electron transfer, as electron acceptors for iron reduction or act as both under various temperature regimes. Furthermore, iron reduction was more favorable under lower temperatures than at mesophilic conditions and dissimilatory iron reducers from the order Desulfuromonadales were enriched during iron reduction.

These findings substantially advance the current state of the art regarding the biotic mechanisms that drive the apparent concurrent iron reduction in methanic zones of marine sediments. Besides providing direct evidence for Fe-AOM, the body of work presented in this thesis demonstrates the various ways iron oxides could facilitate methanogenic organic matter degradation in ferruginous methanic marine sediments. The exact molecular guides for these various processes should be subject of future studies.

Zusammenfassung

Derzeit werden in zahlreichen marinen Habitaten erhöhte Konzentrationen von gelösten Eisenionen (Fe^{2+}) gefunden, was als ein deutliches Signal für die Reduktion von Eisenoxiden in den methanreichen Sedimentschichten der Meere gilt. Die verschiedenen Mechanismen, die zu diesem Fe^{2+}-Eintrag in das Porenwasser führen könnten, werden kontrovers diskutiert. Einerseits wird für einige Habitate der abiotische kryptische Schwefelkreislauf als Ursache für die Eisenreduktion vorgeschlagen, für andere zieht man andererseits bestimmte biotische Prozesse als Erklärung in Betracht, darunter auch für die Schlammzonen um Helgoland (Helgoland Mud Area, „HMA“). Die Eisenoxid-abhängige, anaerobe Oxidation von Methan (Fe-AOM) ist dabei der primär vermutete biotische Prozess hinter der Eisenreduktion in den Methanzonen, aber ebenso könnte sie durch den Abbau organischer Kohlenstoffverbindungen bedingt sein. Es gibt jedoch abseits geochemischer Daten wenig physiologische Beweise dafür, daß die hypothetisierten Prozesse wirklich ablaufen und nur wenig Anhaltspunkte für die daran beteiligten Mikroorganismen.

Der zweite Abschnitt der vorliegenden Arbeit schildert, wie mit Hilfe von radioaktiven Tracern in Kurzzeitexperimenten gezeigt werden konnte, daß Fe-AOM ein plausibler Prozess in der HMA sein kann, wenn auch mit sehr geringen Raten (0.095 ± 0.03 nmol cm^{-3} d^{-1}) unter annähernd den Bedingungen, wie sie auch *in situ* vorliegen. Trotz des geringen Wertes repräsentieren die gefundenden Prozessraten die erste Demonstration von Fe-AOM in einer marinen Umwelt, die die dafür benötigten Vorbedingungen aufweist. Zusätzlich wurde in Sedimenten aus den Methanzonen gezeigt, wie unterschiedliche Eisenoxidtypen (Lepidokrokit, Magnetit, Hematit) Fe-AOM stimulieren. Besonders der Zusatz von kristallinem Magnetit führte zu einer Anreicherung von ANME-2a Organismen nach 250 Tagen. Dies ist der erste klare Hinweis auf eine Beteiligung dieser Organismen am untersuchten Prozess.

Ältere Studien der HMA demonstrierten, daß aromatische Kohlenwasserstoffe das wahrscheinlich bevorzugte Substrat für die Gärung in den Methanzonen darstellen. Dies wiederum könnte die hohe Korrelation zwischen fermentativen Bakterien, methanogenen Archeen - die Gärungsprodukte nutzen - und der Fe^{2+}-Konzentration erklären. Das dritte Kapitel der Arbeit untersuchte diese Möglichkeit näher, zunächst in Sedimentinkubationen, dann in hochangereicherten Kulturen. Mit Benzoat als alleiniger Kohlenstoffquelle führten Anreicherungen mit kristallinen Eisenoxiden (Magnetit und Hematit) zur gleichzeitigen Eisenreduktion und Methanogenese durch Benzoatabbau. Im Gegensatz dazu verlangsamten sich beide Prozesse unter Anwesenheit von niederkristallinem Lepidokrokit. Daraus folgt, daß die simultane Reduktion von hochkristallinen Eisenoxidspezies den Abbau organischer Materie beschleunigt, während niederkristalline Eisenoxide diesen Abbau inhibieren. Daher ist es ein mutmassliches Szenario in der HMA, daß sich abgelagerte kristalline Eisenoxidphasen (die bis zu 1.6% der Sedimenttrockenmasse ausmachen) positiv auf die mikrobiellen Gemeinschaften auswirken. Wahrscheinlich ist die Reduktion dieser Eisenoxide an den methanogenen Abbau organischer Substanzen gekoppelt, die damit zu den erhöhten Fe^{2+}-Konzentrationen im Porenwasser beitragen könnte. Zusätzlich konnten wir die Familie der Halobacteroidaceae erstmals als am Benzoatabbau beteiligt identifizieren.

Im vierten Kapitel wird gezeigt, daß in Sedimentinkubationen mit einem leicht zugänglichen Gärungssubstrat (hier Glukose) die Rolle von Eisenoxiden sich mit der Inkubationstemperatur ändert, indem sie temperaturabhängig als Leiter für den Elektrontransfer, als Elektronenakzeptoren, oder in beiden Rollen simultan fungieren. Eisenreduktion lief unter niedrigeren Temperaturen bevorzugt ab, und dissimilatorische Eisenreduzierer aus der Ordnung Desulfuromonadales wurden dabei angereichert.

Diese Befunde tragen substantiell zur Verbesserung unseres Verständnis von biotischen Prozessen bei, die die mikrobielle Eisenreduktion in methanreichen Sedimentschichten

antreiben. Neben der Führung eines direkten Nachweises für den tatsächlichen Ablauf von Fe-AOM demonstriert diese Arbeit die verschiedenen Möglichkeiten der Beteiligung von Eisenreduktion an methanogenen Abbauwegen in eisenreichen Meeressedimenten. Die exakten molekularen Vorgänge sollten in zukünftigen Studien untersucht werden.

Abbreviations

AOM	Anaerobic oxidation of methane
ANME	Anaerobic methane oxidising archaea
BCR	Benzoyl-CoA reductase
BES	Bromoethanesulfonate
CARD-FISH	Catalysed reporter deposition fluorescence *in situ* hybridization
DEPC	Diethyl pyrocarbonate
DIC	Dissolved inorganic carbon
DIET	Direct interspecies electron transfer
DNA	Deoxyribonucleic acid
dNTP	Deoxyribonucleotide triphosphate
EDS	Energy dispersive X-ray spectroscopy
Fe-AOM	Iron dependent anaerobic oxidation of methane
FTICR-MS	Fourier-transform ion cyclotron resonance mass spectrometry
GC	Gas chromatograph
HMA	Helgoland Mud Area
KeV	Kilo electron volts
LC-MS	Liquid chromatography - mass spectometry
MCR	Methyl-coenzyme M reductase
mcrA	Methyl coenzyme M reductase alpha subunit gene
mDIET	Mineral mediated direct interspecies electron transfer
OTU	Operational taxonomic unit(s)
PCR	Polymerase chain reaction
pmoA	Particulate methane monooxygenase alpha subunit gene
qPCR	Quantitative polymerase chain reaction
RNA	Ribosomal ribonucleic acid
rRNA	Ribosomal ribonucleic acid
S-AOM	Sulfate dependent anaerobic oxidation of methane
SEM	Scanning electron microscope (microscopy)
SIP	Stable isotope probing
SMT	Sulfate methane transition
SRB	Sulfate reducing bacteria
TEAP	Terminal electron accepting processes

Chapter One

General Introduction

1. Anaerobic food chain in marine sediments

About 70 % of the earth is occupied by marine water bodies, underneath which sediments rich in organic carbon accumulate over geological time scales (Parkes et al., 2014). These sediments harbour up to ~ 15,000 * 10^{18} g organic carbon, the biggest pool of organic carbon on earth (Hedges and Keil, 1995; Parkes et al., 2014). Marine sediments also account for a vast diversity of active prokaryotes (bacteria and archaea) that survive under extreme energy limitations by adapting to lifestyles governed by extraordinarily low metabolic activities (D'Hondt et al., 2004; Schippers et al., 2005; Biddle et al., 2006; Lloyd et al., 2013). Despite their extremely low energy requirements, degradation of the organic matter reaching benthic communities from both marine and terrestrial sources is the primary energy source for their metabolic activities (Jørgensen and Boetius, 2007). While the microbes in the surface sediments have access to more labile organic matter, microbial communities in deeper sediments gain energy from degradation of more recalcitrant organic matter depending on sediment age and depth (Middelburg, 1989; Biddle et al., 2006). Thus, microbial activity in deep marine sediments is estimated to be approximately 10, 000 times less than in near-surface sediments (Parkes et al., 2014).

During the degradation of organic carbon, large macromolecules typically undergo a series of exoenzymatic hydrolyses and depolymerisation followed by fermentation of monomeric organic carbon by specialist microbes. The later steps in the mineralisation of organic carbon couple the microbial oxidation of fermentation intermediates (volatile fatty acids, H_2 and acetate) to terminal electron accepting processes (TEAPs; Figure 1).

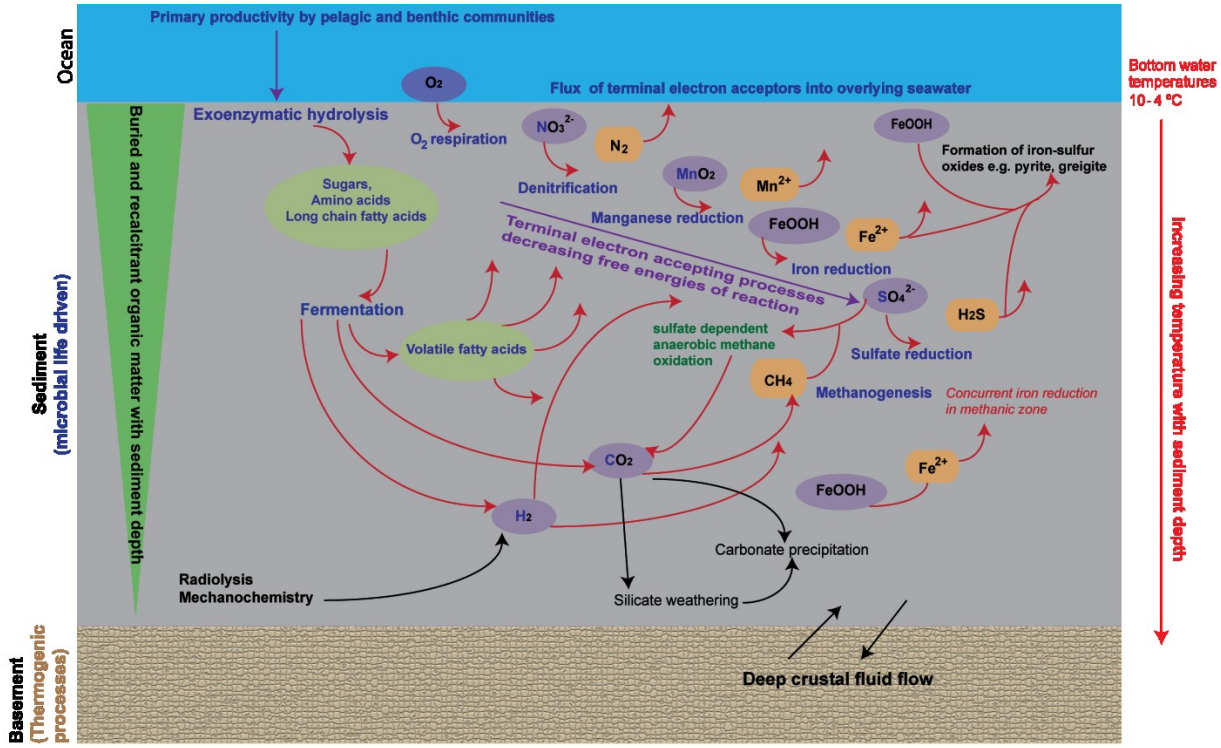

Figure 1: Anaerobic food chain in marine sediment detailing the geochemical zonation of terminal electron accepting processes for mineralisation of organic matter in marine sediments. Adapted from Jørgensen, 2006; and Wehrmann and Riedinger, 2016.

Therefore, distinct geochemical zones are formed based on energy yield from each process (Froelich et al., 1979; Berner, 1981; Jørgensen, 2006) (Table 1).

Table 1: Terminal electron accepting processes and their standard free energy yields following the classical geochemical zonation in marine sediments after Jørgensen (2006).

Pathway	Reaction stoichiometry	ΔG^0 (kJ mol^{-1})
Aerobic respiration	$CH_2O + O_2 \rightarrow CO_2 + H_2O$	-479
Nitrate reduction	$5CH_2O + 4NO_3^- \rightarrow 2N_2 + 4HCO_3^- + CO_2 + 3H_2O$	-453
Mn(IV) reduction	$CH_2O + 3CO_2 + H_2O + 2MnO_2 \rightarrow 2MnO_2 + 4HCO_3^-$	-349
Fe(III) reduction	$CH_2O + 7CO_2 + 4Fe(OH)_3 \rightarrow 4Fe^{2+} + 8HCO_3^- + 3H_2O$	-114
Sulfate reduction	$2CH_2O + SO_4^{2-} \rightarrow H_2S + 2HCO_3^-$	-77
Hydrogenotrophic methanogenesis	$4H_2 + HCO_3^- + H^+ \rightarrow CH_4 + 3H_2O$	-136

The extent of each geochemical zone within the sediments is proposed to be controlled by organic matter fluxes, availability of electron acceptors and sediment accumulation rates (Arndt et al., 2013; Wehrmann and Riedinger, 2016). Consequently, the less available but more thermodynamically favourable electron acceptors (oxygen, nitrate and metal oxides, respectively) are rapidly depleted in the upper few centimetres of surface sediments especially in high productivity regions (D'hondt et al., 2002; D'Hondt et al., 2004; Wehrmann and Riedinger, 2016). The rate of organic matter degradation in sediments ultimately decreases continuously with sediment age and depth, regardless of prevailing redox zonation and potential changes in the degradation pathway (Beulig et al., 2017).

Sulfate is the most available electron acceptor, accounting for 12–29 % of organic carbon flux on the seafloor (Bowles et al., 2014). These estimates are based on recent assessment of global organic matter fluxes to marine sediment (Dunne et al., 2007; Regnier et al., 2013). Below the sulfate zone is the methanic zone, where biogenic methane is being produced (Whiticar et al., 1986; Whiticar, 1999). An interphase between the sulfate zone and the methanic zone, known as the sulfate methane transition (SMT) (Iversen and Jørgensen, 1985), exists where upward diffusing methane from the methanic zone gets in contact with downward diffusing sulfate from the sulfate zone and methane is consequently oxidized. Anaerobic oxidation of methane (AOM) coupled to sulfate reduction strongly controls the fluxes of methane to the atmosphere such that up to 90 % of the methane produced in marine sediment is estimated to be consumed in the SMT (Hinrichs and Boetius, 2003; Knittel and Boetius, 2009). The process is biologically mediated by a specialised consortium of anaerobic methane oxidizing archaea (ANME) and sulfate reducing bacteria (SRB) (Hinrichs et al., 1999; Boetius et al., 2000). Within the methanic zone, sulfate becomes depleted and CO_2 becomes the available electron acceptor for microbial processes. Thus, CO_2 reduction driven methanogenesis predominates (Whiticar et al., 1986; Whiticar, 1999), with hydrogen derived

mostly as an intermediate of organic matter degradation or from radiolysis and mechanochemistry (Wehrmann and Riedinger, 2016) acting as the electron donor (hydrogenotrophic methanogenesis; Figure 1). Detection of micro-molar concentrations of acetate and methanol in some marine environments (Beulig et al., 2017; Zhuang et al., 2018) and the dominance of acetoclastic methanogens like *Methanosaeta* over hydrogenotrophic methanogens in some marine environments (Carr et al., 2018) are indicative of other active methanogenic pathways in the methanic zone. However, as recent data from the Baltic Sea shows, CO_2 reduction driven methanogenesis is favoured over acetoclastic methanogenesis in terms of turnover rates and preferential pathway utilised by the respective methanogens (Beulig et al., 2017).

2. Overlapping geochemical zones in marine sediments

There are indications that the standard model of finely defined geochemical zonation for TEAPs might be an oversimplification of the complex biogeochemical system fuelling the microbial food chain in marine sediments (Wehrmann and Riedinger, 2016). For example, concurrent sulfate reduction and methanogenesis were suggested to occur in the methanic zone (Mitterer, 2010; Treude et al., 2014). The most recent geochemical modelling estimates from over 740 sites globally highlight only a 70 % contribution of AOM to sulfate reduction rates in the SMT (Egger et al., 2018). Therefore, organic matter degradation, coupled to sulfate reduction, likely occurs alongside sulfate driven AOM in the SMT. Although hydrogenotrophic and acetoclastic methanogenesis are the dominant methanogenic pathways in marine sediments, methylotrophic methanogenesis also occurs, with highest rates in the sulfate zone (Zhuang et al., 2016; Xiao et al., 2018; Zhuang et al., 2018). Here, non-competitive substrates (mostly C-1 compounds such as methanol and methylamines) that are not metabolised by sulfate reducers (Oremland et al., 1982; King et al., 1983) are used exclusively by methylotrophic methanogens.

Elevated dissolved iron (Fe^{2+}) concentrations have been observed in the methanic zone of several marine sediments around the world (Table 2). The observations indicate a microbial activity induced iron reduction concurrently occurs in the methanic zone (Oni et al., 2015b). The sites are widely distributed globally varying from coastal sediments to deep sea sediments, and are usually characterised by either high accumulation rates of terrigenous organic matter or non-steady state systems (Table 2).

Table 2: Dissolved iron (Fe^{2+}) concentration ranges below the SMT in many sites around the world from shallow coastal sediments (e.g. the Bothnian Sea) to deep sub-seafloor continental margins (e.g., Peru Margin). Sediment depths were represented otherwise stated where only core depth was given.

Location	Sediment depth sampled	Fe^{2+} concentrations in the methanic zone (µM)	References
Amazon Shelf*	2.5 m[§]	150–500	(Aller et al., 1986)
Amazon Fan	7 m	10–130	(Schulz et al., 1994)
Bering Sea	800 m	0–60	(Takahashi et al., 2011)
Canterbury Basin	1000 m	10–38	(Fulthorpe et al., 2011)
Peru Margin	500 m	2–20	(D'Hondt et al., 2004)
Aarhus Bay	6 m	50–250	(Holmkvist et al., 2011)
Taiwan coast	25 m	2–13	(Lim et al., 2011)
Zambezi Fan	600 cm	3–13	(März et al., 2008)
Argentine Basin	10 m	3–90	(Hensen et al., 2003; Riedinger et al., 2014)
Bothnian Sea	60 cm[§]	250–2000	(Egger et al., 2015)
Black Sea	8 m[§]	20–680	(Egger et al., 2016a)
Baltic Sea	100 m	120–1700	(Egger et al., 2017)
Alaskan Beaufort Sea	5 m	30–80	(Treude et al., 2014)
North Sea (Helgoland Mud Area)	5 m	0–370	(Oni et al., 2015b)

[§]Represent sites where core depths were reported. *Methane concentrations were not measured in the Amazon shelf study (Aller et al., 1986), therefore only the sulfate profile was used to estimate potential SMT at the site.

The source and microbial processes fuelling these dissolved iron concentrations is currently a hot-topic in sub-surface geo-microbiology. The following sections describe the state of the art, potential pathways and mechanisms currently being discussed to drive deep iron reduction.

3. Microbial iron reduction in methanic zone of marine sediments and potential mechanisms

Microbial iron reduction accounts for around 17 % of total carbon mineralisation in a wide range of marine sediments (Thamdrup 2000) and could contribute up to 50 % of oxidised carbon in non-sulfidogenic sediments (Canfield et al 1993, Thamdrup 2000). Until recently, iron reduction was thought to be restricted to the upper few centimetres of marine sediments and could be facilitated by abiotic and biotic metabolisms. A number of abiotic and biotic mechanisms such as cryptic sulfur cycling, anaerobic oxidation of methane coupled to iron reduction and dissimilatory iron reduction have been discussed as possible mechanisms driving concurrent iron reduction in the methanic zone of marine sediments. These factors are discussed below.

3.1 Cryptic sulfur cycling

Sulfate reduction primarily drives biogeochemical sulfur cycling in marine sediments (Jørgensen and Kasten, 2006; Wasmund et al., 2017). Sulfate reduction, however, typically occurs in the surface sediments and the SMT rich in sulfate (up to 28 mM; Wasmund et al., 2017). However, there is molecular evidence that sulfate reducing bacteria constitute a high proportion of bacteria in the methanic zone of some sites (Leloup et al., 2007; Leloup et al., 2009; Schippers and Blazejak, 2011; Aoki et al., 2015). Nevertheless, sulfate concentrations in the methanic zone of these sites are low (< 500 μM). These low sulfate concentrations were referred to as 'background concentrations' (Leloup et al., 2007) and the presence of sulfate in the methanic zone might in fact be due to sulfate contamination coming from sea water that gets in contact with sediment cores during core recovery and pore water extraction (Brunner et al., 2016; Pellerin et al., 2018). Low porewater concentration of sulfate and low availability of reactive organic matter suppresses sulfate reduction in the methanic zone (Holmkvist et al., 2011). In the Aarhus bay sediments for example, sulfate reduction rates in

the methanic zone accounted for only 0.1 % of total sulfate reduction throughout the sediment core analysed (Holmkvist et al., 2011). Therefore, reduction of endogenously formed sulfate might not be the process driving the survival of sulfate reducers in these depths. Other metabolisms that could fuel the survival of sulfate reducing bacteria in the methanic zone could be sulfur disproportionation and iron reduction linked cryptic sulfur cycling (Holmkvist et al., 2011) or fermentation (Holmkvist et al., 2011; Glombitza et al., 2015). The role of fermentation might be less apparent due to the low availability of easily accessible organic matter. Hence, cryptic sulfur cycling, which involves rapid recycling of sulfur species at low sulfate concentrations (Holmkvist et al., 2011; Brunner et al., 2016; Wasmund et al., 2017), was hypothesised as the likely mechanism fuelling the presence of sulfate reducers and iron reduction in the methanic zone of Aarhus bay (Figure 2).

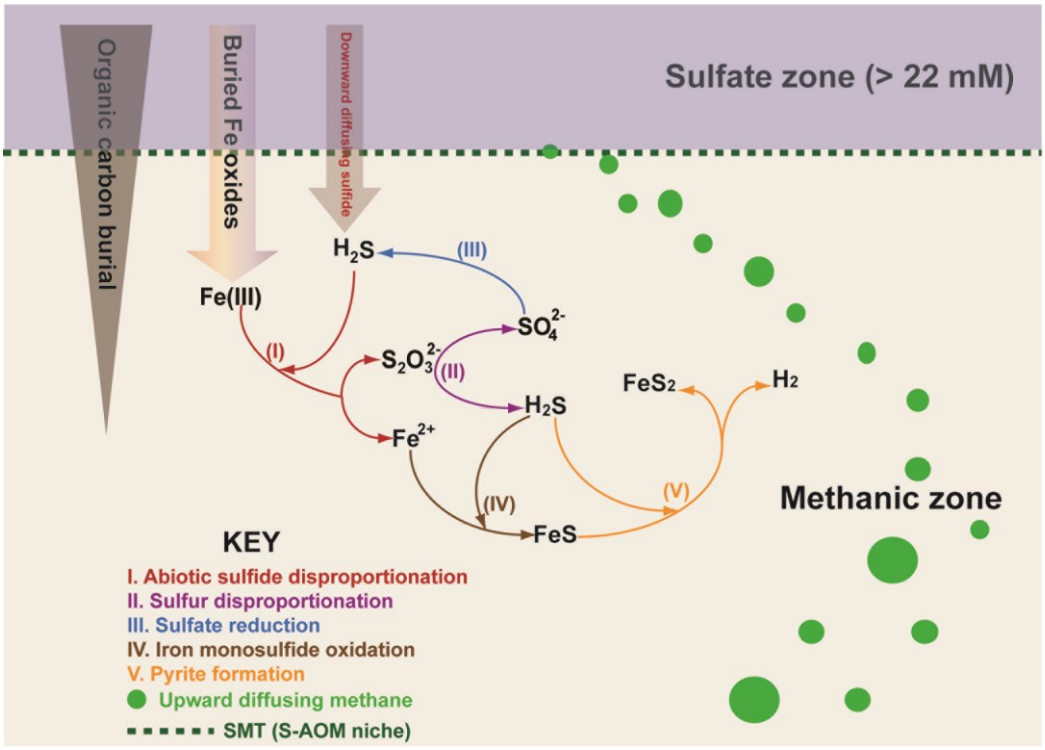

Figure 2: Schematic representation of major reactions involved during abiotic cryptic sulfur cycling in the methanic zone. Scheme modified from Holmkvist et al (2011).

A major constraint for cryptic cycling to occur in the methanic zone is the availability of downward diffusing sulfide from the SMT. In Aarhus Bay, where cryptic sulfur cycling was

proposed to fuel Fe^{2+} dissolution into the pore waters, sulfide produced from sulfate reduction diffuses downwards to the methanic zone, thereby leading to a 'sulfidization front' in the methanic zone (Holmkvist et al., 2011). Because there are deeply buried iron oxides in the methanic zone, abiotic free sulfide oxidation coupled to iron oxide reduction (Poulton et al., 2004) was therefore proposed in a cryptic sulfur cycling process that eventually yields sulfate (Figure 2; Holmkvist et al., 2011). Sulfate reducing bacteria constitute about 8 % of total bacteria cells in the methanic zone of Aarhus Bay, and they were proposed to use the generated sulfate to fuel their survival (Leloup et al., 2009; Holmkvist et al., 2011). A key factor in this hypothesis, however, is the location of the sulfidization front, providing high concentrations of free sulfide that rapidly react with Fe(III) as shown in Figure 2 (Holmkvist et al., 2011). In many other sites with elevated Fe^{2+} concentrations in the methanic zone, the sulfidization front is often distant, as free sulfide concentrations are below detection limits in the methanic zone (März et al., 2008; Lim et al., 2011; Riedinger et al., 2014; Egger et al., 2015). Therefore, other mechanisms might explain the elevated Fe^{2+} concentrations serving as a proxy for on-going iron reduction at other sites.

3.2 Anaerobic oxidation of methane coupled to iron reduction

Sulfate reduction coupled AOM occurs in the SMT of marine sediments and is responsible for 70 % of sulfate reduction in the SMT (Egger et al., 2018). This process was thought to be the only sink for methane in anoxic marine sediments, accounting for 2 % of methane oxidised in natural environments globally (Reeburgh, 2007; Saunois et al., 2016). The coupling of AOM to other electron acceptors such as nitrate has also been shown (Raghoebarsing et al., 2006). Nitrate profiles decrease with depth in sub-surface marine sediments (Froelich et al., 1979), therefore nitrate dependent AOM is unlikely. The first study that demonstrated the potential for other electron acceptors other than sulfate and nitrate to facilitate AOM stimulated methane oxidation activity in incubations amended with iron and

manganese oxides from cold seep sediments (Beal et al., 2009). A similar study also showed that addition of iron oxides to cold seep sediments stimulates higher rates of AOM (Sivan et al., 2014). However, both studies did not assess, if and to what extent background sulfate concentrations may have contributed to the observed methane oxidation activity. It was previously observed that background sulfate concentrations detected in marine sediments (70–100 μM) can stimulate S-AOM (Segarra et al., 2015; Timmers et al., 2016). Another important finding from cold seep sediments successfully excluded the possible sulfate involvement during AOM while demonstrating the potential for ANME-2a and ANME-2c to use artificial electron acceptors (ferric citrate, 9,10-anthraquinone-2,6-disulfonate) to uncouple AOM from sulfate reduction (Scheller et al., 2016). ANME-1 archaea were also shown to uncouple AOM from sulfate reduction at deeper depths in incubation experiments from metalliferous hydrothermal vent sediments (Wankel et al., 2012). Besides these stimulation experiments from marine sediments, a number of studies have suggested the occurrence of Fe-AOM by both near *in situ* and long-term enrichment studies from terrestrial environments and coastal sediments (Sivan et al., 2011; Chang et al., 2012; Segarra et al., 2013; Egger et al., 2015; Segarra et al., 2015; Ettwig et al., 2016; Bar-Or et al., 2017; Martinez-Cruz et al., 2017; Tu et al., 2017; Cai et al., 2018). While these studies showed the turnover of methane coupled to iron oxide reduction, the involved microorganisms and proposed mechanism vary (Figure 3). For example, ANME-2d archaea (*Candidatus* 'Methanoperedens'), enriched in bioreactors with materials from freshwater sediments, can couple methane oxidation to Fe(III) reduction without a bacterial partner (Ettwig et al., 2016; Cai et al., 2018). In terrestrial mud volcanoes, ANME-2a were proposed to be capable of coupling AOM to iron reduction together with deltaproteobacterial iron reducing partners from the order Desulfuromonadales (Chang et al., 2012; Tu et al., 2017).

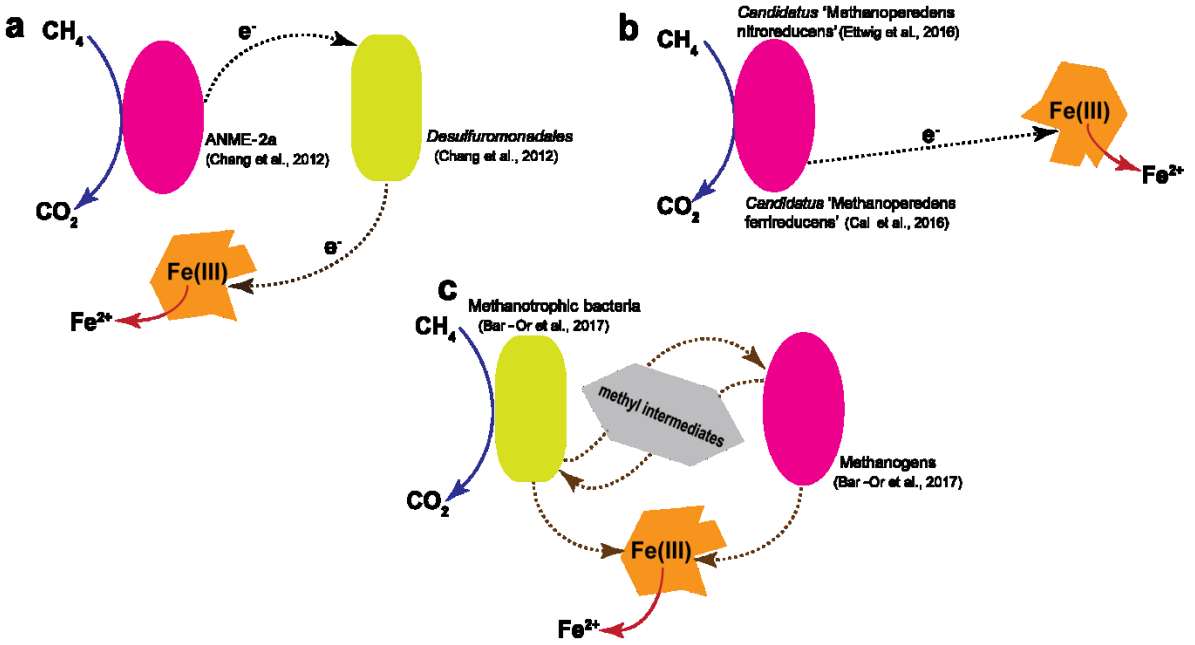

Figure 3: Proposed mechanisms for Fe-AOM. **(a)** Syntrophic coupling of CH_4 oxidation to iron reduction by ANME-2a archaea and dissimilatory iron reducing Desulfuromonadales bacteria **(b)** direct coupling of CH_4 oxidation to iron reduction by novel ANME-2d archaea **(c)** proposed complex metabolic coupling of Fe-AOM where methanotrophic bacteria directly or indirectly activates CH_4 and methyl (unconfirmed) intermediates are metabolised with syntrophic partners (Methanogens). Fe(III) provides final outlet for electrons from both partners. Authors demonstrated the importance of methanogens, as 2-bromoethanesulfonate addition inhibits methane oxidation completely.

Methanotrophic bacteria appear to be primarily involved in methane turnover during Fe-AOM (Bar-Or et al., 2017; Martinez-Cruz et al., 2017) in ferruginous lake sediments. Bar-Or et al., (2017) also demonstrated by inhibiting methanogenesis with 2-bromoethanesulfonate (a specific inhibitor of the methyl-coenzyme M reductase [MCR] enzyme, crucial a key enzyme for of methanogenesis and anaerobic methanotrophy) that methanogens are crucial for AOM by methanotrophic bacteria. However, the mechanism governing this type of methane turnover in anaerobic incubations, and the metabolic intermediates that facilitate Fe(III) reduction were not clearly explained yet. Recently, a biochemical framework was used to demonstrate that pure cultures of *Methanosarcina acetivorans* reversed their methanogenic pathway into an AOM pathway facilitated by Fe(III) dependent respiration (Yan et al., 2018). Therefore, unlike sulfate dependent AOM whose mechanism is based on syntrophic interactions facilitated by direct interspecies electron transfer (McGlynn et al.,

2015; Wegener et al., 2015), Fe-AOM metabolism appears to be mediated by both bacteria and archaea with or without syntrophic partners (Figure 3).

Given these indications that Fe-AOM is feasible in different natural environments, it is currently being proposed based on geochemical models from pore water profiles of iron, sulfate and methane that Fe-AOM occurs in the methanic zone of many of these deep iron reduction sites (Riedinger et al., 2014; Egger et al., 2015; Egger et al., 2016a; Egger et al., 2016b; Rooze et al., 2016; Egger et al., 2017). The juxtaposition of deeply buried iron oxides, alongside elevated methane concentrations in the absence of sulfate and appreciable amounts of reactive organic matter (Riedinger et al., 2014), is the strongest premise for this hypothesis. However, whether this process indeed occurs *in situ* and at what rates it occurs is not known. Consequently, the microbial key players for Fe-AOM in these deep sub-seafloor sediments are unknown as well.

3.3 Dissimilatory iron reduction

Microorganisms that couple the oxidation of organic or inorganic electron donors to the reduction of iron oxides (dissimilatory iron reducers) have a strong influence on the geochemistry of many natural environments (Lovley, 1997; Thamdrup, 2000; Kappler and Straub, 2005). Bacteria from the deltaproteobacterial order Desulfuromonadales are widely known as dissimilatory iron reducers and have been implicated for iron reduction in surface marine sediments (Lovley, 1997; Lovley, 2006; Vandieken et al., 2006; Vandieken and Thamdrup, 2013). Sequences affiliated with the order Desulfuromonadales were found in the methanic zone of the Helgoland Mud Area sediments, albeit at very low relative abundance (0.01–0.1%; Oni et al., 2015b). Dissimilatory iron reducers require electron donors similar to those required by methanogens, i.e., acetate and hydrogen (Lovley and Phillips, 1986; Roden and Wetzel, 1996). In theory, iron reduction should outcompete methanogenesis (see Table 1), but this does not seem to be the case, as active biogenic methane formation is on-going in

many of these sites (Riedinger et al., 2014; Egger et al., 2017). In addition, methanogens themselves can switch from methane production to iron reduction (Bond and Lovley, 2002; Van Bodegom et al., 2004; Zhang et al., 2012; Zhang et al., 2013; Sivan et al., 2016), facilitated by methanophenazines that serve as redox carriers in their cell membranes and thus act as electron shuttles (Beifuss et al., 2000; Sivan et al., 2016). However, whether (I) dissimilatory iron reduction is on-going or (II) the potential dissimilatory iron reducers detected in low abundance in the sediments are active or (III) methanogens themselves reduce iron in the sediments *in situ* has not been demonstrated yet.

3.4 Fermentative iron reduction

Microorganisms that convert simple sugars and other fermentable substrates to volatile fatty acids, acetate and hydrogen are capable of transferring up to 5 % of reducing equivalents generated during fermentation to iron oxides (Lovley and Phillips, 1986, 1988; Lovley, 2006). Despite being a minor pathway for electron flow in fermentative microorganisms (Lovley, 1997), the ability to fortuitously reduce iron oxides confers ecological advantages on fermenting organisms (Dobbin et al., 1999; Lehours et al., 2010). The subsurface environments, where deep iron reduction has been observed, harbour distinct microbial communities dominated by fermenting microorganisms whose distribution through the sediments are tightly linked to the dissolved iron profile (Oni et al., 2015b; Oni et al., 2015a). In the iron-oxide rich Helgoland Mud Area methanic sediments, Fourier transform ion cyclotron resonance mass spectrometry (FTICR-MS) was used to characterise the bioavailable fractions of organic matter potentially utilised by fermenting organisms. The results suggested that aromatic hydrocarbons were depleted and consequently likely degraded in the methanic zone by respective organisms.

Aromatic hydrocarbons represent some of the most abundant classes of organic compounds on earth (Carmona et al., 2009; Fuchs et al., 2011; Rabus et al., 2016) and their capability as

growth substrates for many fermentative bacteria has been well studied (Harwood et al., 1998; Gibson and Harwood, 2002; McInerney et al., 2008; Carmona et al., 2009; Sieber et al., 2010; Rabus et al., 2016; Nobu et al., 2017). Recently, members of the *Bathyarchaeota* phylum were linked to growth on aromatic lignin monomers (Yu et al., 2018), thus extending the scope of aromatic hydrocarbon degraders in the environment beyond bacteria to archaea as well. Because aromatic compounds are chemically inert and recalcitrant, they are mechanistically difficult to access by respective microorganisms living in anoxic environments such as marine sediments (Rabus et al., 2016). Activation of aromatic compounds by fermentative bacteria is also endergonic under standard conditions (McInerney et al., 2008). One strategy employed by fermenting organisms to overcome these energetic barriers and access aromatic compounds is to establish syntrophic interactions with sulfate reducers or methanogens. These syntrophic partners ensure that fermentative intermediates like acetate, H_2 and formate are kept at concentrations that are sufficiently low to facilitate organic matter degradation by fermenting partners (Harwood et al., 1998; Gibson and Harwood, 2002; McInerney et al., 2008; Rabus et al., 2016). It is possible that fermenting organisms also fortuitously reduce iron by using iron oxides as outlet to overcome thermodynamic barriers while degrading recalcitrant aromatic compound. Besides iron reducers are also capable of aromatic carbon degradation (Lovley and Lonergan, 1990; Lovley et al., 1993; Lonergan et al., 1996). The existence of an iron oxide driven fermentative metabolism could confer ecological advantage on microbial life in the energy limited deep biosphere by enhancing the rates of recalcitrant organic matter degradation. In the Helgoland Mud Area where aromatic compounds appear to be degraded in the methanic zone, and fermentative organisms are tightly linked to dissolved Fe^{2+} profile (Oni et al., 2015b; Oni et al., 2015a), it is feasible that fermentative bacteria, and or iron reducers together with methanogens are involved in a complex syntrophic relationship. Such

interaction would facilitate effective degradation of aromatic compounds in methanic zone, leading to faster methanogenesis rates while iron oxides are concurrently reduced allowing for dissolution of Fe^{2+} in porewater. A missing link to support these ideas is an experimental evidence, where aromatic monomers or compounds like benzoate that act as central intermediates during the degradation of most aromatic hydrocarbons (Carmona et al., 2009) are metabolised coupled to concurrent iron reduction and methanogenesis by a consortia of fermenting organisms and methanogens. Besides, knowledge on microorganisms that degrade aromatic hydrocarbons in marine sediments is unknown.

4. Direct interspecies electron transfer as a novel and more efficient electron transfer mechanism

Interspecies electron transfer, discovered by Bryant et al. (1967), is a key mechanism utilised in syntrophic methanogenic communities to overcome energy barriers (Stams and Plugge, 2009; Sieber et al., 2012). Transfer of diffusible intermediates of organic matter degradation such as H_2/formate is a well-known type of interspecies electron transfer (Morris et al., 2013; Schink and Stams, 2001; Sieber et al., 2014; Shrestha and Rotaru, 2015). Direct interspecies electron transfer (DIET) is a novel, 'electrical' and potentially faster alternative form of interspecies electron transfer (Cheng and Call, 2016; Lovley, 2016; Lovley, 2017). First discovered in syntrophic co-cultures of *Geobacter metallireducens* and *Geobacter sulfurreducens* (Summers et al., 2010), DIET is currently being suggested to proffer advantages to microorganisms under some environmental conditions (Lovley, 2017). Strategies that participating organisms explore to facilitate DIET include (I) electron transfer with biological appendages such as electrically conductive pili or outer membrane cytochromes (II) abiotic conduits such as minerals, electrodes or carbon material (Shrestha and Rotaru, 2015; Lovley, 2017). DIET might also have a biogeochemical significance: Anaerobic consortia mediating anaerobic oxidation coupled to sulfate reduction were shown

to transfer electrons via DIET (McGlynn et al., 2015; Wegener et al., 2015). Furthermore, DIET could also be important in syntrophic photosynthesis (Ha et al., 2017).

The potential role of crystalline iron minerals to facilitate mineral mediated DIET (mDIET; Shrestha & Rotaru, 2015) in natural environments has been studied using *in vitro* microcosms designed to metabolise carbon substrates to methane. In rice field soils, *Geobacter metallireducens*, known iron reducer in these environments, opted to participate in DIET with acetoclastic methanogen *Methanosarcina* in the presence of either hematite or magnetite (Kato et al., 2012). This resulted in enhancement of methanogenesis both in terms of increased process rate and reduced lag phase. A similar syntrophic association was subsequently shown in other rice field soils (Zhou et al., 2014; Li et al., 2015; Yang et al., 2015; Zhuang et al., 2015), anaerobic digesters (Cruz Viggi et al., 2014; Rotaru et al., 2014), river sediments (Jiang et al., 2013), lake sediments (Zhang and Lu, 2016), and coastal sediments (Rotaru et al., 2018). While the carbon substrate metabolised, syntrophic partners and methanogenic pathway may vary in the aforementioned studies, the potential relevance of this mechanism and the potential for crystalline iron minerals to facilitate electron transfer in natural environments was established. Therefore, mDIET could play a similar role in ferruginous sub-seafloor sediments given the relatively large fractions of crystalline iron oxides present *in situ,* but this needs to be demonstrated.

5. Temperature control of methanogenesis and iron reduction in marine sediments

Temperature is an important environmental factor that controls rates of biogeochemical processes (Arndt et al., 2013). About 85 % of global oceans have average temperatures below 5 ºC (Jørgensen, 2006), to which dominant microbial communities have to adapt optimally (Arndt et al., 2013). Therefore, *in situ* activity rates at lower temperatures are not intrinsically slower, especially for organisms in permanently cold sediments (Jørgensen, 2006). Most isolated strains of iron reducers in pure culture are mesophilic (Lovley et al., 2004) and few

psychrophilic iron reducers have been isolated from surface arctic sediments (Vandieken et al., 2006). There is so far no available data showing that microbes from these deep iron reduction sites actually reduce crystalline iron oxide fractions present in the sediments under psychrophilic conditions. Dissimilatory iron reducers in sub-glacial sediments reduced poorly crystalline ferrihydrite at faster rates at psychrophilic conditions (Nixon et al., 2017). It is yet unknown whether iron reduction in marine sediments also proceeds similarly such that lower temperatures favour higher rates of iron reduction.

Influence of temperature on methanogenesis on the other hand has been well studied from sedimentary and terrestrial environments. Previous studies showed that methanogenesis is favoured at mesophilic temperatures compared to psychrophilic (Zeikus and Winfrey, 1976; Van Hulzen et al., 1999; Fey and Conrad, 2000; Yao and Conrad, 2000). As discussed in section 4 above, crystalline iron oxides might also accelerate methane production in natural environments via mDIET. These mDIET stimulating studies were however carried out at either mesophilic or thermophilic temperatures. Given the slower process of methanogenesis at cold temperatures which predominates in marine sediments (Jørgensen, 2006), the availability of crystalline iron oxides in the methanic zone could enable accelerated methanogenesis in these environments. However, the potential for mDIET to occur under psychrophilic conditions that predominate in subsurface marine sediments is yet unknown Therefore, a gap exists in literature to identify what potential roles (either reduction or conduit function) crystalline iron oxides play at cold temperatures in marine sediments.

6. Study site and aims of thesis

The Helgoland Mud Area, located on the German bight of the North Sea is an area of fine grained mud with high sedimentation rates resulting in co-deposition of terrestrially derived organic matter and metal oxides (Hebbeln et al., 2003). Previous work in the area showed that metal oxide reduction (iron and manganese oxides) concurrently occurs in the methanic zone,

with iron oxide reduction being more predominant based on pore water concentrations of dissolved constituents (Oni et al., 2015b). Initial investigations into the microbial community composition in methanic zone sediments showed a tight correlation between distinct microbial communities and the dissolved iron profile suggesting iron reduction is microbial activity driven (Oni et al., 2015b).

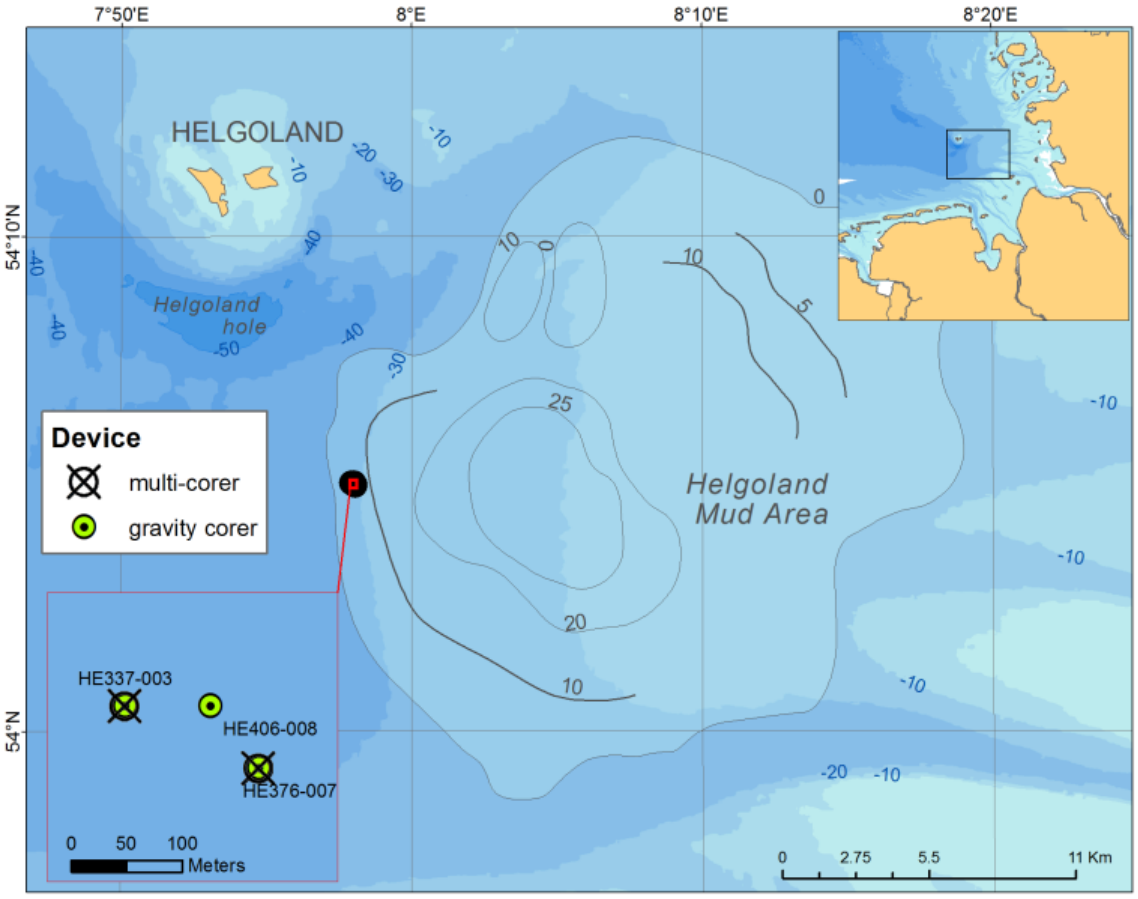

Figure 4: Map of the Helgoland Mud Area study site (Oni et al., 2015b). While fresh cores were collected for this project during a 2015 expedition to the site, the sampling locations were similar to those of the station HE376-007 listed on the map.

Indications from the water-extractable organic matter fractions also suggested aromatic hydrocarbons are preferentially degraded by fermenting microorganisms in the methanic zone (Oni et al., 2015a). In the present study, I aimed at the following objectives:

A. Provide experimental evidence for Fe-AOM in the methanic zone of Helgoland Mud Area sediments, obtain activity rates at close to *in situ* conditions and identify the microorganisms that are involved.

B. Set up enrichment cultures using a substrate (benzoate) that models the type of organic matter preferentially degraded *in situ*. By stimulating methanogenic benzoate degradation with crystalline iron oxides, I investigated how fermentative iron reduction during organic matter degradation could play a role in Fe^{2+} dissolution into the pore waters in addition to Fe-AOM. I specifically aimed to stimulate concurrent iron reduction during methanogenic benzoate degradation, enrich the microbial communities involved and investigate the ecological advantage conferred on the microbial communities by adding crystalline iron oxides to the enrichments.

C. The influence of temperature on microbial utilisation of crystalline iron oxides either as electron acceptors or as conduits to facilitate methanogenesis in marine sediments via mDIET was studied systematically. The aim of this study was to shed more light on how crystalline iron oxides, which were previously thought to be not bioavailable, could be serving microbial communities under different temperature regimes in sedimentary settings.

References

Aller, R.C., Mackin, J.E., and Cox, R.T. (1986) Diagenesis of Fe and S in Amazon inner shelf muds: Apparent dominance of Fe reduction and implications for the genesis of ironstones. *Cont. Shelf Res.* **6**: 263-289.
Aoki, M., Kakiuchi, R., Yamaguchi, T., Takai, K., Inagaki, F., and Imachi, H. (2015) Phylogenetic diversity of *aprA* genes in subseafloor sediments on the northwestern Pacific margin off Japan. *Microbes Environ.* **30**: 276-280.

Arndt, S., Jørgensen, B.B., LaRowe, D.E., Middelburg, J., Pancost, R., and Regnier, P. (2013) Quantifying the degradation of organic matter in marine sediments: A review and synthesis. *Earth Sci. Rev.* **123**: 53-86.

Bar-Or, I., Elvert, M., Eckert, W., Kushmaro, A., Vigderovich, H., Zhu, Q. et al. (2017) Iron-coupled anaerobic oxidation of methane performed by a mixed bacterial-archaeal community based on poorly reactive minerals. *Environ. Sci. Technol.* **51**: 12293-12301.

Beal, E.J., House, C.H., and Orphan, V.J. (2009) Manganese- and iron-dependent marine methane oxidation. *Science* **325**: 184-187.

Beifuss, U., Tietze, M., Bäumer, S., and Deppenmeier, U. (2000) Methanophenazine: structure, total synthesis, and function of a new cofactor from methanogenic archaea. *Angew. Chem. Int. Ed.* **39**: 2470-2472.

Berner, R.A. (1981) A new geochemical classification of sedimentary environments. *J. Sed. Res.* **51**: 359-365.

Beulig, F., Røy, H., Glombitza, C., and Jørgensen, B. (2017) Control on rate and pathway of anaerobic organic carbon degradation in the seabed. *Proc. Nat. Acad. Sci.* **115**: 367 - 372.

Biddle, J.F., Lipp, J.S., Lever, M.A., Lloyd, K.G., Sørensen, K.B., Anderson, R. et al. (2006) Heterotrophic archaea dominate sedimentary subsurface ecosystems off Peru. *Proc. Nat. Acad. Sci.* **103**: 3846-3851.

Boetius, A., Ravenschlag, K., Schubert, C.J., Rickert, D., Widdel, F., Gieseke, A. et al. (2000) A marine microbial consortium apparently mediating anaerobic oxidation of methane. *Nature* **407**: 623-626.

Bond, D.R., and Lovley, D.R. (2002) Reduction of Fe(III) oxide by methanogens in the presence and absence of extracellular quinones. *Environ. Microbiol.* **4**: 115-124.

Bowles, M.W., Mogollón, J.M., Kasten, S., Zabel, M., and Hinrichs, K.U. (2014) Global rates of marine sulfate reduction and implications for sub–sea-floor metabolic activities. *Science* **344**: 889-891.

Brunner, B., Arnold, G.L., Røy, H., Müller, I.A., and Jørgensen, B.B. (2016) Off limits: Sulfate below the sulfate-methane transition. *Front. Earth Sci.* **4**: 75.

Bryant, M., Wolin, E., Wolin, M., and Wolfe, R. (1967) *Methanobacillus omelianskii*, a symbiotic association of two species of bacteria. *Arch. Mikrobiol.* **59**: 20-31.

Cai, C., Leu, A.O., Xie, G.J., Guo, J., Feng, Y., Zhao, J.-X. et al. (2018) A methanotrophic archaeon couples anaerobic oxidation of methane to Fe(III) reduction. *ISME J.* **12**: 1929-1939.

Carmona, M., Zamarro, M.T., Blázquez, B., Durante-Rodríguez, G., Juárez, J.F., Valderrama, J.A. et al. (2009) Anaerobic catabolism of aromatic compounds: a genetic and genomic view. *Microbiol. Mol. Biol. Rev.* **73**: 71-133.

Carr, S.A., Schubotz, F., Dunbar, R.B., Mills, C.T., Dias, R., Summons, R.E., and Mandernack, K.W. (2018) Acetoclastic *Methanosaeta* are dominant methanogens in organic-rich Antarctic marine sediments. *ISME J.* **12**: 330-342.

Chang, Y.-H., Cheng, T.-W., Lai, W.J., Tsai, W.-Y., Sun, C.H., Lin, L.H., and Wang, P.L. (2012) Microbial methane cycling in a terrestrial mud volcano in eastern Taiwan. *Environ. Microbiol.* **14**: 895-908.

Cheng, Q., and Call, D.F. (2016) Hardwiring microbes via direct interspecies electron transfer: Mechanisms and applications. *Environ. Sci. Process. Impacts* **18**: 968-980.

Cruz Viggi, C., Rossetti, S., Fazi, S., Paiano, P., Majone, M., and Aulenta, F. (2014) Magnetite particles triggering a faster and more robust syntrophic pathway of methanogenic propionate degradation. *Environ. Sci. Technol.* **48**: 7536-7543.

D'hondt, S., Rutherford, S., and Spivack, A.J. (2002) Metabolic activity of subsurface life in deep-sea sediments. *Science* **295**: 2067-2070.

D'Hondt, S., Jørgensen, B.B., Miller, D.J., Batzke, A., Blake, R., Cragg, B.A. et al. (2004) Distributions of microbial activities in deep subseafloor sediments. *Science* **306**: 2216-2221.

Dobbin, P.S., Carter, J.P., García-Salamanca San Juan, C., von Hobe, M., Powell, A.K., and Richardson, D.J. (1999) Dissimilatory Fe(III) reduction by *Clostridium beijerinckii* isolated from freshwater sediment using Fe(III) maltol enrichment. *FEMS Microbiol. Lett.* **176**: 131-138.

Dunne, J.P., Sarmiento, J.L., and Gnanadesikan, A. (2007) A synthesis of global particle export from the surface ocean and cycling through the ocean interior and on the seafloor. *Glob. Biogeochem. Cycles* **21**: GB4006.

Egger, M., Riedinger, N., Mogollón, J.M., and Jørgensen, B.B. (2018) Global diffusive fluxes of methane in marine sediments. *Nat. Geo.* **11**: 421-425.

Egger, M., Kraal, P., Jilbert, T., Sulu-Gambari, F., Sapart, C.J., Röckmann, T., and Slomp, C.P. (2016a) Anaerobic oxidation of methane alters sediment records of sulfur, iron and phosphorus in the Black Sea. *Biogeosciences* **13**: 5333.

Egger, M., Lenstra, W., Jong, D., Meysman, F.J., Sapart, C.J., van der Veen, C. et al. (2016b) Rapid sediment accumulation results in high methane effluxes from coastal sediments. *PloS one* **11**: e0161609.

Egger, M., Rasigraf, O., Sapart, C.l.J., Jilbert, T., Jetten, M.S., Röckmann, T. et al. (2015) Iron-mediated anaerobic oxidation of methane in brackish coastal sediments. *Environ. Sci. Technol.* **49**: 277-283.

Egger, M., Hagens, M., Sapart, C.J., Dijkstra, N., van Helmond, N.A., Mogollón, J.M. et al. (2017) Iron oxide reduction in methane-rich deep Baltic Sea sediments. *Geochim. Cosmochim. Acta* **207**: 256-276.

Ettwig, K.F., Zhu, B., Speth, D., Keltjens, J.T., Jetten, M.S.M., and Kartal, B. (2016) Archaea catalyze iron-dependent anaerobic oxidation of methane. *Proc.Nat. Acad. Sci.* **113**: 12792-12796.

Fey, A., and Conrad, R. (2000) Effect of temperature on carbon and electron flow and on the archaeal community in methanogenic rice field soil. *Appl. Environ. Microbiol.* **66**: 4790-4797.

Froelich, P.N., Klinkhammer, G.P., Bender, M.L., Luedtke, N.A., Heath, G.R., Cullen, D. et al. (1979) Early oxidation of organic matter in pelagic sediments of the eastern equatorial Atlantic: suboxic diagenesis. *Geochim. Cosmochim. Acta* **43**: 1075-1090.

Fuchs, G., Boll, M., and Heider, J. (2011) Microbial degradation of aromatic compounds—from one strategy to four. *Nat. Rev. Microbiol.* **9**: 803.

Fulthorpe, C.S., Hoyanagi, K., Blum, P., and Expedition, I. (2011) IODP expedition 317: Exploring the record of sea-level change off New Zealand. *Sci. Dril.* **12**: 4-14.

Gibson, J., and Harwood, S.C. (2002) Metabolic diversity in aromatic compound utilization by anaerobic microbes. *Annu. Rev. Microbiol.* **56**: 345-369.

Glombitza, C., Jaussi, M., Røy, H., Seidenkrantz, M.S., Lomstein, B.A., and Jørgensen, B.B. (2015) Formate, acetate, and propionate as substrates for sulfate reduction in sub-arctic sediments of Southwest Greenland. *Front. Microbiol.* **6**: 846.

Ha, P.T., Lindemann, S.R., Shi, L., Dohnalkova, A.C., Fredrickson, J.K., Madigan, M.T., and Beyenal, H. (2017) Syntrophic anaerobic photosynthesis via direct interspecies electron transfer. *Nat. Commun.* **8**: 13924.

Harwood, C.S., Burchhardt, G., Herrmann, H., and Fuchs, G. (1998) Anaerobic metabolism of aromatic compounds via the benzoyl-CoA pathway. *FEMS Microbiol. Rev.* **22**: 439-458.

Hebbeln, D., Scheurle, C., and Lamy, F. (2003) Depositional history of the Helgoland Mud Area, German Bight, North Sea. *Geo-Mar. Lett.* **23**: 81-90.

Hedges, J.I., and Keil, R.G. (1995) Sedimentary organic matter preservation: an assessment and speculative synthesis. *Mar. Chem.* **49**: 81-115.

Hensen, C., Zabel, M., Pfeifer, K., Schwenk, T., Kasten, S., Riedinger, N. et al. (2003) Control of sulfate pore-water profiles by sedimentary events and the significance of anaerobic oxidation of methane for the burial of sulfur in marine sediments. *Geochim. Cosmochim. Acta* **67**: 2631-2647.

Hinrichs, K.-U., and Boetius, A. (2003) The anaerobic oxidation of methane: New insights in microbial ecology and biogeochemistry. In *Ocean Margin Systems*. Wefer, G., Billett, D., Hebbeln, D., Jørgensen, B.B., Schlüter, M., and van Weering, T.C.E. (eds). Berlin, Heidelberg: Springer Berlin Heidelberg, pp. 457-477.

Hinrichs, K.-U., Hayes, J.M., Sylva, S.P., Brewer, P.G., and DeLong, E.F. (1999) Methane-consuming archaebacteria in marine sediments. *Nature* **398**: 802-805.

Holmkvist, L., Ferdelman, T.G., and Jørgensen, B.B. (2011) A cryptic sulfur cycle driven by iron in the methane zone of marine sediment (Aarhus bay, Denmark). *Geochim. Cosmochim. Acta* **75**: 3581-3599.

Iversen, N., and Jørgensen, B. (1985) Anaerobic methane oxidation rates at the sulfate-methane transition in marine sediments from Kattegat and Skagerrak (Denmark). *Limnol. Oceanogr.* **30**: 944-955.

Jiang, S., Park, S., Yoon, Y., Lee, J.H., Wu, W.M., Phuoc Dan, N. et al. (2013) Methanogenesis facilitated by geobiochemical iron cycle in a novel syntrophic methanogenic microbial community. *Environ. Sci. Technol.* **47**: 10078-10084.

Jørgensen, B.B. (2006) Bacteria and Marine Biogeochemistry. In *Marine Geochemistry*. Schulz, H.D., and Zabel, M. (eds). Berlin, Heidelberg: Springer Berlin Heidelberg, pp. 169-206.

Jørgensen, B.B., and Kasten, S. (2006) Sulfur cycling and methane oxidation. In *Marine Geochemistry.* Schulz, H.D., and Zabel, M. (eds). Berlin, Heidelberg: Springer, pp. 271-309.

Jørgensen, B.B., and Boetius, A. (2007) Feast and famine – microbial life in the deep-sea bed. *Nat. Rev. Microbiol.* **5**: 770-781.

Kappler, A., and Straub, K.L. (2005) Geomicrobiological cycling of iron. *Rev. Mineral. Geochem.* **59**: 85-108.

Kato, S., Hashimoto, K., and Watanabe, K. (2012) Methanogenesis facilitated by electric syntrophy via (semi) conductive iron-oxide minerals. *Environ. Microbiol.* **14**: 1646-1654.

King, G.M., Klug, M.J., and Lovley, D.R. (1983) Metabolism of acetate, methanol, and methylated amines in intertidal sediments of Lowes Cove, Maine. *Appl. Environ. Microbiol.* **45**: 1848-1853.

Knittel, K., and Boetius, A. (2009) Anaerobic oxidation of methane: Progress with an unknown process. *Annu. Rev. Microbiol.* **63**: 311-334.

Lehours, A.C., Rabiet, M., Morel-Desrosiers, N., Morel, J.-P., Jouve, L., Arbeille, B. et al. (2010) Ferric iron reduction by fermentative strain BS2 isolated from an iron-rich anoxic environment (Lake Pavin, France). *Geomicrobiol. J.* **27**: 714-722.

Leloup, J., Loy, A., Knab, N.J., Borowski, C., Wagner, M., and Jørgensen, B.B. (2007) Diversity and abundance of sulfate-reducing microorganisms in the sulfate and methane zones of a marine sediment, Black Sea. *Environ. Microbiol.* **9**: 131-142.

Leloup, J., Fossing, H., Kohls, K., Holmkvist, L., Borowski, C., and Jørgensen, B.B. (2009) Sulfate-reducing bacteria in marine sediment (Aarhus Bay, Denmark): abundance and diversity related to geochemical zonation. *Environ. Microbiol.* **11**: 1278-1291.

Li, H., Chang, J., Liu, P., Fu, L., Ding, D., and Lu, Y. (2015) Direct interspecies electron transfer accelerates syntrophic oxidation of butyrate in paddy soil enrichments. *Environ. Microbiol.* **17**: 1533-1547.

Lim, Y.C., Lin, S., Yang, T.F., Chen, Y.G., and Liu, C.-S. (2011) Variations of methane induced pyrite formation in the accretionary wedge sediments offshore southwestern Taiwan. *Mar. Petrol. Geol.* **28**: 1829-1837.

Lloyd, K.G., May, M.K., Kevorkian, R.T., and Steen, A.D. (2013) Meta-analysis of quantification methods shows that archaea and bacteria have similar abundances in the subseafloor. *Appl. Environ. Microbiol.* **79**: 7790-7799.

Lonergan, D.J., Jenter, H.L., Coates, J.D., Phillips, E., Schmidt, T.M., and Lovley, D.R. (1996) Phylogenetic analysis of dissimilatory Fe(III)-reducing bacteria. *J. Bacteriol.* **178**: 2402-2408.

Lovley, D. (2006) Dissimilatory Fe(III)-and Mn(IV)-reducing prokaryotes. In *The prokaryotes*: Springer, pp. 635-658.

Lovley, D.R. (1997) Microbial Fe(III) reduction in subsurface environments. *FEMS Microbiol. Rev.* **20**: 305-313.

Lovley, D.R. (2016) Happy together: Microbial communities that hook up to swap electrons. *ISME J*. **11**: 327–336.

Lovley, D.R. (2017) Syntrophy goes electric: Direct interspecies electron transfer. *Annu. Rev. Microbiol.* **71**: 643-664.

Lovley, D.R., and Phillips, E.J. (1986) Organic matter mineralization with reduction of ferric iron in anaerobic sediments. *Appl. Environ. Microbiol.* **51**: 683-689.

Lovley, D.R., and Phillips, E.J. (1988) Novel mode of microbial energy metabolism: Organic carbon oxidation coupled to dissimilatory reduction of iron or manganese. *Appl. Environ. Microbiol.* **54**: 1472-1480.

Lovley, D.R., and Lonergan, D.J. (1990) Anaerobic oxidation of toluene, phenol, and p-cresol by the dissimilatory iron-reducing organism, GS-15. *Appl. Environ. Microbiol.* **56**: 1858-1864.

Lovley, D.R., Giovannoni, S.J., White, D.C., Champine, J.E., Phillips, E., Gorby, Y.A., and Goodwin, S. (1993) *Geobacter metallireducens* gen. nov. sp. nov., a microorganism capable of coupling the complete oxidation of organic compounds to the reduction of iron and other metals. *Arch. Microbiol.* **159**: 336-344.

Lovley, D.R., Holmes, D.E., and Nevin, K.P. (2004) Dissimilatory Fe(III) and Mn(IV) reduction. *Adv. Microb. Physiol.* **49**: 219–286.

Martinez-Cruz, K., Leewis, M.C., Herriott, I.C., Sepulveda-Jauregui, A., Anthony, K.W., Thalasso, F., and Leigh, M.B. (2017) Anaerobic oxidation of methane by aerobic methanotrophs in sub-Arctic lake sediments. *Sci. Total Environ.* **607-608**: 23-31.

März, C., Hoffmann, J., Bleil, U., De Lange, G., and Kasten, S. (2008) Diagenetic changes of magnetic and geochemical signals by anaerobic methane oxidation in sediments of the Zambezi deep-sea fan (SW Indian Ocean). *Mar. Geol.* **255**: 118-130.

McGlynn, S.E., Chadwick, G.L., Kempes, C.P., and Orphan, V.J. (2015) Single cell activity reveals direct electron transfer in methanotrophic consortia. *Nature* **526**: 531-535.

McInerney, M.J., Struchtemeyer, C.G., Sieber, J., Mouttaki, H., Stams, A.J., Schink, B. et al. (2008) Physiology, ecology, phylogeny, and genomics of microorganisms capable of syntrophic metabolism. *Annals New York Acad. Sci.* **1125**: 58-72.

Middelburg, J.J. (1989) A simple rate model for organic matter decomposition in marine sediments. *Geochim. Cosmochim. Acta* **53**: 1577-1581.

Mitterer, R.M. (2010) Methanogenesis and sulfate reduction in marine sediments: A new model. *Earth Planet. Sci. Lett.* **295**: 358-366.

Morris, B.E., Henneberger, R., Huber, H., and Moissl-Eichinger, C. (2013) Microbial syntrophy: Interaction for the common good. *FEMS Microbiol. Rev.* **37**: 384-406.

Nixon, S.L., Telling, J.P., Wadham, J.L., and Cockell, C.S. (2017) Viable cold-tolerant iron-reducing microorganisms in geographically diverse subglacial environments. *Biogeosciences* **14**: 1445-1455.

Nobu, M.K., Narihiro, T., Liu, M., Kuroda, K., Mei, R., and Liu, W.T. (2017) Thermodynamically diverse syntrophic aromatic compound catabolism. *Environ. Microbiol*. **19**: 4576-4586.

Oni, O.E., Schmidt, F., Miyatake, T., Kasten, S., Witt, M., Hinrichs, K.-U., and Friedrich, M.W. (2015a) Microbial communities and organic matter composition in surface and subsurface sediments of the Helgoland Mud Area, North Sea. *Front. Microbiol.* **6**: 1290.

Oni, O.E., Miyatake, T., Kasten, S., Richter-Heitmann, T., Fischer, D., Wagenknecht, L. et al. (2015b) Distinct microbial populations are tightly linked to the profile of dissolved iron in the methanic sediments of the Helgoland Mud Area, North Sea. *Front. Microbiol.* **6**: 1-15.

Oremland, R.S., Marsh, L.M., and Polcin, S. (1982) Methane production and simultaneous sulphate reduction in anoxic, salt marsh sediments. *Nature* **296**: 143-145.

Parkes, R.J., Cragg, B., Roussel, E., Webster, G., Weightman, A., and Sass, H. (2014) A review of prokaryotic populations and processes in sub-seafloor sediments, including biosphere: geosphere interactions. *Mar. Geol.* **352**: 409-425.

Pellerin, A., Antler, G., Røy, H., Findlay, A., Beulig, F., Scholze, C. et al. (2018) The sulfur cycle below the sulfate-methane transition of marine sediments. *Geochim. Cosmochim. Acta*. **239**: 74-89.

Poulton, S.W., Krom, M.D., and Raiswell, R. (2004) A revised scheme for the reactivity of iron (oxyhydr)oxide minerals towards dissolved sulfide. *Geochim. Cosmochim. Acta* **68**: 3703-3715.

Rabus, R., Boll, M., Heider, J., Meckenstock, R.U., Buckel, W., Einsle, O. et al. (2016) Anaerobic microbial degradation of hydrocarbons: From enzymatic reactions to the environment. *J. Mol. Microbiol. Biotechnol.* **26**: 5-28.

Raghoebarsing, A.A., Pol, A., Van de Pas-Schoonen, K.T., Smolders, A.J., Ettwig, K.F., Rijpstra, W.I.C. et al. (2006) A microbial consortium couples anaerobic methane oxidation to denitrification. *Nature* **440**: 918-921.

Reeburgh, W.S. (2007) Oceanic Methane Biogeochemistry. *Chem. Rev.* **107**: 486-513.

Regnier, P., Friedlingstein, P., Ciais, P., Mackenzie, F.T., Gruber, N., Janssens, I.A. et al. (2013) Anthropogenic perturbation of the carbon fluxes from land to ocean. *Nat. Geo.* **6**: 597.

Riedinger, N., Formolo, M.J., Lyons, T.W., Henkel, S., Beck, A., and Kasten, S. (2014) An inorganic geochemical argument for coupled anaerobic oxidation of methane and iron reduction in marine sediments. *Geobiology* **12**: 172-181.

Roden, E.E., and Wetzel, R.G. (1996) Organic carbon oxidation and suppression of methane production by microbial Fe(III) oxide reduction in vegetated and unvegetated freshwater wetland sediments. *Limnol. Oceanogr.* **41**: 1733-1748.

Rooze, J., Egger, M., Tsandev, I., and Slomp, C.P. (2016) Iron-dependent anaerobic oxidation of methane in coastal surface sediments: Potential controls and impact. *Limnol. Oceanogr.* **61**: S267-S282.

Rotaru, A.-E., Shrestha, P.M., Liu, F., Shrestha, M., Shrestha, D., Embree, M. et al. (2014) A new model for electron flow during anaerobic digestion: Direct interspecies electron transfer to *Methanosaeta* for the reduction of carbon dioxide to methane. *Energy Environ. Sci.* **7**: 408-415.

Rotaru, A.-E., Calabrese, F., Stryhanyuk, H., Musat, F., Shrestha, P.M., Weber, H.S. et al. (2018) Conductive particles enable syntrophic acetate oxidation between *Geobacter* and *Methanosarcina* from coastal sediments. *Mbio* **9**: e00226-00218.

Saunois, M., Bousquet, P., Poulter, B., Peregon, A., Ciais, P., Canadell, J.G. et al. (2016) The global methane budget 2000-2012. *Earth Syst. Sci. Data Discuss.* **8**: 1-54.

Scheller, S., Yu, H., Chadwick, G.L., McGlynn, S.E., and Orphan, V.J. (2016) Artificial electron acceptors decouple archaeal methane oxidation from sulfate reduction. *Science* **351**: 703-707.

Schink, B., and Stams, A.J. (2001) Syntrophism among prokaryotes: In *The Prokaryotes: An Evolving Electronic Resource for the Microbiological Community*. M. Dworkin, et al., Eds. New York: Springer-Verlag Springer.

Schippers, A., and Blazejak, A. (2011) Real-time PCR quantification and diversity analysis of the functional genes *aprA* and *dsrA* of sulfate-reducing prokaryotes in marine sediments of the Peru continental margin and the Black Sea. *Front. Microbiol.* **2**: 253.

Schippers, A., Neretin, L.N., Kallmeyer, J., Ferdelman, T.G., Cragg, B.A., Parkes, R.J., and Jørgensen, B.B. (2005) Prokaryotic cells of the deep sub-seafloor biosphere identified as living bacteria. *Nature* **433**: 861-864.

Schulz, H.D., Dahmke, A., Schinzel, U., Wallmann, K., and Zabel, M. (1994) Early diagenetic processes, fluxes, and reaction rates in sediments of the South Atlantic. *Geochim. Cosmochim. Acta* **58**: 2041-2060.

Segarra, K.E.A., Comerford, C., Slaughter, J., and Joye, S.B. (2013) Impact of electron acceptor availability on the anaerobic oxidation of methane in coastal freshwater and brackish wetland sediments. *Geochim. Cosmochim. Acta* **115**: 15-30.

Segarra, K.E.A., Schubotz, F., Samarkin, V., Yoshinaga, M.Y., Hinrichs, K.U., and Joye, S.B. (2015) High rates of anaerobic methane oxidation in freshwater wetlands reduce potential atmospheric methane emissions. *Nat. Commun.* **6**: 7477.

Shrestha, P.M., and Rotaru, A.E. (2015) Plugging in or going wireless: Strategies for interspecies electron transfer. *Front. Microbiol.* **5**: 237.

Sieber, J.R., McInerney, M.J., and Gunsalus, R.P. (2012) Genomic insights into syntrophy: The paradigm for anaerobic metabolic cooperation. *Annu. Rev. Microbiol.* **66**: 429-452.

Sieber, J.R., Le, H.M., and McInerney, M.J. (2014) The importance of hydrogen and formate transfer for syntrophic fatty, aromatic and alicyclic metabolism. *Environ. Microbiol.* **16**: 177-188.

Sieber, J., McInerney, M., Plugge, C., Schink, B., and Gunsalus, R. (2010) Methanogenesis: Syntrophic metabolism. In *Handbook of Hydrocarbon and Lipid Microbiology*: Springer, pp. 337-355.

Sivan, O., Shusta, S., and Valentine, D. (2016) Methanogens rapidly transition from methane production to iron reduction. *Geobiology* **14**: 190-203.

Sivan, O., Antler, G., Turchyn, A.V., Marlow, J.J., and Orphan, V.J. (2014) Iron oxides stimulate sulfate-driven anaerobic methane oxidation in seeps. *Proc.Nat. Acad. Sci.* **111**: E4139-E4147.

Sivan, O., Adler, M., Pearson, A., Gelman, F., Bar-Or, I., John, S.G., and Eckert, W. (2011) Geochemical evidence for iron-mediated anaerobic oxidation of methane. *Limnol. Oceanogr.* **56**: 1536-1544.

Stams, A.J., and Plugge, C.M. (2009) Electron transfer in syntrophic communities of anaerobic bacteria and archaea. *Nat. Rev. Microbiol.* **7**: 568-577.

Summers, Z.M., Fogarty, H.E., Leang, C., Franks, A.E., Malvankar, N.S., and Lovley, D.R. (2010) Direct exchange of electrons within aggregates of an evolved syntrophic coculture of anaerobic bacteria. *Science* **330**: 1413-1415.

Takahashi, K., Ravelo, A.C., and Alvarez Zarikian, C. (2011) IODP expedition 323: Pliocene and pleistocene paleoceanographic changes in the Bering Sea. *Sci. Dril.* **11**: 4-13.

Thamdrup, B. (2000) Bacterial manganese and iron reduction in aquatic sediments. In *Advances in Microbial Ecology*. Schink, B. (ed). Boston, MA: Springer US, pp. 41-84.

Timmers, P.H.A., Suarez-Zuluaga, D.A., van Rossem, M., Diender, M., Stams, A.J.M., and Plugge, C.M. (2016) Anaerobic oxidation of methane associated with sulfate reduction in a natural freshwater gas source. *ISME J.* **10**: 1400-1412.

Treude, T., Krause, S., Maltby, J., Dale, A.W., Coffin, R., and Hamdan, L.J. (2014) Sulfate reduction and methane oxidation activity below the sulfate-methane transition zone in Alaskan Beaufort Sea continental margin sediments: Implications for deep sulfur cycling. *Geochim. Cosmochim. Acta* **144**: 217-237.

Tu, T.-H., Wu, L.-W., Lin, Y.-S., Imachi, H., Lin, L.-H., and Wang, P.-L. (2017) Microbial community composition and functional capacity in a terrestrial ferruginous, sulfate-depleted mud volcano. *Front. Microbiol.* **8**: 2137.

Van Bodegom, P.M., Scholten, J.C., and Stams, A.J. (2004) Direct inhibition of methanogenesis by ferric iron. *FEMS Microbiol. Ecol.* **49**: 261-268.

Van Hulzen, J., Segers, R., Van Bodegom, P., and Leffelaar, P. (1999) Temperature effects on soil methane production: an explanation for observed variability. *Soil Biol. Biochem.* **31**: 1919-1929.

Vandieken, V., and Thamdrup, B. (2013) Identification of acetate-oxidizing bacteria in a coastal marine surface sediment by RNA-stable isotope probing in anoxic slurries and intact cores. *FEMS Microbiol. Ecol.* **84**: 373-386.

Vandieken, V., Mußmann, M., Niemann, H., and Jørgensen, B.B. (2006) *Desulfuromonas svalbardensis* sp. nov. and *Desulfuromusa ferrireducens* sp. nov., psychrophilic, Fe(III)-reducing bacteria isolated from Arctic sediments, Svalbard. *Int. J. Syst. Evol. Microbiol.* **56**: 1133-1139.

Wankel, S.D., Adams, M.M., Johnston, D.T., Hansel, C.M., Joye, S.B., and Girguis, P.R. (2012) Anaerobic methane oxidation in metalliferous hydrothermal sediments: influence on carbon flux and decoupling from sulfate reduction. *Environ. Microbiol.* **14**: 2726-2740.

Wasmund, K., Mußmann, M., and Loy, A. (2017) The life sulfuric: microbial ecology of sulfur cycling in marine sediments. *Environ. Microbiol. Rep*. **9**: 323-344.

Wegener, G., Krukenberg, V., Riedel, D., Tegetmeyer, H.E., and Boetius, A. (2015) Intercellular wiring enables electron transfer between methanotrophic archaea and bacteria. *Nature* **526**: 587-590.

Wehrmann, L.M., and Riedinger, N. (2016) The sedimentary deep subseafloor biosphere. In *Reference Module in Earth Systems and Environmental Sciences*: Elsevier.

Whiticar, M.J. (1999) Carbon and hydrogen isotope systematics of bacterial formation and oxidation of methane. *Chem. Geol.* **161**: 291-314.

Whiticar, M.J., Faber, E., and Schoell, M. (1986) Biogenic methane formation in marine and freshwater environments: CO_2 reduction vs. acetate fermentation–isotope evidence. *Geochim. Cosmochim. Acta* **50**: 693-709.

Xiao, K.Q., Beulig, F., Røy, H., Jørgensen, B.B., and Risgaard-Petersen, N. (2018) Methylotrophic methanogenesis fuels cryptic methane cycling in marine surface sediment. *Limnol. Oceanogr.* **63**: 1519-1527.

Yan, Z., Joshi, P., Gorski, C.A., and Ferry, J.G. (2018) A biochemical framework for anaerobic oxidation of methane driven by Fe(III)-dependent respiration. *Nat. Commun.* **9**: 1642.

Yang, Z., Shi, X., Wang, C., Wang, L., and Guo, R. (2015) Magnetite nanoparticles facilitate methane production from ethanol via acting as electron acceptors. *Sci. Rep.* **5**: 16118

Yao, H., and Conrad, R. (2000) Effect of temperature on reduction of iron and production of carbon dioxide and methane in anoxic wetland rice soils. *Biol. Fert. Soils* **32**: 135-141.

Yu, T., Wu, W., Liang, W., Lever, M.A., Hinrichs, K.-U., and Wang, F. (2018) Growth of sedimentary *Bathyarchaeota* on lignin as an energy source. *Proc. Nat. Acad. Sci.***115**: 6022-6027.

Zeikus, J., and Winfrey, M. (1976) Temperature limitation of methanogenesis in aquatic sediments. *Appl. Environ. Microbiol.* **31**: 99-107.

Zhang, J., and Lu, Y. (2016) Conductive Fe_3O_4 nanoparticles accelerate syntrophic methane production from butyrate oxidation in two different lake sediments. *Front. Microbiol.* **7**:1316.

Zhang, J., Dong, H., Liu, D., and Agrawal, A. (2013) Microbial reduction of Fe(III) in smectite minerals by thermophilic methanogen *Methanothermobacter thermautotrophicus*. *Geochim. Cosmochim. Acta* **106**: 203-215.

Zhang, J., Dong, H., Liu, D., Fischer, T.B., Wang, S., and Huang, L. (2012) Microbial reduction of Fe(III) in illite–smectite minerals by methanogen *Methanosarcina mazei*. *Chem. Geol.* **292**: 35-44.

Zhou, S., Xu, J., Yang, G., and Zhuang, L. (2014) Methanogenesis affected by the co-occurrence of iron(III) oxides and humic substances. *FEMS Microbiol. Ecol.* **88**: 107-120.

Zhuang, G.-C., Elling, F.J., Nigro, L.M., Samarkin, V., Joye, S.B., Teske, A., and Hinrichs, K.-U. (2016) Multiple evidence for methylotrophic methanogenesis as the dominant methanogenic pathway in hypersaline sediments from the Orca Basin, Gulf of Mexico. *Geochim. Cosmochim. Acta* **187**: 1-20.

Zhuang, G.-C., Heuer, V.B., Lazar, C.S., Goldhammer, T., Wendt, J., Samarkin, V.A. et al. (2018) Relative importance of methylotrophic methanogenesis in sediments of the Western Mediterranean Sea. *Geochim. Cosmochim. Acta*. **224**: 171-186.

Zhuang, L., Tang, J., Wang, Y., Hu, M., and Zhou, S. (2015) Conductive iron oxide minerals accelerate syntrophic cooperation in methanogenic benzoate degradation. *J. Hazard. Mat.* **293**: 37-45.

Chapter Two

Rates and microbial players of iron-driven anaerobic oxidation of methane in methanic marine sediments

Declaration on the contribution of David A. Aromokeye to chapter two

Name of the candidate:	David A. Aromokeye
Title of the thesis:	Iron oxide driven methanogenesis and methanotrophy in methanic sediments of Helgoland Mud Area, North Sea
Authors of manuscript:	David A. Aromokeye, Ajinkya C. Kulkarni, Marcus Elvert, Gunter Wegener, Susann Henkel, Sarah Coffinet, Thilo Eickhorst, Oluwatobi E. Oni, Tim Richter-Heitmann, Heidi Taubner, Lea Wunder, Xiuran Yin, Qingzeng Zhu, Kai-Uwe Hinrichs, Sabine Kasten, Michael W. Friedrich
Article submitted:	Submitted to Proceedings of the National Academy of Sciences of the United States of America

Contribution of the candidate in % of the total work load

Experimental concept and design:	ca. 50 %
Experimental work/acquisition of experimental data:	ca. 50 %
Data analysis and interpretation:	ca. 50 %
Preparation of figures and tables:	ca. 50 %
Drafting of manuscript:	ca. 50 %

Rates and microbial players of iron-driven anaerobic oxidation of methane in methanic marine sediments

David A. Aromokeye[1,2,3‡], Ajinkya C. Kulkarni[1,2,3‡], Marcus Elvert[2,4], Gunter Wegener[2,5], Susann Henkel[2,6], Sarah Coffinet[2], Thilo Eickhorst[7], Oluwatobi E. Oni[1], Tim Richter-Heitmann[1], Heidi Taubner[2,4], Lea Wunder[1], Xiuran Yin[1,2,3], Qingzeng Zhu[2], Kai-Uwe Hinrichs[2,4], Sabine Kasten[2,4,6], Michael W. Friedrich[1,2]*

[1]Microbial Ecophysiology Group, Faculty of Biology/Chemistry, University of Bremen, Bremen, Germany

[2]MARUM – Center for Marine Environmental Sciences, University of Bremen, Bremen, Germany

[3]International Max Planck Research School for Marine Microbiology, Max Planck Institute for Marine Microbiology, Bremen, Germany

[4]University of Bremen, Faculty of Geosciences, Bremen, Germany

[5]Max Planck Institute for Marine Microbiology, Bremen, Germany

[6]Alfred Wegener Institute Helmholtz Centre for Polar and Marine Research, Bremerhaven, Germany

[7]Faculty of Biology/Chemistry, University of Bremen, Bremen, Germany

‡ Contributed equally to the manuscript

* Corresponding author

Correspondence:

Michael W. Friedrich,

Microbial Ecophysiology Group, Faculty of Biology/Chemistry, University of Bremen, PO

Box 33 04 40, D-28334 Bremen, Germany

Email: michael.friedrich@uni-bremen.de

Abstract

In marine environments, the flux of methane from the seabed is largely controlled by anaerobic oxidation of methane (AOM) coupled to sulfate reduction. Recent studies suggest an additional iron-oxide dependent methane sink in the methanic zone but direct proof of iron-oxide coupled anaerobic oxidation of methane (Fe-AOM) is still lacking. Using short-term radiotracer experiments, we demonstrate Fe-AOM in samples from the iron-oxide rich methanic zone of the Helgoland Mud Area, North Sea, with methane oxidation rates of 0.095 ± 0.03 nmol cm^{-3} d^{-1}. In comparison, sulfate dependent AOM (S-AOM) rates in the sulfate methane transition were 59 times higher (5.6 ± 2.5 nmol cm^{-3} d^{-1}). The iron oxide phases lepidocrocite, hematite, and magnetite facilitated Fe-AOM in long-term sediment slurry incubations from the methanic zone when sulfate reduction was inhibited. Especially amendment with magnetite triggered substantial Fe-AOM activity; in this incubation anaerobic methane oxidizing archaea of the ANME-2a clade were particularly enriched. We show that Fe-AOM is a hidden methane sink in methanic marine sediments containing mineral-bound ferric iron, and is therefore an important component in the global methane budget that has the potential to sustain microbial life in the deep biosphere.

Significance Statement

The anaerobic oxidation of methane (AOM) in marine sediments is a crucial biological filter that mitigates the flux of the greenhouse methane into the atmosphere. Previous studies extensively documented a coupling of AOM to sulfate reduction. More recently, some evidence hinted towards metal oxide dependent AOM as additional methane sink in marine sediments. Here, we used a multi-pronged approach to show iron oxide driven AOM (Fe-AOM) occurs in the methanic zone of iron-oxide rich marine sediments and especially identified ANME-2a as a key microorganism involved. Given the larger volume of methanic

zones compared to the sulfate methane transition where sulfate dependent AOM occurs, Fe-AOM could contribute significantly to global methane budgets from marine environments.

Introduction

In marine sediments globally, methanogenic archaea naturally form large amounts of the potent greenhouse gas methane (1). Because of a rather effective biological filter, the anaerobic oxidation of methane (AOM), an estimated 90 % of this methane is consumed before escaping from the sediment (2, 3). AOM is commonly mediated by a consortium of anaerobic methane oxidizing archaea (ANME) and sulfate reducing bacteria (2-5), which results in the establishment of a sulfate methane transition (SMT) (6, 7), a reactive layer into which methane from the subsurface and sulfate from seawater diffuse. In addition to sulfate-coupled AOM (S-AOM), the role of other electron acceptors as additional sinks for methane in marine sediments is not fully established. Metal oxides such as those of iron and manganese have been suggested to serve as additional electron acceptors in AOM (8) in a number of terrestrial and marine environments (9-26). To date, only few highly enriched cultures from freshwater samples exist, in which *Candidatus* 'Methanoperedens nitroreducens' and *Ca.* 'Methanoperedens ferrireducens' (also known as members of the clade ANME-2d) were unequivocally shown to couple iron oxide reduction to anaerobic methane oxidation (Fe-AOM) (17, 18):

$$CH_4 + 8Fe(OH)_3 + 15H^+ \rightarrow HCO_3^- + 8Fe^{2+} + 21H_2O \qquad \text{(I)}$$

Although Fe-AOM is thermodynamically feasible, especially with the highly soluble iron citrate (16, 17), direct proof for the occurrence of the process in marine environments, where solid phase iron oxides are present in high abundance, remains elusive. Recently, Fe-AOM has been suggested to occur ubiquitously in the methanic zone of marine sediments (9-15). Elevated concentrations of dissolved Fe^{2+} in porewater, low to undetectable concentrations of

sulfate, high contents of buried reactive iron oxides and the presence of methane have been suggested as signpost of geochemical feasibility of Fe-AOM in methanic sediments (9-15). In fact, geochemical modeling suggests Fe-AOM as the likely major mechanism driving iron oxide reduction in the methanic zone of marine sediments (10-15).

The existence of an additional methane sink in the vast methanic zone of continental shelf and margin sediments fueled by iron oxides might hold important implications for the cycles of iron and carbon and for microbial life in the energy-limited deep sedimentary biosphere. Here, we investigated methanic sediments of the Helgoland Mud Area in the North Sea, which are characterized by high concentrations of dissolved Fe and methane, undetectable sulfate, as well as high amounts of buried reactive iron oxides (15) (Figs. 1, S1, S3). In a multi-pronged approach including geochemical analysis of porewater and sediments, radio and stable isotope labeling experiments, molecular biology and lipid stable isotope probing (SIP), we demonstrate the presence of Fe-AOM, provide activity rates at near *in situ* conditions and identified ANME-2a as a key microorganism of this process.

Results and Discussion

Direct evidence for iron-driven methane oxidation in methanic sediments

For measuring AOM activity, we carried out short-term $^{14}CH_4$ incubation experiments at near *in situ* temperatures of 10 ºC (27) using sediments from the methanic zone and the SMT (see methods). In methanic zone sediment incubations, methane was oxidized at a rate of 0.27 ± 0.01 nmol cm^{-3} d^{-1} (Fig. 1c). For comparison, in SMT sediment incubations, the methane oxidation rate (5.6 ± 2.5 nmol cm^{-3} d^{-1}) was 14 to 31 times higher (Fig. 1c). Because minimal sulfate concentrations (ranging from 70–100 µM) were shown to stimulate S-AOM (28, 29), molybdate, a known inhibitor of sulfate reduction (30), was added to a set of replicate incubations. Yet, methane oxidation (0.095 ± 0.03 nmol cm^{-3} d^{-1}) was detected under

inhibition of sulfate reduction in the incubations with methanic sediments, indicating a decoupling of AOM from sulfate reduction below the SMT (Fig. 1c). Similarly, AOM under molybdate inhibition was found in the methanic zone of Alaskan Beaufort Sea sediment, albeit at substantial *in situ* sulfate concentrations (30–500 μM) (25). In contrast, sediments from the methanic zone of the Helgoland Mud Area are sulfate-depleted and replete with metal oxides (15) (mostly iron oxides ranging from 0.49–1.64 wt %, Fig. S1; but also manganese oxides ranging from 0.02–0.11 wt %; Fig. S2). These metal oxides potentially serve as electron acceptors during AOM. Although elevated dissolved Mn concentrations suggest ongoing manganese reduction at these depths, Mn concentrations were between 2–10 fold lower than Fe concentrations (Fig. S3). Thus, iron oxide reduction is quantitatively more important than manganese reduction, and consequently, AOM below the SMT is predominantly driven by the presence and the reduction of iron oxides. The mode of AOM in the SMT was different from the methanic zone because molybdate addition inhibited S-AOM completely in the SMT (Fig. 1c). In contrast, Fe-AOM occurred in the methanic zone, even when sulfate reduction was inhibited. Thus, Fe-AOM in the sulfate-depleted methanic zone is not a side reaction of S-AOM (31) and probably requires specifically adapted microorganisms.

In order to pinpoint microorganisms involved in Fe-AOM at our study site, its microbial community composition was studied at various sediment depths. Based on sequencing of the functional gene marker *mcrA* encoding the methyl coenzyme M reductase alpha subunit (32, 33), we detected phylogenetically diverse ANME populations in sediments from the methanic zone (Fig. 2a). An "ANME-1-related" clade (34) dominated the methane metabolizing microbial community (up to 55 % of *mcrA* genes; Fig. 2a). Moreover, estimates of absolute *mcrA* gene copy numbers of the different ANME phylotypes showed that ANME-2a (5, 35) and ANME-3 (36) archaea, previously identified as key players during S-AOM, were

abundant in the sediments from the methanic zone (Fig. 2b). Of these groups, ANME-2a was the most abundant, particularly at 220 cm depth (6.0×10^6 copies per gram wet weight; Fig. 2b) and was also dominant based on *mcrA* gene sequencing (44 %; Fig 2a). In addition, the distribution profile of *mcrA* gene copies of ANME-1-related clade correlates strongly with the dissolved Fe concentration across all depths (Pearson's r=0.64, 95 % CI 0.23–0.86, $p<0.01$; Figs. 1b, 2b, Table S3). Domain-specific cell counts based on catalysed reporter deposition fluorescence *in situ* hybridization (CARD-FISH) revealed potentially active archaeal cells in the methanic zone (at least 3.9×10^6 cells per gram wet weight; Fig. 2c). Thus, methanic sediments of the Helgoland Mud Area harbor several abundant ANME groups known from S-AOM (5, 34, 36, 37) that are potentially involved in Fe-AOM *in situ.*

Iron oxide amendment increases Fe-AOM activity in the methanic zone

The crystalline iron oxides lepidocrocite, hematite and magnetite are quantitatively important as potential Fe-AOM electron acceptors in the methanic zone of the Helgoland Mud Area (15) (Fig S1). Therefore, we conducted enrichments with $^{13}CH_4$ to identify those iron oxides that were preferentially utilized by Fe-AOM mediating microorganisms and compared these results with enrichments from the sulfate zone (Figs. 3a, 3b). Over 250 days, δ^{13}C-DIC values, serving as a proxy for methane oxidation, increased continuously in sediment incubations from both geochemical zones (Fig. 3). In methanic zone incubations performed under inhibition of sulfate reduction, iron oxide addition, and in particular magnetite, resulted in higher levels of methane oxidation compared to the control incubation amended with $^{13}CH_4$ and molybdate (Fig. 3b). In contrast, excess sulfate amendment (30 mM) resulted in lower rates of methane oxidation. In sulfate zone sediment incubations, lepidocrocite and molybdate addition led to lower rates of methane oxidation than sulfate addition (Fig. 3a), indicating that the presence of iron oxides did not stimulate AOM under inhibition of sulfate reduction. Hence, our slurry incubations demonstrate that a geochemical niche separation

possibly occurs in the environment with sulfate and ferric iron as electron acceptors for methane oxidation in the sulfate zone and methanic zone, respectively. Among the reactive iron minerals present in the methanic zone, magnetite stimulated Fe-AOM most strongly, suggesting that this iron mineral could be important for *in situ* Fe-AOM. Similar findings were obtained from incubation experiments with lake sediments (19) and supported by a geochemical modeling study on Baltic Sea sediments (11).

Microbial key players involved in Fe-AOM

Potential key players for AOM in our long-term $^{13}CH_4$ incubation experiments were identified by 16S rRNA gene sequencing, *mcrA* gene qPCR of specific ANME phylotypes, lipid SIP of bacterial fatty acids and archaeal ethers, as well as *pmoA* gene amplification and cloning. In methanic zone sediment incubations showing Fe-AOM, 16S rRNA gene sequences of detected archaeal methane-oxidizers were affiliated to ANME-1b, ANME-2a/2b, ANME-3 (up to 8.5 % of all archaeal sequences; Fig. 5a) but not ANME-2c/2d (Figs. S7, S9). More importantly, in magnetite-molybdate incubations, ANME-2a/2b increased strongly in relative 16S rRNA gene sequence abundance (7 % to 40 % of ANMEs) and ANME-2a specific *mcrA* gene copies (50-fold, Fig. 4) between 120 and 250 days. Thus, in concert with the highest methane oxidation activity recorded (Fig. 3b), ANME-2a performed Fe-AOM under inhibition of sulfate reduction in magnetite added incubations of methanic zone sediment. Moreover, ANME-1-related and ANME-3 were stimulated as well in the other Fe-AOM incubations (Figs. 4, 5a). However, a similar trend was observed without molybdate addition and in N_2 amended controls (Figs. S7, S8). The stimulation of ANMEs in the N_2 controls might have been due to methane supply via co-occurring methanogenesis in these incubations (Fig. S12) recently termed “cryptic methane cycling” and detected in the SMT of Aarhus bay and other marine sediments (38-40).

In order to exclude the possible involvement of methanotrophic bacteria in Fe-AOM (19, 20), we studied ^{13}C uptake from $^{13}CH_4$ into bacterial lipids. Given the substantially lower incorporation of ^{13}C-label in bacterial fatty acids (Fig. 5b, Table S5) and the absence of a specific pattern related to methanotrophic bacteria compared to lake sediment incubations (19, 20), there was no evidence to support direct uptake of label from CH_4 into bacteria in samples from both, the sulfate zone and the methanic zone. Generally, this rather hints towards the incorporation of ^{13}C-DIC or another unknown metabolic intermediate or a mixture of both. Lipid SIP results were corroborated by the lack of detection of *pmoA* genes, a molecular marker for methanotrophic bacteria (41) in Fe-AOM performing incubations (Fig. S13, Table S4). Thus, in contrast to Fe-AOM in lake sediments, methanotrophic bacteria were not involved in our marine sediment incubations.

In other environments, ANMEs perform Fe-AOM either alone (17, 18), or potentially together with iron-reducing Desulfuromonadales as syntrophic partners (21, 22). However, microbial communities performing Fe-AOM in marine iron oxide-rich and sulfate-depleted methanic sediments were not identified until now. Our multi-pronged approach allowed us to show for the first time that ANME-2a performs Fe-AOM (Figs. 3, 4, 5). Unexpectedly, investigation of archaeal ether lipids in Fe-AOM incubations did not show any ^{13}C-label incorporation (Table S7), suggesting that ANMEs were neither directly assimilating CH_4, nor indirectly incorporating DIC into their biomass, with the latter previously shown to be the dominant mode for their relatives mediating S-AOM (42). This is, moreover, in accordance with archaeal lipid isotopes from Fe-AOM incubations using lake sediments where associated methanogens were similarly found with only marginal incorporation of ^{13}C-label (19). In contrast, we found clear indication for incorporation of label into archaeal lipids (Table S7) in incubations from the sulfate zone as expected for S-AOM (42, 43) that occurs at a much higher rate compared to Fe-AOM (Figs. 1c, 3). The bacterial community composition

analysis based on 16S rRNA gene sequencing showed that potential iron-reducing partner bacteria from the order Desulfuromonadales (21, 22) were present in all $^{13}CH_4$ amended incubations (up to 6.4 %, Figs. 5a, S10). However, whether they are syntrophic partners of ANME in Fe-AOM requires further research.

Environmental significance of Fe-AOM

By showing (I) the turnover of $^{14}CH_4$ and $^{13}CH_4$ to CO_2 (II) the presence of ANME phylotypes in the methanic zone of the Helgoland Mud Area and (III) increased gene copy numbers of these microorganisms in incubation experiments stimulating Fe-AOM, our study provides direct evidence for Fe-AOM in marine sediments. At our study site of the Helgoland Mud Area, Fe-AOM in the methanic zone occurs at a low lower rate of 0.095 ± 0.03 nmol cm^{-3} d^{-1}, which is only roughly ~ 2 % of that of S-AOM (5.6 ± 2.5 nmol cm^{-3} d^{-1}) in the SMT (Fig. 1c). Modeled estimates from coastal sediments of the Bothnian Sea also suggested a 3 % vs. 97 % contribution of Fe-AOM and S-AOM, respectively, to methane consumption (10). In general, Fe-AOM rates based on either $^{13}CH_4$ enrichment incubations or modeling approaches are low (8, 10, 11, 23, 24). But given the estimated global volume of sediments below the SMT (10^8 km^3 or 32 % of total subsurface), considerable amounts of methane could be consumed locally over substantial time-scales in the methanic zone before upward diffusion into the SMT (45).

Our study shows that Fe-AOM is an additional sink for methane in marine sediments, especially in environments characterized by high sedimentation rates facilitating the burial of reactive iron oxides underneath the SMT. Such environments bearing elevated Fe^{2+} concentrations as indicator for ongoing iron reduction are widely distributed from shallow sediments on coastal shelves to deep subseafloor settings at lower continental margins (9-15, 25, 46-54). Besides, Fe-AOM might have been an important methane sink in the early Archean before the accumulation of sulfate in the ocean (55) and it was previously suggested

that Fe-AOM should be considered in methane oxidation budgets (9). Our study provides the first rate estimates for Fe-AOM in iron oxide-rich methanic marine sediments. Now, an extensive evaluation of this process on a global scale is required to complement current diagenetic models (10-14) and improve our understanding of methane budgets in marine environments.

Acknowledgements

The authors thank the captain, crew and scientists of RV HEINCKE for the multi-year sampling campaigns to the Helgoland Mud Area. We also thank Jenny Wendt, Xavier Prieto and Mirja Meiners for their technical support. We thank Martina Stickan for proof-reading the manuscript. This work was supported by the Deutsche Forschungsgemeinschaft (DFG) Cluster of Excellence 309 "The Ocean in the Earth System - MARUM - Center for Marine Environmental Sciences", the Max Planck Society, the Alfred Wegener Institute Helmholtz Centre for Polar and Marine Research and the University of Bremen. The Gottfried Wilhelm Leibniz Program of the DFG (grant Hi 616-14-1) is acknowledged for purchase of the isotope ratio infrared spectrometer used in this study.

Author contributions

D.A.A., A.C.K., O.E.O., M.E., G.W., S.K. and M.W.F. designed the study. S.H., S.K., D.A.A. and A.C.K. performed geochemical sampling and analysis. G.W., A.C.K. and D.A.A. performed $^{14}CH_4$ experiments. A.C.K. D.A.A. and T.E. performed molecular biology assessments on sediment samples. D.A.A., O.E.O., H.T. and A.C.K. performed the $^{13}CH_4$ incubation experiments. A.C.K., D.A.A., X.Y. and L.W. performed molecular biology assessments on the $^{13}CH_4$ incubations. D.A.A., Q.Z., S.C. and M.E. performed lipid stable isotope probing on the $^{13}CH_4$ incubations. Figures production and statistical analysis were performed by T.R.H., supported by A.C.K. and D.A.A. G.W., M.E., K.U.H., S.K. and

M.W.F. obtained funding for this research. D.A.A. and A.C.K. contributed equally and together with M.W.F. wrote the article with contribution from all co-authors.

Additional information

Raw sequence data used in this study can be accessed from GenBank Short Reads Archive with accession number SRP156177. Clone sequences used in this study for qPCR were deposited to Genbank and have been assigned the accession numbers MH917693-MH917696. Geochemical dataset have been submitted to the PANGAEA data publisher for Earth & Environmental Sciences database under the following temporary doi https://doi.pangaea.de/10.1594/PANGAEA.893768.

References

1. Reeburgh WS (2007) Oceanic Methane Biogeochemistry. *Chem. Rev.* 107(2):486-513.

2. Hinrichs K-U & Boetius A (2003) The anaerobic oxidation of methane: New insights in microbial ecology and biogeochemistry. *Ocean Margin Systems*, eds Wefer G, Billett D, Hebbeln D, Jørgensen BB, Schlüter M, & van Weering TCE (Springer Berlin Heidelberg, Berlin, Heidelberg), pp 457-477.

3. Knittel K & Boetius A (2009) Anaerobic oxidation of methane: Progress with an unknown process. *Annu. Rev. Microbiol.* 63(1):311-334.

4. Hinrichs K-U, Hayes JM, Sylva SP, Brewer PG, & DeLong EF (1999) Methane-consuming archaebacteria in marine sediments. *Nature* 398:802-805.

5. Boetius A, *et al.* (2000) A marine microbial consortium apparently mediating anaerobic oxidation of methane. *Nature* 407:623-626.

6. Iversen N & Jørgensen B (1985) Anaerobic methane oxidation rates at the sulfate-methane transition in marine sediments from Kattegat and Skagerrak (Denmark). *Limnol. Oceanogr.* 30(5):944-955.

7. Niewöhner C, Hensen C, Kasten S, Zabel M, & Schulz H (1998) Deep sulfate reduction completely mediated by anaerobic methane oxidation in sediments of the upwelling area off Namibia. *Geochim. Cosmochim. Acta* 62(3):455-464.

8. Beal EJ, House CH, & Orphan VJ (2009) Manganese- and iron-dependent marine methane oxidation. *Science* 325(5937):184-187.

9. Riedinger N, *et al.* (2014) An inorganic geochemical argument for coupled anaerobic oxidation of methane and iron reduction in marine sediments. *Geobiology* 12(2):172-181.

10. Egger M, *et al.* (2015) Iron-mediated anaerobic oxidation of methane in brackish coastal sediments. *Environ. Sci. Technol.* 49(1):277-283.

11. Egger M, *et al.* (2017) Iron oxide reduction in methane-rich deep Baltic Sea sediments. *Geochim. Cosmochim. Acta* 207:256-276.

12. Egger M, *et al.* (2016) Anaerobic oxidation of methane alters sediment records of sulfur, iron and phosphorus in the Black Sea. *Biogeosciences* 13(18):5333-5355.

13. Egger M, *et al.* (2016) Rapid sediment accumulation results in high methane effluxes from coastal sediments. *PloS One* 11(8):e0161609.

14. Rooze J, Egger M, Tsandev I, & Slomp CP (2016) Iron-dependent anaerobic oxidation of methane in coastal surface sediments: Potential controls and impact. *Limnol. Oceanogr.* 61(S1):S267-S282.

15. Oni OE, *et al.* (2015) Distinct microbial populations are tightly linked to the profile of dissolved iron in the methanic sediments of the Helgoland Mud Area, North Sea. *Front. Microbiol.* 6:365.

16. Scheller S, Yu H, Chadwick GL, McGlynn SE, & Orphan VJ (2016) Artificial electron acceptors decouple archaeal methane oxidation from sulfate reduction. *Science* 351(6274):703-707.

17. Ettwig KF, *et al.* (2016) Archaea catalyze iron-dependent anaerobic oxidation of methane. *Proc. Nat. Acad. Sci.* 113(45):12792-12796.

18. Cai C, *et al.* (2018) A methanotrophic archaeon couples anaerobic oxidation of methane to Fe(III) reduction. *ISME J.* 12:1929-1939.

19. Bar-Or I, *et al.* (2017) Iron-coupled anaerobic oxidation of methane performed by a mixed bacterial-archaeal community based on poorly reactive minerals. *Environ. Sci. Technol.* 51(21):12293-12301.

20. Martinez-Cruz K, *et al.* (2017) Anaerobic oxidation of methane by aerobic methanotrophs in sub-Arctic lake sediments. *Sci. Total Environ.* 607-608:23-31.

21. Chang Y-H, *et al.* (2012) Microbial methane cycling in a terrestrial mud volcano in eastern Taiwan. *Environ. Microbiol.* 14(4):895-908.

22. Tu T-H, *et al.* (2017) Microbial community composition and functional capacity in a terrestrial ferruginous, sulfate-depleted mud volcano. *Front. Microbiol.* 8:2137.

23. Sivan O, *et al.* (2011) Geochemical evidence for iron-mediated anaerobic oxidation of methane. *Limnol. Oceanogr.* 56(4):1536-1544.

24. Segarra KEA, Comerford C, Slaughter J, & Joye SB (2013) Impact of electron acceptor availability on the anaerobic oxidation of methane in coastal freshwater and brackish wetland sediments. *Geochim. Cosmochim. Acta* 115:15-30.

25. Treude T, *et al.* (2014) Sulfate reduction and methane oxidation activity below the sulfate-methane transition zone in Alaskan Beaufort Sea continental margin sediments: Implications for deep sulfur cycling. *Geochim. Cosmochim. Acta* 144:217-237.

26. Wankel SD, *et al.* (2012) Anaerobic methane oxidation in metalliferous hydrothermal sediments: Influence on carbon flux and decoupling from sulfate reduction. *Environ. Microbiol.* 14(10):2726-2740.

27. Oehler T, Schlüter M, & Schückel U (2015) Seasonal dynamics of the biogenic silica cycle in surface sediments of the Helgoland Mud Area (southern North Sea). *Cont. Shelf Res.* 107(Supplement C):103-114.

28. Segarra KEA, *et al.* (2015) High rates of anaerobic methane oxidation in freshwater wetlands reduce potential atmospheric methane emissions. *Nat. Commun.* 6:7477.

29. Timmers PHA, *et al.* (2016) Anaerobic oxidation of methane associated with sulfate reduction in a natural freshwater gas source. *ISME J.* 10(6):1400-1412.

30. Oremland RS & Taylor BF (1978) Sulfate reduction and methanogenesis in marine sediments. *Geochim. Cosmochim. Acta* 42(2):209-214.

31. Sivan O, Antler G, Turchyn AV, Marlow JJ, & Orphan VJ (2014) Iron oxides stimulate sulfate-driven anaerobic methane oxidation in seeps. *Proc. Nat. Acad. Sci.* 111(40):E4139-E4147.

32. Hales BA*, et al.* (1996) Isolation and identification of methanogen-specific DNA from blanket bog peat by PCR amplification and sequence analysis. *Appl. Environ. Microbiol.* 62(2):668-675.

33. Luton PE, Wayne JM, Sharp RJ, & Riley PW (2002) The *mcrA* gene as an alternative to 16S rRNA in the phylogenetic analysis of methanogen populations in landfill. *Microbiol.* 148(11):3521-3530.

34. Takeuchi M*, et al.* (2011) A distinct freshwater-adapted subgroup of ANME-1 dominates active archaeal communities in terrestrial subsurfaces in Japan. *Environ. Microbiol.* 13(12):3206-3218.

35. Orphan VJ, House CH, Hinrichs K-U, McKeegan KD, & DeLong EF (2001) Methane-consuming archaea revealed by directly coupled isotopic and phylogenetic analysis. *Science* 293(5529):484-487.

36. Niemann H*, et al.* (2006) Novel microbial communities of the Haakon Mosby mud volcano and their role as a methane sink. *Nature* 443(7113):854-858.

37. Orphan VJ, House CH, Hinrichs K-U, McKeegan KD, & DeLong EF (2002) Multiple archaeal groups mediate methane oxidation in anoxic cold seep sediments. *Proc. Nat. Acad. Sci.* 99(11):7663-7668.

38. Xiao KQ, Beulig F, Røy H, Jørgensen BB, & Risgaard-Petersen N (2018) Methylotrophic methanogenesis fuels cryptic methane cycling in marine surface sediment. *Limnol. Oceanogr.* 63(4):1519-1527.

39. Beulig F, Røy H, Glombitza C, & Jørgensen B (2017) Control on rate and pathway of anaerobic organic carbon degradation in the seabed. *Proc. Nat. Acad. Sci.* 115:376-372.

40. Maltby J*, et al.* (2018) Microbial methanogenesis in the sulfate-reducing zone of sediments in the Eckernförde Bay, SW Baltic Sea. *Biogeosciences* 15(1):137-157.

41. Murrell JC, McDonald IR, & Bourne DG (1998) Molecular methods for the study of methanotroph ecology. *FEMS Microbiol. Ecol.* 27(2):103-114.

42. Kellermann MY*, et al.* (2012) Autotrophy as a predominant mode of carbon fixation in anaerobic methane-oxidizing microbial communities. *Proc. Nat. Acad. Sci.* 109(47):19321-19326

43. Wegener G, Krukenberg V, Ruff SE, Kellermann MY, & Knittel K (2016) Metabolic capabilities of microorganisms involved in and associated with the anaerobic oxidation of methane. *Front. Microbiol.* 7:46.

44. Bowles MW, Mogollón JM, Kasten S, Zabel M, & Hinrichs K-U (2014) Global rates of marine sulfate reduction and implications for sub–sea-floor metabolic activities. *Science* 344(6186):889-891.

45. Aller RC, Mackin JE, & Cox RT (1986) Diagenesis of Fe and S in Amazon inner shelf muds: Apparent dominance of Fe reduction and implications for the genesis of ironstones. *Cont. Shelf Res.* 6(1):263-289.

46. März C, Hoffmann J, Bleil U, De Lange G, & Kasten S (2008) Diagenetic changes of magnetic and geochemical signals by anaerobic methane oxidation in sediments of the Zambezi deep-sea fan (SW Indian Ocean). *Mar. Geol.* 255(3):118-130.

47. Holmkvist L, Ferdelman TG, & Jørgensen BB (2011) A cryptic sulfur cycle driven by iron in the methane zone of marine sediment (Aarhus Bay, Denmark). *Geochim. Cosmochim. Acta* 75(12):3581-3599.

48. Lim YC, Lin S, Yang TF, Chen Y-G, & Liu C-S (2011) Variations of methane induced pyrite formation in the accretionary wedge sediments offshore southwestern Taiwan. *Mar. Petrol. Geol.* 28(10):1829-1837.

49. D'Hondt S*, et al.* (2004) Distributions of microbial activities in deep subseafloor sediments. *Science* 306(5705):2216-2221.

50. Schulz HD, Dahmke A, Schinzel U, Wallmann K, & Zabel M (1994) Early diagenetic processes, fluxes, and reaction rates in sediments of the South Atlantic. *Geochim. Cosmochim. Acta* 58(9):2041-2060.

51. Kasten S, Freudenthal T, Gingele FX, & Schulz HD (1998) Simultaneous formation of iron-rich layers at different redox boundaries in sediments of the Amazon deep-sea fan. *Geochim. Cosmochim. Acta* 62(13):2253-2264.

52. Fulthorpe CS, Hoyanagi K, Blum P, & Expedition I (2011) IODP expedition 317: Exploring the record of sea-level change off New Zealand. *Sci. Dril.* 12:4-14.

53. Takahashi K, Ravelo AC, & Alvarez Zarikian C (2011) IODP expedition 323: Pliocene and pleistocene paleoceanographic changes in the Bering Sea. *Sci. Dril.* 11:4-13.

54. Konhauser K, Newman D, & Kappler A (2005) The potential significance of microbial Fe(III) reduction during deposition of precambrian banded iron formations. *Geobiology* 3(3):167-177.

Figures

Fig. 1

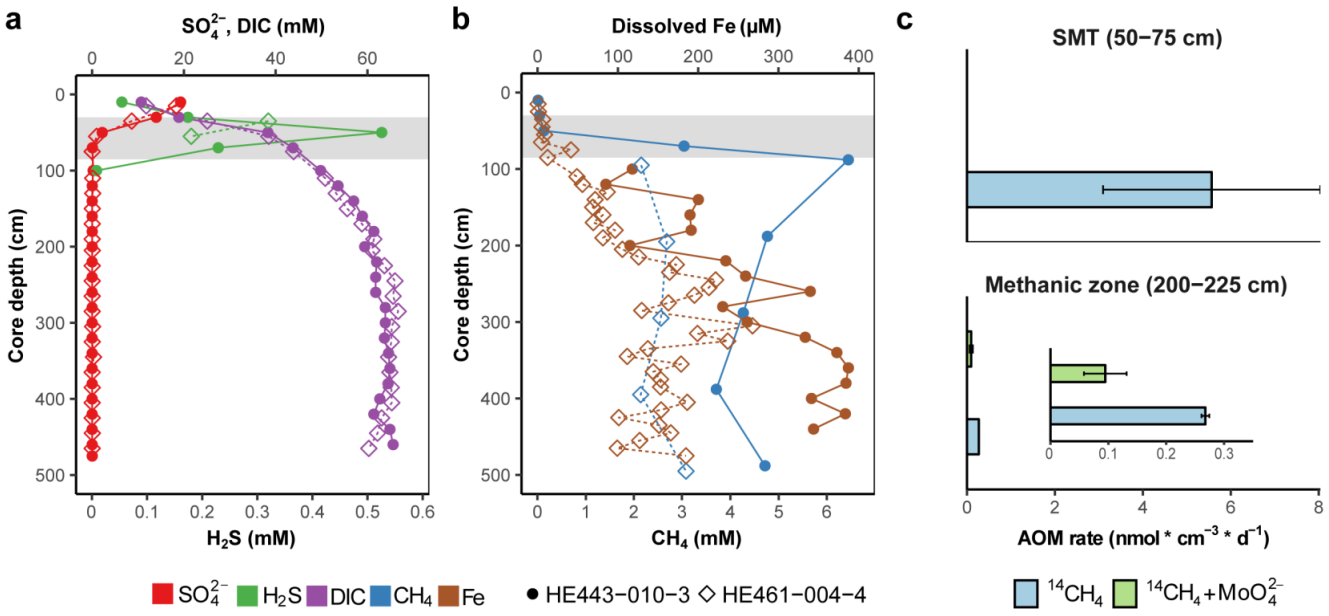

Figure 1: Geochemical profiles and near *in situ* rates of anaerobic methane oxidation in the Helgoland Mud Area. (**a)** Distribution of DIC, sulfate, and sulfide (**b)** concentrations of dissolved Fe (µM) and methane (mM) over depth (**c)** rates of methane turnover based on a $^{14}CH_4$ in samples from the SMT (50–75 cm), n = 3, and the methanic zone (200–225 cm), n = 2, error bar represent 1 s.d. of biological replicates. INSET: scale adjusted activity rates in the methanic zone. Grey bars within the profiles reflect the SMT. See Table S1 for sediment sampling information for the various porewater and molecular analysis. Using $^{14}CH_4$, rates of methane turnover were below abiotic control samples in $^{14}CH_4$ and molybdate treatment from the SMT and in the methanic zone samples from depths 300–325 cm and 400–425 cm after 8 days.

Fig. 2

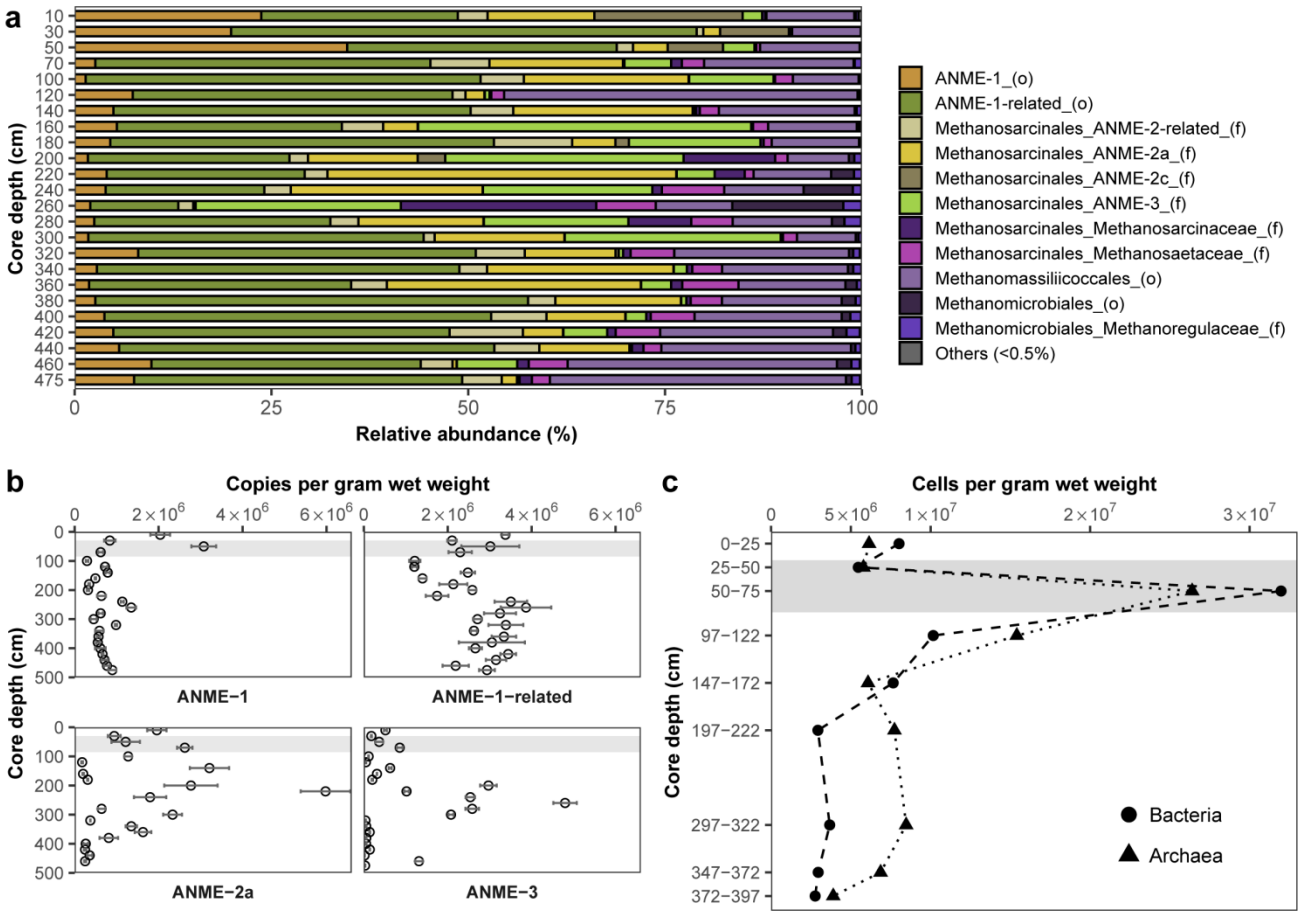

Figure 2: Distribution and abundance of microorganisms in the Helgoland Mud Area core. Relative abundances of **(a)** *mcrA* genes and **(b)** *mcrA* gene copies of ANME. Error bars represent 1 s.d. of technical qPCR triplicates. **(c)** Cell counts of potentially active bacteria and archaea based on CARD-FISH. Grey bars within the profiles depict the SMT.

Fig. 3

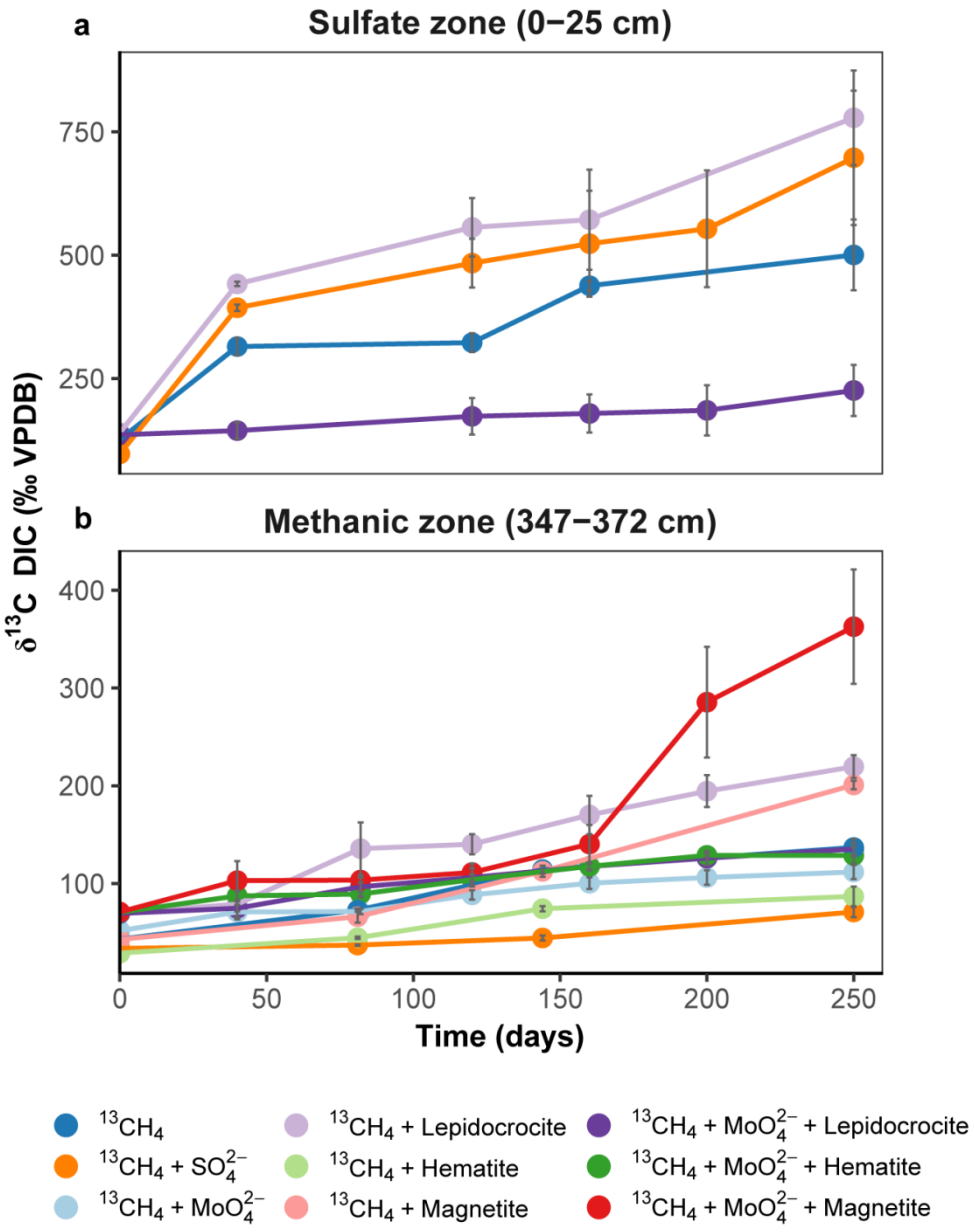

Figure 3: Change in $\delta^{13}C$ DIC values over 250 days in slurry incubation experiments with Helgoland Mud Area sediments. (a) Sulfate zone (0–25 cm) and **(b)** the methanic zone (347–372 cm) with $^{13}CH_4$ tracer, n = 3, error bars represent 1 s.d. of biological replicates. The ^{13}C-increase in the DIC pool serves as proxy for AOM. DIC isotope values in control incubations are provided in Fig. S4.

Fig. 4

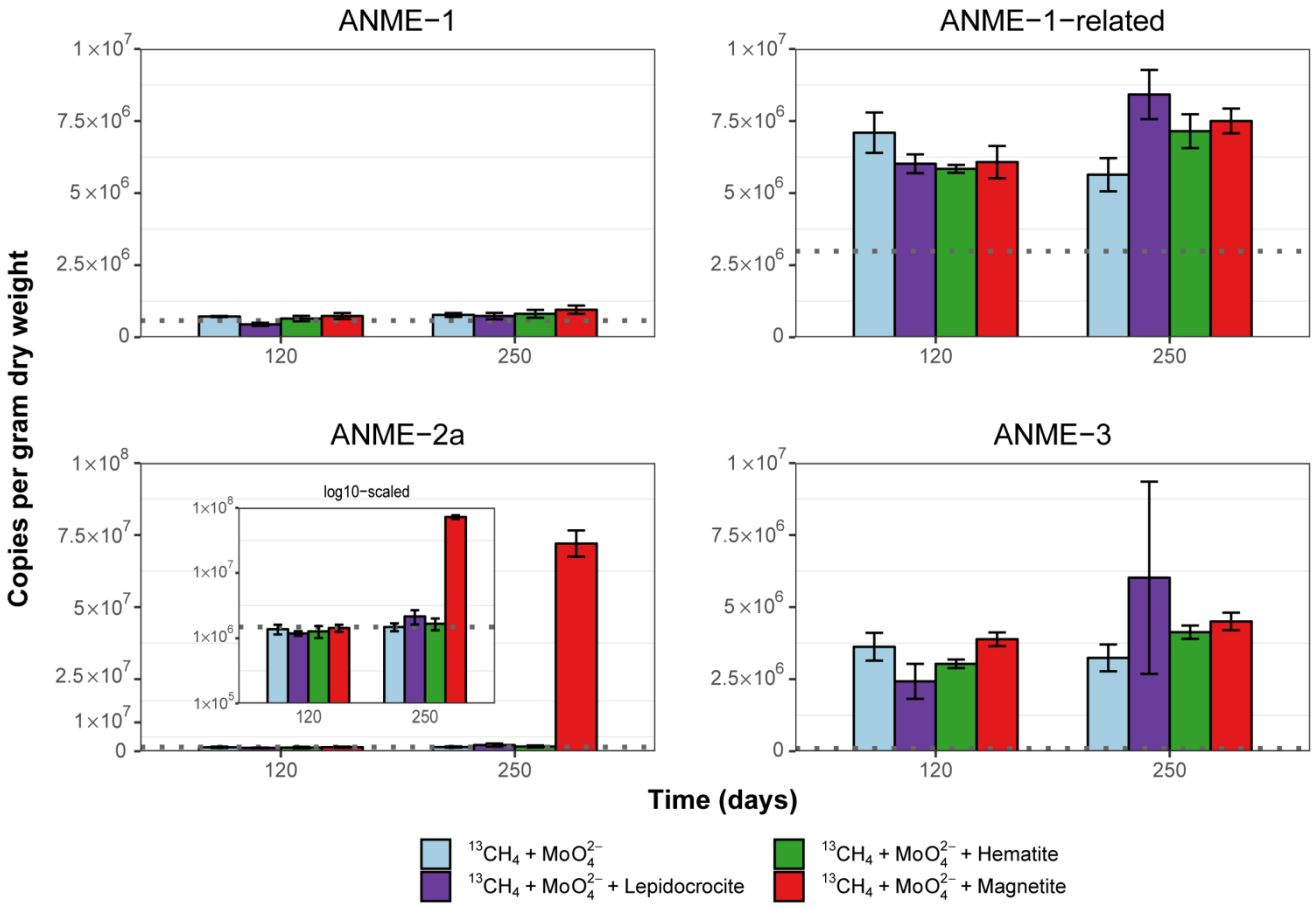

Figure 4: Abundance of *mcrA* gene copies assigned to different ANME clades in the methanic zone after 120 and 250 days of incubation in molybdate amended incubations from the methanic zone. Grey line in each plot represents estimates of gene copies of the different ANME subtype at respective incubation depths (see Fig. 2b) as indication for increasing gene copies during the 250 day incubation experiment. *mcrA* copies across all incubations with or without molybdate from the sulfate zone and methanic zone are provided in Fig. S8. INSET: log scaled adjusted *mcrA* gene copies of ANME-2a. Error bars represent 1 s.d. of technical qPCR replicates.

Fig. 5

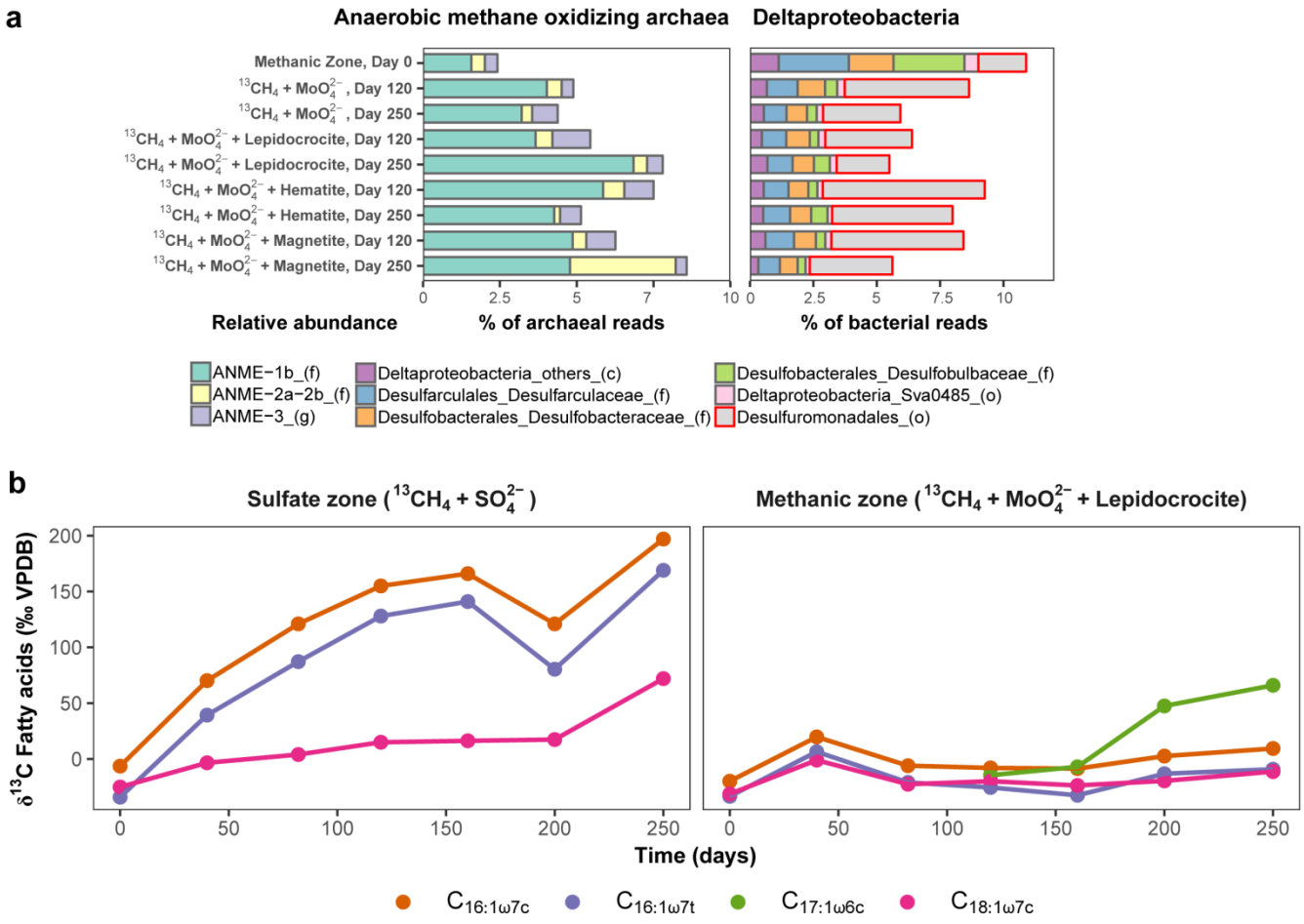

Figure 5: Molecular fingerprints providing insights into microbial activity during $^{13}CH_4$ oxidation and potential key players involved in Fe-AOM. (a) Relative abundances of ANME and Deltaproteobacteria based on 16S rRNA gene sequencing in the Fe-AOM incubations from the methanic zone after 120 and 250 days. Relative abundance based on total sum scaling of bacterial and archaeal 16S rRNA genes is provided in Fig S7, S9-S11. **(b)** Development of carbon isotopic composition of dominant bacterial fatty acids (‰ VPDB) over time during S-AOM in the sulfate zone (supplemented with sulfate) and Fe-AOM in the methanic zone (supplemented with molybdate and lepidocrocite). Complete list of $\delta^{13}C$ values of fatty acids and total uptake by each fatty acid is given in Table S5 and S6.

Materials and Methods and Supplementary Information

Rates and microbial players of iron-driven anaerobic oxidation of methane in methanic marine sediments

David A. Aromokeye[1,2,3‡], Ajinkya C. Kulkarni[1,2,3‡], Marcus Elvert[2,4], Gunter Wegener[2,5], Susann Henkel[2,6], Sarah Coffinet[2], Thilo Eickhorst[7], Oluwatobi E. Oni[1], Tim Richter-Heitmann[1], Heidi Taubner[2,4], Lea Wunder[1], Xiuran Yin[1,2,3], Qingzeng Zhu[2], Kai-Uwe Hinrichs[2,4], Sabine Kasten[2,4,6], Michael W. Friedrich[1,2]*

[1]Microbial Ecophysiology Group, Faculty of Biology/Chemistry, University of Bremen, Bremen, Germany

[2]MARUM – Center for Marine Environmental Sciences, University of Bremen, Bremen, Germany

[3]International Max Planck Research School for Marine Microbiology, Max-Planck-Institute for Marine Microbiology, Bremen, Germany

[4]University of Bremen, Faculty of Geosciences, Bremen, Germany

[5]Max Planck Institute for Marine Microbiology, Bremen, Germany

[6]Alfred Wegener Institute Helmholtz Centre for Polar and Marine Research, Bremerhaven, Germany

[7]Faculty of Biology/Chemistry, University of Bremen, Bremen, Germany

‡ Contributed equally to the manuscript

* Corresponding author:

Correspondence:

Michael W. Friedrich,

Microbial Ecophysiology Group, Faculty of Biology/Chemistry, University of Bremen, PO

Box 33 04 40, D-28334 Bremen, Germany

Email: michael.friedrich@uni-bremen.de

Materials and Methods

Sampling from the Helgoland Mud Area

This study took a multi-year sampling approach to the Helgoland Mud Area (Table S1). Sediment samples were obtained from gravity cores collected during RV HEINCKE cruises HE406 (July, 2013), HE443 (May, 2015) and HE461 (April, 2016) (Table S1). As data from previous campaign show (see reference (1) and Fig. 1a, 1b), the geochemical zonation of the sediments at the study sites are consistent over the years. Porewater sampling of gravity cores HE443-010-3 and HE461-004-1 for dedicated geochemical analysis was done on board using rhizon samplers (2, 3). Sediment samples for solid phase geochemical analysis (Table S1) were collected as described in reference (1).

Geochemical and molecular assessments were done on samples that were directly taken on board after the gears were retrieved. The gravity core HE443-077-1 was stored on board at 4 ºC and sectioned immediately (at 25 cm intervals) after the expedition and stored in the dark at 4 ºC in 2.6 L anoxic jars. Within 3 months after collection, these sediments were used for $^{13}CH_4$ incubation experiments. Potential for anaerobic oxidation of methane (AOM) was investigated with fresh sediments from HE461-064-1 gravity core sectioned and used for $^{14}CH_4$ experiments a week after core retrieval.

Table S1: Sampling information for all gravity cores retrieved from the Helgoland Mud Area.

Sampling objective	Sampling date	Station name	Coordinates	
			Latitude	Longitude
Total Fe and Mn quantification and sequential extraction	July 2013	HE406-004-2	54° 6.03' N	07° 59.01' E
Total Fe quantification and sequential extraction	July 2013	HE406-008-2	54° 5.01' N	07° 58.04' E
Total Fe quantification and sequential extraction, porewater profiles, *mcrA* gene sequencing and qPCR	May 2015	HE443-010-3	54° 05.19' N	07° 58.21' E
Long-term experiments with $^{13}CH_4$ (including molecular analyses), CARD-FISH counts of active bacteria and archaea	May 2015	HE443-077-1	54° 05.23' N	07° 58.04' E
Porewater profiles	April 2016	HE461-004-4	54° 05.20' N	07° 57.99' E
Determination AOM rates experiment	April 2016	HE461-064-1	54° 05.20' N	07° 57.99' E

Geochemical analyses

Sulfate, hydrogen sulfide, and CH_4 measurements were done from porewater and sediment slurry (for CH_4) samples as described in reference (1). For dissolved inorganic carbon (DIC) measurements, 2 mL of porewater samples were filled into 2 mL glass vials without headspace and DIC was measured directly after the cruise using a SEAL nutrient analyzer (based on the procedure described by Hall and Aller (4) using the Dickson standard for calibration). Dissolved Fe and Mn concentrations in porewater were determined by inductively coupled plasma-optical emission spectrometry (Iris Intrepid II ICP-OES).

For the determination of total iron and manganese contents in the solid phase, about 50 mg of freeze-dried and ground sediment was fully digested in a concentrated acid mixture of 3 mL HCl, 2 mL HNO_3, and 0.5 mL HF using a CEM Mars Xpress microwave system at Alfred Wegener Institute, Bremerhaven. Sequential extractions were performed after Poulton and Canfield (5) using ~50 mg of dry sediment and 5 mL of a) $MgCl_2$ for adsorbed Fe, b) Na-

acetate for Fe-carbonates and surface-reduced Fe(II), c) hydroxylamine-HCl for easily reducible iron oxides (ferrihydrite, lepidocrocite), d) Na-dithionite/citrate for reducible iron oxides (mostly goethite and hematite and some magnetite) and e) ammonium oxalate/oxalic acid for extractable magnetite. Sequential extractions of manganese oxides were done similarly but different operationally defined Mn phases were not determined. However, the extraction gave an indication regarding the quantity of reactive manganese oxides that could be present in the sediment. Fe and Mn measurements in the total digestion and the sequential extraction solutions were performed by ICP-OES.

Determination of methane oxidation rates using a $^{14}CH_4$ assay

Potential for AOM in the iron oxide-rich methanic zone and the sulfate methane transition (SMT) of the Helgoland Mud Area was tested via $^{14}CH_4$ AOM rate measurements. In 15 mL serum vials (*n*=4 per treatment), 7 g of fresh sediment (50–75 cm from the SMT and 200–225 cm, 300–325 cm, 400–425 cm from the methanic zone) was anoxically homogenized (N_2:CO_2; 80%:20%, 152 kPa) with 7 mL sulfate-depleted artificial sea water (ASW; composition [L^{-1}]: 26.4 g NaCl, 11.2 g $MgCl_2 \cdot 6H_2O$, 1.5 g $CaCl_2 \cdot 2H_2O$ and 0.7 g KCl). Sodium molybdate (10 mM; as inhibitor of dissimilatory sulfate reduction) and CH_4 or only CH_4 were supplemented to the treatments. Killed controls (n=4) were similarly prepared using heat inactivated sediments (autoclavation) to account for abiotic reactions. Headspace in the vials was subsequently exchanged with CH_4 (99.999%) and the incubations were allowed to equilibrate at 10 °C for two days, in the dark. After pre-incubation, the headspace in the vials was completely filled with CH_4 saturated sulfate-depleted ASW. 100 µL of dissolved $^{14}CH_4$ (~24 kBq; dissolved in slightly alkaline double-deionized water) was injected into each vial and the slurries were incubated in the dark at 10 °C for 8 days. Afterwards, the incubation was stopped by transferring the samples into 100 mL vials containing 10 mL of 25 g L^{-1} NaOH, to fix the formed radiolabeled DIC pool as solid phase.

The concentration of applied CH_4 was determined from headspace CH_4 using gas chromatography (GC) coupled to flame ionization detection (FID; Focus GC, Thermo Scientific; Porapak-Q column 60/80 mesh, 4 mm length, 2 mm inner diameter). The ^{14}C content of applied CH_4 (activity) was determined by stripping and combusting the headspace CH_4 to CO_2 at 850 °C in a combustion furnace, trapping this gas in scintillation vials containing 7 mL phenethylamine (6). Blanks (air) were measured to estimate background activity within the system at the end of each day. Radioactivity was measured in a liquid scintillation counter (2900TR LSA, Packard) after adding 7 mL Irgasafe Plus (Perkin Elmer, Waltham, USA) scintillation cocktail. Radioactivity in the DIC pool was determined by acid digestion (7) with slight modifications. Briefly, slurries were transferred to 250-mL Erlenmeyer flasks containing an antifoam agent and few drops of bromothymol blue as pH indicator. Serum vials were rinsed with 25 g L^{-1} NaOH 2–3 times to transfer the leftover slurry. A scintillation vial containing 1 mL, 0.5 M NaOH and 1 mL phenethylamine was placed in the plastic loop and flasks were sealed with rubber stoppers to which the plastic loop was attached using a metal wire. Acid digestion was carried out by adding 6 mL of 6 N HCl by passing a needle and a syringe alongside the rubber stopper. Flasks were tightly sealed using metal clamps before shaking at 90 rpm for 4 hours in order to release and trap the DIC in the scintillation vials. Radioactivity was measured as mentioned above after adding 2 mL Irgasafe Plus scintillation cocktail. AOM rates were calculated using the following equation:

$$\text{AOM rate (nmol } g_{dw}^{-1}\ d^{-1}) = (^{14}\text{C-DIC}/^{14}CH_4) \times [CH_4] \times (1/t) \times (1/g_{dw})$$

Where, ^{14}C-DIC is the activity of the AOM product pool, $^{14}CH_4$ is the activity of the reactant pool, $[CH_4]$ is the concentration of headspace CH_4 in nmol, t represents the incubation period and g_{dw} is the dry weight of the sediment samples. Dry weight estimates were obtained from

heat drying slurries as previously prepared in 50-mL tubes at 80 °C for 48 hours. Final rates were calculated after deducting rates measured in killed controls.

Long-term incubations with $^{13}CH_4$ tracer

For the long-term AOM experiments, sediments from the sulfate zone (0–25 cm) and methanic zone (347–372 cm) (see Table S1) were used to set up slurry incubations. Individual anoxic slurries were prepared by mixing 60 mL of sediments with sulfate-depleted ASW (1:3 w/v) in 120-mL serum vials. Headspace of slurries was filled with either CH_4 (99.999 %, core treatments) or N_2 (99.999 %, negative controls). Slurries were incubated at 4 ^{o}C for 14 days to equilibrate the system and ensure the microcosms are completely reduced. Afterwards, 15 % (~ 9 mL) of the headspace of CH_4 carrying slurries was removed using an air tight syringe and replaced with 9 mL $^{13}CH_4$. $^{13}CH_4$ was added to the headspace to track CO_2 formation in form of DIC within incubations from the different sediment layers and with different amendments as a proxy for AOM. From the sulfate zone sediments, treatment sets (n=3) were prepared with the following modifications: (I) $^{13}CH_4$ and 5 mM sodium sulfate; (II) $^{13}CH_4$, 30 mM sodium molybdate and 30 mM lepidocrocite; (III) $^{13}CH_4$ and 30 mM lepidocrocite; (IV) $^{13}CH_4$ (V) N_2 headspace, un-amended slurry; (VI) N_2 headspace and 5 mM sodium sulfate; (VII) N_2 headspace and 30 mM lepidocrocite. To slurry sets (n=3) from the methanic zone, the following treatment modifications were made: (I) $^{13}CH_4$ and 30 mM lepidocrocite; (II) $^{13}CH_4$, 5 mM sodium molybdate and 30 mM lepidocrocite; (III) $^{13}CH_4$ and 30 mM hematite; (IV) $^{13}CH_4$, 5 mM sodium molybdate and 30 mM hematite; (V) $^{13}CH_4$ and 30 mM magnetite; (VI) $^{13}CH_4$, 5 mM sodium molybdate and 30 mM magnetite; (VII) $^{13}CH_4$ and 5 mM sodium molybdate; (VIII) $^{13}CH_4$ and 30 mM sodium sulfate; (IX) $^{13}CH_4$; (X) N_2 headspace, un-amended slurry; (XI) N_2 headspace and 30 mM lepidocrocite; (XII) N_2 headspace and 30 mM hematite; (XIII) N_2 headspace and 30 mM magnetite; (XIV) N_2 headspace and 30 mM sodium sulfate. To be able to carry out lipid stable isotope probing

(SIP) subsequently, we prepared several replicates for sacrificial sampling from two treatment types described above; (I) from the sulfate zone, where we expected to stimulate S-AOM ($^{13}CH_4$ + sulfate) and (II) from the methanic zone, where we expected to stimulate Fe-AOM ($^{13}CH_4$ + molybdate + lepidocrocite). All treatments were incubated at 30 ^{o}C, sampled initially after 12–18 hours (taken as time-point 0) for dissolved Fe^{2+} and DIC measurements and subsequently over the course of 250 days. Replicate samples for lipid SIP were also sacrificially sampled at each time-point (including time-point 0) by directly opening each serum bottle and transferring the contents into a sterile 50-mL falcon tube, which was stored immediately at -20 ºC until lipid extraction. Fe^{2+} formation in aqueous phase was monitored spectrophotometrically, according to reference (8).

For analysis of DIC isotopic composition, 2 mL of sediments from each microcosm, using syringes pre-flushed with N_2, were transferred into 2.5-mL micro-centrifuge tubes pre-flushed with N_2. The tubes were centrifuged at 15,300 *g* for 3 minutes followed by careful transfer of the supernatants into 4-mL glass vials. Vials were stored at -20 ^{o}C until measurements. DIC analysis was done using a Delta Ray Isotope Ratio Infrared Spectrometer (IRIS) with URI Connect and autosampler (Thermo Fisher Scientific, Germany). As preparation of the DIC analysis, 100 µL of 45 % H_3PO_4 was added to gas tight 12-mL exetainer vials with septum caps and flushed for 3 minutes with CO_2 free air using the Delta Ray system. Afterwards, 1 mL of stored liquid sample was transferred into each exetainer vial using a gas tight syringe and left for equilibration at room temperature overnight. During equilibration, the DIC components in the liquid were released as CO_2 into the headspace due to acidification. The headspace was analyzed for carbon isotope ratio of CO_2 as $\delta^{13}C$ DIC against CO_2 reference gas using the Delta Ray IRIS with URI connect.

Concentrations of CH_4 in headspace samples (100 µL) of N_2 controls were measured on a GC (Shimadzu GC-2014, Tokyo, Japan) as described elsewhere (9). CH_4 concentrations formed

in headspace were calculated using the ideal gas law with incubation temperature (30 ºC) as variable.

Molecular analyses of sediments and $^{13}CH_4$ tracer experiments

Nucleic acid extraction

Aliquots of sediments were sampled depth-wise directly on board during porewater sampling from HE443-010-3 gravity core (Table S1) and were immediately frozen at -20 ºC. Using these sediment samples, DNA was extracted from 0.5 g of sediment per depth in duplicates following the phenol-chloroform-isoamylalcohol method (10). Similarly, nucleic acids were extracted at specific time-points (day 0, 120 or 144 and 250) in the $^{13}CH_4$ experiments. Here, ~ 0.5 g sediment pellets, which were stored during sampling from biological triplicates samples of each treatment, were used for the extraction (porewater previously extracted for DIC measurement). 50 µL of DEPC water was added to elute nucleic acids from the first sample replicate. This eluent was subsequently transferred to other sample replicates in order to have the nucleic acids pooled together in one tube.

Next generation sequencing of *mcrA* and 16S rRNA genes

Using polymerase chain reaction (PCR) method, *mcrA* genes were amplified from DNA extracts from sediment samples taken from HE443-010-3 gravity core. The primer pairs mlasF (5'-GGTGGTGTMGGDTTCACMCARTA-3') (11) and ME2mod (5'-TCATBGCRTAGTTNGGRTAGT-3') (12) were used for the amplification. DNA was amplified using AmpliTaq DNA polymerase kit (Thermo Fisher Scientific, Germany) containing 1X PCR buffer, 0.2 mM dNTP mix, 1.5 mM $MgCl_2$, 0.2 mg mL^{-1} bovine serum albumin (BSA), 500 nM of each primer, 1U of AmpliTaq DNA polymerase and 2 µL of diluted DNA in a 50 µL reaction volume. Amplification was done at the following PCR conditions: 95 °C: 5 minutes; 30 cycles at 95 °C: 30 seconds, 50 °C: 45 seconds, 72 °C:

45 seconds and 72 °C: 5 minutes. Amplicons were screened on gel electrophoresis (2 % Agarose, 100V, 60 minutes) and purified using the QIAGEN MinElute kit (QIAGEN, Hilden, Germany) following the manufacturer's instruction. Purified amplicons were sent to MR DNA (Molecular Research LP, Texas, USA) for sequencing on an Illumina MiSeq (2 x 300 bp) sequencing platform.

Bacterial and archaeal 16S rRNA genes were amplified from DNA extracts from the $^{13}CH_4$ incubation experiments using Illumina HiSeq 4000 (2 x 150 bp) amplicon sequencing platform. Primer pairs Bac515F (5'-GTGYCAGCMGCCGCGGTAA-3') (13) and Bac805R (5'-GACTACHVGGGTATCTAATCC-3') (14) were used for targeting bacteria, whereas Arc519F (5'CAGCMGCCGCGGTAA-3') (5'CAGCMGCCGCGGTAA-3') (15) and Arc806R (5'GGACTACVSGGGTATCTAAT-3') (16) were used for targeting archaea. Each primer was synthesized with an additional unique barcode sequence (8 bp long) that facilitated multiplexing of several samples in one sequence library (17). PCR reaction mix (50 µL) contained 1 x KAPA HiFi buffer, 0.3 mM dNTP mix, 0.25 U KAPA HiFi DNA polymerase (KAPA Biosystems, Germany), 1.5 µM each of forward and reverse barcoded primer pairs, and 2 µL of 10-fold diluted DNA template from each sample. PCR cycling conditions include: 95 °C: 5 minutes; 28 cycles at 98 °C: 20 seconds, 60 °C: 20 seconds, 72 °C: 20 seconds; 72 °C: 1 min. PCR products were screened by gel electrophoresis as mentioned before and purified using Monarch® PCR & DNA purification kit (New England Biolabs, Germany). PCR products were quantified using Quant-iT PicoGreen dsDNA assay kit (Invitrogen-Thermo Fischer Scientific, Steinheim, Germany). Based on the estimated quantities from the PicoGreen assay, an equimolar library of samples was constructed. Amplicon library was sequenced at GATC Biotech GmbH, Germany.

Cloning and quantification of *mcrA* genes of anaerobic methane oxidizing archaea (ANME)

Due to the unavailability of cultured strains of methanotrophic archaea, we cloned genes obtained from Helgoland Mud Area sediment samples to use them as standards for quantifying gene copy numbers of ANMEs. DNA extracts from different depths of the Helgoland Mud Area sediments (HE376-007-5 (1); HE443-10-3: this study) were amplified using the primer pairs (I) mcrA-312f (5' CAACBCNGCVATGCAGCAG 3', this study) – ME2mod and (II) mlasF–ME2mod using the AmpliTaq DNA polymerase kit (same as before). The following PCR program was used for the mcrA-312f–ME2mod primer pairs: 95 °C: 5 minutes; 30 cycles at 95 °C: 30 seconds, 55 °C: 1 minute, 72 °C: 1.5 minute; and 72 °C: 5 minutes. PCR products were purified using QIAGEN MinElute kit following the manufacturer's instructions. Purified PCR products were cloned, sequenced and edited as described (1). An in-house *mcrA* gene database was created by acquiring (from https://www.ncbi.nlm.nih.gov/nucleotide/) and manually aligning long (>1000 bp) gene sequences of cultured and published methanogenic, methanotrophic and hydrocarbon degrading archaea in ARB 6.02 (18). Using the RAxML algorithm in ARB, a phylogenetic tree was constructed, to which shorter *mcrA* gene sequences were added using the ARB Parsimony tool. Edited FASTA sequences were imported and translated into their protein sequences in ARB. The protein sequences of clones were manually aligned and imported in the aforementioned *mcrA* gene database using the ARB Parsimony tool in order to determine their taxonomic affiliations (on DNA and protein level). Abundances of specific ANME phylotypes were determined from various sediment depths and from $^{13}CH_4$ tracer experiments using quantitative PCR (qPCR). In order to estimate increase in biomass of ANME phylotypes in the incubations experiments over 250 days, abundances from their respective depths were considered as baseline proxy. qPCR assay was done following

reference (19) with few modifications. Standard templates were prepared by amplifying ANME clones using plasmid specific M13 primer pairs and the AmpliTaq DNA polymerase kit. PCR products were then purified (QIAGEN MinElute kit) and quantified using Quant-iT PicoGreen dye. Takyon ROX SYBR 2X MasterMix (Eurogentec, Seraing, Belgium) was used as a replacement kit instead of the MESA BLUE qPCR kit for the SYBR qPCR assay as recommended by the company. DNA extracted from the incubations and *in situ* sediment samples was quantified using Quant-iT PicoGreen dye and diluted to 500 pg /µL (standards and sulfate zone incubations) and 50 pg /µL (methanic zone incubations). 2 µL of diluted DNA was used as template for all qPCR assays. qPCR assays were run using the following program: 95 °C: 10 minutes; 40 cycles at 95 °C: 30 seconds, 52 °C or 62 °C: 20–30 seconds, 72 °C: 40 seconds. A post amplification melting curve analysis was performed in order to rule out PCR by-products by detecting change in fluorescence every 0.5 °C from 60 °C to 95 °C. qPCR primers, assay conditions, efficiencies and clone information are provided in Table S2.

Table S2: Supporting information for phylotype specific qPCR assays

Target *mcrA* gene	Annealing temperature/time	Average efficiency	R^2	Clone used	Mass of one gene (Da)	Primer sequences (5' - 3')	Reference	Primer concentration	Product length (bp)
ANME-1	62 °C/ 30 seconds	84.45%	>0.99	E-3	878414	F: AYGACCAGYTGTGGTTCGGAACGT R: TCCATGTTSARCTTGTCGCCCTTY		600 nM	175 bp
ANME-2a	62 °C/ 30 seconds	84.96%	>0.99	F-79	862362	F: ATATGGCAGATATTGTCCAGACCTCAAGG R: ATTTATCCCAKCCGTAYTC	Miyazaki et al (20)	600 nM	218 bp
ANME-3	52 °C/ 20 seconds	85.67%	>0.984	AII58	440445	F: AAGGAYATYRSAACCGAATC R: TTGAAAGGTACCATSSKGAAAGACC		400 nM	180 bp
ANME-1 related	52 °C/ 20 seconds	89.08%	>0.99	E-155	870491	F: GAGATCGCVRTVGACATGTTCGG R: GCCCTMACAGAMCCRCCGAAGTG	Zhou et al (21)	400 nM	172 bp

Analysis of *mcrA* and 16S rRNA gene sequences

Sequence analysis was performed on the QIIME 1.8.0 platform (22) based on the analysis pipeline as recommended (23) with modifications. To analyse *mcrA* gene sequences, barcodes were extracted and sequences were reoriented starting with the forward primer sequence. Reoriented reads were joined using a minimum overlap of 50 bases. Joined reads were demultiplexed with a filter quality of Q0 (24). Demultiplexed sequences were quality filtered using USEARCH 10 (expected error value of 0.5) (25). At this step, all sequences were truncated to a length of 352 bp. USEARCH 10 was further used to dereplicate sequences, sort them by their abundances and subject them to remove singletons. OTU clustering and chimera removal was done using the UPARSE-OTU algorithm (26) to create an OTU database. Chimeric sequences were checked and discarded by the UPARSE-OTU algorithm during this step. The truncated, non-dereplicated reads were mapped back to the OTU database to create an OTU table. OTUs were classified for their taxonomy using uclust and an in-house *mcrA* gene database as reference (see *mcrA* genes cloning section). The taxonomic assignment was done on the family level at a sequence identity of 0.7 (27). The OTU table and taxonomy assignment files were merged together using a set of "biom" commands (28) to obtain a tab-delimited text file useful for downstream analysis. A few modifications of the above pipeline were done to analyze 16S rRNA gene sequences. Forward reads were used to analyze the community composition. After extraction of barcodes, forward reads were de-multiplexed, quality filtered and their lengths were truncated to 143 bp. Taxonomic assignment was done on clustered OTUs against the 16S rRNA gene SILVA database (Release 128 for QIIME) (29).

Cloning and amplification of *pmoA* gene

To maximize amplification of *pmoA* genes, a two-step PCR was conducted with AmpliTaq DNA polymerase kit with slight modifications compared to the *mcrA* gene amplification (1.25U of AmpliTaq polymerase and 3 mM $MgCl_2$ were used instead). Primer pairs of A189F (5'-GGNGACTGGGACTTCTGG-3') (30) and 682R (5'-GAASGCNGAGAAGAASGC-3') (30) were used for the first PCR at the following conditions: 94 °C: 4 minutes; 35 cycles at 94 °C: 30 seconds, 50 °C to 60.5 °C (0.3 °C per cycle) and 72 °C for 1 minute; 72 °C: 7 minutes. PCR products were purified using the QIAGEN MinElute kit. Purified products were further amplified using primer pairs A189F and mb661R (5'-CCGGMGCAACGTCYTTACC-3') (31) at the following conditions: 94 °C: 4 minutes; 35 cycles at 94 °C: 30 seconds, 55 °C: 1 minute and 72 °C: 1 minute; 72 °C: 1 minute. Cloning was done (see *mcrA* gene cloning) to identify the unspecific PCR products of ~300-350 bp from the *pmoA* gene PCR amplification (Fig. S13). PCR products from $^{13}CH_4$ + molybdate + magnetite (P) and $^{13}CH_4$ + molybdate + lepidocrocite (L) incubations were purified, cloned and sequenced as per mentioned in *mcrA* gene cloning section. Using BioEdit (32) (version 7.0.9.0), vector sequences were trimmed and the sequences were reoriented (if necessary) by locating the A189F primer sequence. A sorted six-frame translation of the nucleotide sequences was performed in BioEdit and the longest amino acid sequences (110 amino acids; without a stop codon) in the positive frame were selected and stored in the FASTA file format. Amino acid sequence FASTA files were uploaded to the Protein BLAST suite (blastp suite; https://blast.ncbi.nlm.nih.gov/Blast.cgi) and BLAST hits were tabulated in Table S4.

Bacterial and archaeal cell counts using catalyzed reporter deposition-fluorescence in situ hybridization (CARD-FISH)

CARD-FISH was performed as previously described (33) to quantify potentially active bacterial and archaeal cells at different sediment depths of the Helgoland Mud Area (HE443-077-1). Approximately 0.5 g of sediment samples were weighed in 2-mL vials and were fixed in 4 % formaldehyde and 1X phosphate-buffered saline. The 2-mL vials were incubated at 4 °C for 2.5 hours under constant shaking (180 rpm on an overhead shaker). The suspension was centrifuged and the sediment was washed with 1.5 mL of 1X PBS twice. After decanting the supernatant, fixed samples were re-suspended using 1.5 mL 1X PBS:ethanol (v:v) solution. 100 µL of fixed samples were transferred to 900 µL of 1X PBS:ethanol (v:v) solution and sonicated in pulses at 10 % power for 30 seconds (two times paused by 30 seconds) in a cryo-box. 250 µL of sonicated samples were mixed with 10 mL of Milli-Q water (H_2O_{MQ}) and vacuum filtered through a polycarbonate filter (0.22 µm) in order to capture fixed cells on the filter. After air drying, the filter was dipped in molten, 0.2 % low melting point Agarose and allowed to dry at 46 °C. Permeabilization of the cell walls was done using 100 µL solutions of lysozyme (60 minutes, 37 °C) and achromopeptidase (30 minutes, 37 °C). The filters were washed with H_2O_{MQ} after each treatment. Inactivation of endogenous peroxides, hybridization with horseradish peroxidase labeled probes, washing of unbound probes and tyramide signal amplification (with 500 µL amplification buffer) was done as mentioned in reference (32). Bacterial cells were targeted with a mixture of three probes namely, EUB338 (5’ GCTGCCTCCCGTAGGAGT 3’) (34), EUB338II (5’ GCAGCCACCCGTAGGTGT 3’) (34) and EUB338III (5’ GCTGCCACCCGTAGGTGT 3’) (35). Archaeal cells were targeted with the ARC915 probe (5’ GTGCTCCCCCGCCAATTCCT 3’) (34). The filters were mounted on a clean glass slide

containing a drop of VectaShield H-1200 containing DAPI in order to counter-stain cellular DNA. Cells were observed and counted following reference (33).

Lipid SIP

^{13}C incorporation into bacterial and archaeal membrane lipids was monitored during the $^{13}CH_4$ incubations. Sacrificed replicates from each time-point were used to investigate changes in stable carbon isotopic composition of the lipids. While bacterial lipids were continuously monitored over the whole incubation period, archaeal lipids were only determined at the start and the end.

Total lipids were extracted from freeze-dried slurries (10–12 g) following a modified Bligh and Dyer method (36). Afterwards, polar lipid derived fatty acids (PLFAs) of bacteria were released from aliquots (30 %) of the total lipid extract (TLE) and converted into fatty acid methyl esters (FAMEs) (37). Intact and core archaeal lipids from a second TLE aliquot (30 %) were separated by preparative HPLC and ether lipids in each fraction were converted to hydrocarbons (38). Separation was achieved by a LiChrosphere Diol-100 column (250 x 10 mm, 5 µm particle size, Alltech) connected to an Agilent 1200 series HPLC that was equipped with an Agilent 1200 series fraction collector, at 30 °C, with a flow rate of 3 mL min^{-1}. The eluent gradient was 0 % to 24 % B in 15 min, to 100 % B in 5 min and hold for 10 min where eluent A was composed of *n*-hexane and isopropanol (IPA) (90/10; v/v) and eluent B of 100 % IPA. FAMEs and ether-cleaved hydrocarbons were subsequently analyzed by a Thermoquest Trace GC mass spectrometry (GC-MS) system and GC-isotope ratio-MS (GC-IRMS) using a Trace GC ultra-coupled via GC Isolink and a Conflo IV interface to a Thermo Scientific Delta V plus following published protocols (39).

Uptake of $^{13}CH_4$ into PLFAs was calculated as the product of excess ^{13}C and the amount of PLFA carbon based on quantification via GC-FID measurements (39). Excess ^{13}C is the

difference between the fractional abundance (F) of ^{13}C in PLFAs after 250 days relative to the T_0 sample where $F = {}^{13}C/({}^{13}C+{}^{12}C) = R/(R+1)$, with R being derived from the measured $\delta^{13}C$ values as $R = (\delta^{13}C/1000+1) \times R_{VPDB}$.

Statistical analysis and figures production

Correlation analysis and figures were made within the R environment (40, 41). Pearson correlation coefficients (*r*) were calculated along with confidence intervals (95 %). P values were adjusted for multiple testing (False Discovery Rate method).

Supplementary Results and Discussion

Total iron contents and sequentially leached iron mineral phases

Total iron and contents of different iron mineral phases in the Helgoland Mud Area sediments were analyzed following reference (5) (Fig. S1). FeCarb represents carbonate bound solid phase Fe(II) such as siderite, ankerite, but also surface reduced Fe(II) (5, 42). This fraction appears to be the most abundant in the sediment. FeOX1 represents poorly crystalline iron oxides like ferrihydrite and lepidocrocite. FeOX2 derives from crystalline iron oxides (akaganéite, hematite and goethite) and up to 50 % of magnetite (42). FeMag displays the magnetite fractions. These sequentially extracted fractions are abundant in the methanic zone of the Helgoland Mud Area (up to 0.93 wt %).

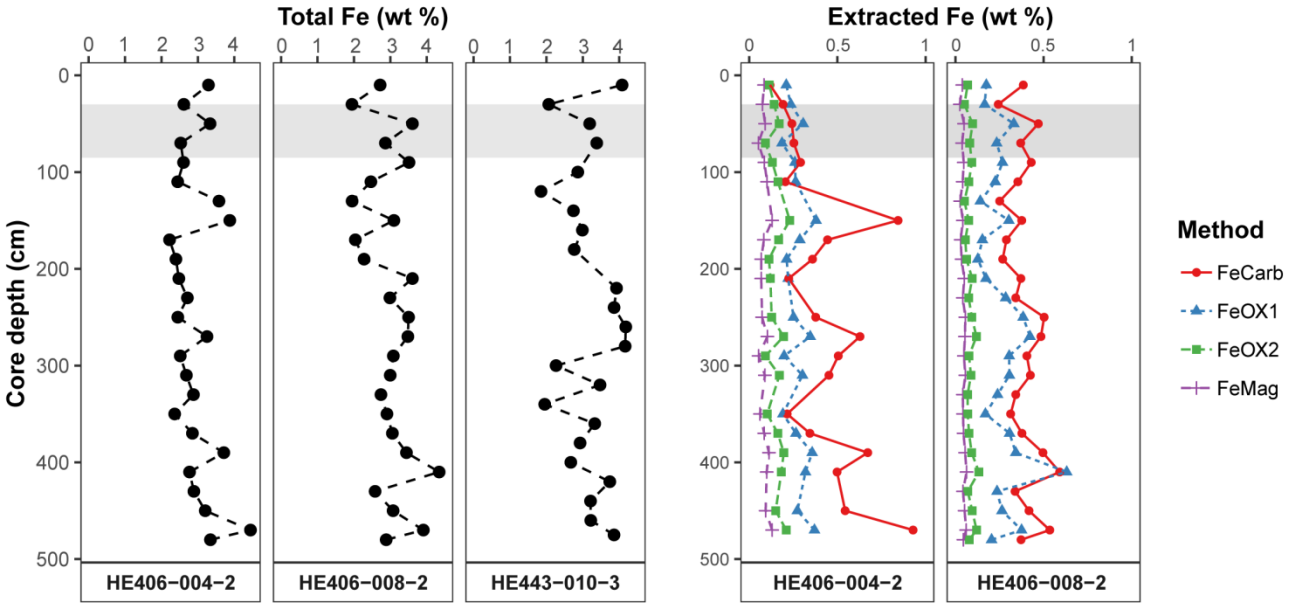

Fig. S1: Total Fe contents and operationally defined iron phases in gravity cores from the Helgoland Mud Area (see Table S1). (FeCarb: sodium acetate extractable, FeOX1: hydroxylamine-HCl extractable, FeOX2: dithionite extractable and FeMag: oxalate extractable iron oxide phases). Grey area represents the SMT.

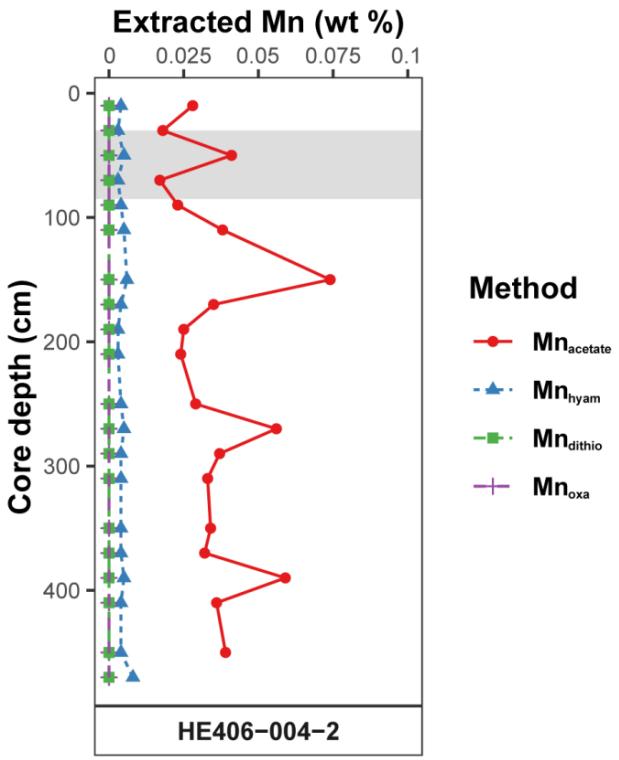

Fig. S2: Operationally defined manganese oxide phases in Helgoland Mud Area obtained from HE406-4-2 gravity core. ($Mn_{acetate}$: sodium acetate extractable, Mn_{hyam}: hydroxylamine-HCl extractable, Mn_{dithio}: dithionite extractable and Mn_{oxa}: oxalate extractable manganese oxide phases). Grey area represents the SMT.

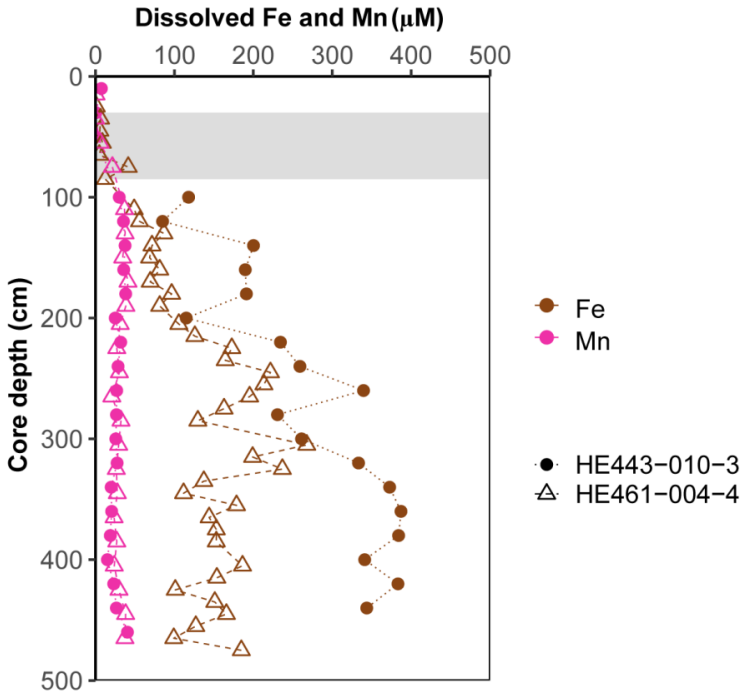

Fig. S3: Dissolved Fe and Mn profiles in gravity cores taken during HE443 and HE461 cruises (see Table S1). Grey area represents the SMT.

Table S3: Correlation analysis of dissolved Fe and Mn profile with *mcrA* gene based copies of different ANME phylotypes. Dissolved Fe and Mn concentrations (in µM), respectively, in the core HE443-010-3, were correlated to absolute gene copy numbers of each phylotype across all depths in the methanic zone. 'n.s.' represents non-significant p-values (> 0.05) and their confidence intervals were thereby not estimated (NA).

ANME phylotype	Dissolved Fe				Dissolved Mn			
	Pearson's *r*	P(adj)	95 % CI upper	95% CI lower	Pearson's *r*	P(adj)	95 % CI upper	95 % CI lower
ANME-1	0.28	n.s.	NA	NA	-0.14	n.s.	NA	NA
ANME-1-related	0.64	0.01	0.23	0.86	-0.67	0.01	-0.87	-0.26
ANME-2a	-0.06	n.s.	NA	NA	0.15	n.s.	NA	NA
ANME-3	-0.08	n.s.	NA	NA	0.10	n.s.	NA	NA

DIC values in control samples from the $^{13}CH_4$ AOM experiments

For the long-term AOM experiments, N_2 headspace filled controls were prepared to show the depletion of δ^{13}C-DIC (Fig. S4) in contrast to the enrichment of δ^{13}C-DIC observed during

AOM (Fig. 3). Results presented in Fig. S4 serve as negative control showing that the increase in δ^{13}C-DIC observed in Fig. 3 is due to the addition of $^{13}CH_4$ to the incubations.

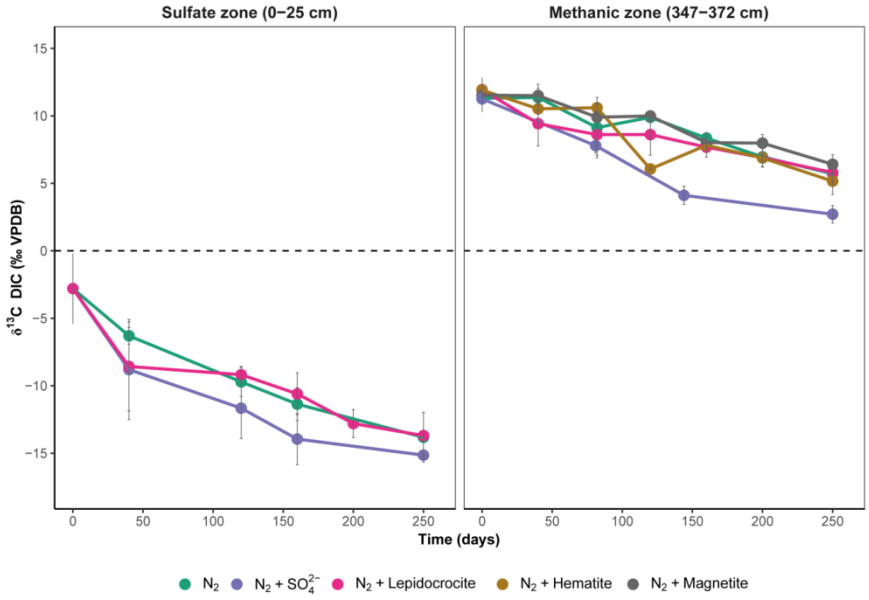

Fig. S4: DIC measurements in control incubations over time showing the ^{13}C depletion of DIC in N_2 headspace filled controls**.**

Dissolved Fe^{2+} measurement across all incubations

As shown in Fig. S1, FeCarb phases, which are representative of Fe(II) phases, are abundant in the sediment. Given that the incubation experiments were carried out using natural sediment samples replete with solid phase Fe(II) fractions, measurement of HCl extractable Fe(II) would potentially leach out Fe(II) fractions already present in the sediment. Consequently, this overprints on the freshly produced Fe(II) from ongoing microbial iron reduction. Therefore, dissolved Fe^{2+} in aqueous phase was measured in real time and directly used as proxy for rates of microbial iron oxide reduction (Fig. S5, Fig. S6). While lepidocrocite amended incubations showed the highest concentrations of dissolved Fe^{2+}, magnetite amended incubations in the methanic zone showed the lowest concentrations of dissolved Fe^{2+} in the headspace.

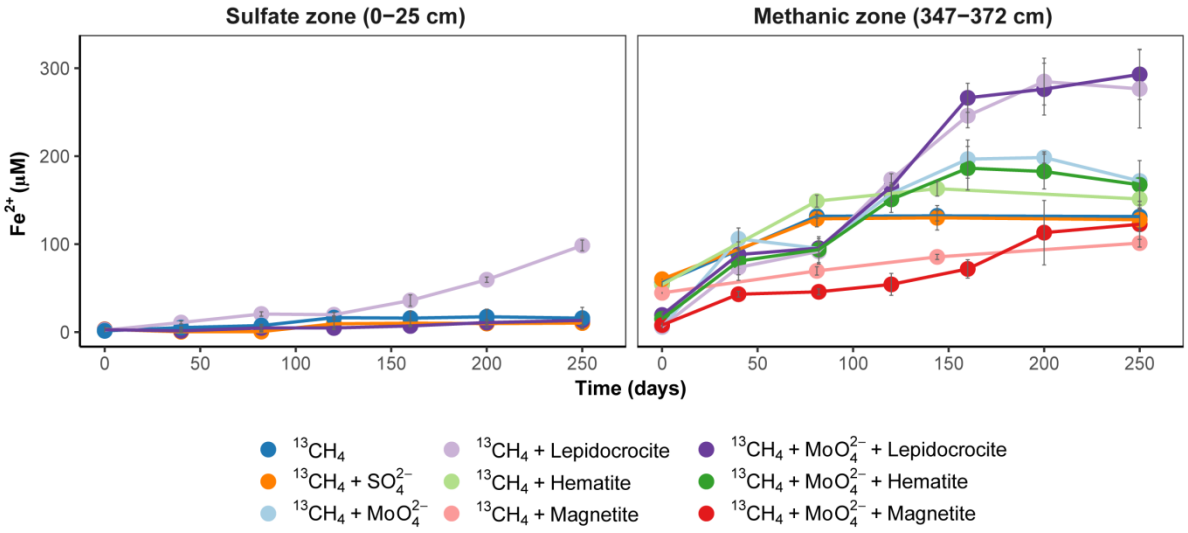

Fig. S5: Dissolved Fe^{2+} measurements over time in incubations with $^{13}CH_4$ in the headspace.

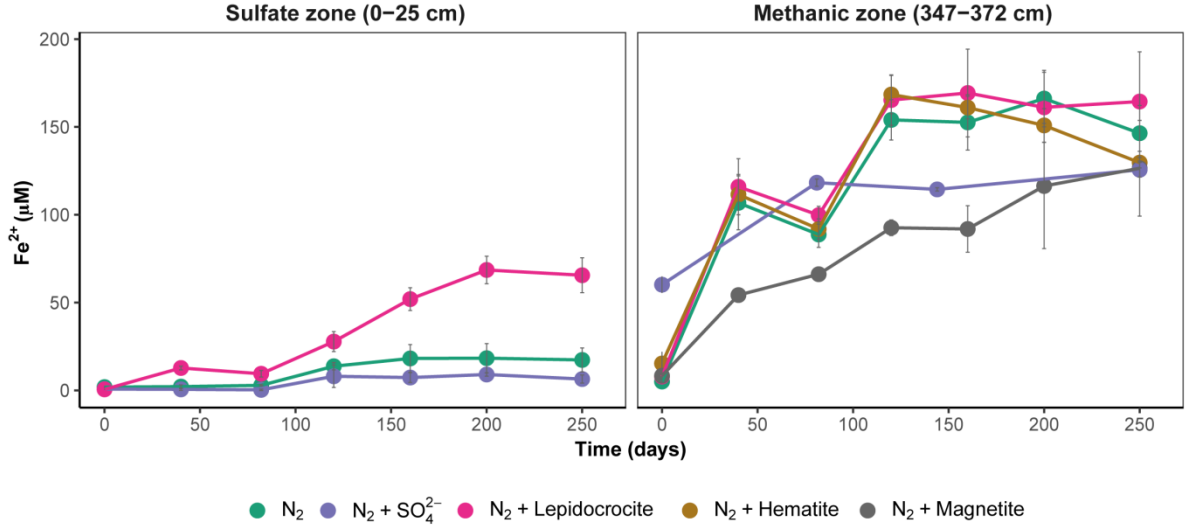

Fig. S6: Dissolved Fe^{2+} measurements over time in control incubations with N_2 in the headspace.

Although the Fe^{2+} concentrations formed in N_2 amended control incubations (Fig. S6) are slightly lower than in parallel incubations with $^{13}CH_4$ in the headspace (Fig. S5), the results show that there are potentially other pathways generating Fe^{2+} in the sediment, mostly due to organic matter in the sediments. The fact that iron oxide reduction in these incubations cannot be totally attributed to Fe-AOM alone shows that these Fe^{2+} data cannot be used for an accurate stoichiometric assessment of Fe-AOM. Future enrichments of sediment free communities from these sediments will allow for such assessments.

Microbial community composition in $^{13}CH_4$ incubation experiments

Extracted DNA in all incubations from the $^{13}CH_4$ experiment was investigated for Fe-AOM key players using 16S rRNA gene sequence and *mcrA* gene qPCR analysis (Figs. S7–S11).

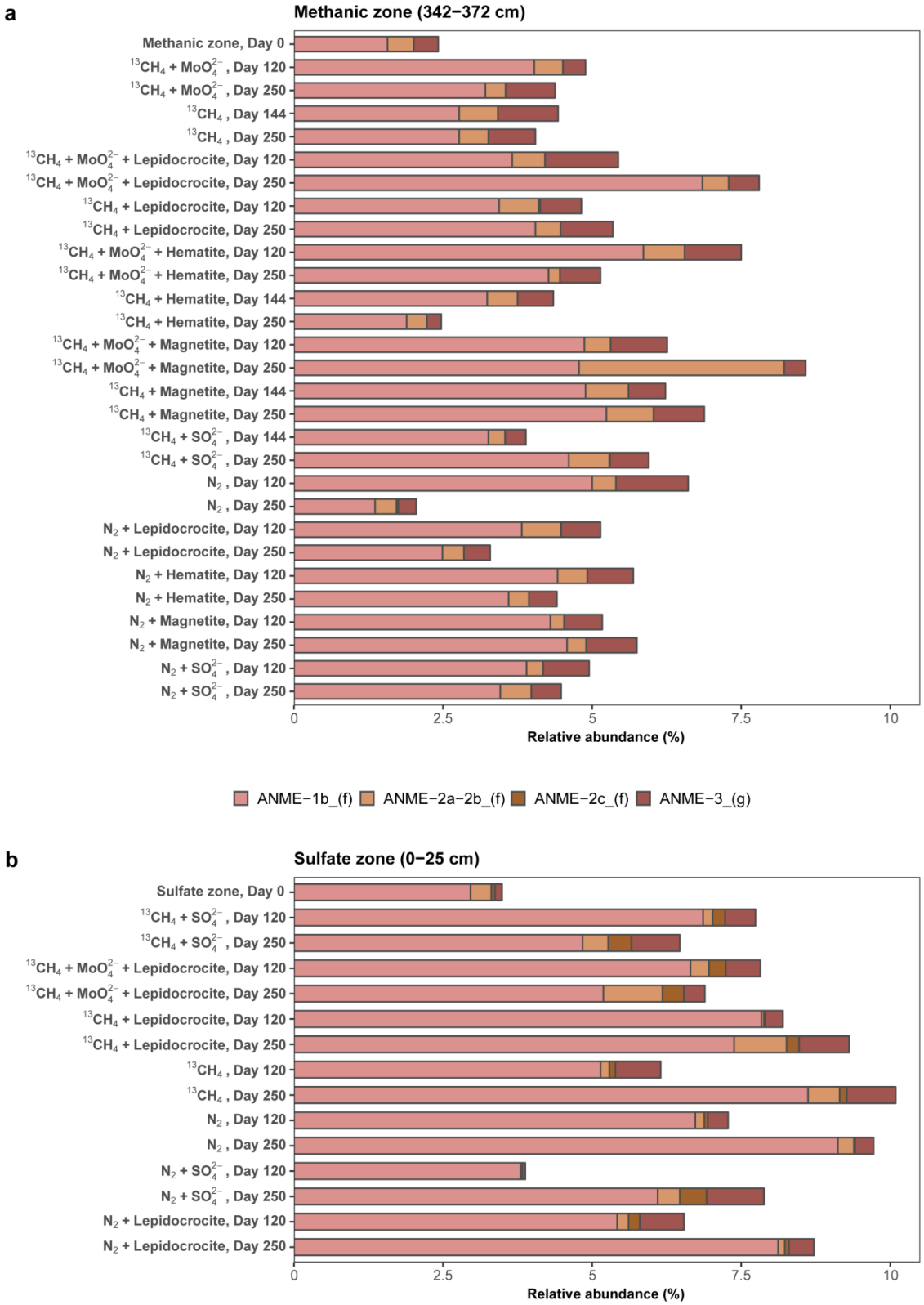

Fig. S7: 16S rRNA genes belonging to known ANME as a fraction of total archaeal 16S rRNA genes in incubations of both geochemical zones.

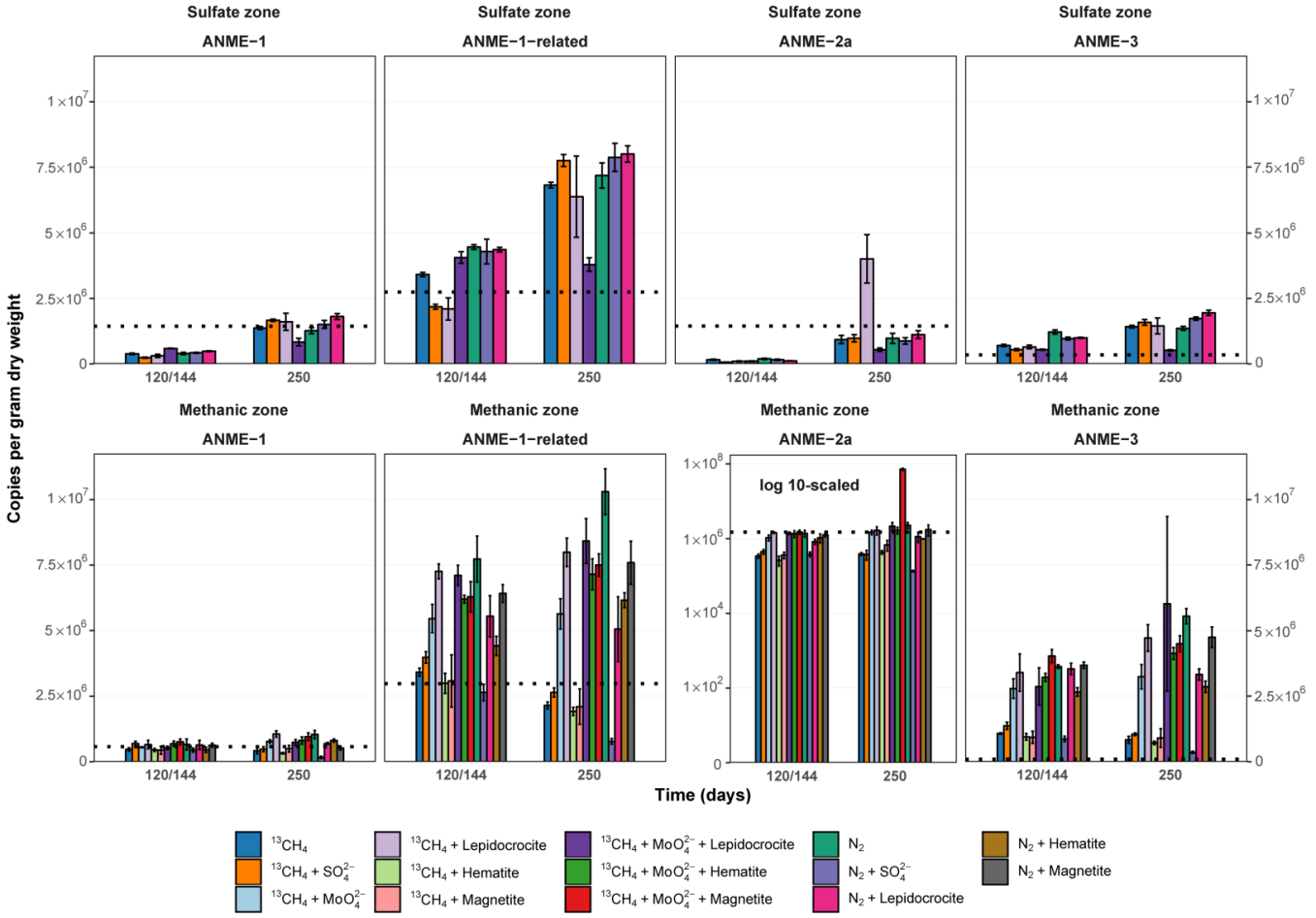

Fig. S8: *mcrA* gene qPCR results of ANMEs from all incubations after either 120 or 144 days as intermediate time-point and after 250 days of incubation. Gene copy numbers were compared with copy numbers from the respective depths (grey baselines) used for setting up the experiment in both geochemical zones.

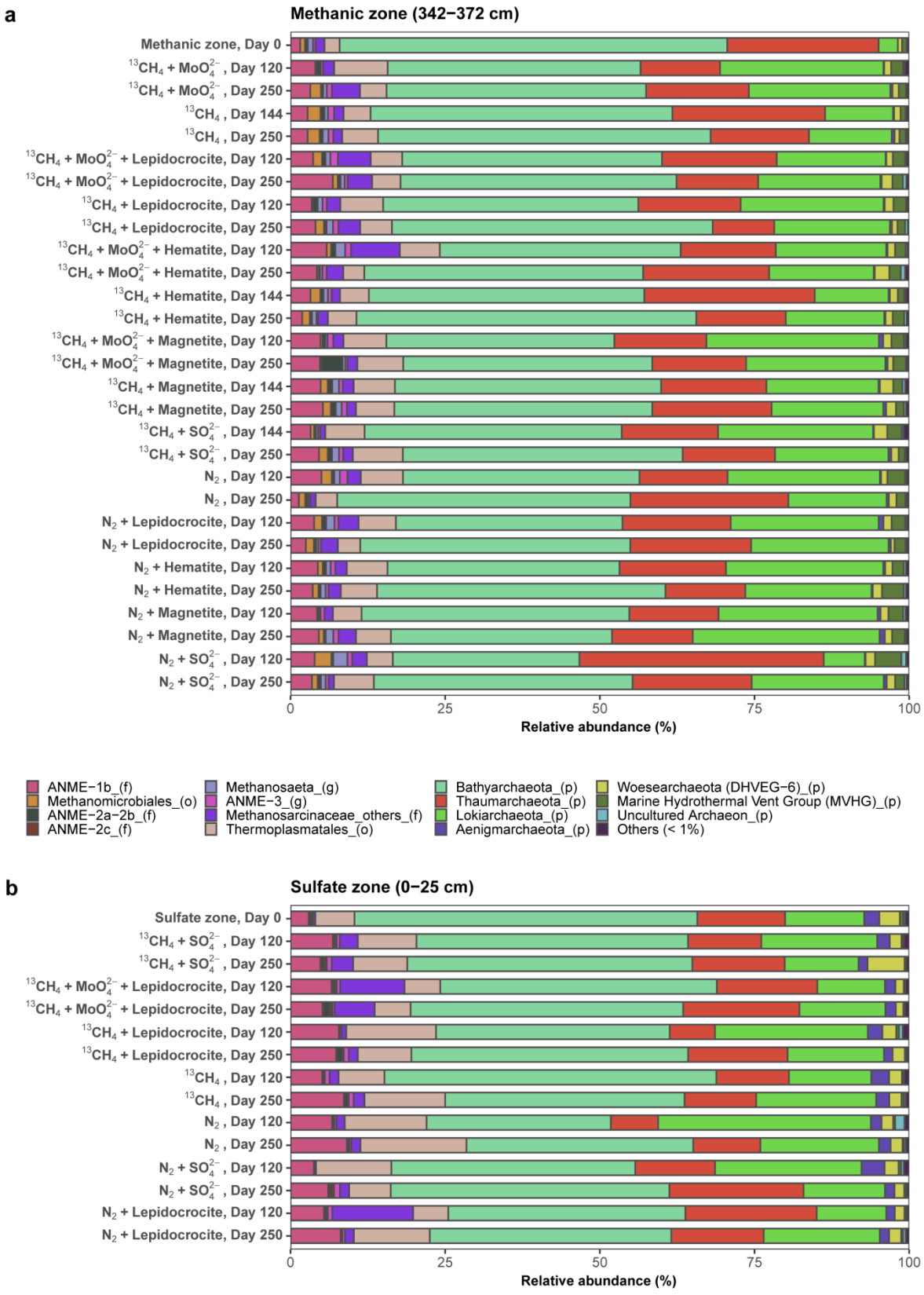

Fig. S9: Total sum scaling of archaeal 16S rRNA genes across all incubations from both geochemical zones.

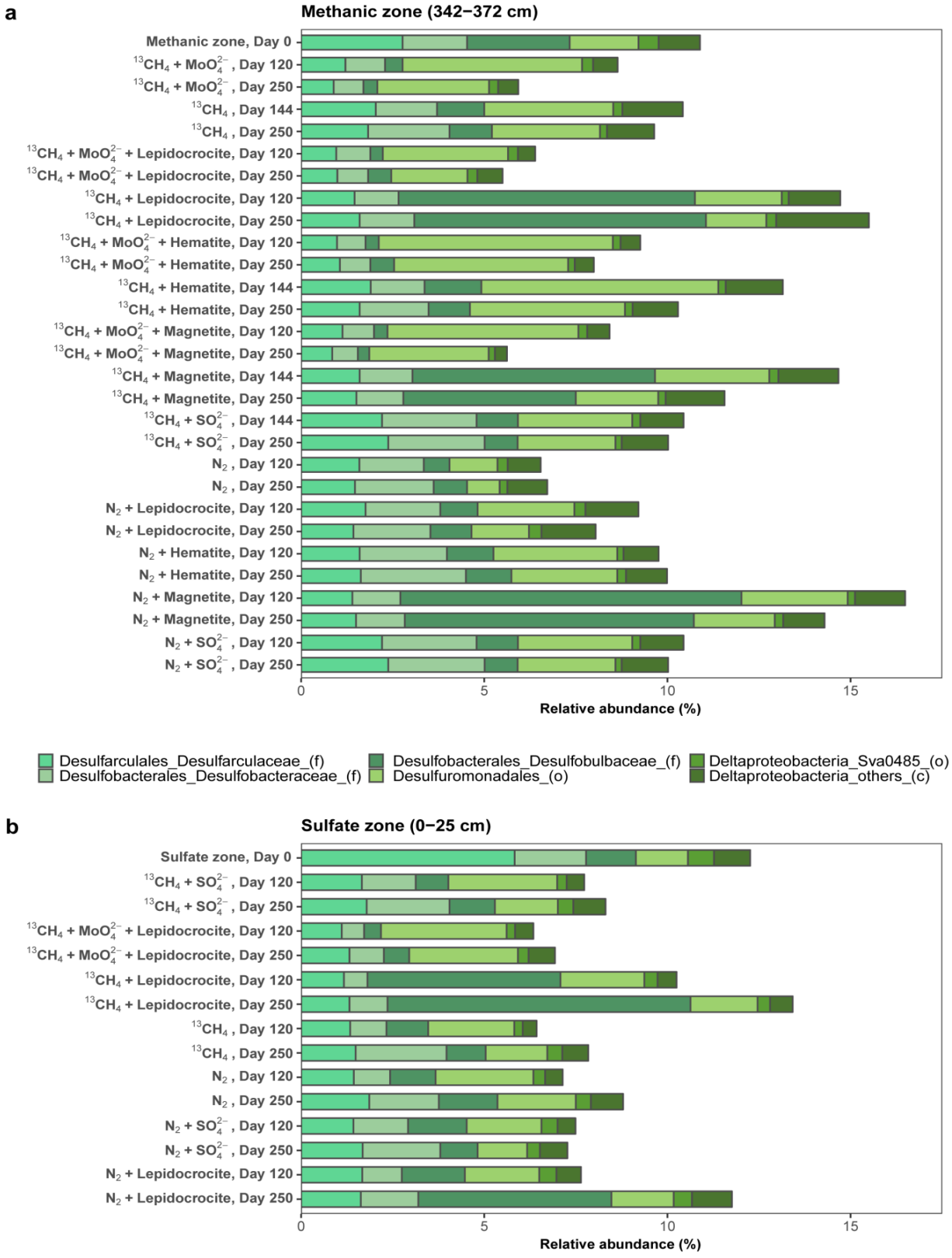

Fig. S10: 16S rRNA sequences belonging to Deltaproteobacteria across all incubations. Sequences belonging to dissimilatory iron reducing family Desulfuromonadales were more abundant, relative to known sulfate reducers, in incubations with molybdate amendment. This indicated that Fe-reducers were predominant in these incubations due to Fe-AOM.

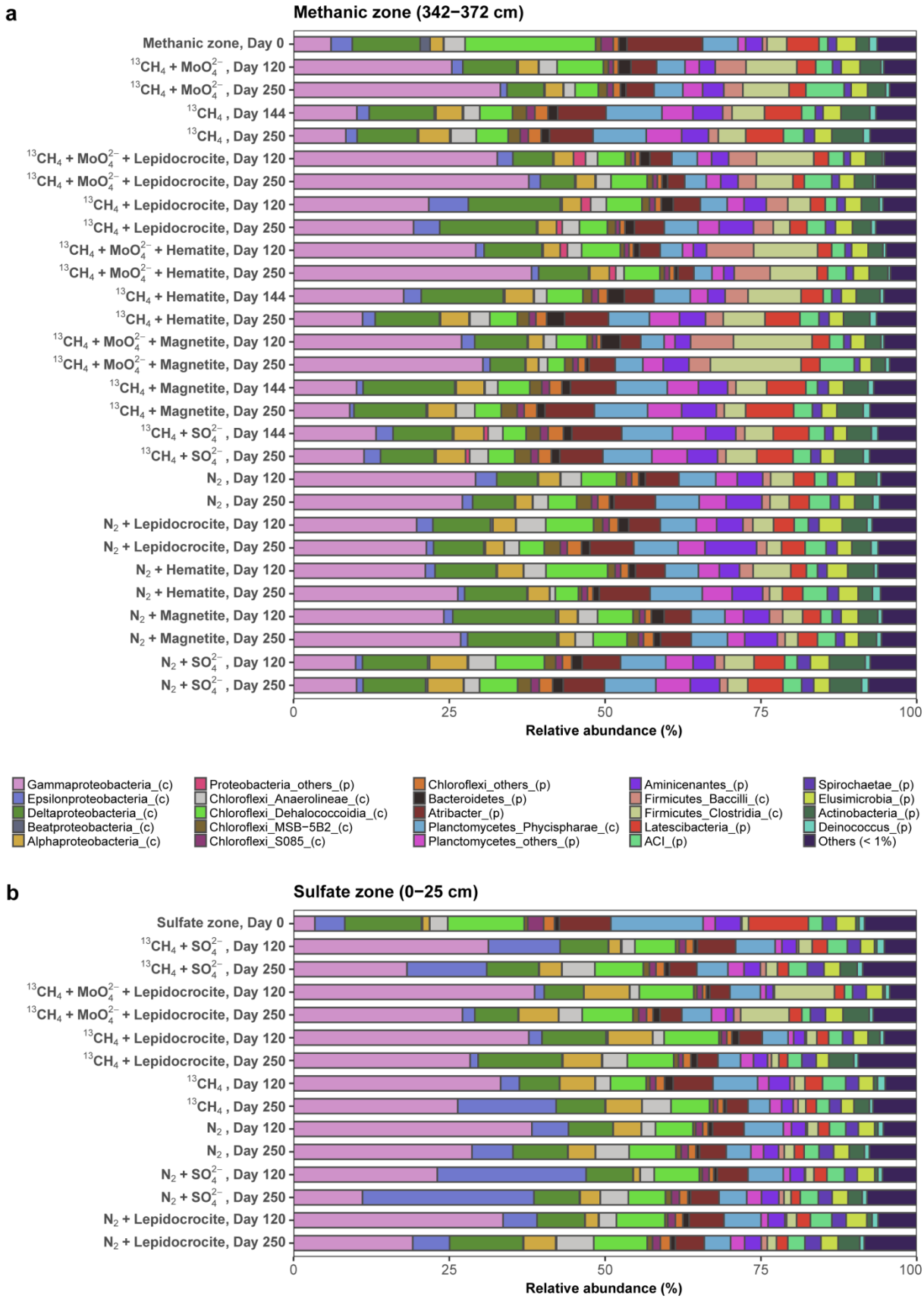

Fig. S11: Total sum scaling of bacteria 16S rRNA genes across all incubations from both geochemical zones.

CH_4 in the headspace of N_2 controls

The microbial community composition dataset shown in Figures S7–S11 showed the presence and stimulation of ANMEs in N_2 filled microcosm controls as well. Therefore, CH_4 in the headspace of controls was measured to check for CH_4 production in the incubations (Fig. S12). Since CH_4 production was observed in the control incubations the amount of CH_4 found in the headspace potentially fueled the survival of ANMEs in the N_2 controls.

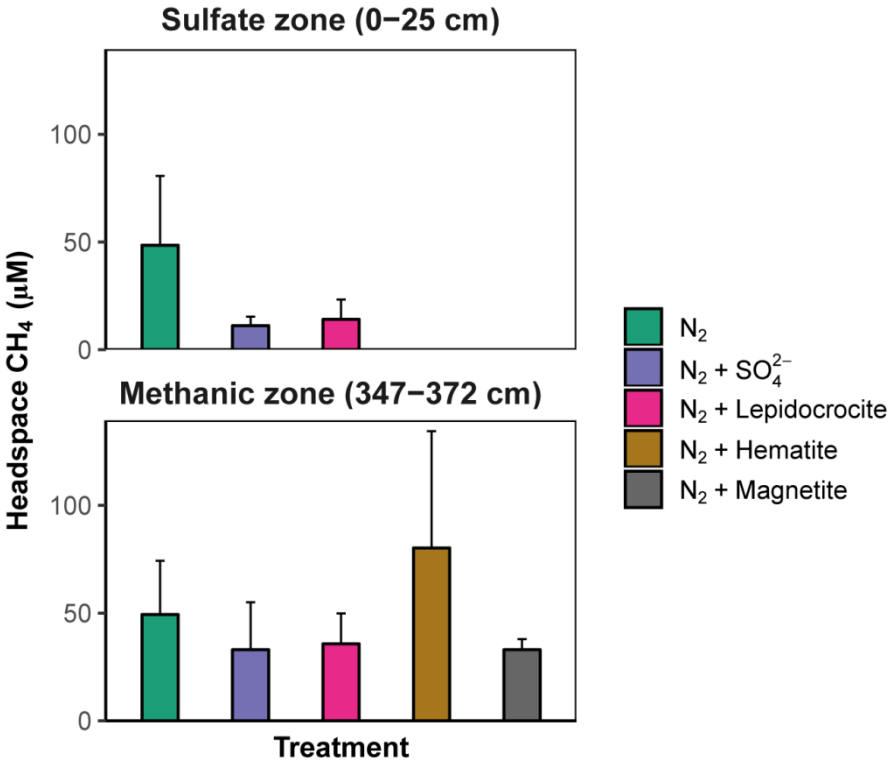

Fig. S12: CH_4 in the headspace of N_2 controls after ~ 500 days.

Although additional carbon source was not added to the sediments, inherent organic matter in the sediments fueled CH_4 production.

pmoA and bacteria PLFA results reveal the absence of aerobic methanotrophs in our incubations

Given the recent evidence that methanotrophic bacteria are involved in Fe-AOM (43), we carried out two-step *pmoA* PCR (see methods section above) to check for the presence of *pmoA* functional gene in our methanic zone treatments. Expected length of PCR product (472 bp) was only found in the initial sediment slurry used for the incubation experiment and not in the treatments after 250 days (Fig. S13); however there was an unspecific amplification at 330 bp whose identity was checked by cloning. The cloned sequences were not closely related to any known methanotrophic bacteria (Table S4) or *pmo*A gene.

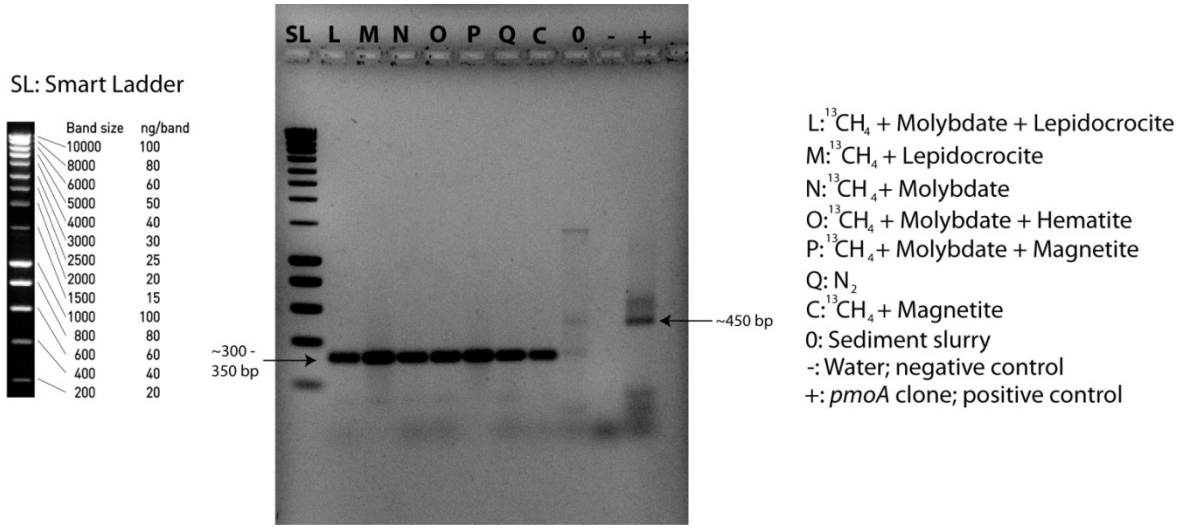

Fig. S13: Unspecific amplification of the *pmoA* gene from incubations (L–Q and C) from the methanic zone.

Table S4: Protein BLAST analysis of sequences from the *pmoA* cloning experiments.

Clone name	Incubation setup	Sequence length (bp)	Translated protein length without stop codons (amino acids)	Protein BLAST hit(s)	Max score	Total score	Query coverage (%)	E value	Indentity (%)	Accession
P5	$^{13}CH_4$ + Molybdate + Magnetite	355	97	APS reductase alpha subunit [Endosymbiont of Sclerolinum contortum]	50.4	50.4	78	1.0E-05	37	CAP03145
				Carbon monoxide dehydrogenase activity/acetyl-CoA synthase, partial [Terrisporobacter glycolicus]	49.7	49.7	23	9.0E-05	96	CCA62924
				Flavin oxidoreductase [Stenotrophomonas chelatiphaga]	48.1	48.1	21	3.0E-04	100	CDQ30636
				Nitrite reductase [uncultured bacterium]	45.8	45.8	26	7.0E-04	82	BAH95949
				Methyl-conenzyme M reductase alpha subunit [uncultured archaeon]	45.8	45.8	23	0.001	88	CBF64715
				Putative heat shock protein isoform a [Lithodes maja]	44.7	44.7	22	0.003	92	CEK41093
				Cytochrome P450 CYP153 alkane hydroxylase [uncultured bacterium]	35.8	35.8	34	6.3	66	CCO96973
P1	$^{13}CH_4$ + Molybdate + Magnetite	333	110	No significant similarity found	-	-	-	-	-	-
P6	$^{13}CH_4$ + Molybdate + Magnetite	333	110	No significant similarity found	-	-	-	-	-	-
P9	$^{13}CH_4$ + Molybdate + Magnetite	333	110	No significant similarity found	-	-	-	-	-	-
L1	$^{13}CH_4$ + Molybdate + Lepidocrocite	332	110	No significant similarity found	-	-	-	-	-	-
L3	$^{13}CH_4$ + Molybdate + Lepidocrocite	333	110	No significant similarity found	-	-	-	-	-	-
L4	$^{13}CH_4$ + Molybdate + Lepidocrocite	333	110	No significant similarity found	-	-	-	-	-	-
L6	$^{13}CH_4$ + Molybdate + Lepidocrocite	333	110	No significant similarity found	-	-	-	-	-	-
L7	$^{13}CH_4$ + Molybdate + Lepidocrocite	333	109	No significant similarity found	-	-	-	-	-	-
L8	$^{13}CH_4$ + Molybdate + Lepidocrocite	333	110	No significant similarity found	-	-	-	-	-	-

Table S5: Development of $\delta^{13}C$ values of fatty acids (in ‰) over 250 days during incubation with $^{13}CH4$ of sediment samples from the sulfate zone (S-AOM) and the methanic zone (Fe-AOM) with the latter supplemented with lepidocrocite (for details see methods); PA: phytanic acid, n.d. : not determined due to low concentration.

S-AOM Time (days)	$C_{14:0}$	$iC_{15:0}$	$aiC_{15:0}$	$C_{15:0}$	$iC_{16:0}$	$C_{16:1\omega7c}$	$C_{16:1\omega7t}$	$C_{16:1\omega5c}$	C_{16}	10-Me $C_{16:0}$	$iC_{17:0}$	$aiC_{17:0}$	$C_{17:1\omega6c}$	$C_{17:0}$	PA	$C_{18:1\omega9c}$	$C_{18:1\omega7c}$	$C_{18:0}$
0	-28.0	-29.2	-34.5	-24.8	-32.0	-6.4	-34.2	-58.2	-27.3	-29.1	-21.8	-32.8	n.d.	-27.3	-22.4	-29.9	-25.1	-28.9
40	-25.4	-23.2	-30.3	-22.4	-30.4	70.2	39.3	-29.8	-19.2	-28.7	-26.2	-31.8	n.d.	-24.7	-22.6	-24.4	-3.4	-28.2
82	-20.9	-18.5	-23.9	-18.2	-25.6	121	87.2	25.0	-14.0	n.d.	n.d.	n.d.	n.d.	-27.6	-21.7	-18.1	4.0	-27.5
120	-20.4	-17.4	-25.3	-9.1	-23.9	155	128	27.2	-6.9	n.d.	-24.7	-26.4	n.d.	-25.4	-22.2	-14.3	15.0	-24.5
160	-16.8	-13.2	-9.9	-12.9	-19.8	166	141	63.4	-7.7	n.d.	n.d.	n.d.	n.d.	-27.4	-22.9	-4.5	16.3	-27.3
200	-21.9	-15.5	-13.1	-23.4	-11.7	121	80.4	30.6	-19.4	n.d.	-22.6	-14.7	n.d.	-31.1	-25.0	-16.9	17.4	-27.8
250	1.1	10.2	-11.5	5.2	-10.6	197	169	49.6	32.0	334	-27.2	-9.3	n.d.	-29.0	-22.5	-7.5	72.0	-28.2

Fe-AOM Time (days)	$C_{14:0}$	$iC_{15:0}$	$aiC_{15:0}$	$C_{15:0}$	$iC_{16:0}$	$C_{16:1\omega7c}$	$C_{16:1\omega7t}$	$C_{16:1\omega5c}$	C_{16}	10-Me $C_{16:0}$	$iC_{17:0}$	$aiC_{17:0}$	$C_{17:1\omega6c}$	$C_{17:0}$	PA	$C_{18:1\omega9c}$	$C_{18:1\omega7c}$	$C_{18:0}$
0	-27.7	-27.5	-30.3	-24.3	-33.5	-19.9	-33.4	-38.8	-28.4	n.d.	-30.6	-31.9	n.d.	-31.2	-21.5	-29.4	-31.3	-30.1
40	-26.0	-23.7	-27.4	-23.6	-30.8	19.8	6.5	-18.9	-18.4	n.d.	-34.5	-37.4	n.d.	-29.4	-21.3	-22.5	-1.0	-29.5
82	-27.6	-26.2	-29.3	-24.6	-26.0	-6.0	-21.0	-25.7	-24.9	-12.1	n.d.	n.d.	n.d.	-29.2	-23.3	-23.6	-22.6	-29.2
120	-27.6	-25.7	-29.1	-24.3	-24.1	-8.0	-25.5	-33.6	-25.1	-19.4	-29.7	-32.1	-14.5	-31.6	-20.0	-27.7	-19.9	-30.5
160	-27.5	-25.7	-28.9	-24.8	-24.9	-8.6	-32.5	-25.6	-26.1	-21.8	n.d.	n.d.	-7.0	-30.6	-23.1	-24.6	-23.7	-29.2
200	-24.6	-24.2	-27.2	-18.7	-29.5	2.6	-13.2	-15.0	-20.9	24.3	-34.3	-34.0	47.5	-32.5	-22.5	-20.8	-19.6	-29.5
250	-23.1	-24.1	-27.5	-10.1	-27.5	9.4	-9.2	7.6	-13.1	27.3	-22.6	-26.2	66.0	-23.7	-23.7	-4.1	-11.3	-30.1

Table S6: Total uptake of $^{13}CH4$ into bacterial fatty acids (in ng ^{13}C/g dw) after 250 days based on the excess of ^{13}C relative to the original sediment (T_0 sample) during incubation of sediment samples from the sulfate zone (S-AOM) and the methanic zone (Fe-AOM) with the latter supplemented with lepidocrocite (for details see methods). Negative ^{13}C-uptake of fatty acids because of absence of increase in $\delta^{13}C$ values over the incubation period is considered zero. n.d.: not determined due to low concentration. *: Fatty acids with no $\delta^{13}C$ value in the T_0 sample. To calculate ^{13}C-uptake for these, the average $\delta^{13}C$ value of all other fatty acids is used, i.e. -30‰.

	$C_{14:0}$	$iC_{15:0}$	$aiC_{15:0}$	$C_{15:0}$	$iC_{16:0}$	$C_{16:1\omega7c}$	$C_{16:1\omega7t}$	$C_{16:1\omega5c}$	C_{16}	10-Me $C_{16:0}$	$iC_{17:0}$	$aiC_{17:0}$	$C_{17:1\omega6c}$	$C_{17:0}$	$C_{18:1\omega9c}$	$C_{18:1\omega7c}$	$C_{18:0}$
S-AOM	0.08	0.04	0.04	0.03	0.02	0.27	0.07	0.05	1.06	0.59	0	0.01	n.d.	0	0.03	0.10	0.01
Fe-AOM	0.03	0.01	0.01	0.03	0.01	0.11	0.02	0.02	0.50	0.05*	0.01	0.00	0.11*	0.01	0.06	0.03	0.00

Table S7: $\delta^{13}C$ values (in ‰) of phytane (phy) and biphytanes (bphy) derived from archaeal membrane core lipids (CL, left panels) and intact polar lipids (IPL, right panels) over 250 days of incubation with $^{13}CH4$ of sediment samples from the sulfate zone (S-AOM) and the methanic zone (Fe-AOM) with the latter supplemented with lepidocrocite (for details see methods); n.d. : not determined due to low concentration.

S-AOM Time (days)	phy	bphy 0	bphy 1	bphy 2	bphy 3	phy	bphy 0	bphy 1	bphy 2	bphy 3
0	-59	-26	n.d.	-22	-20	-33.0	-33.0	n.d.	-29	-21
250	-52	-28	n.d.	n.d.	n.d.	n.d.	+7	+124	+58	+33

Fe-AOM Time (days)	phy	bphy 0	bphy 1	bphy 2	bphy 3	phy	bphy 0	bphy 1	bphy 2	bphy 3
0	-31	-28	n.d.	-25	-19	-32	-36	n.d.	-29	-19
250	-30	-27	n.d.	-26	-19	-32	-35	n.d.	-30	-18

References

1. Oni OE*, et al.* (2015) Distinct microbial populations are tightly linked to the profile of dissolved iron in the methanic sediments of the Helgoland Mud Area, North Sea. *Front. Microbiol.* 6:365.

2. Seeberg-Elverfeldt J, Schlüter M, Feseker T, & Kölling M (2005) Rhizon sampling of porewaters near the sediment-water interface of aquatic systems. *Limnol. Oceanogr.: Meth.* 3(8):361-371.

3. Dickens GR, Kölling M, Smith DC, & Schnieders L (2007) Rhizon sampling of pore waters on scientific drilling expeditions: An example from the IODP expedition 302, Arctic coring expedition (ACEX). *Sci. Dril.* 4:22-25.

4. Hall PJ & Aller RC (1992) Rapid, small-volume, flow injection analysis for SCO_2, and NH^{4+} in marine and freshwaters. *Limnol. Oceanogr.* 37(5):1113-1119.

5. Poulton SW & Canfield DE (2005) Development of a sequential extraction procedure for iron: implications for iron partitioning in continentally derived particulates. *Chem. Geol.* 214(3-4):209-221.

6. Crill PM & Martens CS (1986) Methane production from bicarbonate and acetate in an anoxic marine sediment. *Geochim. Cosmochim. Acta* 50(9):2089-2097.

7. Joye SB*, et al.* (2004) The anaerobic oxidation of methane and sulfate reduction in sediments from Gulf of Mexico cold seeps. *Chem. Geol.* 205(3-4):219-238.

8. Viollier E, Inglett P, Hunter K, Roychoudhury A, & Van Cappellen P (2000) The ferrozine method revisited: Fe(II)/Fe(III) determination in natural waters. *Appl. Geochem.* 15(6):785-790.

9. Aromokeye DA*, et al.* (2018) Temperature controls crystalline iron oxide utilization by microbial communities in methanic ferruginous marine sediment incubations. *Front. Microbiol.* 9:2574.

10. Lueders T, Manefield M, & Friedrich MW (2004) Enhanced sensitivity of DNA-and rRNA-based stable isotope probing by fractionation and quantitative analysis of isopycnic centrifugation gradients. *Environ. Microbiol.* 6(1):73-78.

11. Steinberg LM & Regan JM (2008) Phylogenetic comparison of the methanogenic communities from an acidic, oligotrophic fen and an anaerobic digester treating municipal wastewater sludge. *Appl. Environ. Microbiol.* 74(21):6663-6671.

12. Mori K, Iino T, Suzuki K-I, Yamaguchi K, & Kamagata Y (2012) Aceticlastic and NaCl-requiring methanogen "*Methanosaeta pelagica*" sp. nov., isolated from marine tidal flat sediment. *Appl. Environ. Microbiol.* 78(9):3416-3423.

13. Parada AE, Needham DM, & Fuhrman JA (2016) Every base matters: Assessing small subunit rRNA primers for marine microbiomes with mock communities, time series and global field samples. *Environ. Microbiol.* 18(5):1403-1414.

14. Herlemann DPR*, et al.* (2011) Transitions in bacterial communities along the 2000 km salinity gradient of the Baltic Sea. *ISME J.* 5(10):1571-1579.

15. Ovreås L, Forney L, Daae FL, & Torsvik V (1997) Distribution of bacterioplankton in meromictic Lake Saelenvannet, as determined by denaturing gradient gel electrophoresis of PCR-amplified gene fragments coding for 16S rRNA. *Appl. Environ. Microbiol.* 63(9):3367-3373.

16. Takai K & Horikoshi K (2000) Rapid detection and quantification of members of the archaeal community by quantitative PCR using fluorogenic probes. *Appl. Environ. Microbiol.* 66(11):5066-5072.

17. Hamady M, Walker JJ, Harris JK, Gold NJ, & Knight R (2008) Error-correcting barcoded primers for pyrosequencing hundreds of samples in multiplex. *Nat. Meth.* 5(3):235-237.

18. Ludwig W*, et al.* (2004) ARB: a software environment for sequence data. *Nucl. Acids Res.* 32(4):1363-1371.

19. Reyes C*, et al.* (2017) Potentially active iron, sulfur, and sulfate reducing bacteria in Skagerrak and Bothnian Bay sediments. *Geomicrobiology J.* 34(10):840-850.

20. Miyazaki J*, et al.* (2009) Molecular characterization of potential nitrogen fixation by anaerobic methane-oxidizing archaea in the methane seep sediments at the number 8 Kumano Knoll in the Kumano Basin, offshore of Japan. *Appl. Environ. Microbiol.* 75(22):7153-7162.

21. Zhou Z, Han P, & Gu J-D (2014) New PCR primers based on *mcrA* gene for retrieving more anaerobic methanotrophic archaea from coastal reedbed sediments. *Appl. Microbiol. Biotechnol.* 98(10):4663-4670.

22. Caporaso JG*, et al.* (2010) QIIME allows analysis of high-throughput community sequencing data. *Nat. Meth.* 7(5):335-336.

23. Pylro VS*, et al.* (2014) Data analysis for 16S microbial profiling from different benchtop sequencing platforms. *J. Microbiol. Meth.* 107:30-37.

24. Caporaso JG*, et al.* (2011) Global patterns of 16S rRNA diversity at a depth of millions of sequences per sample. *Proc. Nat. Acad. Sci.* 108(Supplement 1):4516-4522.

25. Edgar RC (2010) Search and clustering orders of magnitude faster than BLAST. *Bioinformatics* 26(19):2460-2461.

26. Edgar RC (2013) UPARSE: Highly accurate OTU sequences from microbial amplicon reads. *Nat. Meth.* 10(10):996-998.

27. Yang S, Liebner S, Alawi M, Ebenhöh O, & Wagner D (2014) Taxonomic database and cut-off value for processing *mcrA* gene 454 pyrosequencing data by MOTHUR. *J. Microbiol. Meth.* 103:3-5.

28. McDonald D*, et al.* (2012) An improved Greengenes taxonomy with explicit ranks for ecological and evolutionary analyses of bacteria and archaea. *ISME J.* 6(3):610-618.

29. Quast C*, et al.* (2012) The SILVA ribosomal RNA gene database project: Improved data processing and web-based tools. *Nucl. Acids Res.* 41(D1):D590-D596.

30. Holmes AJ, Costello A, Lidstrom ME, & Murrell JC (1995) Evidence that participate methane monooxygenase and ammonia monooxygenase may be evolutionarily related. *FEMS Microbiol. Lett.* 132(3):203-208.

31. Smith KS, Costello AM, & Lidstrom ME (1997) Methane and trichloroethylene oxidation by an estuarine methanotroph, *Methylobacter* spp. strain BB5.1. *Appl. Environ. Microbiol.* 63(11):4617-4620.

32. Hall TA (1999) BioEdit: a user-friendly biological sequence alignment editor and analysis program for Windows 95/98/NT. *Nucl. Acids Symp. Ser.*, (London: Information Retrieval Ltd., c1979-c2000.), pp 95-98.

33. Schmidt H & Eickhorst T (2014) Detection and quantification of native microbial populations on soil-grown rice roots by catalyzed reporter deposition-fluorescence in situ hybridization. *FEMS Microbiol. Ecol.* 87(2):390-402.

34. Amann RI*, et al.* (1990) Combination of 16S rRNA-targeted oligonucleotide probes with flow cytometry for analyzing mixed microbial populations. *Appl. Environ. Microbiol.* 56(6):1919-1925.

35. Daims H, Brühl A, Amann R, Schleifer K-H, & Wagner M (1999) The domain-specific probe EUB338 is insufficient for the detection of all bacteria: Development and evaluation of a more comprehensive probe set. *Syst. Appl. Microbiol.* 22(3):434-444.

36. Sturt HF, Summons RE, Smith K, Elvert M, & Hinrichs KU (2004) Intact polar membrane lipids in prokaryotes and sediments deciphered by high-performance liquid chromatography/electrospray ionization multistage mass spectrometry-new biomarkers for biogeochemistry and microbial ecology. *Rapid Commun. Mass Spectrom.* 18(6):617-628.

37. Elvert M, Boetius A, Knittel K, & Jørgensen BB (2003) Characterization of specific membrane fatty acids as chemotaxonomic markers for sulfate-reducing bacteria involved in anaerobic oxidation of methane. *Geomicrobiology J.* 20(4):403-419.

38. Lin YS*, et al.* (2010) Intramolecular stable carbon isotopic analysis of archaeal glycosyl tetraether lipids. *Rapid Commun. Mass Spectrom.* 24(19):2817-2826.

39. Kellermann MY*, et al.* (2012) Autotrophy as a predominant mode of carbon fixation in anaerobic methane-oxidizing microbial communities. *Proc. Nat. Acad. Sci.* 109(47):19321-19326

40. Wickham H (2016) *ggplot2: elegant graphics for data analysis* (Springer).

41. Team RC (2018) R: A language and environment for statistical computing, R foundation for statistical computing, Austria, 2015. (ISBN 3-900051-07-0: URL http://www.R-project.org).

42. Henkel S, Kasten S, Poulton SW, & Staubwasser M (2016) Determination of the stable iron isotopic composition of sequentially leached iron phases in marine sediments. *Chem. Geol.* 421:93-102.

43. Bar-Or I*, et al.* (2017) Iron-coupled anaerobic oxidation of methane performed by a mixed bacterial-archaeal community based on poorly reactive minerals. *Environ. Sci. Technol.* 51(21):12293-12301.

Chapter Three

Concurrent crystalline iron oxide reduction and methanogenesis from benzoate degradation by marine sediment derived enrichment cultures

Declaration on the contribution of David A. Aromokeye to chapter three

Name of the candidate:	David A. Aromokeye
Title of the thesis:	Iron oxide driven methanogenesis and methanotrophy in methanic sediments of Helgoland Mud Area, North Sea
Authors of manuscript:	David A. Aromokeye, Oluwatobi E. Oni, Jan Tebben, Jenny Wendt, Rolf Nimzyk, Sten Littmann, Ajinkya Kulkarni, Tim Richter-Heitmann, Kai-Uwe Hinrichs, Marcus Elvert, Tilmann Harder, Sabine Kasten and Michael W. Friedrich
Manuscript status:	In preparation for submission to ISME journal.

Contribution of the candidate in % of the total work load

Experimental concept and design:	ca. 70 %
Experimental work/acquisition of experimental data:	ca. 85 %
Data analysis and interpretation:	ca. 90 %
Preparation of figures and tables:	ca. 70 %
Drafting of manuscript:	ca. 90 %

Concurrent crystalline iron oxide reduction and methanogenesis from benzoate degradation by marine sediment derived enrichment cultures

David A. Aromokeye[1,2], Oluwatobi E. Oni[1,2], Jan Tebben[3,4], Jenny Wendt[2,5], Rolf Nimzyk[6], Sten Littmann[7], Ajinkya Kulkarni[1,2], Tim Richter-Heitmann[1], Kai-Uwe Hinrichs[2,5], Marcus Elvert[2,5], Tilmann Harder[4,5], Sabine Kasten[2,3,5] and Michael W. Friedrich[1,2]

[1]Microbial Ecophysiology Group, Faculty of Biology/Chemistry, University of Bremen, Bremen, Germany

[2]MARUM – Center for Marine Environmental Sciences, University of Bremen, Bremen, Germany

[3]Alfred Wegener Institute Helmholtz Centre for Polar and Marine Research, Bremerhaven, Germany

[4]Department of Chemistry, University of Bremen, Bremen, Germany

[5]University of Bremen, Faculty of Geosciences, Bremen, Germany

[6]Department of Microbe-Plant Interactions, Faculty of Biology/Chemistry, University of Bremen, Bremen, Germany

[77]Department of Biogeochemistry, Max Planck Institute for Marine Microbiology, Bremen, Germany

Running title: Concurrent iron reduction and methanogenesis

Abstract

Elevated dissolved iron (Fe^{2+}) concentrations have been recently detected in methanic zones of multiple marine environments; the source is currently attributed to abiotic and biotic reactions. Here, using a targeted cultivation approach with sediments from Helgoland Mud Area, North Sea, we present an additional explanation that biotic organoclastic iron reduction contributes to the Fe^{2+} pool and enhances methanogenic degradation of complex organic matter in iron-oxide rich methanic sediments. Based on previous observations that aromatic hydrocarbons were likely preferentially degraded by microbes in the methanic zone, benzoate, a model aromatic substrate, was provided initially to sediment incubations and subsequently in enrichment cultures obtained from the sediment incubations. In the presence of crystalline iron oxides (magnetite and hematite), concurrent iron reduction and methanogenesis was stimulated from benzoate degradation with methanogenesis being the dominant electron sink. Growth on and concurrent reduction of crystalline magnetite facilitated benzoate degradation to CH_4 but poorly crystalline lepidocrocite inhibited the process. In addition to known benzoate degraders from other environments, Clostridia family Halobacteroidaceae were dominant (33–52 %) in one of the enrichments suggesting we unmasked previously unknown benzoate degraders from marine sediments. The presence of genes involved in all steps of the benzoate degradation pathway in various metagenomic bins suggests a syntrophic mode of benzoate consumption in the highly enriched cultures. The findings presented here simulates a possible scenario for iron reduction *in situ* and indicates that organoclastic iron reduction possibly contributes to the elevated Fe^{2+} observed in the methanic zone of multiple marine sediments.

Introduction

The final steps during microbial mineralisation of organic matter in marine sediments are largely controlled by available terminal electron accepting processes (TEAP). These TEAPs couple the downstream oxidation of fermentation products from organic matter degradation over a redox cascade based on availability and thermodynamic feasibility. This well-known redox cascade (Froelich et al., 1979; Jørgensen, 2006) results in the establishment of distinct biogeochemical zones wherein microbial oxygen respiration is followed by nitrate reduction, metal oxide (manganese and iron) reduction, sulfate reduction and CO_2 reduction, respectively. There is evidence that some biogeochemical zones overlap in marine sediment such that more than one TEAP concurrently occurs in distinct zones. An example is the detection of dissolved iron (Fe^{2+}) in the methanic zone below the sulfate methane transition (SMT) of high accumulation marine sediments. This observation from multiple marine environments indicates active co-occurrence of microbial iron reduction and methanogenesis in the methanic zone (Riedinger et al., 2014; Oni et al., 2015b; Egger et al., 2017).

A number of hypotheses have been put forward to explain the potential mechanisms that could fuel the co-existence of microbial iron reduction in a biogeochemical zone where methanogenesis is the dominant TEAP. Cryptic sulfur cycling is one (Holmkvist et al., 2011), while anaerobic oxidation of methane coupled to iron reduction (Fe-AOM) is another (Riedinger et al., 2014; Egger et al., 2015; Oni et al., 2015b; Egger et al., 2017). Dissimilatory iron reduction could also occur at these depths but requires similar electron donors (acetate and H_2) as methanogenesis (Lovley and Phillips, 1986; Roden and Wetzel, 1996). One potential mechanism that has not been so far investigated is fermentation based organoclastic iron reduction. Sequential extraction of iron oxides from a number of these sites (Oni et al., 2015b; Egger et al., 2017) indicates both crystalline and poorly crystalline phases are abundant in the methanic zone. Besides, recent findings from rice field soils, lake and

marine sediments show that these crystalline iron oxides accelerate methanogenic degradation of organic matter (Kato et al., 2012; Jiang et al., 2013; Aromokeye et al., 2018a; Rotaru et al., 2018). Fermentative iron reduction has also been previously shown in pure culture studies to account for up to 5 % of electrons during organic matter degradation (Lovley and Phillips, 1986, 1988; Lovley, 2006). Thus, a complex biogeochemical interplay between iron minerals, organic matter fermentation and methanogenesis might be on-going in iron oxide rich methanic sediments such that both iron reduction and methanogenesis are concurrently fuelled during organic matter degradation.

In previous studies, we investigated the Helgoland Mud Area (HMA), a high accumulation marine sediment with high Fe^{2+} concentrations in the methanic zone (Oni et al., 2015b) and performed molecular characterisation on the nature of bio-available fraction of the organic matter utilized by the microbial communities therein (Oni et al., 2015a). The results suggested that terrestrially derived aromatic compounds are preferentially degraded in the methanic zone. Benzoate is the central intermediate in the anaerobic degradation pathway of most aromatic compounds (Carmona et al., 2009; Fuchs et al., 2011). Therefore, benzoate is widely used as a model compound to study anaerobic degradation of aromatic hydrocarbons (Gibson and Harwood, 2002; Carmona et al., 2009). Methanogenic benzoate degradation requires a complex syntrophic community of bacteria and archaea (Hopkins et al., 1995; Schink, 1997; Schöcke and Schink, 1997) to be thermodynamically feasible under environmental conditions according to the following equation:

$$4C_6H_5COO^- + 4H^+ \rightarrow 15CH_4 + 13CO_2;\ \Delta G^{0'} = -624 \text{ KJ per 4 mol benzoate}$$

Here, we cultivated methanogenic benzoate degrading microbial communities from the methanic zone of the HMA, and provided these microbial communities with iron oxides that differ in their crystallinity: both in sediment slurry incubations and over 5 successive sediment-free planktonic enrichments. By providing benzoate as the only carbon source for

these microbial communities, a similar scenario as the environment (HMA) was simulated with a type of substrate preferentially degraded *in situ* (Oni et al., 2015a). The results we present show (1) how the presence and concurrent reduction of crystalline iron oxides facilitate methanogenic benzoate degradation (2) ecological advantage of microbe-crystalline mineral interaction during organic matter degradation and (3) novel benzoate degrading communities enriched from these iron oxide-rich methanic marine sediments.

Materials and Methods

Benzoate degradation experiment within sediment slurry

Geochemical profiles and depositional history of sampling site, the Helgoland Mud Area is previously described (Hebbeln et al., 2003; Oni et al., 2015b; Aromokeye et al., 2018b). For the current study, sediments were taken during RV HEINCKE research expedition HE-443 (54° 05.23' N; 007° 58.04' E) in May 2015 and preserved prior to incubation set up as described elsewhere (Aromokeye et al., 2018a). In order to study methanogenic degradation of benzoate in the presence of iron minerals, sediment samples from depths in the methanic zone (247–279 cm) were used. Several anoxic slurry incubations (1:3 w/v) were made in 120-mL serum vials with sulfate-free artificial sea water (ASW; composition [L^{-1}]: 26.4 g NaCl, 11.2 g $MgCl_2$, 1.5 g $CaCl_2.2H_2O$ and 0.7 g KCl). To triplicate vials, 5mM sodium benzoate and 30 mM iron oxides (lepidocrocite, hematite or magnetite; LanXess GmbH, Germany) were added. In addition, slurry incubations (*n=3*) devoid of either sodium benzoate or the aforementioned iron oxides (30 mM) were prepared to serve as background controls. Since samples were taken from depths of active methanogenesis (Oni et al., 2015b) and it is our goal to study methanogenic degradation of benzoate, it was necessary to create conditions favourable for methanogenesis to occur. Test experiments, incubated at 10 °C did not result in methanogenesis even after 200 days until the vials were transferred to 30 °C (Oni, 2015).

For this reason, we decided to incubate the slurries prepared in this study at 30 °C, in the dark.

Cultivation of sediment-free benzoate degrading enrichment cultures

A modified strictly anaerobic sterile salt water enrichment medium was used for cultivation of the enrichment cultures following Widdel et al (1983). The bicarbonate-buffered (30 mM) sulfate depleted basal medium contained 20 g/L NaCl, 3 g/L $MgCl_2.6H_20$, 0.5 g/L KCl, 0.2 g/L KH_2PO_4, 0.25 g/L NH_4Cl, and 0.15 g/L $CaCl_2.2H_2O$ and 2 mM $Na_2S.9H_2O$ as reducing agent. Trace elements, vitamin solution and selenite-tungsten were added respectively as previously described (Widdel, 1980; Widdel and Pfennig, 1981; Widdel et al., 1983).The pH of the complete medium was between 7–7.2 before dispensing into serum bottles and used for cultivation. Headspace of serum bottles were flushed and completely filled with N_2-CO_2 (80:20 %). In the initial transfer from sediment slurry incubations, 2 mL of slurry from the sediment incubation from respective treatment types were transferred into salt water media described above and cultivated with 5 mM benzoate and 30 mM respective iron oxide (50 mL final volume). After methanogenesis was observed, these cultures served as 1st generation transfers. For subsequent transfers, 5 mL from the previous generation amounting to 10 % of media volume was transferred. The cultivation media became completely sediment free after the 2nd generation transfer. Continuous transfer was done until the 5th generation transfer where several triplicates were made with similar concentration of benzoate and or iron oxides.

Analytical methods

Methane concentrations in incubation headspace samples (100 µl) were monitored over time as previously described (Aromokeye et al., 2018a). Because of the difficulty of getting an accurate determination of iron reduction kinetics by measuring total Fe(II) produced in

sediment incubations (Aromokeye et al., 2018a), Fe^{2+} formation in aqueous phase of sediment incubations was monitored spectrophotometrically (Viollier et al., 2000). However in the sediment free enrichment cultures, total Fe(II) was measured as described (Aromokeye et al., 2018a). It was possible to accurately determine total Fe(II) because the provided iron oxide is only iron oxide present in the enrichment medium unlike the slurry incubations.

To quantify benzoate concentration in both the sediment incubations and sediment free enrichment cultures, sterile deionised-water diluted 200 µl aliquot of supernatant (stored at -20 °C before analysis) obtained from centrifuged (20,000 x *g*) 1 ml sediment slurry was derivatized to benzoic acid which was then measured using LC-MS. LC–MS analysis was performed with a Vanquish UPLC system coupled to a Q Exactive Plus mass spectrometer (Thermo Fisher Scientific, Germany), using a heated electrospray ionization (HESI-II) source. Separation was performed on a C18 column (C18 BEH, 100 x 2 mm, 1,7 µm particle size, ACQUITY Waters, equipped with guard-column) with a flowrate of 0.45 mL/min (solvent A: H_2O + 0.1 % formic acid (FA), solvent B: acetonitrile (ACN) + 0.1 % FA). After injection, the samples were eluted isocratically at 8 % B for 4 min, followed by a gradient to 99 % B and held for 0.7 min. The re-equilibration phase at 8 % B was 2.5 min. MS spectra were acquired in full MS mode with a resolution of 70,000 in negative mode and a scan range of 70 to 1050 m/z. The auxiliary gas and transfer capillary temperature was set to 350 °C, the spray voltage was 2.9 kV, the sheath gas flow rate was 45 and auxiliary gas rate 15. In order to ascertain high mass accuracy at the low mass range (70–1050 m/z), phenylacetic acid ($C_8H_8O_2$) and pyruvic acid ($C_3H_4O_3$) were added as calibrants at 20 µg per ml to the Negative Ion Calibration Solution (Pierce, Thermo Fisher). To limit the accumulation of salt deposits, the first 0.7 min of each run were discarded to waste. Each pore water sample was diluted 1:20 with water containing the injection standard (phenylacetic acid at a final concentration

of 20 µg per mL). Benzoic acid was quantified relatively to the injection standard and an external calibration curve.

Intermediates from benzoate degradation (butyrate and acetate) were measured from deionised-water diluted aliquots (200 µL) from supernatant of the highly enriched cultures following Heuer et al. (2006). H_2 measurements in the headspace were done at time points where methanogenesis was on-going following Lin et al (2012) but H_2 was undetectable, and the results were not reported.

DNA extraction, 16S rRNA gene amplification and sequencing

DNA was extracted from 1 ml of slurry taken from incubation at certain time-points using a direct lysis protocol (Lueders et al., 2004) with modifications described elsewhere (Aromokeye et al., 2018a). For the enrichment cultures, DNA was extracted from 6 ml of each culture; the 6 ml volume was dispensed into triplicate screw-cap tubes containing zirconium beads (0.1 mm diameter) and centrifuged (15,300 g, 5 mins). Supernatant was removed from each tube, leaving behind ~ 200 µL followed by DNA extraction with phenol-chloroform-isoamylalcohol steps (Lueders et al., 2004). Triplicate DNA extracts from each sample were dissolved together in 50 µL diethyl pyrocarbonate (DEPC) treated water. DNA was stored at -20 ºC until use. For further processing of the sediment free cultures in the 5th generation, biological replicates were analysed separately unlike the sediment cultures where replicates were pooled for sequencing. PCR amplification, bacteria and archaea 16S rRNA Illumina HiSeq 4000 sequencing and subsequent analysis of sequencing methodology were described elsewhere (Aromokeye et al., 2018a).

Metagenomic sequencing and analysis of highly enriched cultures

For metagenomic sequencing, 200 ng of extracted DNA from each of the three highly enriched cultures (BM5, BL5, and B5) were used as starting material. Each DNA sample was

fragmented in a M220 Focused-Ultrasonicator (Covaris Inc., Massachusetts, USA) to an average fragment size of 550 bp according to the Illumina TrueSeq Nano DNA LT Library preparation protocol (Illumina Inc., San Diego, California, USA). The DNA sequencing libraries were created as stated in the manufacturer's protocol. Sequencing run was performed on an Illumina MiSeq Sequencer using MiSeq V3 Reagent Kit according the manufacturer's instructions.

The resulting sequences (BM5 = 6684988, B5 = 6844877, and BL5 = 6281456, paired end reads) were analysed with the MetaWRAP pipeline (Uritskiy and DiRuggiero, 2018). First, sequencing adapters were removed and sequences were quality trimmed using the READ_QC module, a wrapper for that consistently applies quality and adapter trimming to FastQ files. Afterwards, the sequences were assembled with metaSPAdes assembly module (Nurk et al., 2017). For binning of the scaffolds tree different binning-programs, MaxBin2 (Wu et al., 2014), MetaBAT (Wu et al., 2014) and CONCOCT (Alneberg et al., 2014) were used. The MetaWRAP binning refinement uses CheckM (Parks et al., 2015) for quality control and refinement of bins. The MetaWRAP module reassemble_bins was used to improve the bin quality. To classify the bins, the metaWRAP classify_bins module wrapping MEGABLAST (Chen et al., 2015) and Taxator-tk (Dröge et al., 2014) was used. The annotation of the binned sequences was performed with PROKKA (Seemann, 2014) within MetaWRAP. The selection of pathway specific annotations was done with custom Perl scripts. The phylogenomics analysis was performed with ANVI'O phylogenomics pipeline (Eren et al., 2015) which calculates the phylogenomic tree using profile hidden Markov models with HMMER (Eddy, 2011) from a collection of different constitutive proteins/genes (Campbell et al., 2011).

Scanning electron microscopy (SEM)

After ~ 200 days of cultivating BM5, B5 and BL5 cultures, 500 µl aliquots of the triplicates from each of the three cultures were pooled together. 50 µl from each of the three pooled samples were fixed for SEM imaging using paraformaldehyde (PFA) with a final concentration of 2 % for 1h at room temperature. The samples were rinsed 3x with PBS and some drops of the sample material were deposited on silicon wafers (Ted Pella, USA). Sample materials were dehydrated with ethanol of different concentrations (30 %, 50 %, 80 % and 96 % for 10 minutes). After dehydration, the samples were dried using a critical point dryer (CPD 300) (Leica, Wetzlar, Germany). The prepared samples were mounted on an aluminium stub with sticky carbon tape (PLANO GmbH, Wetzlar Germany). Mounted samples were imaged on a scanning electron microscope (Quanta^{TM} 250 FEG, FEI Eindhoven, Netherlands) with either 2 keV (for secondary electron images) or 5 keV (back scattered electron images). An elemental mapping of the samples was performed using energy dispersive X-ray spectroscopy (EDS). For EDS the SEM is equipped with a Bruker double detector system XFlash 6/30 (Bruker Nano GmbH, Berlin, Germany) with an energy resolution <123 eV at Manganese Kα line. EDS maps were made with 15 keV. The mapping data where processed using the Bruker Quantax 400 software package.

Results and Discussion

The potential mechanisms that mediate concurrent microbial iron reduction in the methanic zones of rapidly accumulating marine sediments are currently of high interest in sediment biogeochemistry. Fe-AOM has been the main biotic mechanism hypothesized to majorly contribute to pore water dissolved Fe^{2+} concentrations at these depths (Riedinger et al., 2014; Egger et al., 2015; Egger et al., 2016a; Egger et al., 2016b; Rooze et al., 2016; Egger et al., 2017). Here, we present data supporting an additional explanation. By stimulating microbial communities involved in benzoate degradation, iron reduction and methanogenesis, we show

how iron reduction and methanogenesis could be concurrently fuelled by organic matter degradation. Benzoate degrading microbial communities from the methanic zone of marine sediments have not been previously identified. Therefore, we also present sediment-free microbial communities involved in methanogenic benzoate degradation in marine sediments.

Concurrent iron reduction and methanogenesis in sediment incubations

As model iron oxides in our sediment incubations, hematite (crystalline, semi-conductive), magnetite (crystalline, conductive) and lepidocrocite (poorly crystalline, poorly conductive) were used. We found that in sediment slurry incubations with benzoate and (semi) conductive iron oxides i.e. hematite and magnetite, both methanogenesis and benzoate degradation were accelerated compared to the benzoate only and the lepidocrocite amended incubations, accompanied by a concurrent increase in Fe^{2+} concentrations (Fig. 1a, b, c). Interestingly, increase in Fe^{2+} concentrations reached a plateau at similar time points as when no further increase in methane amounts were observed and benzoate was below detection (90–95 days; Fig. 1a, b, c). In contrast, with benzoate and lepidocrocite, methanogenesis (Fig. 1a) did not occur until no further increase in Fe^{2+} concentrations were observed (after 120 days; Fig. 1b). In control incubations without addition of benzoate, iron reduction occurred, probably fuelled by electrons from organic matter in the sediment. Fe^{2+} concentrations in these controls were however not as high as in benzoate amended incubations. Thus, the concurrent stimulation of crystalline iron reduction and methanogenesis in these sediment incubations was predominantly fuelled by electrons from benzoate degradation. Positive correlation between methanogenesis and iron reduction both *in situ* and in incubation experiments was previously demonstrated during organic matter degradation in terrestrial environments such as arctic tundra soils that are rich in iron oxides and aromatic carbon (Herndon et al., 2015; Yang et al., 2016). Similar processes may also explain high Fe^{2+} concentrations in the methanic zone of the HMA and other marine or limnic settings.

Methanogenic benzoate degraders from marine sediments have not been previously identified. However, the bacteria communities stimulated by benzoate addition to the slurries (mostly families Peptococcaceae and Syntrophomonadaceae; Fig. 1d) were hitherto identified as syntrophic benzoate degraders from other environments (McInerney et al., 2008; Carmona et al., 2009; Sieber et al., 2010). The deltaproteobacterial order Desulfuromonadales harbours organisms known to perform microbial iron reduction in coastal marine sediments (Vandieken et al., 2006; Aromokeye et al., 2018a). This order was found to increase in relative abundance from 1.5 % at day 0 to at least 6 % at day 105 across all benzoate amended incubations (Fig. 1d). In addition to their involvement in iron reduction, these organisms can also potentially transfer electrons via mineral mediated direct interspecies electron transfer (mDIET) to methanogens in the sediment matrix, thus accelerating methanogenesis in magnetite and hematite amended slurries (Kato et al., 2012; Rotaru et al., 2014; Rotaru et al., 2018; Aromokeye et al., 2018a). Therefore, the pathway of utilization of the iron oxides seems to involve both, reduction and use as conduit. Members of the genus *Methanosarcina, Methanosaeta* and the family Methanomicrobiaceae were the dominant methanogens enriched during the phase of active methanogenesis (Fig. 1d). These enriched communities were specifically stimulated by benzoate addition only (Fig. 1d).

Concurrent iron reduction and methanogenesis in 5th generation sediment-free planktonic cultures

Given the distinct observation of concurrent reduction of crystalline iron oxides and methanogenesis in the sediment slurry incubations, we cultivated the microbial communities over 5 successive transfers in an artificial enrichment medium. The aim was (I) to gain a better understanding on how electrons from benzoate degradation fuel both iron reduction and methanogenesis (II) to obtain active enrichment cultures performing benzoate degradation in marine sediments. For the 5th generation physiological experiments, ~ 250

µmol of benzoate was fed to triplicates of the benzoate only enrichment (B5), benzoate-magnetite enrichment (BM5) representing crystalline iron oxides and benzoate-lepidocrocite enrichment (BL5) representing poorly crystalline iron oxides. We monitored methane formation, iron reduction (where possible), build-up and eventual depletion of fermentation intermediates during benzoate degradation.

In BM5, we observed magnetite reduction, alongside methanogenesis during benzoate degradation (Fig. 2), similarly to what was observed during the slurry incubations (Fig. 1). While H_2 was not detected, a transient build-up of acetate (max 200 µmol) and butyrate (max 30 µmols) was observed. CH_4 and Fe(II) concentrations leveled up after 100 days and intermediates were not detected at this time-point reflecting complete degradation of amended benzoate. Bacteria community in the BM5 enrichment sequenced after 100 days of incubation was dominated by members of the genus *Sporotomaculum* (53–62 %), followed by *Syntrophomonas* (11–19 %), and *Therminicola* (5–8 %). Amongst the bacteria taxa detected in low relative abundance, genus *Caldicoprobacter* (2 %), and families Synergistaceae (2 %) and Coriobacteriaceae (2–4 %) which have not been previously associated with benzoate degradation were observed. Within the archaea community, genus *Methanosarcina* (64–73 %) was dominant. *Methanoculleus* (24–28 %) and *Methanosaeta* (2–7 %) were also enriched.

For the B5 enrichment cultivated over time without adding iron oxides, methanogenic benzoate degradation was also evident in triplicates from the 5th transfer. In two of three replicates however, about 200 µmoles of methane was detected after the first 100 days. Subsequently, there was no further increase in methane amounts, despite monitoring CH_4 until 200 days. In the third replicate, 520 µmoles of methane was produced already after 121 days. Methanogenesis thus appeared to be inhibited in two of 3 replicates such that no further increase in CH_4 amounts were observed in both cultures after 121 days. Instead, high

amounts of acetate were measured in both cultures: 1290 and 1330 µmoles after 200 days. There was also a transient build-up of butyrate (up to 69 µmoles) over the 200 days. The enriched bacterial community which was sequenced after 131 days showed that clostridial family Halobacteroidaceae was dominant (33–52 %). Bacillales was also dominant (13–33 %). *Syntrophomonas* (14–40%), Synergistaceae (4–8 %) and *Desulfotomaculum* (2–10 %) were also enriched. Amongst the archaea community, both *Methanosarcina* and *Methanoculleus* were dominant (Fig. 3). Unlike the BM5 enrichment, *Methanosaeta* were not enriched in high proportions in the B5 enrichment.

The potential for the B5 enrichment to reduce crystalline iron and produce methane simultaneously was also investigated. Another triplicate set up was prepared at the start of the 5th transfer and amended with 30 mM magnetite. Similarly to the BM5, the enrichment B5 could also reduce magnetite and produce methane concurrently, albeit at slower rates. A transient build-up of butyrate was detected (up to 230 µmoles). More interestingly, the build-up of acetate was not as high as the B5 enrichment without magnetite amendment as more electrons could be transferred to methane while magnetite was also partly reduced. Inhibitory effects of acetate on syntrophic benzoate degradation either by adding a thermodynamic barrier or by affecting the proton electrochemical gradient was previously demonstrated (Dolfing and Tiedje, 1988; Hopkins et al., 1995; Schöcke and Schink, 1997). Under such conditions, thermodynamic barriers placed by acetate accumulation were removed by providing the co-cultures with an acetate oxidizing syntroph (Schöcke and Schink, 1997). Here, we show that crystalline magnetite could remove such thermodynamic barrier caused by acetate accumulation. The microbial community composition after 197 days was similar to the habitual B5 enrichment. Therefore the same community, enriched over four generation of successive transfers without iron oxides, which struggled to completely convert acetate to

methane, could as well reduce iron and produce more methane concurrently, when available (Fig. 3).

For the BL5 enrichment cultivated with poorly crystalline lepidocrocite, benzoate degradation was slower and incomplete after 200 days (Fig. 4) compared to the BM5 and B5 enrichments (Figs. 2 and 3). Between 29–79 μmols of benzoate was measured after 197 days, much more than the 3 μmols found in the B5 culture after 121 days or the non-detection of benzoic acid in BM5 cultures after 100 days. The trend was similar to the initial sediment slurry incubations where lepidocrocite amendment also slowed down benzoate degradation compared to other benzoate amended set-ups (Fig. 1). Inhibitory effects of poorly crystalline lepidocrocite on benzoate degradation was rather unexpected, as this is ideally a more reactive iron oxide compared to hematite and magnetite (Lovley and Phillips, 1986), and should facilitate benzoate degradation. Although butyrate was not detected in the time-points sampled, benzoate and acetate were still detected after 200 days showing that methanogenic benzoate degradation was limited by lepidocrocite addition. Therefore, while crystalline iron oxides facilitate methanogenic benzoate degradation, poorly crystalline lepidocrocite constrains the process (Figs. 1–4) but iron reduction was more pronounced with lepidocrocite (Figs. 1b, 4). Unlike BM5 grown with magnetite, methanogenesis did not start in BL5 around the same time as iron reduction. Instead, there was a build-up of Fe(II) without methane formation for the first 100 days. However, during methanogenesis, iron reduction was still on-going such that increased methane amounts were accompanied by increased Fe(II) amounts (Fig. 4). The bacterial community composition after 197 days was dominated by *Desulfotomaculum* (20–37 %), *Therminicola* (11–26 %), *Syntrophomonas* (2–18 %), Coriobacteriaceae (13–18 %) and *Thiohalomonas* (2–14 %). The archaea community was dominated by *Methanosarcina* (73–92 %) and *Methanoculleus* (7–9 %). Uncultured Methanomicrobiales Archaeon EJ-E01 was enriched in one of the triplicates (15 %; Fig. 4).

Similarly to the initial sediment incubations (Fig. 1), we show that even after several transfers, the highly enriched cultures performing methanogenic benzoate degradation concurrently reduce iron oxides, when available. Electron balance calculations from benzoate revealed that both methanogenesis and iron reduction must have been fuelled by electrons from benzoate degradation but methanogenesis, when feasible, is the dominant electron sink: both in the sediment incubations and in the highly enriched cultures (Tables 1 and 2). Both acetate and butyrate as intermediates of benzoate degradation were also completely degraded from the system when methanogenesis was favourable. Members of the Peptococcaceae family; in particular, the genus *Sporotomaculum* were previously shown to ferment 3-hydroxybenzoate to butyrate and acetate in pure cultures (Brauman et al., 1998). A similar pathway might have been used to ferment benzoate by the Peptococcaceae families (*Desulfotomaculum*, and *Sporotomaculum*) enriched in our cultures. The formation of butyrate as intermediate is particularly interesting as this point to a secondary fermentation pathway to convert butyrate to acetate and or H_2, in addition to benzoate fermentation in the enrichments. Methanogenic benzoate degradation and the complete disappearance of intermediates from the system were fastest in the BM5 culture enriched with magnetite (Fig. 2). Removal of the high amounts of acetate in the B5 enrichment when provided with magnetite (Fig. 3b) further illuminated the beneficial role crystalline iron oxides play to facilitate organic matter degradation in the environment.

While previously known benzoate degraders enriched from other environments such as *Desulfotomaculum*, *Sporotomaculum* and *Syntrophomonas* (Harwood et al., 1998; Gibson and Harwood, 2002; McInerney et al., 2008; Rabus et al., 2016) were enriched, we also found evidence for enrichment of microorganisms which have not been previously linked to benzoate degradation in these marine sediment derived enrichment cultures. An example is family Halobacteroidaceae who are known as strictly anaerobic, gram negative fermentative

halophiles (Oren, 2014). This family was highly enriched only in the benzoate cultivation without iron oxides, since the 2nd transfer (See Fig. S1–S3) and persisted until the 5th generation (Fig. 3). It is clear from bacteria community dataset that these are novel benzoate degraders enriched from the methanic marine sediments. In addition, the Synergistaceae family from the phylum Synergistetes and NJ-1n from the phylum Tenericutes was also enriched in the BM5 and B5 enrichment and in the previous transfers (Figs. 2, 3, S1, S2). The phylum Synergistetes and Tenericutes are present in unamended sediments from HMA but in very low relative abundance (0.1 % of bacteria, Fig. 1d). Here, we show physiological data identifying benzoate as a potential substrate they thrive on. Interestingly, known dissimilatory iron reducers from the order Desulfuromonadales were not enriched in these cultures, despite the apparent high amount of Fe(II) produced. Instead, we found other organisms such as *Therminicola* who are capable of dissimilatory iron reduction (Wrighton et al., 2008; Byrne-Bailey et al., 2010) but are from the Peptococcaceae family of known benzoate degraders and actinobacterial sequences from the family Coriobacteriaceae which have been previously enriched with iron oxides (Lentini et al., 2012). Therefore, it is highly probable that iron reduction in these cultures is tightly linked to benzoate degradation (organoclastic iron reduction). The lack of increased Fe(II) amounts in controls without microbial cells (Fig. S4) also supports this conclusion that iron reduction in the enrichments is microbial activity driven.

SEM imaging reveals microbe-mineral interaction in highly enriched cultures

SEM was done after 200 days of incubating the 5th generation enrichment to identify patterns of microbial interaction with either crystalline magnetite (BM5) or poorly crystalline lepidocrocite (BL5) in comparison to the enrichment without iron oxides (B5). In the BM5 enrichment, microbial cells were observed on the magnetite surface (Fig. 5a). Formation of closely knitted dense aggregates of different cell shapes was not visible from the SEM

retrieved images unlike the control B5 enrichment where closely knitted dense aggregates were observed (Fig. 5b). Although syntrophic interactions was required to metabolise benzoate, the SEM images show that growth of BM5 with magnetite (Fig. 5a) provided an ecological advantage that nullified the need to form closely knitted aggregates observed in B5 enrichment (Fig. 5b). This in turn might have facilitated partial reduction of magnetite while the unreduced portions could still enhance the degradation of benzoate to CH_4. For BL5, the pattern of microbial cell distribution around lepidocrocite was different compared to BM5 grown on magnetite (Fig. 5c). Cell aggregates were formed, but not on the lepidocrocite surface, less dense cell networks were also observed unlike BM5 and B5 culture. Because lepidocrocite is poorly crystalline and not conductive, aggregates were not formed on lepidocrocite (Fig. 5c). As the images suggest, syntrophic communities growing on lepidocrocite mostly established longer cell-lepidocrocite distances, and could not form dense aggregates as seen in the control (B5, Fig. 5b). This probably resulted in the slower rates of benzoate degradation in the BL5 enrichment.

Benzoate degradation pathway in highly enriched cultures points to a syntrophic metabolism

Multiple nearly complete metagenomic bins containing genes involved in the various steps during anaerobic benzoate degradation were recovered from each of the three highly enriched cultures (Fig. 6, Table S1-S3). Each of these metagenomic bins contained genes involved in parts or nearly all the steps in the well-studied pathway known from anaerobic benzoate degraders (Carmona et al., 2009). The upper degradation pathway involves benzoate activation to benzoyl-CoA, dearomatization of benzoyl-CoA and β-oxidation leading to the formation of 3-hydroxypimelyl-CoA. The intermediate formation of pimelyl-CoA and its subsequent conversion to 3-hydroxypimelyl-CoA was ignored in scheme since it was only previously shown for phototrophic α-Proteobacteria *Rhodopseudomonas palustris* (Harwood

et al., 1998). Eventually *R. palustris* converts pimelyl-CoA to 3-hydroxypimelyl-CoA like other known benzoate degraders. In the lower pathway, 3-hydroxypimelyl-CoA is converted to acetyl-CoA which subsequently forms acetate (Fig. 6a). Butyrate was also detected as intermediate in the BM5 and B5 enrichments (Fig. 2–3). Therefore, the pathway for benzoate fermentation to butyrate via crotonyl-CoA and the subsequent butyrate degradation pathway mostly utilised by members of the family Syntrophomonadaceae (Sieber et al., 2010) might have facilitated butyrate degradation in our highly enriched cultures. It is likely that members of the family Syntrophomonadaceae who were also enriched based on bacteria 16S rRNA genes (Fig. 2–4) could be responsible for the turnover of butyrate. Due to time constraint for thesis submission, genes involved in the butyrate degradation pathway were not analysed from the metagenome yet. ATP-independent benzoyl-CoA reductase (BCR) genes (BamB-I), that catalyse the dearomomatization of benzoyl-CoA in obligate anaerobes (Wischgoll et al., 2005; Fuchs, 2008), were not found in the metagenomic bins presented. Instead the classical ATP-dependent BcrC known to be present in facultative anaerobes were found in BM5 and BL5 enrichments (Butler et al., 2007; McInerney et al., 2007). In the B5 enrichment, known analogues of the BCR were not found in the metagenomic bins. This could be due to either an assembly artefact that led to an overlook of the genes or possibly an unknown or previously overlooked gene in benzoate degradation is utilised by the B5 enrichment (Fig. 3). The mode of benzoyl-CoA dearomatization in our enrichments will be explored further in future versions of this manuscript.

With exception to a few bins (bin 10, and 18 for BM5; bin 5 for B5; bin 2 and 7 for BL5), the genes involved in benzoate degradation which were predominantly present in the metagenomic bins were those involved in the lower pathway. This suggests that the activation of benzoate and the upper pathway steps were carried out by these ‘specialists’ bins whose closest taxonomic affiliation based on ANVI’O concatenated protein classification are given

in Table S4 and Figure S5–S7. These observations also point to the syntrophic mode of benzoate degradation by these enrichment cultures.

Implication for iron-oxide rich methanic marine sediments

In comparison to other processes in the anaerobic food chain, genes for organic matter fermentation have been shown to be the most abundant in methane-rich subsurface sediments (Kirchman et al., 2014). It is therefore conceivable that during the degradation of buried organic matter over time by hydrolytic and fermentative bacteria, crystalline, (semi)conductive portion of bound iron minerals in the sediments (Oni et al., 2015b; Aromokeye et al., 2018b) act as a conduit that help channel electrons directly to methanogens thereby accelerating methanogenesis (Kato et al., 2012; Jiang et al., 2013; Zhou et al., 2014; Li et al., 2015; Liu et al., 2015; Zhang and Lu, 2016). The crystalline iron mineral phases may also be partly reduced in the process of mineral-mediated electron transfer between fermentative bacteria and methanogens as shown in Figs. 1–4. The individual contributions of fermentative microorganisms (Lehours et al., 2010) and methanogens (Liu et al., 2011; Sivan et al., 2016) to iron reduction is however unclear and would require further targeted experiments. Iron mineral-mediated electron transfer between organic matter-fermenting bacteria and methanogens has been demonstrated in pure cultures, and enrichment cultures from anaerobic digesters, rice paddy soils and lake sediments (Kato et al., 2012; Jiang et al., 2013; Cruz Viggi et al., 2014; Zhou et al., 2014). In a previous study, we also established the potential for such syntrophic interaction to occur in methanic marine sediments (Aromokeye et al., 2018a). The findings from our slurry incubations and enrichment cultures re-create a scenario that likely explains the connection between organic matter degradation, methanogenesis and high concentrations of pore-water dissolved Fe in iron-oxide rich methanic zones of marine sediments.

Besides Fe-AOM which was also shown to occur in the HMA (Aromokeye et al., 2018b), our study provides an additional perspective regarding the biotic source of dissolved iron in methanic sub-seafloor sediments as shown in the scheme presented in Fig. 7. We argue that some of the Fe^{2+} detected in pore-water of sulfate-depleted methane-rich subsurface sediments like the HMA originates from concurrent organoclastic iron oxide reduction during methanogenic fermentation of complex organic matter. The possibility of co-occurring Fe-AOM and iron reduction-linked methanogenic degradation of organic matter may therefore explain the observed correlation between organic matter degrading bacteria (e.g. Atribacteria (Dodsworth et al., 2013; Nobu et al., 2016) and Burkholderiales (Tong et al., 2015)), and methanogenic/methane oxidizing archaea with high Fe^{2+} concentrations in some methane-rich sub-seafloor environments (Algora et al., 2015; Oni et al., 2015b). Further studies of the mechanistic details of such interdependencies between microbial cycling of organic carbon and iron will be important for understanding how iron oxides support microbial life in the deep biosphere which represents the biggest reservoir of organic carbon on Earth (Whitman et al., 1998).

Acknowledgements

This project was funding by the Deutsche Forschungsgemeinschaft 448 (DFG) Cluster of Excellence 309 "The Ocean in the Earth System - MARUM - Center for Marine Environmental Sciences", the Alfred Wegener Institute Helmholtz Centre for Polar and Marine Research and the University of Bremen. We thank the captain, crew and scientists of the RV HEINCKE expedition 443 to the Helgoland Mud Area in April 2015. We thank the Max Planck Society for the support of the Single Cell Facility at the MPI Bremen. We also thank Xavier Prieto and Daniela Tienken for their technical support. Shreya Tilve is acknowledged for help with cultivation of the enrichment cultures.

Author contribution

D.A.A., O.E.O., and M.W.F. designed the study. D.A.A performed the physiological experiments. J.T. developed methodology and measured benzoic acid in all samples. J.W. performed intermediates measurements. S.L. performed SEM. D.A.A. performed nucleic acid extraction, amplicon sequencing and analysis. R.N. performed metagenomic sequencing and analyzed the data with input from D.A.A. Figures were produced by D.A.A., T.R.H., and S.L. A.C.K., D.A.A., and O.E.O developed the conceptual scheme. D.A.A., O.E.O. and M.W.F. wrote the manuscript and current version has not been reviewed by all co-authors.

References

Algora, C., Vasileiadis, S., Wasmund, K., Trevisan, M., Krüger, M., Puglisi, E., and Adrian, L. (2015) Manganese and iron as structuring parameters of microbial communities in Arctic marine sediments from the Baffin Bay. *FEMS Microbiol Ecol* **91**: fiv056.

Alneberg, J., Bjarnason, B.S., De Bruijn, I., Schirmer, M., Quick, J., Ijaz, U.Z. et al. (2014) Binning metagenomic contigs by coverage and composition. *Nat Meth* **11**: 1144-1146.

Aromokeye, D.A., Richter-Heitmann, T., Oni, O.E., Kulkarni, A., Yin, X., Kasten, S., and Friedrich, M.W. (2018a) Temperature controls crystalline iron oxide utilization by microbial communities in methanic ferruginous marine sediment incubations. *Front Microbiol* **9**: 2574.

Aromokeye, D.A., Kulkarni, A.C., Elvert, M., Wegener, G., Henkel, S., Coffinet, S. et al. (2018b) Rates and microbial players of iron-driven anaerobic methane oxidation in methanic marine sediments. Submitted.

Brauman, A., Müller, J.A., Garcia, J.-L., Brune, A., and Schink, B. (1998) Fermentative degradation of 3-hydroxybenzoate in pure culture by a novel strictly anaerobic bacterium, *Sporotomaculum hydroxybenzoicum* gen. nov., sp. nov. *Int J Syst Evol Microbiol* **48**: 215-221.

Butler, J.E., He, Q., Nevin, K.P., He, Z., Zhou, J., and Lovley, D.R. (2007) Genomic and microarray analysis of aromatics degradation in *Geobacter metallireducens* and comparison to a *Geobacter* isolate from a contaminated field site. *BMC Genomics* **8**: 180.

Byrne-Bailey, K.G., Wrighton, K.C., Melnyk, R.A., Agbo, P., Hazen, T.C., and Coates, J.D. (2010) Complete genome sequence of the electricity-producing "*Thermincola potens*" strain JR. *J Bacteriol* **192**: 4078-4079.

Campbell, B.J., Yu, L., Heidelberg, J.F., and Kirchman, D.L. (2011) Activity of abundant and rare bacteria in a coastal ocean. *Proc Nat Acad Sci* **108**: 12776-12781.

Carmona, M., Zamarro, M.T., Blázquez, B., Durante-Rodríguez, G., Juárez, J.F., Valderrama, J.A. et al. (2009) Anaerobic catabolism of aromatic compounds: a genetic and genomic view. *Microbiol Mol Biol Rev* **73**: 71-133.

Chen, Y., Ye, W., Zhang, Y., and Xu, Y. (2015) High speed BLASTN: An accelerated MegaBLAST search tool. *Nucleic Acids Res* **43**: 7762-7768.

Cruz Viggi, C., Rossetti, S., Fazi, S., Paiano, P., Majone, M., and Aulenta, F. (2014) Magnetite particles triggering a faster and more robust syntrophic pathway of methanogenic propionate degradation. *Environ Sci Technol* **48**: 7536-7543.

Dodsworth, J.A., Blainey, P.C., Murugapiran, S.K., Swingley, W.D., Ross, C.A., Tringe, S.G. et al. (2013) Single-cell and metagenomic analyses indicate a fermentative and saccharolytic lifestyle for members of the OP9 lineage. *Nat Commun* **4**: 1854.

Dolfing, J., and Tiedje, J.M. (1988) Acetate inhibition of methanogenic, syntrophic benzoate degradation. *Appl Environ Microbiol* **54**: 1871-1873.

Dröge, J., Gregor, I., and McHardy, A.C. (2014) Taxator-tk: Precise taxonomic assignment of metagenomes by fast approximation of evolutionary neighborhoods. *Bioinformatics* **31**: 817-824.

Eddy, S.R. (2011) Accelerated profile HMM searches. *PLoS Comput Biol* **7**: e1002195.

Egger, M., Kraal, P., Jilbert, T., Sulu-Gambari, F., Sapart, C.J., Röckmann, T., and Slomp, C.P. (2016a) Anaerobic oxidation of methane alters sediment records of sulfur, iron and phosphorus in the Black Sea. *Biogeosciences* **13**: 5333-5355.

Egger, M., Lenstra, W., Jong, D., Meysman, F.J., Sapart, C.J., van der Veen, C. et al. (2016b) Rapid sediment accumulation results in high methane effluxes from coastal sediments. *PloS One* **11**: e0161609.

Egger, M., Rasigraf, O., Sapart, C.l.J., Jilbert, T., Jetten, M.S., Röckmann, T. et al. (2015) Iron-mediated anaerobic oxidation of methane in brackish coastal sediments. *Environ Sci Technol* **49**: 277-283.

Egger, M., Hagens, M., Sapart, C.J., Dijkstra, N., van Helmond, N.A., Mogollón, J.M. et al. (2017) Iron oxide reduction in methane-rich deep Baltic Sea sediments. *Geochim Cosmochim Acta* **207**: 256-276.

Eren, A.M., Esen, Ö.C., Quince, C., Vineis, J.H., Morrison, H.G., Sogin, M.L., and Delmont, T.O. (2015) Anvi'O: An advanced analysis and visualization platform for 'omics data. *PeerJ* **3**: e1319.

Froelich, P.N., Klinkhammer, G.P., Bender, M.L., Luedtke, N.A., Heath, G.R., Cullen, D. et al. (1979) Early oxidation of organic matter in pelagic sediments of the eastern equatorial Atlantic: suboxic diagenesis. *Geochim Cosmochim Acta* **43**: 1075-1090.

Fuchs, G. (2008) Anaerobic metabolism of aromatic compounds. *Annals New York Acad Sci* **1125**: 82-99.

Fuchs, G., Boll, M., and Heider, J. (2011) Microbial degradation of aromatic compounds—from one strategy to four. *Nat Rev Microbiol* **9**: 803-816.

Gibson, J., and Harwood, S.C. (2002) Metabolic diversity in aromatic compound utilization by anaerobic microbes. *Annu Rev Microbiol* **56**: 345-369.

Harwood, C.S., Burchhardt, G., Herrmann, H., and Fuchs, G. (1998) Anaerobic metabolism of aromatic compounds via the benzoyl-CoA pathway. *FEMS Microbiol Rev* **22**: 439-458.

Hebbeln, D., Scheurle, C., and Lamy, F. (2003) Depositional history of the Helgoland mud area, German Bight, North Sea. *Geo-Marine Letters* **23**: 81-90.

Herndon, E.M., Yang, Z., Bargar, J., Janot, N., Regier, T.Z., Graham, D.E. et al. (2015) Geochemical drivers of organic matter decomposition in arctic tundra soils. *Biogeochemistry* **126**: 397-414.

Heuer, V., Elvert, M., Tille, S., Krummen, M., Mollar, X.P., Hmelo, L.R., and Hinrichs, K.U. (2006) Online $\delta^{13}C$ analysis of volatile fatty acids in sediment/porewater systems by liquid chromatography-isotope ratio mass spectrometry. *Limnol Oceanogr: Meth* **4**: 346-357.

Holmkvist, L., Ferdelman, T.G., and Jørgensen, B.B. (2011) A cryptic sulfur cycle driven by iron in the methane zone of marine sediment (Aarhus Bay, Denmark). *Geochim Cosmochim Acta* **75**: 3581-3599.

Hopkins, B.T., McInerney, M.J., and Warikoo, V. (1995) Evidence for anaerobic syntrophic benzoate degradation threshold and isolation of the syntrophic benzoate degrader. *Appl Environ Microbiol* **61**: 526.

Jiang, S., Park, S., Yoon, Y., Lee, J.-H., Wu, W.-M., Phuoc Dan, N. et al. (2013) Methanogenesis facilitated by geobiochemical iron cycle in a novel syntrophic methanogenic microbial community. *Environ Sci Technol* **47**: 10078-10084.

Jørgensen, B.B. (2006) Bacteria and marine biogeochemistry. In *Marine Geochemistry*. Schulz, H.D., and Zabel, M. (eds). Berlin, Heidelberg: Springer Berlin Heidelberg, pp. 169-206.

Kato, S., Hashimoto, K., and Watanabe, K. (2012) Methanogenesis facilitated by electric syntrophy via (semi) conductive iron-oxide minerals. *Environ Microbiol* **14**: 1646-1654.

Kirchman, D.L., Hanson, T.E., Cottrell, M.T., and Hamdan, L.J. (2014) Metagenomic analysis of organic matter degradation in methane-rich Arctic Ocean sediments. *Limnol Oceanogr* **59**: 548-559.

Lehours, A.-C., Rabiet, M., Morel-Desrosiers, N., Morel, J.-P., Jouve, L., Arbeille, B. et al. (2010) Ferric iron reduction by fermentative strain BS2 isolated from an iron-rich anoxic environment (Lake Pavin, France). *Geomicrobiol J* **27**: 714-722.

Lentini, C.J., Wankel, S.D., and Hansel, C.M. (2012) Enriched iron(III)-reducing bacterial communities are shaped by carbon substrate and iron oxide mineralogy. *Front Microbiol* **3**: 404.

Li, H., Chang, J., Liu, P., Fu, L., Ding, D., and Lu, Y. (2015) Direct interspecies electron transfer accelerates syntrophic oxidation of butyrate in paddy soil enrichments. *Environ Microbiol* **17**: 1533-1547.

Lin, Y.-S., Heuer, V.B., Goldhammer, T., Kellermann, M.Y., Zabel, M., and Hinrichs, K.-U. (2012) Towards constraining H_2 concentration in subseafloor sediment: A proposal for combined analysis by two distinct approaches. *Geochim Cosmochim Acta* **77**: 186-201.

Liu, D., Wang, H., Dong, H., Qiu, X., Dong, X., and Cravotta, C.A. (2011) Mineral transformations associated with goethite reduction by *Methanosarcina barkeri*. *Chem Geol* **288**: 53-60.

Liu, F., Rotaru, A.E., Shrestha, P.M., Malvankar, N.S., Nevin, K.P., and Lovley, D.R. (2015) Magnetite compensates for the lack of a pilin-associated c-type cytochrome in extracellular electron exchange. *Environ Microbiol* **17**: 648-655.

Lovley, D. (2006) Dissimilatory Fe(III)-and Mn(IV)-reducing prokaryotes. In *The prokaryotes*: Springer, pp. 635-658.

Lovley, D.R., and Phillips, E.J. (1986) Organic matter mineralization with reduction of ferric iron in anaerobic sediments. *Appl Environ Microbiol* **51**: 683-689.

Lovley, D.R., and Phillips, E.J. (1988) Novel mode of microbial energy metabolism: Organic carbon oxidation coupled to dissimilatory reduction of iron or manganese. *Appl Environ Microbiol* **54**: 1472-1480.

Lueders, T., Manefield, M., and Friedrich, M.W. (2004) Enhanced sensitivity of DNA-and rRNA-based stable isotope probing by fractionation and quantitative analysis of isopycnic centrifugation gradients. *Environ Microbiol* **6**: 73-78.

McInerney, M.J., Struchtemeyer, C.G., Sieber, J., Mouttaki, H., Stams, A.J., Schink, B. et al. (2008) Physiology, ecology, phylogeny, and genomics of microorganisms capable of syntrophic metabolism. *Annals New York Acad Sci* **1125**: 58-72.

McInerney, M.J., Rohlin, L., Mouttaki, H., Kim, U., Krupp, R.S., Rios-Hernandez, L. et al. (2007) The genome of *Syntrophus aciditrophicus*: Life at the thermodynamic limit of microbial growth. *Proc Nat Acad Sci* **104**: 7600-7605.

Nobu, M.K., Dodsworth, J.A., Murugapiran, S.K., Rinke, C., Gies, E.A., Webster, G. et al. (2016) Phylogeny and physiology of candidate phylum 'Atribacteria'(OP9/JS1) inferred from cultivation-independent genomics. *ISME J* **10**: 273-286.

Nurk, S., Meleshko, D., Korobeynikov, A., and Pevzner, P.A. (2017) metaSPAdes: A new versatile metagenomic assembler. *Genome Res* **27**: 824-834.

Oni, O.E. (2015) Structure and function of microorganisms in the methanic sediments of the Helgoland Mud Area, North Sea, Germany. Bremen, Germany: University of Bremen.

Oni, O.E., Schmidt, F., Miyatake, T., Kasten, S., Witt, M., Hinrichs, K.-U., and Friedrich, M.W. (2015a) Microbial communities and organic matter composition in surface and subsurface sediments of the Helgoland mud area, North Sea. *Front Microbiol* **6**: 1290.

Oni, O.E., Miyatake, T., Kasten, S., Richter-Heitmann, T., Fischer, D., Wagenknecht, L. et al. (2015b) Distinct microbial populations are tightly linked to the profile of dissolved iron in the methanic sediments of the Helgoland Mud Area, North Sea. *Front Microbiol* **6**: 365.

Oren, A. (2014) The order Halanaerobiales, and the families Halanaerobiaceae and Halobacteroidaceae. In *The Prokaryotes: Firmicutes and Tenericutes*. Rosenberg, E., DeLong, E.F., Lory, S., Stackebrandt, E., and Thompson, F. (eds). Berlin, Heidelberg: Springer Berlin Heidelberg, pp. 153-177.

Parks, D.H., Imelfort, M., Skennerton, C.T., Hugenholtz, P., and Tyson, G.W. (2015) CheckM: Assessing the quality of microbial genomes recovered from isolates, single cells, and metagenomes. *Genome Res* **25**: 1043-1055.

Rabus, R., Boll, M., Heider, J., Meckenstock, R.U., Buckel, W., Einsle, O. et al. (2016) Anaerobic microbial degradation of hydrocarbons: From enzymatic reactions to the environment. *J Mol Microbiol Biotechnol* **26**: 5-28.

Riedinger, N., Formolo, M.J., Lyons, T.W., Henkel, S., Beck, A., and Kasten, S. (2014) An inorganic geochemical argument for coupled anaerobic oxidation of methane and iron reduction in marine sediments. *Geobiology* **12**: 172-181.

Roden, E.E., and Wetzel, R.G. (1996) Organic carbon oxidation and suppression of methane production by microbial Fe(III) oxide reduction in vegetated and unvegetated freshwater wetland sediments. *Limnol Oceanogr* **41**: 1733-1748.

Rooze, J., Egger, M., Tsandev, I., and Slomp, C.P. (2016) Iron-dependent anaerobic oxidation of methane in coastal surface sediments: Potential controls and impact. *Limnol Oceanogr* **61**: S267-S282.

Rotaru, A.-E., Shrestha, P.M., Liu, F., Markovaite, B., Chen, S., Nevin, K.P., and Lovley, D.R. (2014) Direct interspecies electron transfer between *Geobacter metallireducens* and *Methanosarcina barkeri*. *Appl Environ Microbiol* **80**: 4599-4605.

Rotaru, A.-E., Calabrese, F., Stryhanyuk, H., Musat, F., Shrestha, P.M., Weber, H.S. et al. (2018) Conductive particles enable syntrophic acetate oxidation between *Geobacter* and *Methanosarcina* from coastal sediments. *Mbio* **9**: e00226-00218.

Schink, B. (1997) Energetics of syntrophic cooperation in methanogenic degradation. *Microbiol Mol Biol Rev* **61**: 262-280.

Schöcke, L., and Schink, B. (1997) Energetics of methanogenic benzoate degradation by *Syntrophus gentianae* in syntrophic coculture. *Microbiol* **143**: 2345-2351.

Seemann, T. (2014) Prokka: Rapid prokaryotic genome annotation. *Bioinformatics* **30**: 2068-2069.

Sieber, J., McInerney, M., Plugge, C., Schink, B., and Gunsalus, R. (2010) Methanogenesis: syntrophic metabolism. In *Handbook of Hydrocarbon and Lipid Microbiology*: Springer, pp. 337-355.

Sivan, O., Shusta, S., and Valentine, D. (2016) Methanogens rapidly transition from methane production to iron reduction. *Geobiology* **14**: 190-203.

Tong, H., Hu, M., Li, F., Chen, M., and Lv, Y. (2015) *Burkholderiales* participating in pentachlorophenol biodegradation in iron-reducing paddy soil as identified by stable isotope probing. *Environ Sci Processes Impacts* **17**: 1282-1289.

Uritskiy, G.V., and DiRuggiero, J. (2018) MetaWRAP-a flexible pipeline for genome-resolved metagenomic data analysis. *Microbiome* **6**: 158.

Vandieken, V., Mußmann, M., Niemann, H., and Jørgensen, B.B. (2006) *Desulfuromonas svalbardensis* sp. nov. and *Desulfuromusa ferrireducens* sp. nov., psychrophilic, Fe(III)-reducing bacteria isolated from Arctic sediments, Svalbard. *Int J Syst Evol Microbiol* **56**: 1133-1139.

Viollier, E., Inglett, P., Hunter, K., Roychoudhury, A., and Van Cappellen, P. (2000) The ferrozine method revisited: Fe(II)/Fe(III) determination in natural waters. *Appl Geochem* **15**: 785-790.

Whitman, W.B., Coleman, D.C., and Wiebe, W.J. (1998) Prokaryotes: The unseen majority. *Proc Nat Acad Sci* **95**: 6578-6583.

Widdel, F. (1980) Anaerober Abbau von fettsäuren und benzoesäure durch neu isolierte arten sulfat-reduzierender Bakterien. In: Georg-August-Universität zu Göttingen.

Widdel, F., and Pfennig, N. (1981) Studies on dissimilatory sulfate-reducing bacteria that decompose fatty acids. *Arch Mircrobiol* **129**: 395-400.

Widdel, F., Kohring, G.-W., and Mayer, F. (1983) Studies on dissimilatory sulfate-reducing bacteria that decompose fatty acids III. Characterization of the filamentous gliding *Desulfonema limicola* gen. nov. sp. nov., and *Desulfonema magnum* sp. nov. *Arch Microbiol* **134**: 286-294.

Wischgoll, S., Heintz, D., Peters, F., Erxleben, A., Sarnighausen, E., Reski, R. et al. (2005) Gene clusters involved in anaerobic benzoate degradation of *Geobacter metallireducens*. *Mol Microbiol* **58**: 1238-1252.

Wrighton, K.C., Agbo, P., Warnecke, F., Weber, K.A., Brodie, E.L., DeSantis, T.Z. et al. (2008) A novel ecological role of the Firmicutes identified in thermophilic microbial fuel cells. *ISME J* **2**: 1146-1156.

Wu, Y.-W., Tang, Y.-H., Tringe, S.G., Simmons, B.A., and Singer, S.W. (2014) MaxBin: An automated binning method to recover individual genomes from metagenomes using an expectation-maximization algorithm. *Microbiome* **2**: 26.

Yang, Z., Wullschleger, S.D., Liang, L., Graham, D.E., and Gu, B. (2016) Effects of warming on the degradation and production of low-molecular-weight labile organic carbon in an Arctic tundra soil. *Soil Biol Biochem* **95**: 202-211.

Zhang, J., and Lu, Y. (2016) Conductive Fe_3O_4 nanoparticles accelerate syntrophic methane production from butyrate oxidation in two different lake sediments. *Front Microbiol* **7**: 1316.

Zhou, S., Xu, J., Yang, G., and Zhuang, L. (2014) Methanogenesis affected by the co-occurrence of iron(III) oxides and humic substances. *FEMS Microbiol Ecol* **88**: 107-120.

Table 1 Electron balance calculations for benzoate degradation in highly enriched cultures showing yield in CH_4 and Fe(II). Addition of 5 mM benzoate as carbon substrate amounted to 250 µmol carbon.

Enrichment	Amount CH_4 (µmol)	% CH_4 yield in methanogenesis	Amount Fe(II) µmol	% yield in iron reduction
BM5	717.6	76.5	340	9.1
BM5	742.7	79.2	285.5	7.6
BM5	575.9	61.4	245	6.5
B5A.1	165.7	17.7	NA	NA
B5A.2	227.9	24.3	NA	NA
B5A.3	535.4	57.1	NA	NA
B5B.1	559.3	59.7	125	3.3
B5B.2	466.7	49.8	184	4.9
B5B.3	356.7	38.	119.5	3.2
BL5	502.4	53.6	454	12.1
BL5	357.6	38.2	368	9.8
BL5	596.5	63.6	565	15.1

B5A: habitual cultivation of the benzoate only enrichment without iron oxides. B5B: amendment of seperate B5 enrichment replicates with magnetite. NA: not applicable

Table 2 Electron yield in CH_4 from original sediment incubations. Addition of 5 mM benzoate as carbon substrate amounted to 187.5 µmol carbon.

Treatment	Amount CH_4 (µmol)	% CH_4 yield in methanogenesis
Benzoate + Hematite	389.5	55.4
Benzoate + Magnetite	383.2	54.5
Benzoate only	353.6	50.3
Benzoate + Lepidocrocite	327.6	46.6

Figures and captions

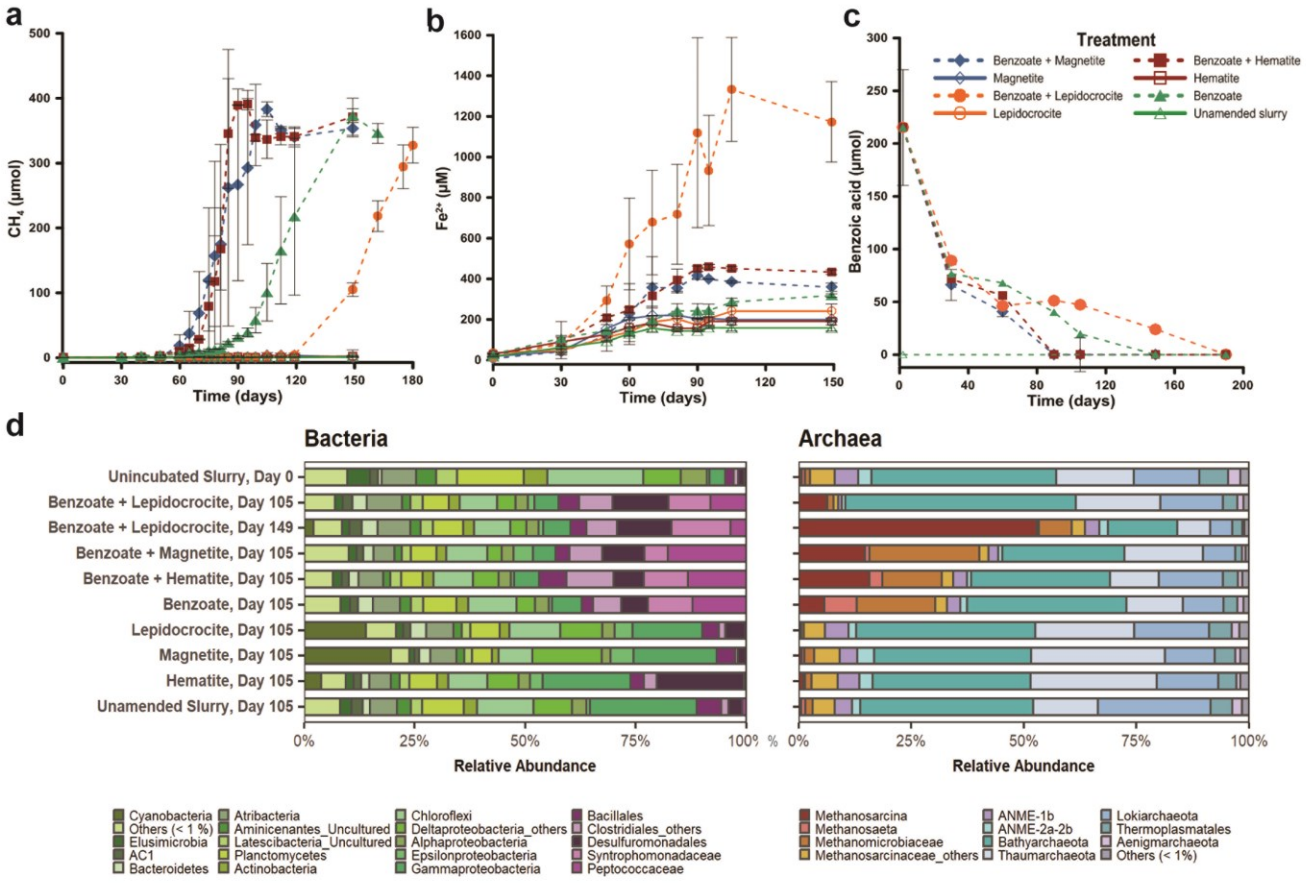

Fig. 1 Concurrent methanogenesis and crystalline iron reduction during benzoate degradation in sediment slurry incubations. **a** enhancement of methanogenesis by (semi)conductive crystalline iron minerals (hematite and magnetite) and inhibition of methanogenesis by non-conductive, poorly crystalline iron lepidocrocite, n = 3, error bars are 1 s.d. **b** concurrent reduction of crystalline iron(III) minerals during phase of active methanogenesis (after day 60). Higher concentrations of dissolved Fe^{2+} were observed in the presence of hematite and magnetite as compared to controls with benzoate only. **c** time course of benzoate degradation in incubations, obtained by measuring the decrease in benzoic acid concentrations. **d** bacteria and archaea communities enriched during the sediment slurry incubations. Two types of colour panels were used for the plots to differentiate communities stimulated during the incubation and presented on either order, family or genus level from the communities whose relative abundance did not increase presented on phylum or class level.

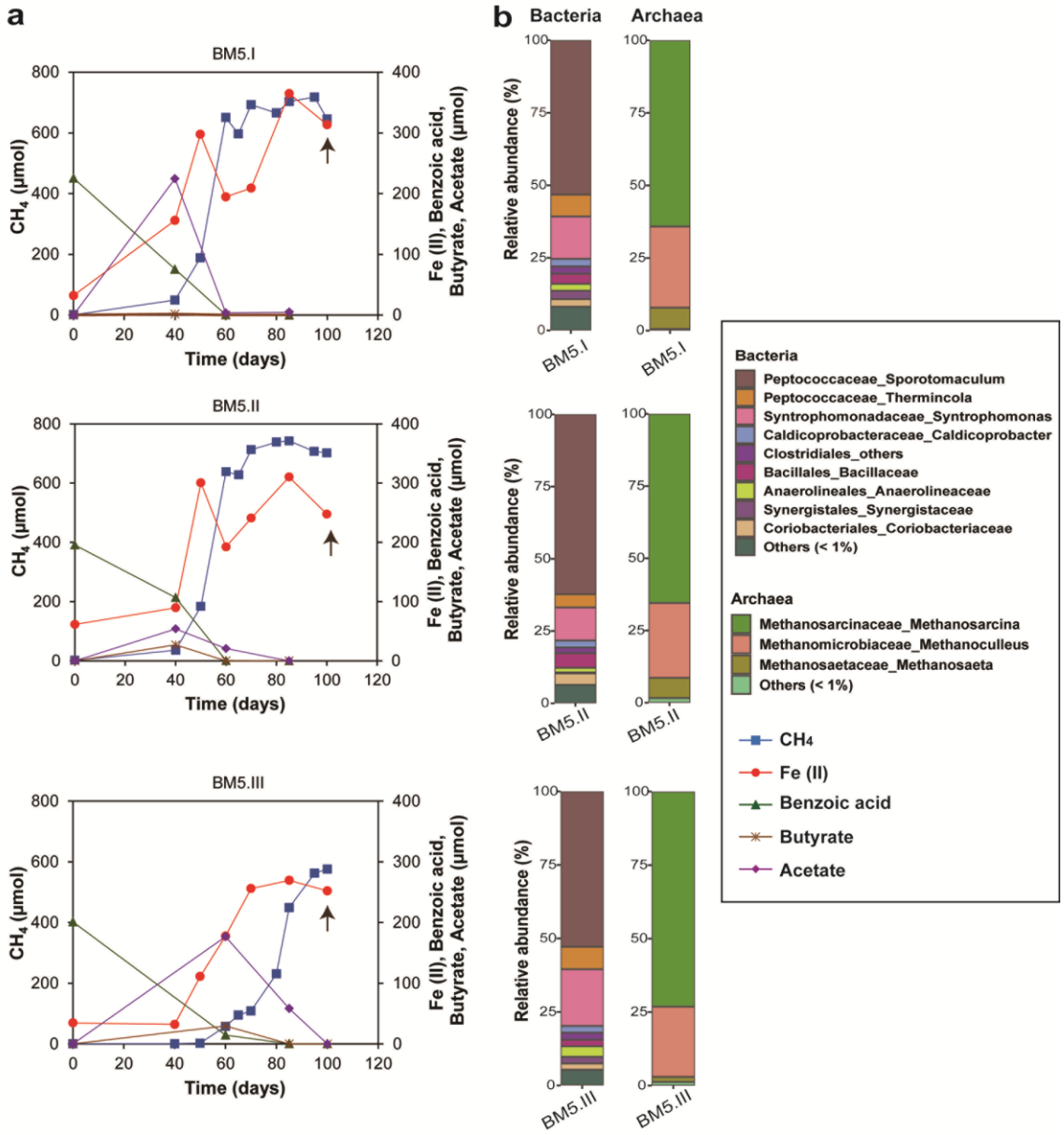

Fig. 2 Concurrent iron reduction and methanogenesis in BM5 enrichment cultivated with benzoate and magnetite as substrates in the 5th generation. **a** Kinetics of benzoic acid degradation, build-up and removal of intermediates (butyrate and acetate), increasing Fe(II) and CH_4 amounts over time. **b** 16S rRNA gene derived bacteria and archaea community composition presented on family or genus level. Brown arrows in the 'a' panel reflect the time point from which DNA was extracted for sequencing.

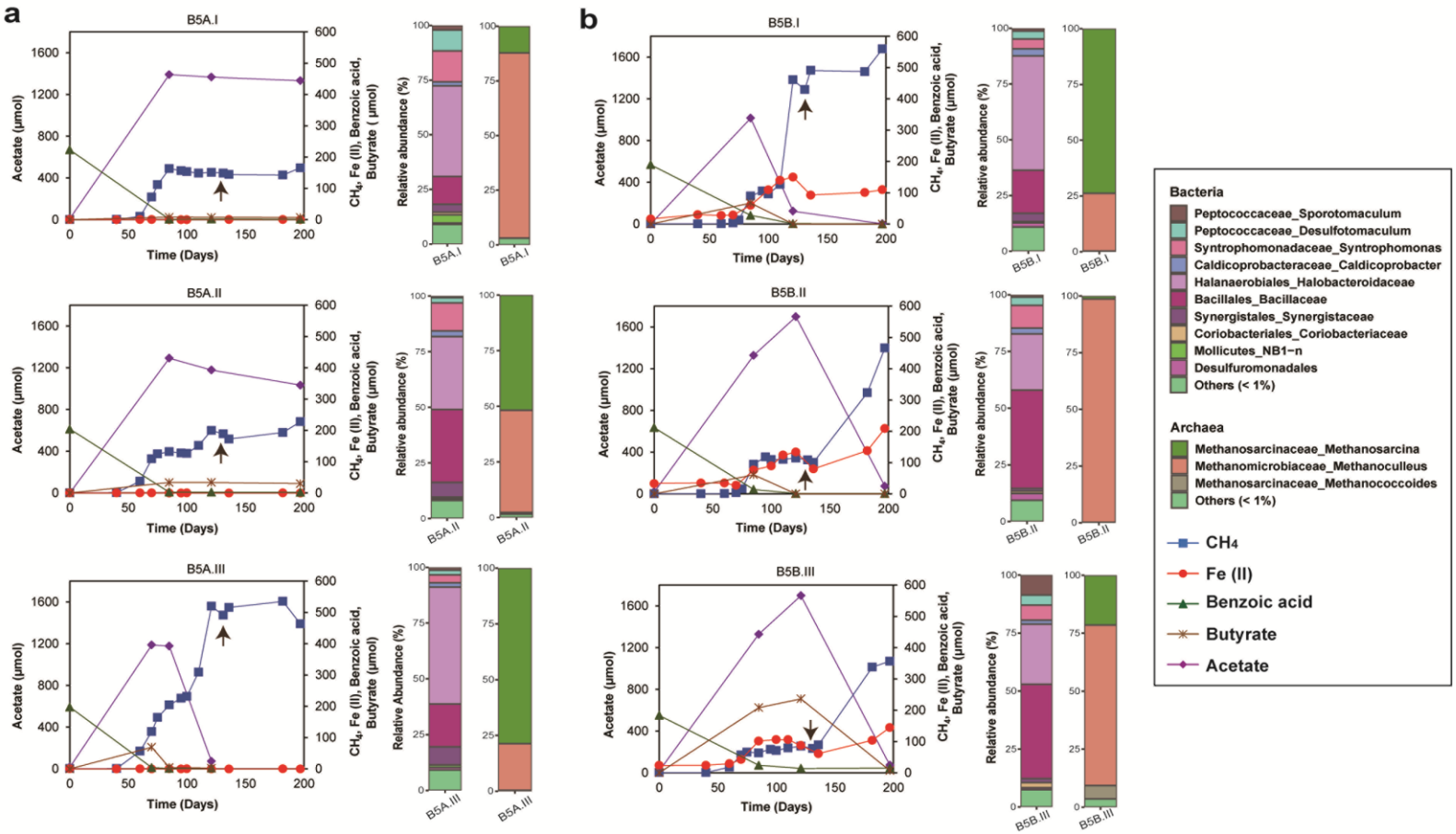

Fig. 3 Kinetics of benzoate degradation and the 16S rRNA derived microbial community composition in B5 enrichment cultivated without iron oxides after 5 transfers. **a** Panel presents time course of intermediate (acetate and butyrate) build-up, methanogenesis and microbial community composition in triplicates from the habitual cultivation. Acetate, first detected after 85 days, stayed in the system until 200 days in 2 of 3 replicates and caused the inhibition of complete benzoate turnover to CH_4. **b** Panel presents kinetics of separate B5 triplicates amended with magnetite demonstrating that acetate accumulation was effectively removed by concurrent magnetite reduction as methanogenesis progressed. Brown arrows in both panels 'a' and 'b' reflect time-point (day 136) sequenced for microbial community composition.

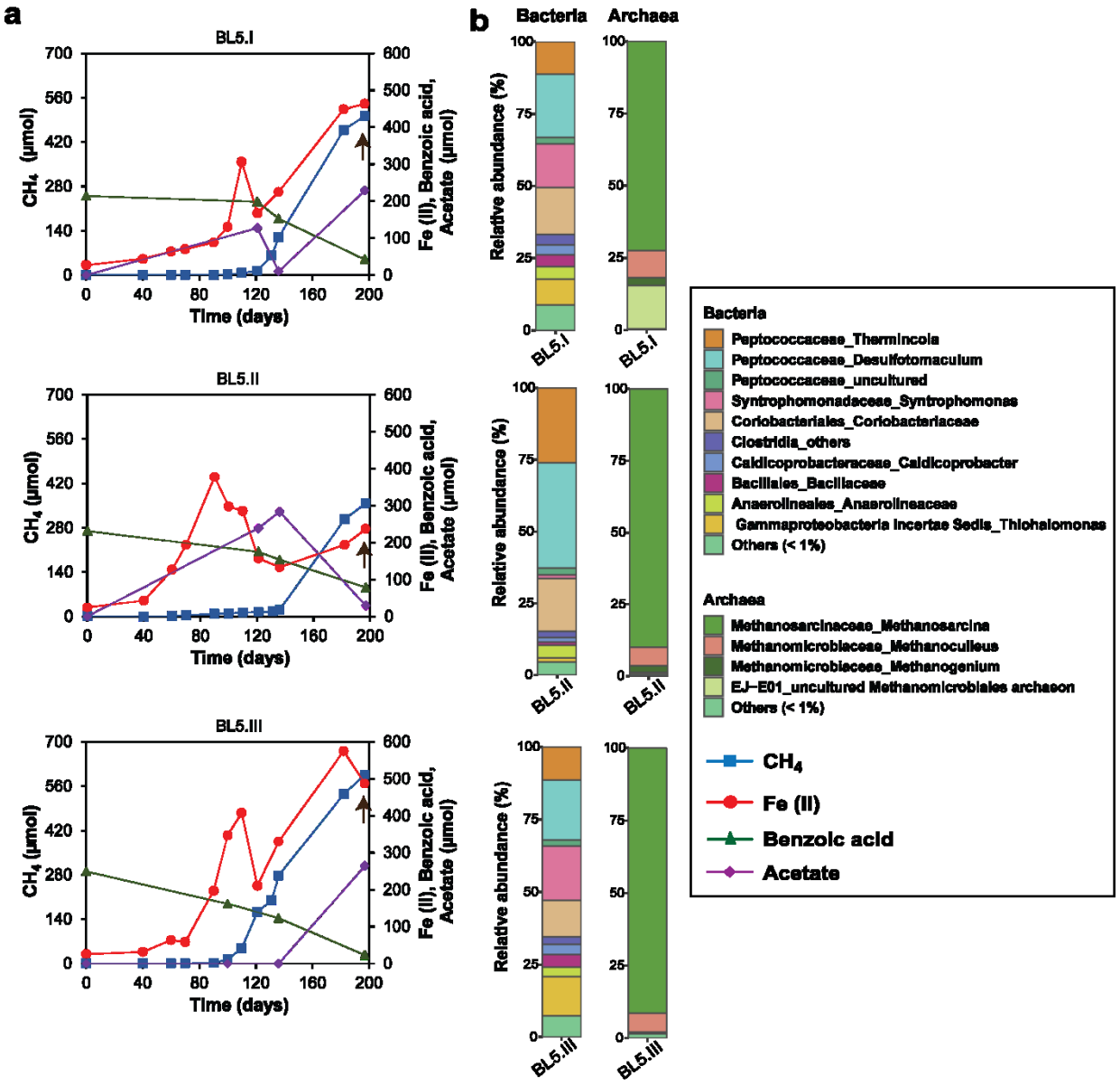

Fig. 4 Kinetics of benzoate degradation and microbial community composition in BL5 enrichment (5th generation) cultivated with lepidocrocite. **a** Time course of benzoate degradation, transient acetate build-up, iron reduction and methanogenesis**. b** 16S rRNA gene derived microbial community composition after 197 days as indicated by brown arrows in the 'a' panel.

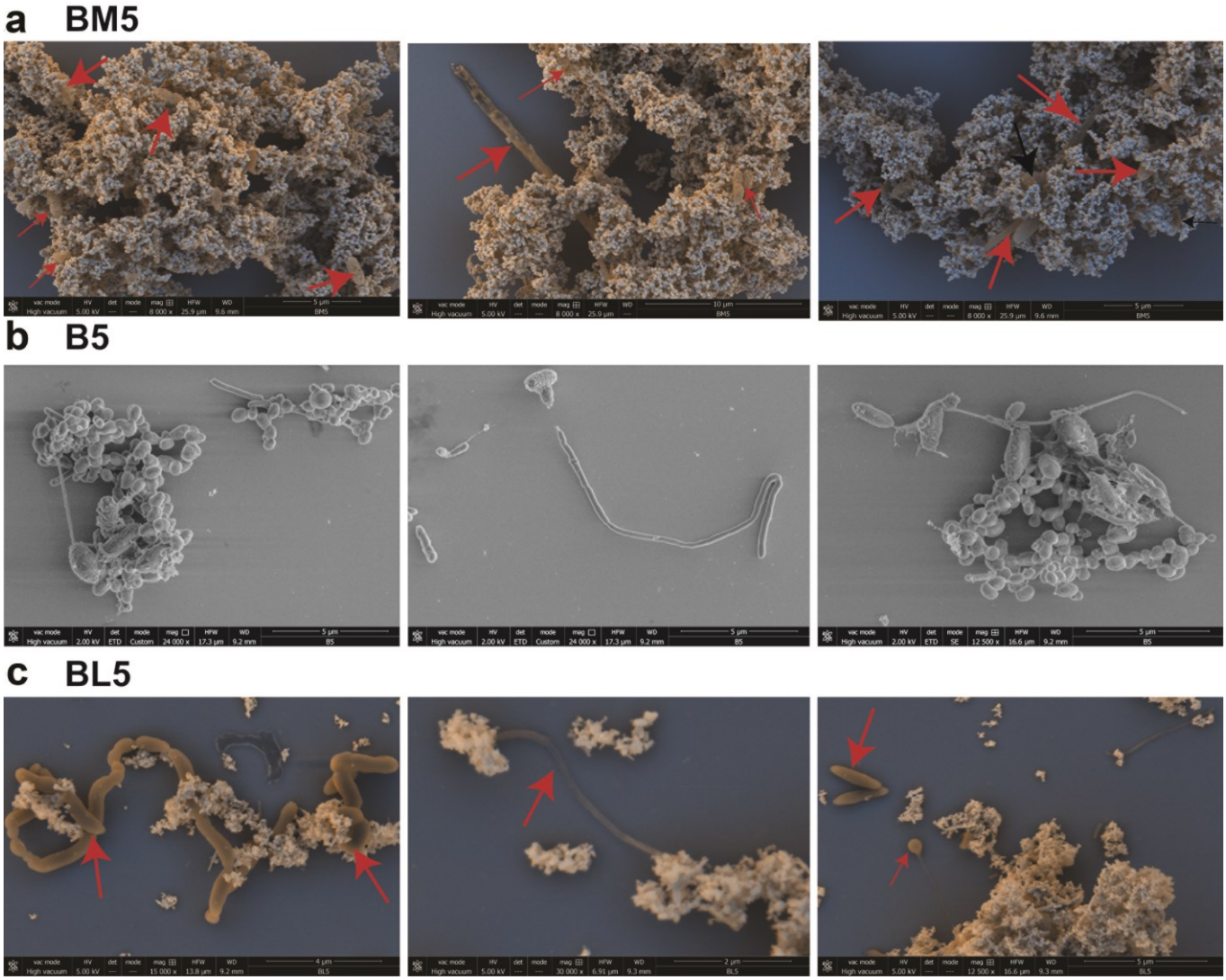

Fig. 5 Scanning electron microscopy images from highly enriched 5th generation cultures after 200 days. **a** BM5 enrichment on magnetite. **b** B5 enrichment cultivated without iron oxides. **c** BL5 enrichment cultivated with lepidocrocite. Images in panels 'a' and 'c' combined images from back scattered (blue colour) and secondary electron (orange colour) images to clearly distinguish between microbial cells and iron oxides. Accordingly, red arrows in the aforementioned panels point towards microbial cells.

a

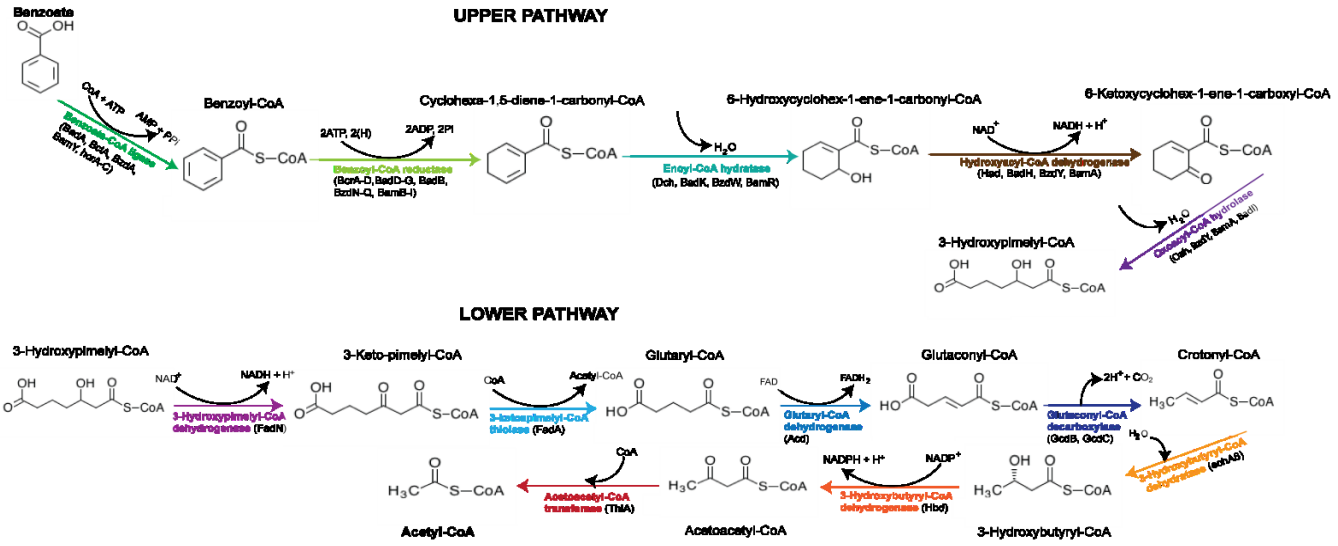

b

Enrichment	Bins	Completeness (%)	Lineage	EC Genes in the anaerobic benzoate degradation pathway																
				Upper pathway									Lower Pathway							
				Step 1				Step 2	Step 3	Step 4		Step 5	Step 6	Step 7	Step 8	Step 9		Step 10	Step 11	Step 12
				BclA	hcrA	hcrB	hcrC	BcrC	Dch	Had	BamA	BamA	FadN	FadA	Acd	GcdB	GcdC	EchA8	Hbd	Thla
BM5	bin.18	98.9	Clostridia	●	●				●		●	●		●	●	●	●	●	●	●
	bin.10	99.1	Firmicutes				●		●	●	●	●			●	●	●	●		●
	bin.9	98.0	Clostridia					●					●	●	●	●	●	●	●	●
	bin.5	94.8	Bacillales			●							●	●				●	●	●
	bin.13	96.9	Clostridiales		●											●	●		●	●
	bin.16	74.7	Clostridia					●						●			●	●	●	●
	bin.15	67.0	Bacteria				●									●	●		●	
	bin.11	98.6	Clostridiales													●	●		●	●
	bin.8	99.2	Clostridia													●	●	●	●	●
	bin.1	90.9	Bacteria											●		●	●			
	bin.4	97.4	Clostridia														●		●	
	bin.19	100.0	Bacteria															●	●	
	bin.2	92.7	Bacteria													●	●			
	bin.6	97.9	Euryarchaeota											●						
	bin.7	99.5	Euryarchaeota											●						
B5	bin.4	93.9	Firmicutes						●	●	●	●			●	●	●	●	●	●
	bin.5	99.7	Clostridia			●							●	●	●	●	●	●	●	●
	bin.7	81.0	Deltaproteobacteria										●	●	●		●	●		
	bin.12	99.3	Bacilli										●	●				●	●	●
	bin.11	73.2	Bacteria													●	●		●	●
	bin.2	97.6	Clostridia													●	●		●	●
	bin.9	97.4	Firmicutes													●	●		●	●
	bin.1	89.3	Bacilli																●	●
	bin.13	100.0	Bacteria															●	●	
	bin.6	60.1	Firmicutes						●							●				
	bin.8	66.1	Bacteria		●															
	bin.10	99.8	Euryarchaeota																	●
BL5	bin.2	99.7	Firmicutes	●	●	●	●	●	●	●			●	●	●	●	●	●	●	●
	bin.7	93.4	Firmicutes	●	●	●			●	●	●	●		●		●	●		●	●
	bin.4	99.9	Firmicutes						●	●	●	●			●	●	●	●		●
	bin.17	99.7	Clostridia					●					●	●	●	●	●	●	●	●
	bin.14	88.7	Deltaproteobacteria										●	●	●	●	●	●		●
	bin.8	82.5	Paenibacillaceae										●	●	●				●	●
	bin.16	90.9	Bacteria		●											●	●	●		
	bin.10	53.2	Bacteria											●	●			●		●
	bin.11	90.9	Bacteria											●		●	●			
	bin.13	57.7	Firmicutes												●	●				
	bin.9	98.7	Clostridiales				●											●	●	
	bin.19	51.6	Firmicutes																●	●
	bin.1	99.5	Clostridia																●	
	bin.18	95.8	Euryarchaeota											●						

Fig. 6 Pathway of benzoate degradation utilised by anaerobic bacteria. **a** The pathway and genes involved in benzoate degradation leading to the formation of acetate is reflected. **b** Presence of genes involved in the various steps of the benzoate degradation pathway in multiple metagenomic bins from highly enriched cultures BM5, B5 and BL5.

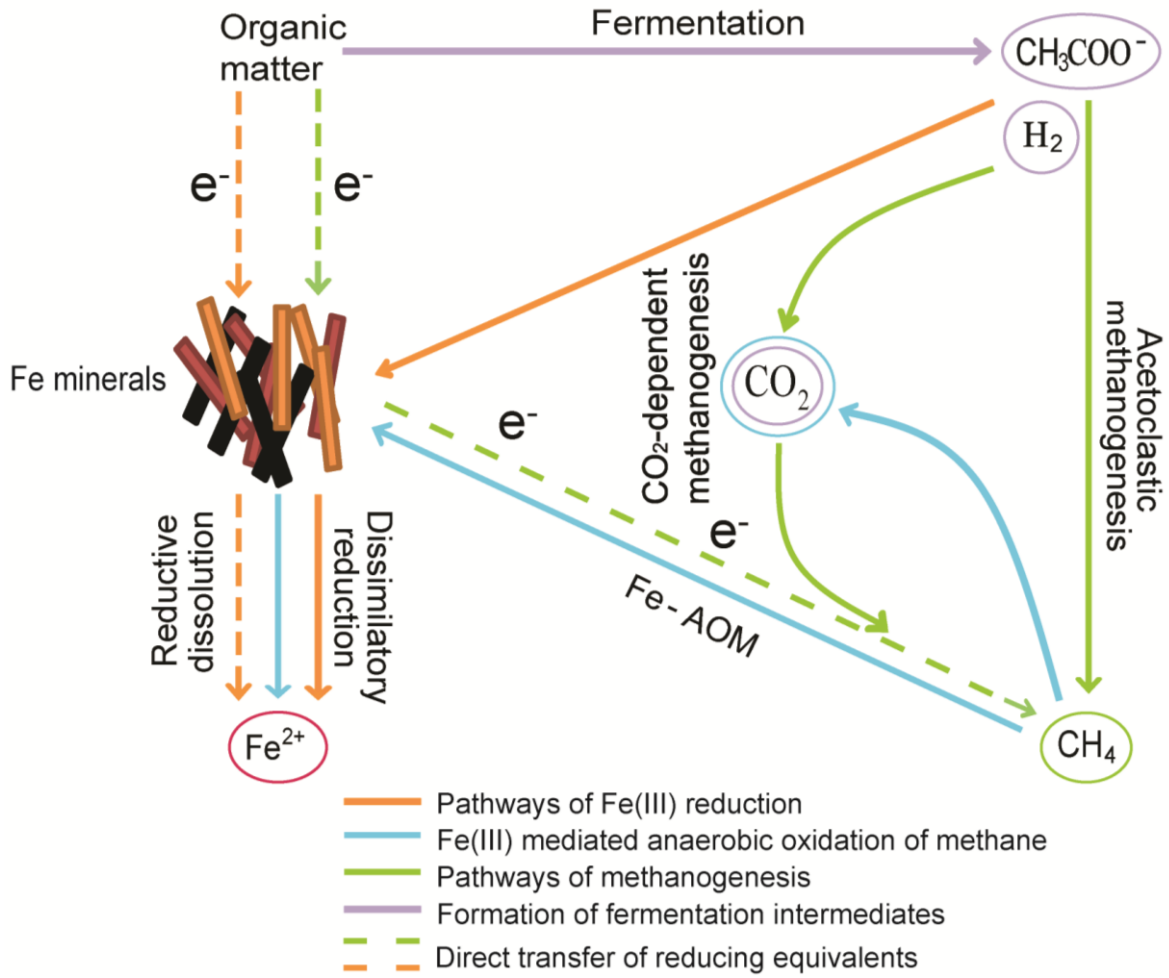

Fig. 7 Schematic description of the various biotic processes that possibly contribute to Fe^{2+} pool detected in porewater of iron-oxide rich methanic marine sediments e.g. Helgoland Mud Area. Previous studies have implicated Fe-AOM as the major mechanism mediating this process but this study shows an additional perspective that organoclastic iron reduction is involved as well. Red, Brown and Black colorations are representative of the various forms of Fe(III) present in the environment.

Supplementary material

Concurrent crystalline iron oxide reduction and methanogenesis from benzoate degradation by marine sediment derived enrichment cultures

David A. Aromokeye[1,2], Oluwatobi E. Oni[1,2], Jan Tebben[3,4], Jenny Wendt[2,5], Rolf Nimzyk[6], Sten Littmann[7], Ajinkya Kulkarni[1,2], Tim Richter-Heitmann[1], Kai-Uwe Hinrichs[2,5], Marcus Elvert[2,5], Tilmann Harder[4,5], Sabine Kasten[2,3,5] and Michael W. Friedrich[1,2*]

[1]Microbial Ecophysiology Group, Faculty of Biology/Chemistry, University of Bremen, Bremen, Germany

[2]MARUM – Center for Marine Environmental Sciences, University of Bremen, Bremen, Germany

[3]Alfred Wegener Institute Helmholtz Centre for Polar and Marine Research, Bremerhaven, Germany

[4]Department of Chemistry, University of Bremen, Bremen, Germany

[5]University of Bremen, Faculty of Geosciences, Bremen, Germany

[6]Department of Microbe-Plant Interactions, Faculty of Biology/Chemistry, University of Bremen, Bremen, Germany

[7]Department of Biogeochemistry, Max Planck Institute for Marine Microbiology, Bremen, Germany

Running title: Concurrent iron reduction and methanogenesis

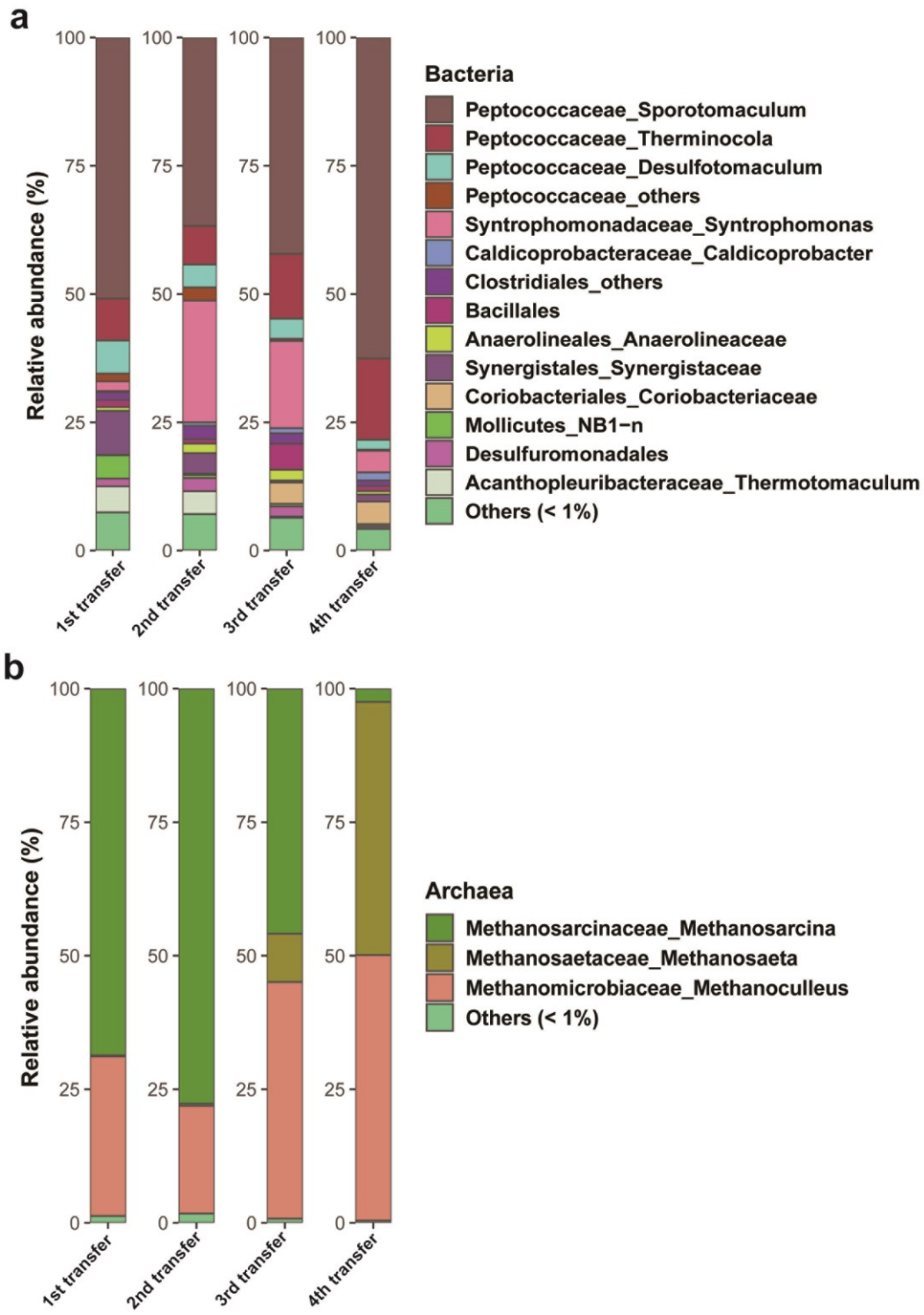

Fig. S1 Microbial community composition after four generation of transfers from the benzoate–magnetite sediment incubations. **a** Bacteria 16S rRNA gene sequences. **b** Archaea 16S rRNA gene sequences. Taxa are presented on order, family or class level for bacteria and on genus level for archaea.

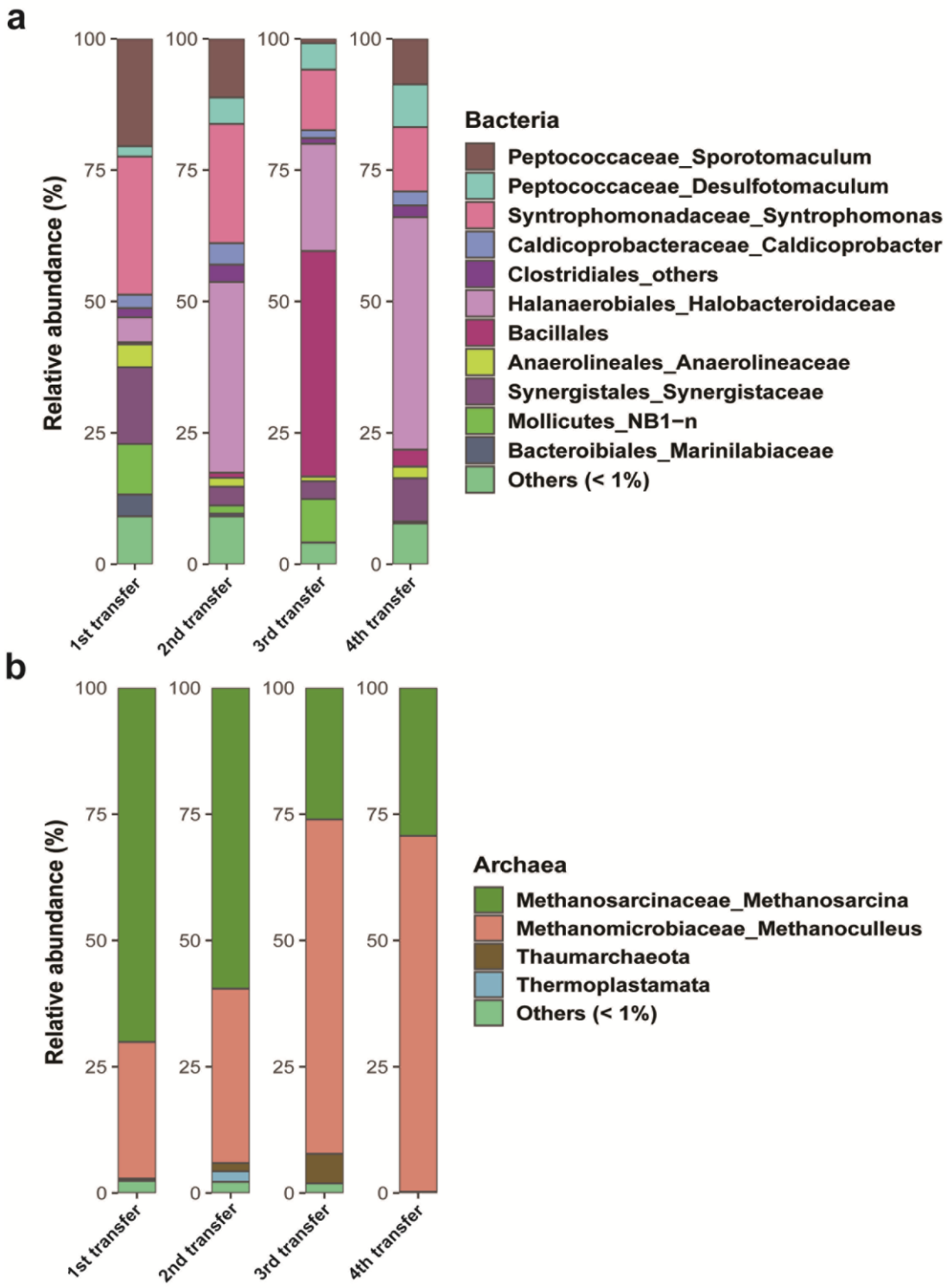

Fig. S2 Microbial community composition after 4 generation of transfers from the benzoate only sediment incubations. **a** Bacteria 16S rRNA gene sequences. **b** Archaea 16S rRNA gene sequences. Taxa are presented on order, family or class level for bacteria and on genus level for archaea.

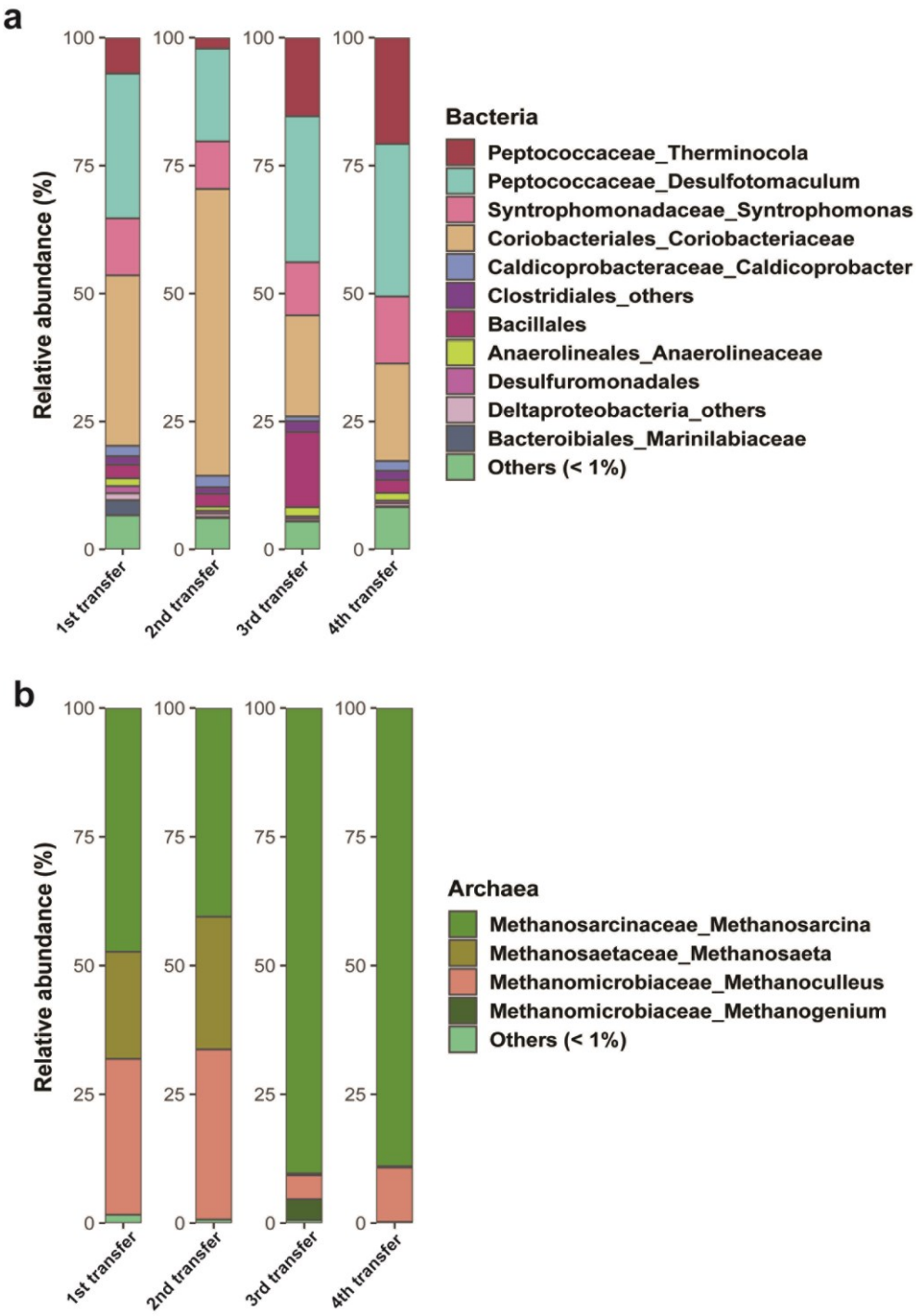

Fig. S3 Microbial community composition after four generation of transfers from the benzoate-lepidocrocite sediment incubations. **a** Bacteria 16S rRNA gene sequences. **b** Archaea 16S rRNA gene sequences. Taxa are presented on order, family or class level for bacteria and on genus level for archaea.

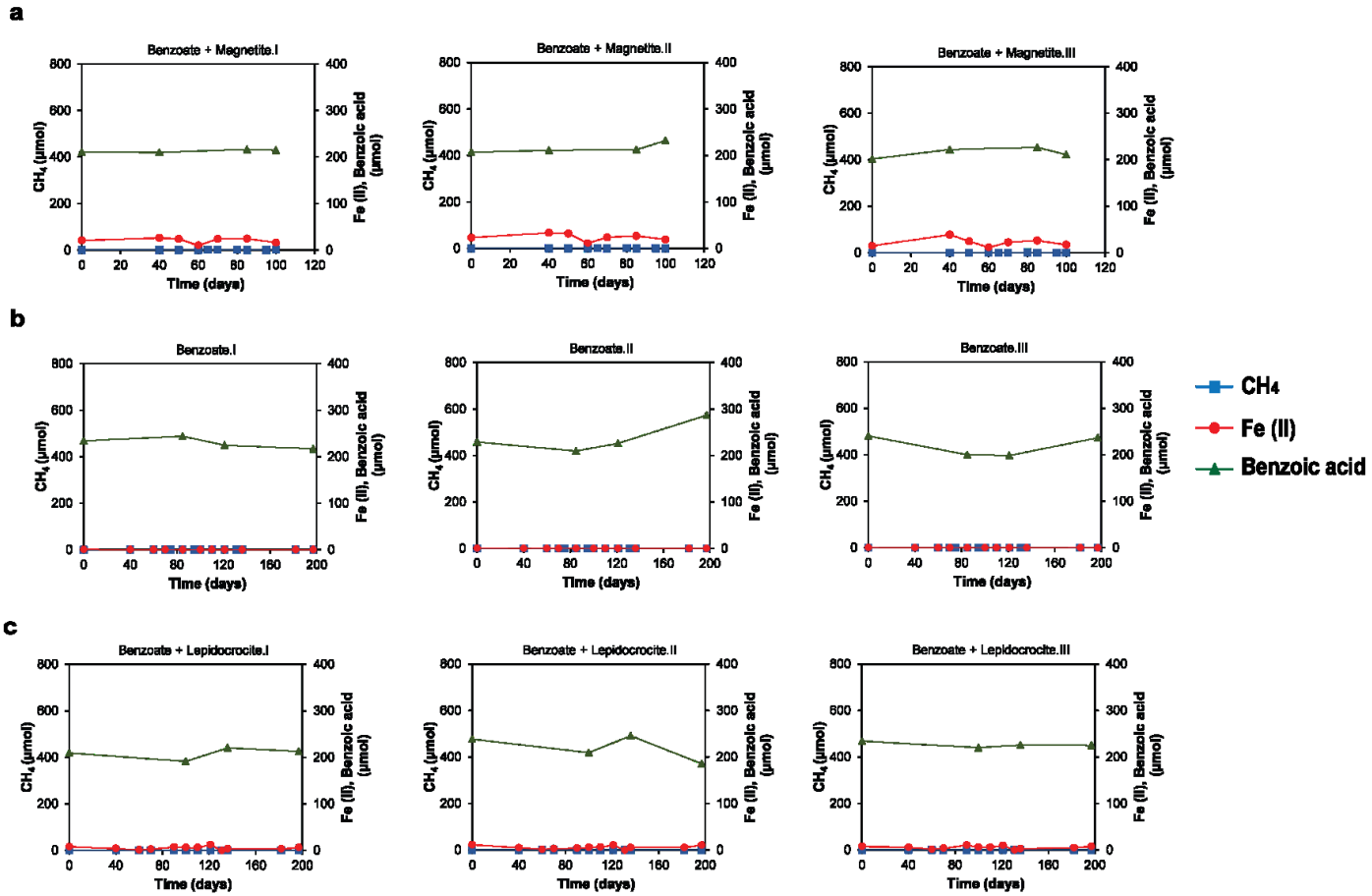

Fig S4 Kinetics of benzoate, methane and Fe(II) in control incubations without microbial cells from the 5th generation experiment. Butyrate and acetate were not detected. The absence of evidence for increased amounts of products or loss of benzoates confirm the processes observed in Fig. 2-4 of main article results from a biotic process.

Table S1 Quality metrics of the metagenomic bins containing genes encoding the various steps in the benzoate degradation pathway from the BM5 enrichment.

Bin	Completeness (%)	Contamination	GC content	Lineage	N50	Size	Coverage	Contigs
bin.1	90.9	2.73	0.45	Bacteria	16930	2894654	7	197
bin.10	99.1	1.59	0.44	Firmicutes	165997	3382841	220	36
bin.11	98.6	0.0	0.37	Clostridiales	92960	3562057	8	88
bin.12	69.9	0.67	0.33	Bacteria	2301	1337031	2.5	622
bin.13	96.9	0.0	0.45	Clostridiales	25790	2750548	12	143
bin.15	87	1.49	0.36	Bacteria	6840	4074501	4	740
bin.16	74.7	4.91	0.45	Clostridia	4224	2976530	3.5	780
bin.18	98.9	5.27	0.42	Clostridia	89471	4156954	8	75
bin.19	100	0.0	0.44	Bacteria	38721	2842865	9	81
bin.2	92.7	2.91	0.49	Bacteria	189548	2855454	30	19
bin.4	97.4	0.55	0.47	Clostridia	106554	3426057	8	49
bin.5	94.8	4.69	0.37	Bacillales	12436	4547570	5	484
bin.6	97.9	0.0	0.46	Euryarchaeota	42539	3653553	260	67
bin.7	99.5	0.65	0.62	Euryarchaeota	102102	2432528	145	24
bin.8	99.2	1.87	0.42	Clostridia	99571	3912647	76	56
bin.9	96	2.94	0.43	Clostridia	24403	3276692	7	179

Table S2 Quality metrics of the metagenomic bins containing genes encoding the various steps in the benzoate degradation pathway from the B5 enrichment.

Bin	Completeness (%)	Contamination	GC content	Lineage	N50	Size	Coverage	Contigs
bin.1	89.3	4.6	0.3	Bacilli	86229	3430657	9	73
bin.10	99.8	0.0	0.46	Euryarchaeota	37529	4163165	300	64
bin.11	73.2	4.8	0.32	Bacteria	5766	3609375	4	686
bin.12	99.3	0.99	0.47	Bacilli	64219	4270005	39	91
bin.13	100	0.0	0.44	Bacteria	230807	3042721	27	15
bin.2	97.6	0.0	0.46	Clostridia	96929	2623609	11	55
bin.4	93.9	0.96	0.45	Firmicutes	55843	3083413	10	91
bin.5	99.7	2.2	0.43	Clostridia	97363	3973561	52	90
bin.6	60.1	1.5	0.43	Firmicutes	3742	2083497	4	616
bin.7	81	3.1	0.51	Deltaproteobacteria	4808	3133879	3	742
bin.8	65.1	1.2	0.52	Bacteria	3136	2641100	2.5	883
bin.9	97.4	2.5	0.38	Firmicutes	250195	5083581	85	43

Table S3 Quality metrics of the metagenomic bins containing genes encoding the various steps in the benzoate degradation pathway from the BL5 enrichment.

Bin	Completeness (%)	Contamination	GC content	Lineage	N50	Size	Coverage
bin.1	99.5	0.38	0.46	Clostridia	150788	3880704	58
bin.10	53.2	0.0	0.43	Bacteria	2899	2276154	3
bin.11	90.9	2.91	0.45	Bacteria	522498	3204169	52
bin.13	57.7	9.01	0.57	Firmicutes	1576	2926831	2
bin.14	88.7	0.97	0.56	Deltaproteobacteria	9980	5040300	7
bin.16	90.9	5.64	0.46	Bacteria	1803718	3345903	19
bin.17	99.7	3.23	0.43	Clostridia	179469	3583623	84
bin.18	95.8	0.0	0.63	Euryarchaeota	10338	2168266	36
bin.19	51.6	1.2	0.38	Firmicutes	1651	1615649	2.5
bin.2	99.7	3.18	0.47	Firmicutes	34814	3844584	14
bin.4	99.9	0.64	0.45	Firmicutes	110545	2838791	88
bin.5	81.1	0.65	0.57	Euryarchaeota	102489	2221645	25
bin.6	99.8	0.0	0.46	Euryarchaeota	40412	3755994	270
bin.7	93.4	2.78	0.44	Firmicutes	153211	4065565	23
bin.8	82.5	2.08	0.35	Paenibacillaceae	10654	3009856	5
bin.9	96.7	0.0	0.45	Clostridiales	40683	2886690	21

Table S4 Bins containing genes involved in benzoate activation and upper pathway of benzoate degradation and their taxonomic lineages based on MetaWrap and ANVI'O based closest relatives.

Enrichment	Bin	Completeness (%)	Lineage (MetaWRAP)	ANVI'O classified closest relative
BM5	10	99.1	Firmicutes	*Desulfotomaculum reducens*
	18	98.9	Firmicutes_Clostridia	*Desulfotomaculum reducens*
B5	4	93.9	Firmicutes	*Desulfotomaculum reducens*
	5	99.7	Firmicutes_Clostridia	*Syntrophomonas wolfei*
BL5	2	99.7	Firmicutes	*Desulfotomaculum reducens*
	7	93.4	Firmicutes	*Dethiobacter alkaliphilus*

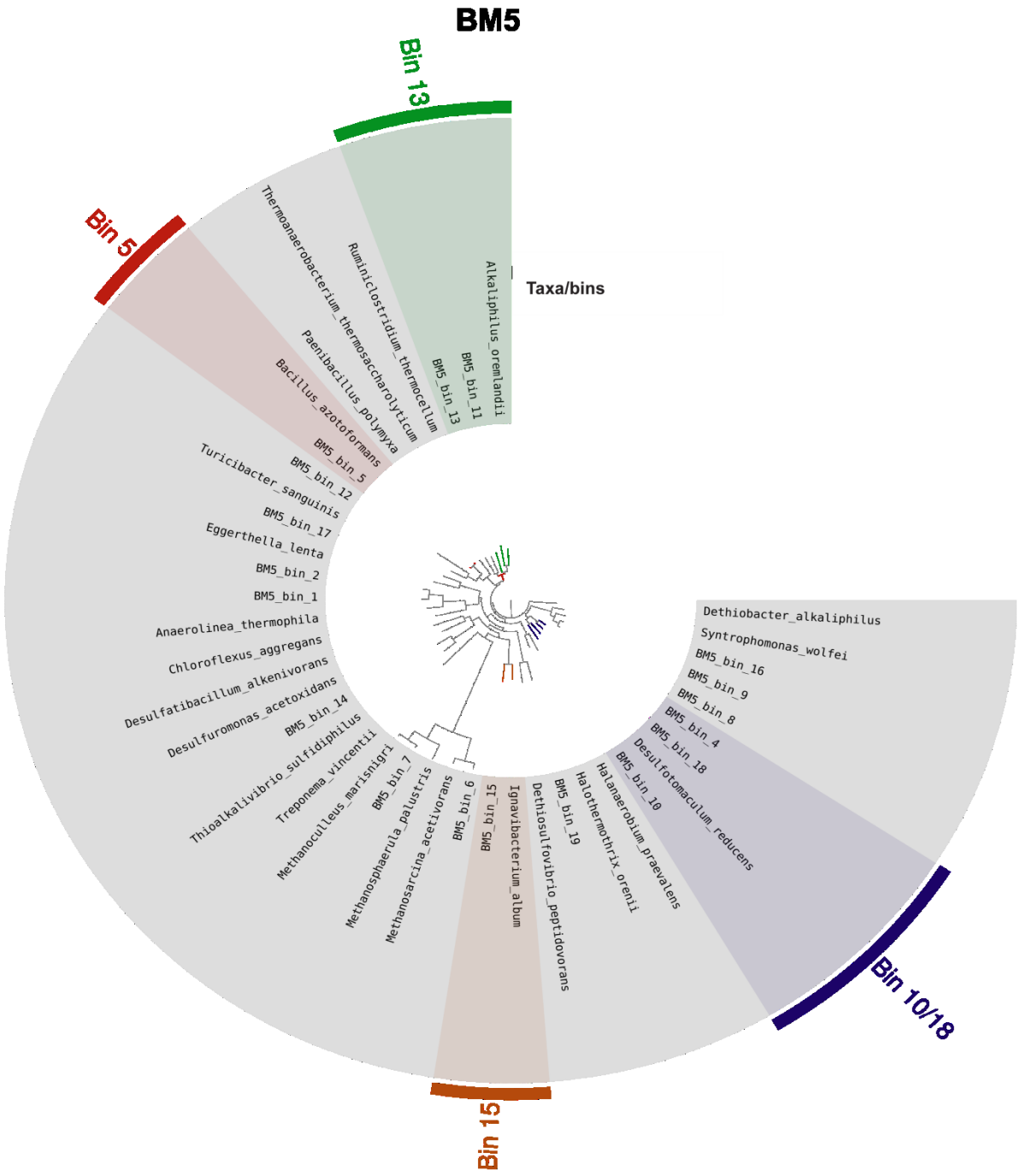

Fig. S5 ANVI'O concatenated proteins based phylogenetic affiliation of metagenomic bins involved in the benzoate degradation pathway (Fig. 6) from the BM5 enrichment.

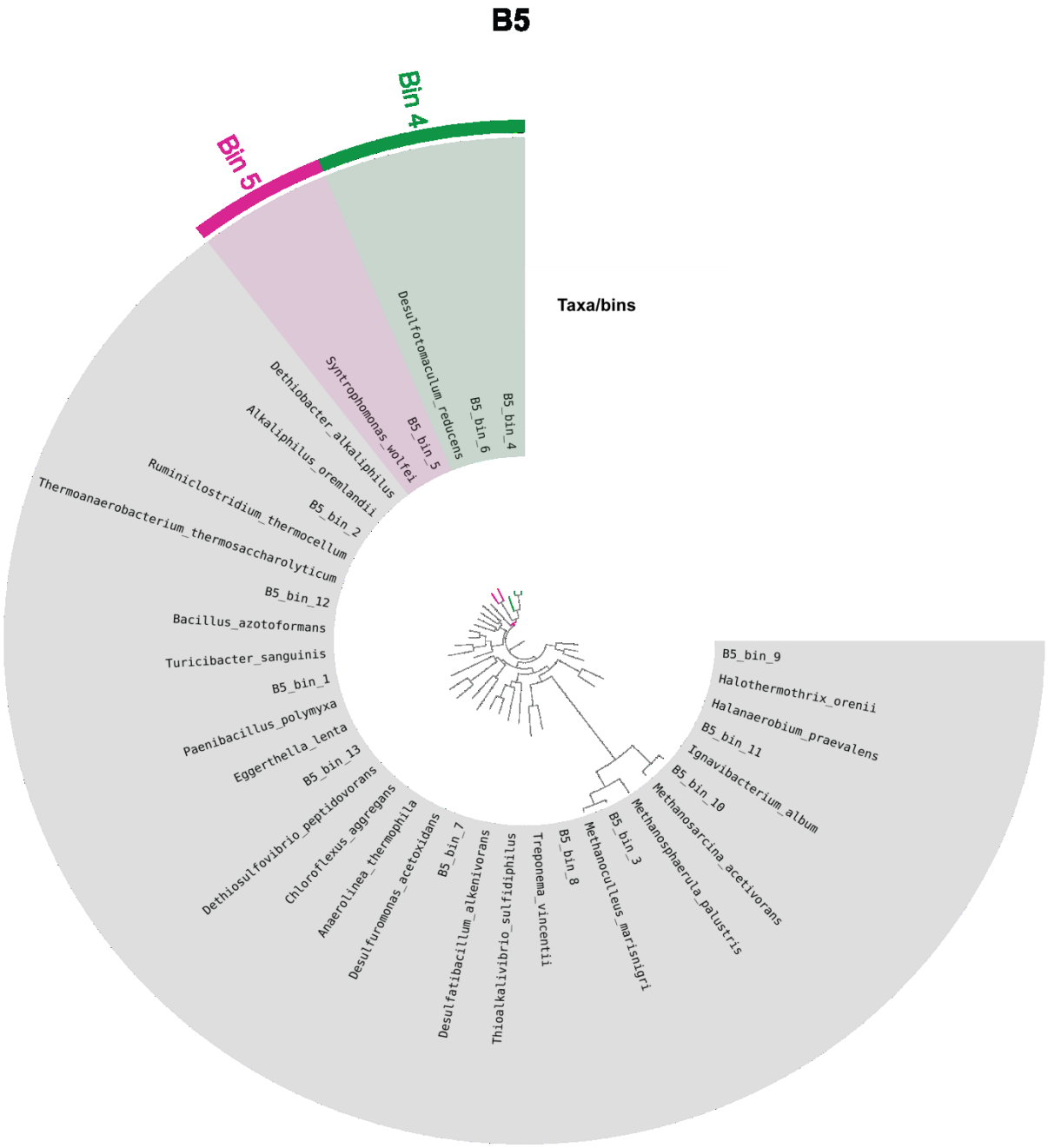

Fig. S6 ANVI'O concatenated proteins based phylogenetic affiliation of metagenomic bins involved in the benzoate degradation pathway (Fig. 6) from the B5 enrichment.

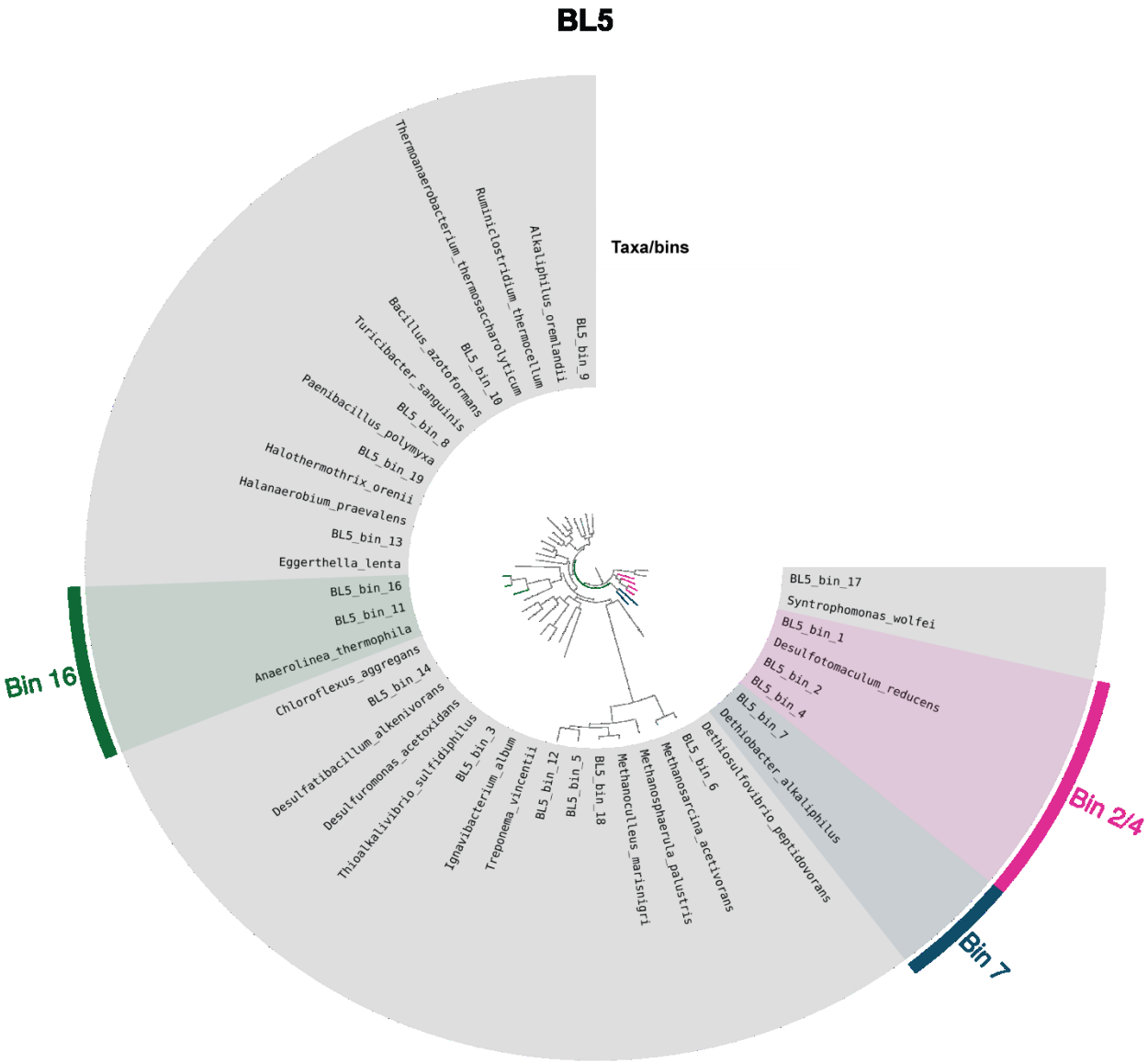

Fig. S7 ANVI'O concatenated proteins based phylogenetic affiliation of metagenomic bins involved in the benzoate degradation pathway (Fig. 6) from the BL5 enrichment.

Chapter Four

Temperature Controls Crystalline Iron Oxide Utilization by Microbial Communities in Methanic Ferruginous Marine Sediment Incubations

Declaration on the contribution of David A. Aromokeye to chapter four

Name of the candidate:	David A. Aromokeye
Title of the thesis:	Iron oxide driven methanogenesis and methanotrophy in methanic sediments of Helgoland Mud Area, North Sea
Authors of manuscript:	David A. Aromokeye, Tim Richter-Heitmann, Oluwatobi E. Oni, Ajinkya Kulkarni, Sabine Kasten and Michael W.Friedrich
Article published:	Frontiers in Microbiology 2018, doi:10.3389/fmicb.2018.02574

Contribution of the candidate in % of the total work load

Experimental concept and design:	ca. 60 %
Experimental work/acquisition of experimental data:	ca. 100 %
Data analysis and interpretation:	ca. 100 %
Preparation of figures and tables:	ca. 60 %
Drafting of manuscript:	ca. 90 %

Temperature Controls Crystalline Iron Oxide Utilization by Microbial Communities in Methanic Ferruginous Marine Sediment Incubations

David A. Aromokeye[1,2,3], Tim Richter-Heitmann[1], Oluwatobi E. Oni[1,2], Ajinkya Kulkarni[1,2,3], Xiuran Yin[1,2,3], Sabine Kasten[2,4,5] and Michael W. Friedrich[1,2,*].

[1]Microbial Ecophysiology Group, Faculty of Biology/Chemistry, University of Bremen, Bremen, Germany

[2]MARUM, Center for Marine Environmental Sciences, University of Bremen, Bremen, Germany

[3]International Max Planck Research School for Marine Microbiology, Max-Planck-Institute for Marine Microbiology, Bremen, Germany

[4]Alfred Wegener Institute Helmholtz Centre for Polar and Marine Research, Bremerhaven, Germany

[5]University of Bremen, Faculty of Geosciences, Bremen, Germany

*Correspondence:

Michael W. Friedrich,

[1]Microbial Ecophysiology Group, Faculty of Biology/Chemistry & MARUM, University of Bremen, PO Box 33 04 40, D-28334 Bremen, Germany

Email: michael.friedrich@uni-bremen.de

Keywords: DIET, temperature control, marine sediment, iron reduction, methanogenesis, microbial community analysis

Running title: Temperature control of microbe-iron oxide interactions

Abstract

Microorganisms can use crystalline iron minerals for iron reduction linked to organic matter degradation or as conduits for direct interspecies electron transfer (mDIET) to syntrophic partners, e.g., methanogens. The environmental conditions that lead either to reduction or conduit use are so far unknown. We investigated microbial community shifts and interactions with crystalline iron minerals (hematite and magnetite) in methanic ferruginous marine sediment incubations during organic matter (glucose) degradation at varying temperatures. Iron reduction rates increased with decreasing temperature from 30 °C to 4 °C. Both hematite and magnetite facilitated iron reduction at 4 ºC, demonstrating that microorganisms in the methanic zone of marine sediments can reduce crystalline iron oxides under psychrophilic conditions. Methanogenesis occurred, however at higher rates with increasing temperature. At 30 ºC, both hematite and magnetite accelerated methanogenesis onset and maximum process rates. At lower temperatures (10 ºC and 4 ºC), hematite could still facilitate methanogenesis but magnetite served more as an electron acceptor for iron reduction than as a conduit. Different temperatures selected for different key microorganisms: at 30 ºC, members of genus *Orenia,* Halobacteroidaceae, at 10 ºC, *Photobacterium* and the order Clostridiales, and at 4 ºC *Photobacterium* and *Psychromonas* were enriched. Members of the order Desulfuromonadales harbouring known dissimilatory iron reducers were also enriched at all temperatures. Our results show that crystalline iron oxides predominant in some natural environments can facilitate electron transfer between microbial communities at psychrophilic temperatures. Furthermore, temperature has a critical role in determining the pathway of crystalline iron oxide utilization in marine sediment shifting from conduction at 30 °C to predominantly iron reduction at lower temperatures.

Introduction

Iron oxide minerals are ubiquitous in natural environments (Straub et al., 2001; Kappler and Straub, 2005; Braunschweig et al., 2013) and exist chemically as amorphous, poorly crystalline or crystalline phases (Cornell and Schwertmann, 2003). Microbial reduction of amorphous and poorly crystalline iron oxide phases is thermodynamically more favourable than using crystalline phases (Weber et al., 2006); therefore, microorganisms preferentially utilize less crystalline phases for dissimilatory and fermentation-linked iron reduction (Munch and Ottow, 1980; Munch and Ottow, 1983; Lovley and Phillips, 1986; 1987; Lovley, 1991). There is growing evidence that the more crystalline iron oxide mineral phases may nevertheless support microbial metabolism either as (I) terminal electron acceptors during oxidation of complex organic matter or fermentation end products such as acetate and H_2 (Lentini et al., 2012; Hori et al., 2015) or as (II) conduits for electron transfer between microorganisms living in syntrophic association (Kato et al., 2012; Liu et al., 2015).

Several incubation studies with marine sediments have previously demonstrated the feasibility of microbial reduction of amorphous iron(III) and poorly crystalline phases like ferrihydrite under psychrophilic (Zhang et al., 1999; Stapleton Jr et al., 2005; Roh et al., 2006; Vandieken et al., 2006), mesophilic (Roden and Lovley, 1993) and thermophilic conditions (Kashefi and Lovley, 2003; Kashefi et al., 2008; Manzella et al., 2013). Microbial reduction of crystalline iron oxides such as goethite (α-FeOOH), hematite (α-Fe_2O_3) and magnetite ($Fe(II)Fe(III)_2O_4$) was previously demonstrated under mesophilic (Roden and Zachara, 1996; Lentini et al., 2012; Hori et al., 2015) but not under psychrophilic conditions. Meanwhile, elevated concentrations of dissolved Fe^{2+} have been detected in the methanic zone of some sub-seafloor sediments bearing appreciable amounts of these crystalline mineral phases (e.g. Hensen et al., 2003; Riedinger et al., 2005; März et al., 2008; Riedinger et al., 2014; Oni et al., 2015a, Egger et al., 2017). Therefore, microbial reduction of crystalline iron oxides could

be a prime metabolic process in these sediment layers. Despite the large body of work on iron reduction at varying temperature conditions and in various environments, knowledge of the diversity of microorganisms involved in crystalline iron mineral reduction in cold marine sediments is still limited.

Mineral-mediated electron transfer between metabolically dependent microbes is particularly important in methanogenic environments such as flooded rice field soils (Kato et al., 2012; Zhou et al., 2014). Despite mineral-meditated direct interspecies electron transfer (mDIET) being central to the functioning of methane-producing microbial communities, the environmental factors that govern these interactions are yet to be studied (Shrestha and Rotaru, 2014). In contrast to other environments such as rice field soils (Kato et al., 2012; Zhou et al., 2014; Li et al., 2015; Zhuang et al., 2015) freshwater (Jiang et al., 2013; Zhang and Lu, 2016) and coastal sediments (Rotaru et al., 2018), microbial communities capable of mDIET in methanic marine sediments are not known.

Although it is established that microorganisms from different environments can reduce crystalline iron minerals or utilise them as conduits to facilitate electron transfer to syntrophic partners, controls of these interactions under different environmental conditions are not known yet. Here, we posit that temperature controls the mode of crystalline iron minerals utilisation, either reduction, conduction or both. To address this hypothesis, we specifically studied (1) the role of crystalline iron minerals during microbial community shifts in marine sediment incubations under varying temperature conditions, (2) the potential for reduction of crystalline iron minerals in sub-seafloor sediments at different temperatures and (3) identified microbial populations that can interact with crystalline iron minerals in marine sediments under varying temperature regimes.

Materials and Methods

Sampling Site

The Helgoland Mud Area is a highly depositional site of fine-grained mud located in the German Bight, North Sea. The depositional history and geochemical profiles of this site were previously described (Hebbeln et al., 2003; Oni et al., 2015a). Samples were collected using a gravity corer (5 m core length) during RV HEINCKE research expedition HE 443 (54° 05.23' N; 007° 58.04' E) in May 2015. The core HE443/077-1 was stored at 4 °C on board, transported to the laboratory within a few days of core retrieval, and sliced into 25-cm sections. Each 25-cm section was stored at 4 °C in 2.6-L jars, under a headspace of N_2 (99.999 % purity, Linde, Germany).

Incubation Experiments

Anoxic 50-mL slurry incubations were prepared in 120-ml serum vials with sediment from 416–441 and 441–466 cm depths and anoxic sulphate-free artificial sea water (ASW; composition [L^{-1}]: 26.4 g NaCl, 11.2 g $MgCl_2 \cdot 6H_2O$, 1.5 g $CaCl_2 \cdot 2H_2O$ and 0.7 g KCl) at a ratio of 1:3 (w/v) under a headspace of N_2. Incubations (n=9) were supplemented by adding ~ 1020 µmoles of iron oxides (hematite or magnetite; LanXess, Germany) and 68 µmoles of glucose as electron donor. Control incubations ("glucose only", n = 9) were supplemented with 68 µmoles glucose only (Table S1). Control sediment slurry incubations containing iron oxides only were considered not necessary as previous incubation studies with subsurface sediments from the Helgoland mud area demonstrated that endogenous organic matter is not reactive enough to stimulate iron reduction and methanogenesis within tolerable laboratory incubation times (approx. 200 days; (Oni, 2015). The sediments of the Helgoland Mud Area are rich in different phases of iron minerals (up to 0.8 wt %; Oni et al., 2015a). Hence, adding a carbon source (glucose) to the sediment even without adding iron oxides stimulated microbial iron reduction in the sediments. The potential for reduction of amended hematite

(HG) or magnetite (MG) was evaluated by comparing the amount of Fe^{2+} formed in crystalline iron-treated incubations to those of the "glucose only" control (G). Triplicates of each treatment set were incubated statically in the dark at 4 °C, 10 °C, or 30 °C. Triplicate supplementary incubations were set up at 30 °C, for testing the effect of the inhibitor 2-bromoethanesulfonate (BES) on methanogenesis and iron reduction in the presence of crystalline iron oxides. This was achieved by adding ~ 15mM BES to freshly prepared triplicate slurries ("glucose only", magnetite and glucose, hematite and glucose). Another set-up in duplicates was done for all treatments across all temperatures to investigate the effects of pH during glucose fermentation (Table S2).

Analytical Methods

All incubations were first sampled after approximately 12 hours at respective temperatures, and designated as "day 0". One millilitre of slurry was collected under anoxic conditions in 1.5 ml reaction tubes pre-flushed with N_2. HCl extractable Fe(II) was determined for each sample first by mixing 100 µl of slurry from each sample with 100 µl 0.5 M HCl. The mixture was subsequently incubated at room temperature for 24 hours. Afterward, the supernatant was collected by centrifugation (15,300 *g*, 5 mins) followed by spectrophotometric determination of Fe(II). However, we observed high amounts of HCl extractable Fe(II) at day 0 that likely originated from precipitated iron carbonate (e.g., siderite) and sulphur compounds (e.g., FeS) within sediment samples. Given the large background of sediment indigenous Fe(II) compounds, it was not possible to determine accurately the amount of freshly formed Fe(II) over the course of the incubation, which precipitates rather rapidly (Figure S1). Therefore, the aqueous Fe^{2+} measured was used as a proxy for evaluating iron reduction kinetics. This was done by centrifugation of freshly collected anoxic slurry and directly adding 100 µl of supernatant from each centrifuged sample (15,300 *g*, 5 mins) to ferrozine reagent following

Viollier et al. (2000). The rest of the slurry was stored at -20 °C and subsequently used for DNA extraction where required.

Methane concentrations in incubation headspace samples (100 µl) were monitored over time using a gas chromatograph (GC) (Shimadzu GC-2014, Tokyo, Japan) coupled to a methanizer (nickel reactor, CP 11952, Agilent, Germany). GC was equipped with a flame ionisation detector and a packed column (Porapak Q, 2 m x 1/8"; inner diameter 2 mm, mesh range: 80/100; Agilent, Waldbronn, Germany). H_2 served both as carrier gas (99.999 % purity; 500 kPa, 30 ml min^{-1} flow rate) and combustion gas (40 kPa). Compressed air (50 kPa) was used for combustion, while make-up gas was N_2 (500 kPa). Temperature conditions were as follows; detector (200 °C), injector (120 °C), column (70 °C), and methanizer (350 °C). Chromatographic data was recorded using a Peak Simple data system (model 2002, SRI, Bad Honnef, Germany). Methane amounts formed in headspace were calculated using the ideal gas law with incubation temperature as variable. Methanogenesis rates were systematically evaluated for each time-point by dividing the methane concentration change by the time elapsed between two successive time-points measured per replicate ($\Delta[CH_4]*\Delta t^{-1}$).

Nucleic Acid Extraction

One millilitre of slurry from individual incubations, at specific time points, was used for nucleic acid extraction following a modified protocol from Lueders et al. (2004). Nucleic acids were precipitated from aqueous supernatant by adding 2 volumes of 30 % polyethylene glycol (PEG-6000) followed by centrifugation (15,300 *g*, 90 mins at 4 °C). Pellets were washed twice with 500 µl 70 % ethanol (15,300 *g*, 5 mins at 4 °C) followed by elution in 50 µl diethylpyrocarbonate (DEPC) treated water (Carl Roth, Germany). Nucleic acid concentrations were measured with NanoDrop 1000 spectrophotometer (Peqlab Biotechnologie, Erlangen, Germany). For further processing, day 0 samples from the “glucose

only" incubations were taken as day 0 for all incubations. All extracted nucleic acids were stored at -20 °C until use.

Amplification of 16S rRNA Genes and Illumina Hiseq Sequencing

Illumina amplicon sequencing PCR was prepared using primers targeting 16S rRNA genes of either Bacteria or Archaea. Bacteria targeting primers used were Bac515F (5'-GTGYCAGCMGCCGCGGTAA-3'; Parada et al., 2016) and Bac805R (5'-GACTACHVGGGTATCTAATCC-3'; Herlemann et al., 2011). Archaea targeting primers were Arc519F (5'CAGCMGCCGCGGTAA-3'; Ovreås et al., 1997) and Arc806R (GGACTACVSGGGTATCTAAT; Takai & Horikoshi, 2000). Each primer had in addition a unique barcode sequences (8 bp; Hamady et al., 2008) that facilitated multiplexing of several samples in one sequence library.

PCR reaction mix (50 µl) contained 1 x KAPA HiFi buffer, 0.3 mM dNTP mix, 0.25 U KAPA HiFi DNA polymerase (KAPA Biosystems, Germany), 1.5 µM each of forward and reverse primer pairs, and 2 µl of 10x diluted DNA template from each sample. Thermal cycling conditions include initial denaturation at 95 °C for 5 min, final denaturation at 98 °C for 20 sec, 20 sec of annealing at 60 °C, extension at 72 °C for 20 sec and final elongation at 72 °C for 1 min. A total of 28 PCR cycles were run. PCR products were screened by gel electrophoresis before purification using Monarch® PCR & DNA purification kit (New England Biolabs, Germany). PCR products were quantified using Quant-iT PicoGreen dsDNA assay kit (Thermo Fisher Scientific, USA). Based on the measured quantities by PicoGreen, a library of samples was constructed using equimolar amounts from each amplicon. Amplicon library was sequenced at GATC GmbH (Konstanz, Germany) using the Illumina 2*150 base pairs HiSeq 4000 Platform.

Sequence Analysis

Sequence analysis was performed on the QIIME 1.8.0 platform (Caporaso et al., 2010) based on the 16S rRNA gene profiling analysis pipeline recommended by Pylro et al. (2014) with modifications. Forward reads were used as inputs for analysis from which barcodes were extracted followed by de-multiplexing with a Q20 filter quality (Caporaso et al., 2011). De-multiplexed sequences were further quality filtered with USEARCH 8.1 (Edgar, 2010). All sequences were truncated to a length of 143 bp. USEARCH 8.1 was further used to de-replicate sequences, sort them by their abundances and remove singletons. OTU clustering was done using the UPARSE-OTU algorithm (Edgar, 2013) to create an OTU database. Chimeric sequences were automatically discarded by the UPARSE-OTU algorithm during this step. The truncated, non-dereplicated reads were mapped back to the OTU database to create an OTU table. OTUs were classified for their taxonomy based on a 97 % identity threshold using UCLUST (Edgar, 2010) and SILVA database as reference. The final OTU table was used for taxonomic annotations in the downstream analysis of community composition. Bacteria sequence reads from archaea OTU table and Archaea sequence reads from Bacteria OTU table were removed after which absolute numbers of the remaining reads in the respective OTU tables were processed for microbial community analysis (Table S3-S4). For graphical representation, abundance data from the OTU table was scaled to the sum of observation in each sample. The raw sequence data for this study have been submitted to GenBank Short Reads Archive (SRA) under the accession number SRP123441.

Statistical Analysis

Significant influence of hematite and magnetite amendment to methane formation rates was inferred by performing post hoc analysis with Tukey procedures for each temperature and time point. The general linear hypothesis test for triplicates with default adjustments for

multiple testing was applied (Hothorn et al., 2008) within the R environment (R Core Team 2018; R version 3.4.4).

Results

Microbial Iron Reduction and Methanogenesis

Microbial iron reduction, tracked by increasing Fe^{2+} concentrations in the aqueous phase over incubation time, was evident across all temperatures (Figure 1A, B and C). At 4 °C, Fe^{2+} concentrations were considerably higher in magnetite-glucose amended (MG) and hematite-glucose amended (HG) incubations in comparison to the "glucose only" control (G). This implies that reduction of magnetite and hematite occurred, albeit more pronounced in the case of magnetite (Figure 1A). At 10 °C, iron reduction was more pronounced in MG incubations than in G and HG incubations (Figure 1B). Reduction of the crystalline iron oxides was not observed at 30 °C as similar concentrations of Fe^{2+} were detected in G, MG and HG incubations (Figure 1C). In general, the potential for microbial iron reduction increased with decrease in temperature from 30 °C to 4 °C (Figure 2). By comparing the maximum amounts of Fe^{2+} observed in each treatment (Figure 2), we could show that in the MG treatments at 4 ºC, 2.5-fold more Fe^{2+} were detected than at 30 ºC. Similarly, hematite also stimulated 1.8-fold more Fe^{2+} at 4 ºC compared to the same treatments at 30 ºC. Although additional iron oxides were not added to the G treatments, 1.4-fold more Fe^{2+} was measured at 4 ºC compared to 30 ºC.

As a measure for the occurrence of mDIET as implied in previous studies (see Lovley 2017 and references therein), we followed methane formation in all incubations assuming that the presence of (semi)conductive iron minerals such as hematite and magnetite would facilitate more efficient electron transfer to methanogenic archaea. Methanogenesis occurred after Fe^{2+} concentrations in the aqueous phase levelled off across all temperatures (Figure 1D, 1E, 1F). Based on the amounts of CH_4 measured in the headspace across all incubations and the expected stoichiometry from glucose fermentation assuming all 68 µmoles electrons from

glucose is turned over to CH_4, methanogenesis was the dominant sink for electrons across all temperatures (Table 1). At 30 °C, onset of methanogenesis was observed after 23 days and continued until 47 days (Figure 1F). Methanogenesis started much later at 10 °C (after 120 days) and continued until no further increase in CH_4 amounts was detected after 216 days (Figure 1E). At 4 ºC, onset of methanogenesis was not observed after the initial 200 days. However, we observed after two years (~ 780 days, Figure 1D) that methanogenesis was completed in HG incubations but continued in the MG and G incubations (898 days). Methanogenesis rates were lower with decrease in temperature from 30 ºC to 4 ºC (Figure 3A, 3B, 3C). Across all temperatures, hematite enhanced methanogenesis in HG incubations such that both the onset and the maximum rates of methane formation were reached faster compared to G incubations (Figure 3A, 3B, 3C). Magnetite, similarly to hematite also enhanced the onset and maximum rates of methanogenesis; however, this was only observed at 30 ºC (Figure 3C). At 10 ºC, the enhanced onset of methanogenesis with magnetite was observed in only 2 of 3 replicates (Figure 3B). At 4 ºC, addition of magnetite did not enhance methanogenesis (Figure 3A). In summary, we found that hematite enhanced methanogenesis both in terms of acceleration and maximum process rates, whereas the magnetite only improved its acceleration (i.e., the time between process onset and reaching maximum process rates), compared to incubations without iron oxide amendments.

In order to assess the role of methanogenesis in electron flow through iron oxides, methanogenesis was specifically inhibited by adding BES (15 mM) to incubations (30 ºC). Based on the Fe^{2+}concentrations measured, there was no difference in the rates of iron reduction in the presence of hematite and magnetite when compared to the glucose + BES incubations (Figure S2).

Microbial Community Shifts at Varying Incubation Temperatures

Microbial community composition in slurry incubations was analysed in order to identify key microorganisms involved in glucose and iron oxide utilization. Because of the different temperature regimes applied, microbial activities were different, which is reflected in the different time intervals of sampling (see Figure S3, S4, S5). At 4 ºC, the genera *Photobacterium* and *Psychromonas* were dominant and their relative abundance was highest after 21 days (ranging from 24–34 % respectively; Figure 4). While sequences related to *Psychromonas* were not observed at 10 ºC, *Photobacterium* spp. were enriched (10–15 % after 90 days; Figure 4). Both *Psychromonas* and *Photobacterium* populations were absent at 30 ºC; Figure 4. Members of the order Clostridiales were observed across all temperatures and were mostly dominant at 10 ºC (up to 36 % at day 90). Within the order Clostridiales, the genus *Fusibacter* was observed across all temperatures (Figure S7). However, there were differences in the other dominant Clostridiales family or genus observed at the different temperatures. For example, *Alkalibacter* spp. was low in relative abundance at 4 ºC (<1 %); enriched at 10 ºC (3–6 % after 90 days) in all treatments and was only observed in the magnetite amended treatment at 30 ºC (4 %, day 23). Family JTB 215 and Clostridiaceae_1 were only enriched at 30 ºC (Figure S7). GoM-GC232-4463-Bac1 was enriched at 10 ºC and 30 ºC but not at 4 ºC (Figure S7). Representatives of the order NB1-n (phylum Tenericutes) were present, but only at 10 ºC after 200 days (4–8 %; Figure 4). At 30 ºC, members of the genus *Orenia* were enriched (26–36 % after 23 days; Figure 4) but were not observed under psychrophilic conditions.

Known iron-reducing taxa detected in enrichments were related to the order Desulfuromonadales and the genus *Sulfurospirillum* (family Campylobacteraceae, class Epsilonproteobacteria) (Figure 5). At low temperatures, where we obtained indications that magnetite (4 ºC and 10 ºC) and hematite (4 ºC) reduction occurred, members of the order

Desulfuromonadales were more abundant in MG and HG compared to the control, G (Figure 4). While Desulfuromonadales were also present at 30 ºC, their relative abundance was lower in the iron oxide amendments (Figure 5). This correlated with the observations that hematite and magnetite were not reduced at 30 ºC (Figure 1). Within Desulfuromonadales, genus *Desulfuromonas* was the dominant taxa enriched at 4 ºC and 10 ºC (up to 11 %; Figure S8). In contrast at 30 ºC, the genus *Pelobacter* was dominant (up to 10 %; Figure S8). The relative abundance of *Pelobacter* was less than 0.5 % at 4 ºC and 10 ºC (Figure S8). *Desulfuromonas* were only enriched in the magnetite amended treatment (4.2 ± 0.5 % at day 50) at 30 ºC. At 4 ºC, the relative abundance of members of the genus *Sulfurospirillum* in MG was higher after 83 days (9 ± 1.8 %) compared to HG (3 ± 0.2 %) and G (4.08 ± 2 %). *Sulfurospirillum* was not enriched at 10 ºC or 30 ºC.

Among Archaea, *Methanosarcina* were the only methanogens enriched across all incubations regardless of incubation temperature (Figure 6). Generally, the relative abundance of other Archaea taxa did not change except at time-points when methanogenesis occurred and *Methanosarcina* was enriched (Figure S3-S5).

Discussion

Crystalline Iron Oxides Utilisation Under Temperature Control

Iron oxide minerals are known as electron acceptors but their important role as conductors for facilitating microbial interspecies electron transfer was only recently recognized (Kato et al., 2012; Jiang et al., 2013; Cruz Viggi et al., 2014; Zhou et al., 2014). Conversely, factors are unknown that determine whether iron oxides are reduced in dissimilatory fashion or used to facilitate electron flow between microbial populations in the environment. Here, we demonstrate that temperature has a pronounced effect on crystalline iron oxide utilization in marine sediment incubations. A shift from low (i.e., 4–10 °C) to high temperature (i.e. 30 °C) resulted in lower iron reduction rates indicated by higher amounts of Fe^{2+} detected at lower

temperatures (Figure 2). Consequently, electron transfer towards methanogenesis was enhanced in the presence of hematite or magnetite, especially at 30 ºC (Figure 3A, 3B, 3C). Thus, temperature appears to be a prime regulator controlling the mode (reduction or conduction) of iron oxide utilization by microorganisms in marine sediments. The underlying mechanisms are most likely multifactorial encompassing (1) community composition changes, (2) the reaction thermodynamics and pathways of degradation involved, and (3) specific adaptations to temperature.

Firstly, temperature is known to have a strong effect on metabolic adaptation and microbial community composition, both, for planktonic and benthic microorganisms (Fuhrman, 2009; Robador et al., 2009; Blake et al., 2015). Bottom water temperatures overlying the sediments of the Helgoland Mud Area are fluctuating annually between 2 °C in March and 19 °C in August (Oehler et al., 2015). Thus, incubations at 4 °C and 10 °C reflected seasonal *in situ* temperatures, whereas 30 °C reflected a strong temperature shift. Not surprisingly, induced by different temperature regimes and glucose amendment, different key microorganisms were enriched (Figure S3, S4, S5) similar to other studies (Upton et al., 1990; Robador et al., 2009; Adams et al., 2010; Blake et al., 2015). In addition to their largely different taxonomic affiliations, temperature selected for communities that differed in their capabilities of crystalline iron oxide utilization (Figure 2, 3). Secondly, thermodynamics of the reactions involved seems to favour different physiological guilds competing for common electron donors. For example, methanogenesis is known to be thermodynamically more feasible under warmer (mesophilic) temperatures (Zeikus and Winfrey, 1976; Van Hulzen et al., 1999; Fey and Conrad, 2000; Yao and Conrad, 2000) than under lower temperatures (Conrad and Wetter, 1990), and can have a strong effect on carbon fractionation in temperature dependent methanogenesis (Fey et al., 2004). Nevertheless, methanogenic activity in freshwater and arctic wetland sediments has been observed over a wide temperature range from 1 °C to 45 °C (Zeikus and Winfrey, 1976; Franzmann et al., 1992; Simankova et al., 2003; Blake et al.,

2015). Some methanogenic isolate are psychrophiles. For example, *Methanogenium frigidum*, isolated from Ace Lake in Antarctica, which grows optimally at 15 °C but not above 18 - 20 °C (Franzmann et al., 1997). Sequences of methanogenic archaea were detected in sediments of the Helgoland Mud Area (Oni et al., 2015b) suggesting a potential for methanogenesis in these sediments. Although we did not observe methanogenesis at 4 °C during the initial time-course of the experiments (200 days), its subsequent occurrence was only a matter of incubation time (~ 780 days). *Methanosarcina* were the only methanogens enriched from our incubations regardless of incubation temperature or addition of crystalline iron oxides (Figure 6) and majority of the electrons from glucose fermentation ended up being used by *Methanosarcina* for methane formation (Table 1). Microorganisms are known for specific temperature adaptations such as membrane fluidity, composition and expressed amount of enzymes, as well as specific regulation response for coping with temperature stress (D'Amico et al., 2006; De Maayer et al., 2014). Our results show that microbial iron reduction was more feasible at lower temperatures (4 °C and 10 °C) than at 30 °C, to the extent that both amended crystalline iron minerals were reduced at 4 °C (Figure 1A, 2). When methanogenesis was BES inhibited in 30 °C incubations (Figure S2), reduction of magnetite and hematite still remained low. Similar Bacteria communities were observed in the BES incubations when compared to the 30 °C incubations without BES (Figure S5 and S6). Thus, the absence of enhanced iron reduction with magnetite or hematite addition at 30 °C was not due to the onset and transfer of electrons from glucose fermentation to methanogenesis. Rather, the microorganisms enriched in the sediments at 4 °C and 10 °C are better adapted to perform crystalline iron oxide reduction than those enriched at 30 °C. Similarly, iron reduction rates increased with a decrease in temperature from 15 °C to 4 °C in ferrihydrite reducing slurry incubations from glacial sediments (Nixon et al., 2017).

The observed strong increase in methanogenesis rates (up to twofold) in the presence of hematite (Figure 1 and 3) suggests that (semi)conductive hematite may have served as conduit in our marine sediment incubations, facilitating mDIET. This is also the first study that demonstrates that mineral mediated enhancement of methanogenesis can occur at psychrophilic temperatures down to 4 ºC. Therefore, mDIET based enhancement of methanogenesis, which has only been previously demonstrated in enrichments from rice field soils and river sediments (see Lovley 2017); can also enhance methanogenesis in cold marine sediments. Electrons from glucose fermentation were likely shunted to methanogens via the (semi)conductive, crystalline iron minerals (i.e. hematite and magnetite). Similarly, Kato et al (2012) found an enhancement of methane formation in rice field soil incubations, which was accompanied by stimulated growth of *Geobacter* spp in incubations amended with hematite and magnetite. Comparable effects on methanogenesis were observed with magnetite at 30 °C, but at 10 °C and 4 °C, magnetite served preferentially as an electron acceptor than as a conduit (Figure 1, 2, 3). At 4 °C, hematite apparently played a dual role, acting initially, as an electron acceptor and subsequently facilitating electron transfer when the conditions were favourable for methanogenesis to occur. More Fe^{2+} was observed in hematite + glucose incubations compared to the glucose amended control but methanogenesis was subsequently enhanced in hematite amended incubations (Figure 1A, 1D, 3A). Likewise, Zhou et al. (2014), in rice field soil enrichments incubated at 30 °C, observed a similar effect in the presence of magnetite.

Since sediment incubations are less defined than pure culture studies, other potential mechanisms could have been operative in addition to or instead of mDIET. Magnetite could have served as electron acceptor (Yang et al. 2015), or as part of an iron redox cycle, could have been important in the production of H_2 from acetate to support hydrogenotrophic methanogenesis (Jiang et al. 2013); however, iron reduction was not observed in our

incubations concurrently while methanogenesis was on-going (Figure. 1). More research is required to elucidate the exact mechanism for enhanced methanogenesis in the presence of crystalline iron oxides.

Crystalline Iron Oxide Reducing Bacteria Under Psychrophilic Conditions

Due to easier accessibility by microorganisms and thermodynamic favourability (Weber et al., 2006), poorly crystalline iron minerals have been mostly used in studying iron reduction in samples from sedimentary environments (Roden and Lovley, 1993; Zhang et al., 1999; Vandieken et al., 2006; Hori et al., 2015). This has led to the lack of knowledge of the diversity of microorganisms capable of reducing crystalline iron minerals, despite their abundance in natural environments (Hori et al., 2015).

The increase in the relative abundance of *Sulfurospirillum* with increasing concentration of Fe^{2+} (Figure 1A, 5) implies their involvement in dissimilatory reduction of magnetite at 4 °C. Members of the genus *Sulfurospirillum* have been previously linked to growth with poorly crystalline iron oxides at mesophilic temperatures. For example, *Sulfurospirillum barnesii* can use amorphous Fe(III) and ferrihydrite as terminal electron acceptors (Stolz et al., 1999; Zobrist et al., 2000) while *S. deleyianum* is capable of ferrihydrite dependent growth coupled to sulphur cycling (Straub and Schink, 2004; Lohmayer et al., 2014). The increase in relative abundance of Desulfuromonadales over time in the 4 ºC incubations correlated with the iron reduction kinetics, i.e. a higher relative abundance of Desulfuromonadales sequences was observed in incubations with higher Fe^{2+} concentration (Figure 1A, 5). At 10 ºC in incubations with added magnetite, a higher abundance of Desulfuromonadales sequences also correlated with the higher Fe^{2+} concentrations measured (Figure 4, 1B). Along with the different temperature regimes, the dominant genus enriched within the Desulfuromonadales order were clearly different. *Desulfuromonas* was dominant at lower temperatures while *Pelobacter* was dominant at 30 ºC (Figure S8). *Desulfuromonas* species are capable of

reducing poorly crystalline iron oxides in marine surface sediments (Roden and Lovley, 1993; Vandieken et al., 2006). Here, we show they are involved in magnetite reduction as well under psychrophilic conditions in the marine sub-surface.

mDIET-Linked Microorganisms Under Mesophilic and Psychrophilic Conditions

Most known members of the family Halobacteroidaceae ferment carbohydrates to acetate, ethanol, H_2, and CO_2 (Oren, 2014). Besides, some species are homoacetogenic but can also use a variety of electron acceptors, e.g., selenate, arsenate, and iron oxides (Oren, 2014). Therefore, the dominance of the genus *Orenia,* regardless of the presence or absence of the crystalline iron oxides within the enriched communities at 30 °C (Figure 4), suggests that members of the genus *Orenia* were largely responsible for glucose fermentation. In addition, *Orenia* might have been involved in iron reduction together with *Pelobacter spp.*, who are capable of fermentative and dissimilatory Fe(III) reduction (Lovley et al., 1995). Syntrophic interactions that occur between microbes and iron minerals during methanogenic fermentation of organic matter mediate the electron transfer during these interactions (Kato et al., 2012; Yang et al., 2015). Although an isolated species within the genus, *Orenia metallireducens* strain Z6, can reduce both poorly crystalline and crystalline iron oxides (Dong et al., 2016), the reduction of amended magnetite and hematite was not detectable based on a lack of increasing Fe^{2+} concentrations at 30 °C. Thus, it is likely that the enriched members of the genus *Orenia* detected here shuttled electrons from glucose fermentation to *Methanosarcina* via mDIET to the amended hematite or magnetite; this in turn accelerated the onset of methane formation and enhanced the process rates (Figure 3C).

The enrichment of members of the known psychrophilic genera *Photobacterium* and *Psychromonas* at 4 ºC might be linked to glucose fermentation (Seo et al., 2005; Auman et al., 2006). Enrichment of different Clostridiales sub-groups at different temperatures (Figure S7) demonstrates the versatility of the order Clostridiales to thrive at various temperature regimes.

The order Clostridiales is well known for harbouring a wide variety of fermenting microorganisms. For example, the genus *Fusibacter* which was enriched across all temperatures studied (Figure S7) has been shown to be capable of glucose metabolism (Ravot et al., 1999; Hania et al., 2012; Fadhlaoui et al., 2015; Smii et al., 2015). Some organisms within the order Clostridiales are also exoelectrogens (Jiang et al., 2013; Fuller et al., 2014; Moscoviz et al., 2017), thus, they can potentially transfer electrons to methanogens directly via mDIET in our incubations. This in turn, may have resulted in the enhanced rates of methanogenesis observed at 10 ºC and 4 ºC.

Conclusion

Our results open a new window into understanding environmental regulators of microbial interaction and utilization of crystalline iron minerals. We identified temperature as one of the regulators important for the mode of crystalline iron mineral utilization by microorganisms. We also demonstrate the potential for mDIET to occur in sub-surface marine sediments and at temperatures down to 4 ºC. Thus, crystalline iron oxides may facilitate electron transfer between microorganisms thriving in anoxic cold sediments in addition to serving as electron acceptors. This extended role of crystalline iron oxides in microbial metabolism could have an impact on the biogeochemical cycling of carbon in sedimentary environments by accelerating the rate of organic carbon biomineralisation. More work is certainly required to identify specific molecular adaptations to iron reduction or utilization as conduit under temperature control.

Funding

This work was supported by the Deutsche Forschungsgemeinschaft (DFG) Cluster of Excellence 309 "The Ocean in the Earth System – MARUM – Center for Marine Environmental Sciences", the Alfred Wegener Institute Helmholtz Centre for Polar and Marine Research and the University of Bremen.

Acknowledgements

The authors thank the captain, crew and scientists of RV HEINCKE expedition 443 to the Helgoland Mud Area.

Author contributions

DAA, OO, TR and MWF designed the experiments. DAA performed the experiments and data analysis with support from OO, AK, XY, TR, and MWF. MWF secured funding for this research. SK carried out the HE433 expedition and provided sediment samples for the experiments. DAA (90 %) and MWF (10 %) wrote the manuscript with contributions from all co-authors.

Conflict of Interest Statement

The authors declare no conflict of interest preventing the publication of this article.

References

Adams, H.E., Crump, B.C., and Kling, G.W. (2010). Temperature controls on aquatic bacterial production and community dynamics in arctic lakes and streams. *Environ. Microbiol.* 12(5)**,** 1319-1333. doi: 10.1111/j.1462-2920.2010.02176.x.

Auman, A.J., Breezee, J.L., Gosink, J.J., Kampfer, P., and Staley, J.T. (2006). *Psychromonas ingrahamii* sp. nov., a novel gas vacuolate, psychrophilic bacterium isolated from Arctic polar sea ice. *Int. J. Syst. Evol. Microbiol.* 56(Pt 5)**,** 1001-1007. doi:10.1099/ijs.0.64068-0.

Blake, L.I., Tveit, A., Øvreås, L., Head, I.M., and Gray, N.D. (2015). Response of methanogens in Arctic sediments to temperature and methanogenic substrate availability. *PloS one* 10(6)**,** e0129733. doi: 10.1371/journal.pone.0129733

Braunschweig, J., Bosch, J., and Meckenstock, R.U. (2013). Iron oxide nanoparticles in geomicrobiology: From biogeochemistry to bioremediation. *New Biotechnol.* 30(6)**,** 793-802. doi: http://dx.doi.org/10.1016/j.nbt.2013.03.008.

Caporaso, J.G., Kuczynski, J., Stombaugh, J., Bittinger, K., Bushman, F.D., Costello, E.K., et al. (2010). QIIME allows analysis of high-throughput community sequencing data. *Nat. Meth.* 7(5)**,** 335-336.

Caporaso, J.G., Lauber, C.L., Walters, W.A., Berg-Lyons, D., Lozupone, C.A., Turnbaugh, P.J., et al. (2011). Global patterns of 16S rRNA diversity at a depth of millions of sequences per sample. *Proc. Natl. Acad. Sci.* 108(Supplement 1)**,** 4516-4522. doi: 10.1073/pnas.1000080107

Conrad, R., and Wetter, B. (1990). Influence of temperature on energetics of hydrogen metabolism in homoacetogenic, methanogenic, and other anaerobic bacteria. *Arch. Microbiol.* 155(1)**,** 94-98. doi: 10.1007/bf00291281.

Cornell, R.M., and Schwertmann, U. (2003). *The iron oxides: structure, properties, reactions, occurrences and uses.* 2nd Edition. VCH Weinheim. John Wiley & Sons.

Cruz Viggi, C., Rossetti, S., Fazi, S., Paiano, P., Majone, M., and Aulenta, F. (2014). Magnetite particles triggering a faster and more robust syntrophic pathway of methanogenic propionate degradation. *Environ. Sci. Technol.* 48(13)**,** 7536-7543. doi: 10.1021/es5016789

D'Amico, S., Collins, T., Marx, J.-C., Feller, G., and Gerday, C. (2006). Psychrophilic microorganisms: Challenges for life. *EMBO Rep.* 7(4)**,** 385-389. doi: 10.1038/sj.embor.7400662.

De Maayer, P., Anderson, D., Cary, C., and Cowan, D.A. (2014). Some like it cold: Understanding the survival strategies of psychrophiles. *EMBO Rep.* 15(5)**,** 508-517. doi: 10.1002/embr.201338170.

Dong, Y., Sanford, R.A., Boyanov, M.I., Kemner, K.M., Flynn, T.M., O'Loughlin, E.J., et al. (2016). *Orenia metallireducens* sp. nov. strain Z6, a novel metal-reducing member of the phylum Firmicutes from the deep subsurface. *Appl. Environ. Microbiol.* 82(21)**,** 6440-6453. doi: 10.1128/aem.02382-16

Edgar, R.C. (2010). Search and clustering orders of magnitude faster than BLAST. *Bioinformatics* 26(19)**,** 2460-2461. doi: 10.1093/bioinformatics/btq461

Edgar, R.C. (2013). UPARSE: highly accurate OTU sequences from microbial amplicon reads. *Nat. Meth.* 10(10)**,** 996-998. doi: 10.1038/nmeth.2604

Egger, M., Hagens, M., Sapart, C.J., Dijkstra, N., van Helmond, N.A., Mogollón, J.M., et al. (2017). Iron oxide reduction in methane-rich deep Baltic Sea sediments. *Geochim. Cosmochim. Acta*. 207: 256-276. doi: 10.1016/j.gca.2017.03.019

Fadhlaoui, K., Hania, W.B., Postec, A., Fauque, G., Hamdi, M., Ollivier, B., et al. (2015). *Fusibacter fontis* sp. nov., a sulfur-reducing, anaerobic bacterium isolated from a mesothermic Tunisian spring. *Int. J. Syst. Evol. Microbiol.* 65(10)**,** 3501-3506. doi: 10.1099/ijsem.0.000445

Fey, A., Claus, P., and Conrad, R. (2004). Temporal change of 13C-isotope signatures and methanogenic pathways in rice field soil incubated anoxically at different temperatures. *Geochim. Cosmochim. Acta*. 68(2)**,** 293-306. doi: 10.1016/S0016-7037(03)00426-5.

Fey, A., and Conrad, R. (2000). Effect of temperature on carbon and electron flow and on the archaeal community in methanogenic rice field soil. *Appl. Environ. Microbiol.* 66(11)**,** 4790-4797. doi: 10.1128/aem.66.11.4790-4797.2000

Franzmann, P.D., Liu, Y., Balkwill, D.L., Aldrich, H.C., Conway De Macario, E., and Boone, D.R. (1997). *Methanogenium frigidum* sp. nov., a psychrophilic, H_2-using methanogen from Ace Lake, Antarctica. *Int. J. Syst. Evol. Microbiol.* 47(4)**,** 1068-1072. doi: doi:10.1099/00207713-47-4-1068.

Franzmann, P.D., Springer, N., Ludwig, W., Conway De Macario, E., and Rohde, M. (1992). A methanogenic archaeon from Ace Lake, Antarctica: *Methanococcoides burtonii* sp. nov. *Syst. Appl. Microbiol.* 15(4)**,** 573-581. doi: https://doi.org/10.1016/S0723-2020(11)80117-7.

Fuhrman, J.A. (2009). Microbial community structure and its functional implications. *Nature* 459(7244)**,** 193-199.

Fuller, S.J., McMillan, D.G., Renz, M.B., Schmidt, M., Burke, I.T., and Stewart, D.I. (2014). Extracellular electron transport-mediated Fe(III) reduction by a community of alkaliphilic bacteria that use flavins as electron shuttles. *Appl. Environ. Microbiol.* 80(1)**,** 128-137. doi: 10.1128/aem.02282-13

Hamady, M., Walker, J.J., Harris, J.K., Gold, N.J., and Knight, R. (2008). Error-correcting barcoded primers for pyrosequencing hundreds of samples in multiplex. *Nat. Meth.* 5(3)**,** 235-237.

Hania, W.B., Fraj, B., Postec, A., Fadhlaoui, K., Hamdi, M., Ollivier, B., et al. (2012). *Fusibacter tunisiensis* sp. nov., isolated from an anaerobic reactor used to treat olive-mill wastewater. *Int. J. Syst. Evol. Microbiol.* 62(6)**,** 1365-1368. doi: 10.1099/ijs.0.034603-0

Hebbeln, D., Scheurle, C., and Lamy, F. (2003). Depositional history of the Helgoland Mud Area, German Bight, North Sea. *Geo-Mar. Lett.* 23(2)**,** 81-90. doi: 10.1007/s00367-003-0127-0

Hensen, C., Zabel, M., Pfeifer, K., Schwenk, T., Kasten, S., Riedinger, N., et al. (2003). Control of sulfate pore-water profiles by sedimentary events and the significance of anaerobic oxidation of methane for the burial of sulfur in marine sediments. *Geochim. Cosmochim. Acta* 67(14)**,** 2631-2647. doi: 10.1016/S0016-7037(03)00199-6

Herlemann, D.P.R., Labrenz, M., Jurgens, K., Bertilsson, S., Waniek, J.J., and Andersson, A.F. (2011). Transitions in bacterial communities along the 2000 km salinity gradient of the Baltic Sea. *ISME J.* 5(10)**,** 1571-1579. doi: 10.1038/ismej.2011.41.

Hori, T., Aoyagi, T., Itoh, H., Narihiro, T., Oikawa, A., Suzuki, K., et al. (2015). Isolation of microorganisms involved in reduction of crystalline iron(III) oxides in natural environments. *Front. Microbiol.* 6**,** 386. doi: 10.3389/fmicb.2015.00386

Hothorn, T., Bretz, F., and Westfall, P. (2008). Simultaneous inference in general parametric models. *Biomet. J.* 50(3)**,** 346-363. doi: 10.1002/bimj.200810425

Jiang, S., Park, S., Yoon, Y., Lee, J.-H., Wu, W.-M., Phuoc Dan, N., et al. (2013). Methanogenesis facilitated by geobiochemical iron cycle in a novel syntrophic methanogenic microbial community. *Environ. Sci. Technol.* 47(17)**,** 10078-10084. doi: 10.1021/es402412c.

Kappler, A., and Straub, K.L. (2005). Geomicrobiological cycling of iron. *Rev. Miner. Geochem.* 59(1)**,** 85-108. doi: 10.2138/rmg.2005.59.5

Kashefi, K., and Lovley, D.R. (2003). Extending the upper temperature limit for life. *Science* 301(5635)**,** 934-934. doi: 10.1126/science.1086823

Kashefi, K., Shelobolina, E.S., Elliott, W.C., and Lovley, D.R. (2008). Growth of thermophilic and hyperthermophilic Fe(III)-reducing microorganisms on a ferruginous smectite as the sole electron acceptor. *Appl. Environ. Microbiol.* 74(1)**,** 251-258. doi: 10.1128/aem.01580-07

Kato, S., Hashimoto, K., and Watanabe, K. (2012). Methanogenesis facilitated by electric syntrophy via (semi) conductive iron-oxide minerals. *Environ. Microbiol.* 14(7)**,** 1646-1654. doi: 10.1111/j.1462-2920.2011.02611.x

Lentini, C.J., Wankel, S.D., and Hansel, C.M. (2012). Enriched iron(III)-reducing bacterial communities are shaped by carbon substrate and iron oxide mineralogy. *Front. Microbiol.* 3**,** 404. doi: 10.3389/fmicb.2012.00404

Li, H., Chang, J., Liu, P., Fu, L., Ding, D., and Lu, Y. (2015). Direct interspecies electron transfer accelerates syntrophic oxidation of butyrate in paddy soil enrichments. *Environ. Microbiol.* 17(5)**,** 1533-1547. doi: 10.1111/1462-2920.12576

Liu, F., Rotaru, A.E., Shrestha, P.M., Malvankar, N.S., Nevin, K.P., and Lovley, D.R. (2015). Magnetite compensates for the lack of a pilin-associated c-type cytochrome in extracellular electron exchange. *Environ. Microbiol.* 17(3)**,** 648-655. doi: 10.1111/1462-2920.12485

Lohmayer, R., Kappler, A., Lösekann-Behrens, T., and Planer-Friedrich, B. (2014). Sulfur species as redox partners and electron shuttles for ferrihydrite reduction by *Sulfurospirillum deleyianum*. *Appl. Environ. Microbiol.* 80(10)**,** 3141-3149. doi: 10.1128/aem.04220-13

Lovley, D.R. (1991). Dissimilatory Fe(III) and Mn(IV) reduction. *Microbiol. Rev.* 55(2)**,** 259-287.

Lovley, D.R. (2017). Syntrophy goes electric: Direct interspecies electron transfer. *Annu. Rev. Microbiol.* 71(1)**,** 643-664. doi: 10.1146/annurev-micro-030117-020420.

Lovley, D.R., Phillips, E., Lonergan, D.J., and Widman, P.K. (1995). Fe(III) and S^0 reduction by *Pelobacter carbinolicus*. *Appl. Environ. Microbiol.* 61(6)**,** 2132-2138.

Lovley, D.R., and Phillips, E.J. (1986). Organic matter mineralization with reduction of ferric iron in anaerobic sediments. *Appl. Environ. Microbiol.* 51(4)**,** 683-689.

Lovley, D.R., and Phillips, E.J. (1987). Rapid assay for microbially reducible ferric iron in aquatic sediments. *Appl. Environ. Microbiol.* 53(7)**,** 1536-1540.

Lueders, T., Manefield, M., and Friedrich, M.W. (2004). Enhanced sensitivity of DNA-and rRNA-based stable isotope probing by fractionation and quantitative analysis of isopycnic centrifugation gradients. *Environ. Microbiol.* 6(1)**,** 73-78. doi: 10.1046/j.1462-2920.2003.00536.x

Manzella, M.P., Reguera, G., and Kashefi, K. (2013). Extracellular electron transfer to Fe(III) oxides by the hyperthermophilic archaeon *Geoglobus ahangari* via a direct contact mechanism. *Appl. Environ. Microbiol.* 79(15)**,** 4694-4700. doi: 10.1128/aem.01566-13

März, C., Hoffmann, J., Bleil, U., De Lange, G., and Kasten, S. (2008). Diagenetic changes of magnetic and geochemical signals by anaerobic methane oxidation in sediments of the Zambezi deep-sea fan (SW Indian Ocean). *Mar. Geol.* 255(3)**,** 118-130. doi: 10.1016/j.margeo.2008.05.013

Moscoviz, R., de Fouchécour, F., Santa-Catalina, G., Bernet, N., and Trably, E. (2017). Cooperative growth of *Geobacter sulfurreducens* and *Clostridium pasteurianum* with subsequent metabolic shift in glycerol fermentation. *Sci. Rep.* 7**,** 44334. doi:10.1038/srep44334

Munch, J., and Ottow, J. (1983). Reductive transformation mechanism of ferric oxides in hydromorphic soils. *Ecol. Bull.* 383-394.

Munch, J.C., and Ottow, J.C.G. (1980). Preferential reduction of amorphous to crystalline iron oxides by bacterial activity. *Soil Sci.* 129(1)**,** 15-21. doi: 10.1097/00010694-198001000-00004

Nixon, S.L., Telling, J.P., Wadham, J.L., and Cockell, C.S. (2017). Viable cold-tolerant iron-reducing microorganisms in geographically diverse subglacial environments. *Biogeosciences* 14(6)**,** 1445-1455. doi: 10.5194/bg-14-1445-2017.

Oehler, T., Schlüter, M., and Schückel, U. (2015). Seasonal dynamics of the biogenic silica cycle in surface sediments of the Helgoland Mud Area (southern North Sea). *Cont. Shelf Res.* 107(Supplement C)**,** 103-114. doi: 10.1016/j.csr.2015.07.016

Oni, O.E. (2015) Structure and function of microorganisms in the methanic sediments of the Helgoland mud area, North Sea, Germany. PhD Thesis. Bremen, Germany. University of Bremen. URL: https://elib.suub.uni-bremen.de/peid=D00105135

Oni, O.E., Miyatake, T., Kasten, S., Richter-Heitmann, T., Fischer, D., Wagenknecht, L., et al. (2015a). Distinct microbial populations are tightly linked to the profile of dissolved

iron in the methanic sediments of the Helgoland mud area, North Sea. *Front. Microbiol.* 6**,** 365. doi: 10.3389/fmicb.2015.01290

Oni, O.E., Schmidt, F., Miyatake, T., Kasten, S., Witt, M., Hinrichs, K.-U., et al. (2015b). Microbial communities and organic matter composition in surface and subsurface sediments of the Helgoland mud area, North Sea. *Front. Microbiol.* 6**,** 1290.

Oren, A. (2014). "The order Halanaerobiales, and the families Halanaerobiaceae and Halobacteroidaceae", in *The Prokaryotes:* Firmicutes and Tenericutes*,* eds. E. Rosenberg, E.F. DeLong, S. Lory, E. Stackebrandt & F. Thompson. (Berlin, Heidelberg: Springer Berlin Heidelberg), 153-177. doi: 10.1007/978-3-642-30120-9_218

Ovreås, L., Forney, L., Daae, F.L., and Torsvik, V. (1997). Distribution of bacterioplankton in meromictic Lake Saelenvannet, as determined by denaturing gradient gel electrophoresis of PCR-amplified gene fragments coding for 16S rRNA. *Appl. Environ. Microbiol.* 63(9)**,** 3367-3373.

Parada, A.E., Needham, D.M., and Fuhrman, J.A. (2016). Every base matters: assessing small subunit rRNA primers for marine microbiomes with mock communities, time series and global field samples. *Environ. Microbiol.* 18(5)**,** 1403-1414. doi: 10.1111/1462-2920.13023.

Pylro, V.S., Roesch, L.F.W., Morais, D.K., Clark, I.M., Hirsch, P.R., and Tótola, M.R. (2014). Data analysis for 16S microbial profiling from different benchtop sequencing platforms. *J. Microbiol. Meth.* 107**,** 30-37. doi: 10.1016/j.mimet.2014.08.018

R Core Team (2018) . R: A language and environment for statistical computing. R Foundation for Statistical Computing, Vienna, Austria. URL https://www.R-project.org/.

Ravot, G., Magot, M., Fardeau, M.-L., Patel, B.K., Thomas, P., Garcia, J.-L., et al. (1999). *Fusibacter paucivorans* gen. nov., sp. nov., an anaerobic, thiosulfate-reducing bacterium from an oil-producing well. *Int. J. Syst. Evol. Microbiol.* 49(3)**,** 1141-1147. doi: 10.1099/00207713-49-3-1141

Riedinger, N., Pfeifer, K., Kasten, S., Garming, J.F.L., Vogt, C., and Hensen, C. (2005). Diagenetic alteration of magnetic signals by anaerobic oxidation of methane related to a change in sedimentation rate. *Geochim. Cosmochim. Acta* 69(16)**,** 4117-4126. doi: 10.1016/j.gca.2005.02.004

Riedinger, N., Formolo, M.J., Lyons, T.W., Henkel, S., Beck, A., and Kasten, S. (2014). An inorganic geochemical argument for coupled anaerobic oxidation of methane and iron reduction in marine sediments. *Geobiology* 12(2)**,** 172-181. doi: 10.1111/gbi.12077

Robador, A., Brüchert, V., and Jørgensen, B.B. (2009). The impact of temperature change on the activity and community composition of sulfate-reducing bacteria in arctic versus temperate marine sediments. *Environ. Microbiol.* 11(7)**,** 1692-1703. doi: 10.1111/j.1462-2920.2009.01896.x

Roden, E.E., and Lovley, D.R. (1993). Dissimilatory Fe(III) reduction by the marine microorganism *Desulfuromonas acetoxidans*. *Appl. Environ. Microbiol.* 59(3)**,** 734-742.

Roden, E.E., and Zachara, J.M. (1996). Microbial reduction of crystalline iron(III) oxides: Influence of oxide surface area and potential for cell growth. *Environ. Sci .Technol.* 30(5)**,** 1618-1628. doi: 10.1021/es9506216

Roh, Y., Gao, H., Vali, H., Kennedy, D.W., Yang, Z.K., Gao, W., et al. (2006). Metal reduction and iron biomineralization by a psychrotolerant Fe(III)-reducing bacterium, *Shewanella* sp. strain PV-4. *Appl. Environ. Microbiol.* 72(5)**,** 3236-3244. doi: 10.1128/aem.72.5.3236-3244.2006

Rotaru, A.-E., Calabrese, F., Stryhanyuk, H., Musat, F., Shrestha, P.M., Weber, H.S., et al. (2018). Conductive particles enable syntrophic acetate oxidation between *Geobacter* and *Methanosarcina* from coastal sediments. *Mbio* 9(3)**,** e00226-00218. doi: 10.1128/mBio.00226-18

Seo, H.J., Bae, S.S., Lee, J.H., and Kim, S.J. (2005). *Photobacterium frigidiphilum* sp. nov., a psychrophilic, lipolytic bacterium isolated from deep-sea sediments of Edison Seamount. *Int. J. Syst. Evol. Microbiol.* 55(Pt 4)**,** 1661-1666. doi: 10.1099/ijs.0.63338-0.

Shrestha, P.M., and Rotaru, A.-E. (2014). Plugging in or going wireless: Strategies for interspecies electron transfer. *Front. Microbiol.* 5**,** 237. doi:10.3389/fmicb.2014.0023.

Simankova, M.V., Kotsyurbenko, O.R., Lueders, T., Nozhevnikova, A.N., Wagner, B., Conrad, R., et al. (2003). Isolation and characterization of new strains of methanogens from cold terrestrial habitats. *Sys. Appl. Microbiol.* 26(2)**,** 312-318. doi: 10.1078/072320203322346173.

Smii, L., Hania, W.B., Cayol, J.-L., Joseph, M., Hamdi, M., Ollivier, B., et al. (2015). *Fusibacter bizertensis* sp. nov., isolated from a corroded kerosene storage tank. *Int. J. Syst. Evol. Microbiol.* 65(1)**,** 117-121. doi: 10.1099/ijs.0.066183-0

Stapleton Jr, R.D., Sabree, Z.L., Palumbo, A.V., Moyer, C.L., Devol, A.H., Roh, Y., et al. (2005). Metal reduction at cold temperatures by *Shewanella* isolates from various marine environments. *Aquat. Microb. Ecol.* 38(1)**,** 81-91. doi:10.3354/ame038081

Stolz, J.F., Ellis, D.J., Blum, J.S., Ahmann, D., Lovley, D.R., and Oremland, R.S. (1999). Note: *Sulfurospirillum barnesii* sp. nov. and *Sulfurospirillum arsenophilum* sp. nov., new members of the *Sulfurospirillum* clade of the ε-Proteobacteria. *Int. J. Syst. Evol. Microbiol.* 49(3)**,** 1177-1180. doi: 10.1099/00207713-49-3-1177

Straub, K.L., Benz, M., and Schink, B. (2001). Iron metabolism in anoxic environments at near neutral pH. *FEMS Microbiol. Ecol.* 34(3)**,** 181-186. doi: 10.1111/j.1574-6941.2001.tb00768.x

Straub, K.L., and Schink, B. (2004). Ferrihydrite-dependent growth of *Sulfurospirillum deleyianum* through electron transfer via sulfur cycling. *Appl. Environ. Microbiol.* 70(10)**,** 5744-5749. doi: 10.1128/aem.70.10.5744-5749.2004

Takai, K., and Horikoshi, K. (2000). Rapid detection and quantification of members of the archaeal community by quantitative PCR using fluorogenic probes. *Appl. Environ. Microbiol.* 66(11)**,** 5066-5072. doi: 10.1128/aem.66.11.5066-5072.2000

Upton, A.C., Nedwell, D.B., and Wynn-Williams, D.D. (1990). The selection of microbial communities by constant or fluctuating temperatures. *FEMS Microbiol. Lett.* 74(4)**,** 243-252. doi: 10.1111/j.1574-6968.1990.tb04070.

Van Hulzen, J., Segers, R., Van Bodegom, P., and Leffelaar, P. (1999). Temperature effects on soil methane production: an explanation for observed variability. *Soil Biol. Biochem.* 31(14)**,** 1919-1929. doi: 10.1016/S0038-0717(99)00109-1

Vandieken, V., Mußmann, M., Niemann, H., and Jørgensen, B.B. (2006). *Desulfuromonas svalbardensis* sp. nov. and *Desulfuromusa ferrireducens* sp. nov., psychrophilic, Fe (III)-reducing bacteria isolated from Arctic sediments, Svalbard. *Int. J. Syst. Evol. Microbiol.* 56(5)**,** 1133-1139. doi: 10.1099/ijs.0.63639-0

Viollier, E., Inglett, P., Hunter, K., Roychoudhury, A., and Van Cappellen, P. (2000). The ferrozine method revisited: Fe(II)/Fe(III) determination in natural waters. *Appl. Geochem.* 15(6)**,** 785-790. doi: 10.1016/S0883-2927(99)00097-9

Weber, K.A., Achenbach, L.A., and Coates, J.D. (2006). Microorganisms pumping iron: anaerobic microbial iron oxidation and reduction. *Nat. Rev. Microbiol.* 4(10)**,** 752-764. doi: 10.1038/nrmicro1490

Yang, Z., Shi, X., Wang, C., Wang, L., and Guo, R. (2015). Magnetite nanoparticles facilitate methane production from ethanol via acting as electron acceptors. *Sci. Rep.* 5, 16118. doi: 10.1038/srep16118

Yao, H., and Conrad, R. (2000). Effect of temperature on reduction of iron and production of carbon dioxide and methane in anoxic wetland rice soils. *Biol. Fert. Soils* 32(2)**,** 135-141. doi: /10.1007/s003740000

Zeikus, J., and Winfrey, M. (1976). Temperature limitation of methanogenesis in aquatic sediments. *Appl. Environ. Microbiol.* 31(1)**,** 99-107.

Zhang, C., Stapleton, R.D., Zhou, J., Palumbo, A.V., and Phelps, T.J. (1999). Iron reduction by psychrotrophic enrichment cultures. *FEMS Microbiol. Ecol.* 30(4)**,** 367-371. doi: 10.1111/j.1574-6941.1999.tb00664.x

Zhang, J., and Lu, Y. (2016). Conductive Fe_3O_4 nanoparticles accelerate syntrophic methane production from butyrate oxidation in two different lake sediments. *Front. Microbiol.* 7, 1316. doi: 10.3389/fmicb.2016.01316

Zhou, S., Xu, J., Yang, G., and Zhuang, L. (2014). Methanogenesis affected by the co-occurrence of iron (III) oxides and humic substances. *FEMS Microbiol. Ecol.* 88(1)**,** 107-120. doi: 10.1111/1574-6941.12274

Zhuang, L., Tang, J., Wang, Y., Hu, M., and Zhou, S. (2015). Conductive iron oxide minerals accelerate syntrophic cooperation in methanogenic benzoate degradation. *J. Hazard. Mater.* 293**,** 37-45. doi: 10.1016/j.jhazmat.2015.03.039

Zobrist, J., Dowdle, P.R., Davis, J.A., and Oremland, R.S. (2000). Mobilization of arsenite by dissimilatory reduction of adsorbed arsenate. *Environ. Sci. Technol.* 34(22)**,** 4747-4753. doi: 10.1021/es001068h

Table 1. Average amounts of methane formed and maximum methanogenesis rates per treatment across temperatures

Temperature	Treatment	Average maximum CH_4 amount measured (µmol)	% Expected CH_4 accounted for	Maximum CH_4 formation rate (nmol * ml Slurry^{-1} day^{-1})
4 ºC	Glucose	93.8 ± 27.5	46	1.9 ± 1.5
	Magnetite + Glucose	67 ± 5.8	32.9	1.9 ± 0.3
	Hematite + Glucose	163.1 ± 17.8	80	5.6 ± 0.6
10 ºC	Glucose	103.2 ± 17	50.6	83.5 ± 22
	Magnetite + Glucose	111.7 ± 16.3	54.8	79 ± 12.7
	Hematite + Glucose	136.3 ± 7.2	66.8	141.1 ± 36
30 ºC	Glucose	94.3 ± 8.8	46.2	179.2 ± 38
	Magnetite + Glucose	90.4 ± 2.2	44.3	180 ± 12.7
	Hematite + Glucose	114.7 ± 6.3	56.2	233.7 ± 4.2

Figures

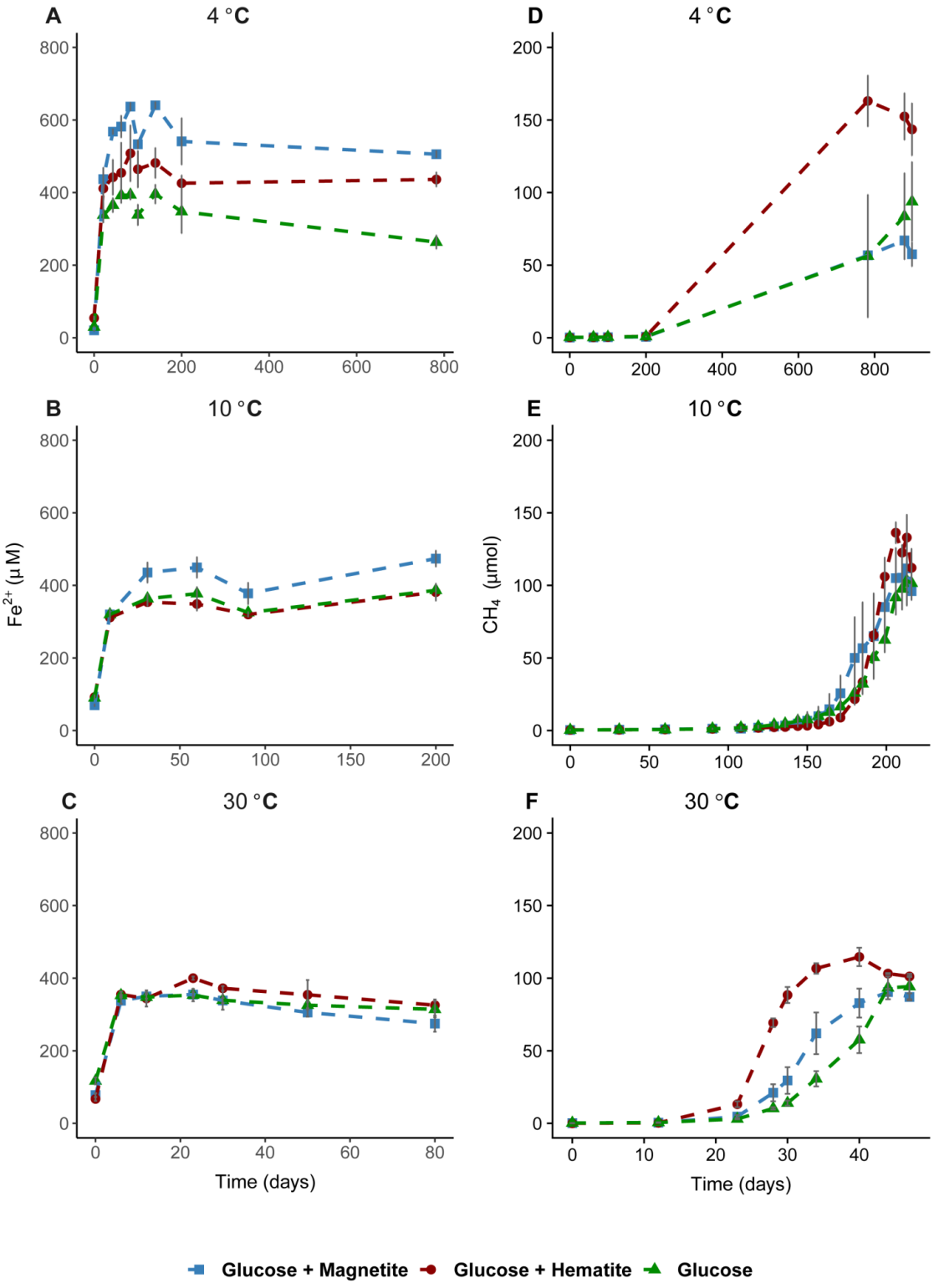

Figure 1: Time course of iron reduction and methane formation in sediment incubations. Left column plots show time course of iron reduction at 4 °C (A), 10 °C (B), and 30 °C (C). Fe^{2+} was measured over time until a stable concentration was observed in the aqueous phase across all temperatures. Right column plots show time course of methane formation at 4 °C (D), 10 °C (E), and 30 °C (F). In panel A, the 800-day time point was added to demonstrate that iron reduction was not on-going in the methanogenesis phase.

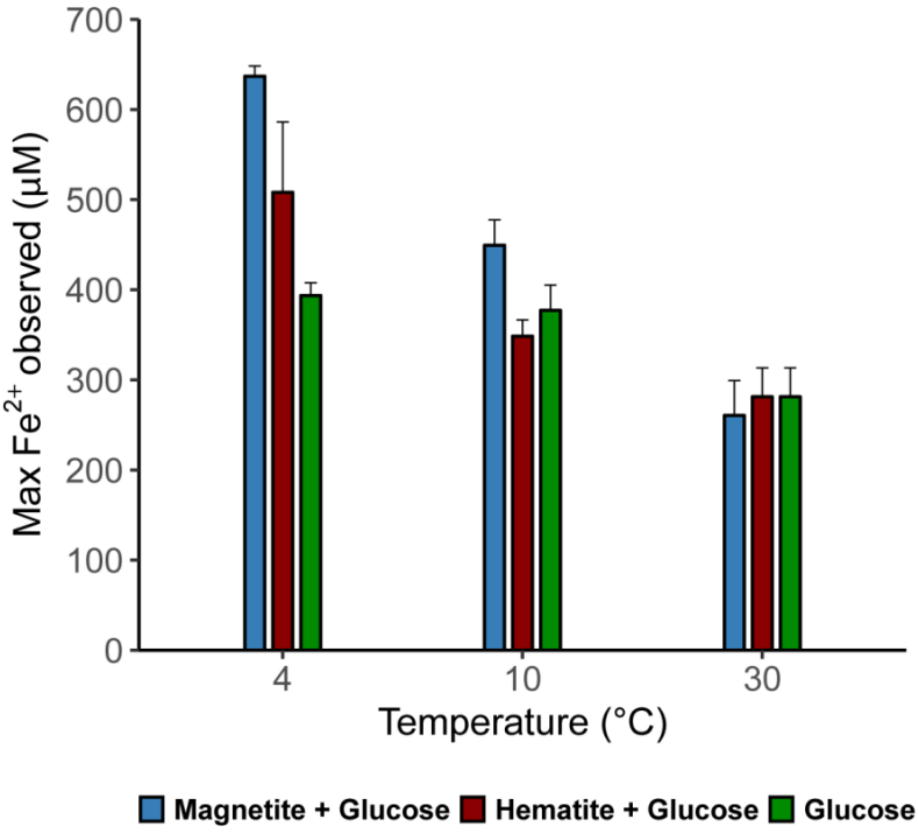

Figure 2: Maximum dissolved Fe (µM) measured in the various treatments across all temperatures showing the effect of crystalline iron minerals on iron reduction in sediment incubations.

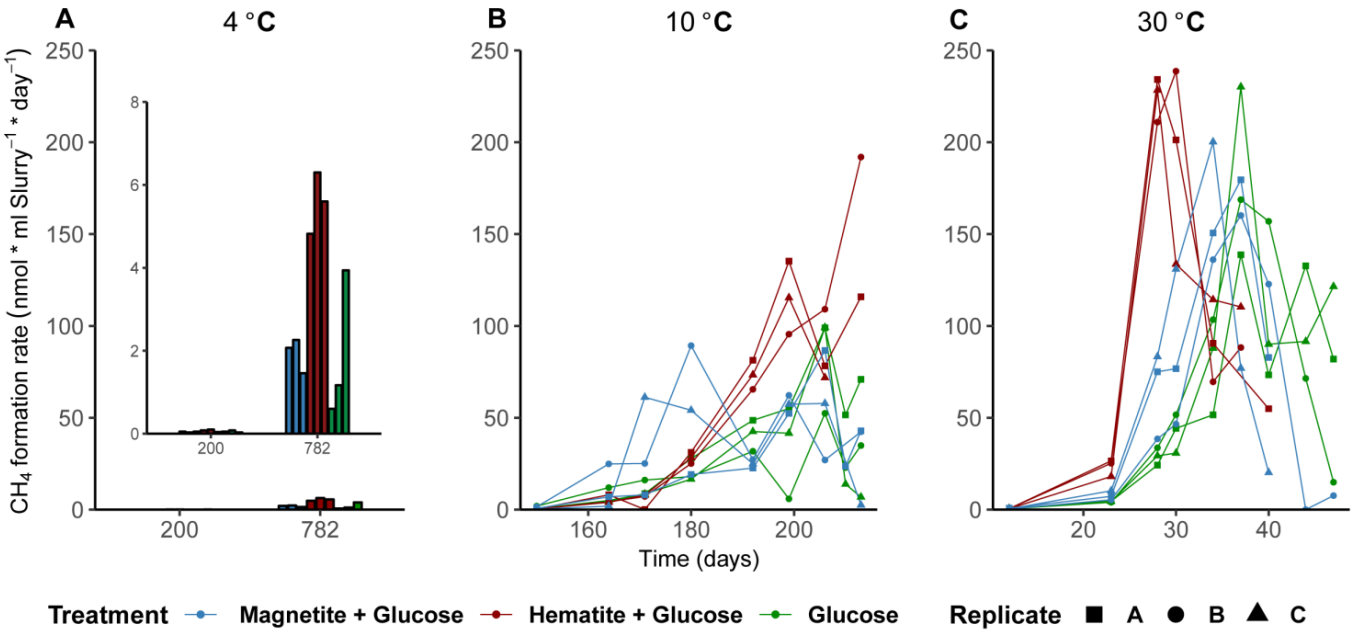

Figure 3: Effect of crystalline iron minerals on methane formation in sediment incubations. Methane formation rates at 4 °C (A), 10 °C (B), and 30 °C (C). Bar plots were displayed for methane formation rates at 4 ºC because fewer time-points were measured (Figure 1D).

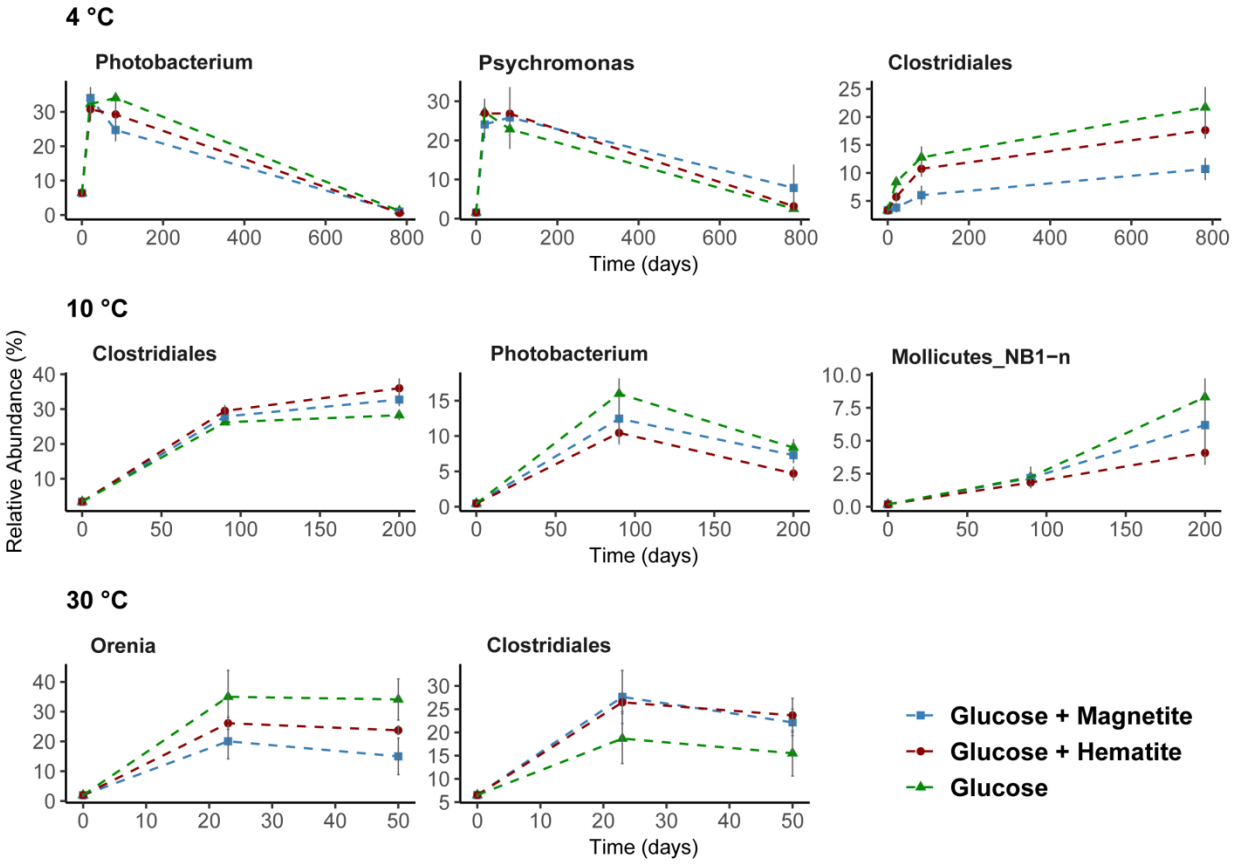

Figure 4: Dominant bacteria communities enriched over time at 4 °C, 10 ºC and 30 ºC determined by 16S rRNA gene analysis. A threshold of relative abundance increase of 5 % was used to determine key taxa (from order to genus level) compared to controls. Percentages show relative abundance of individual genus or order. Data presented here are reflecting the main bacteria taxa that were stimulated by glucose addition to slurry incubations.

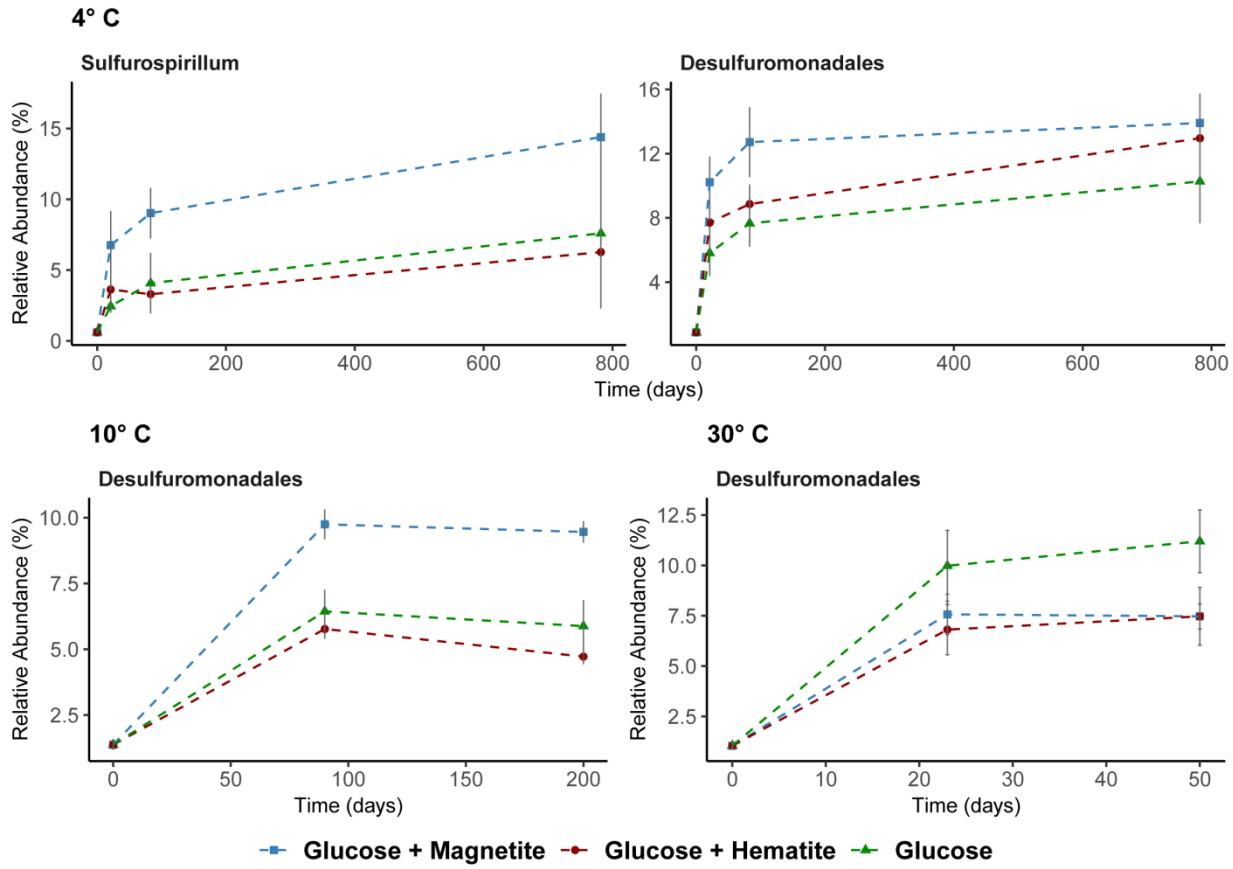

Figure 5: Potential iron reducing bacteria based on 16S rRNA gene analysis across all temperatures. *Sulfurospirillum* shown at 4 ºC only; were below 1 % relative abundance at other temperatures.

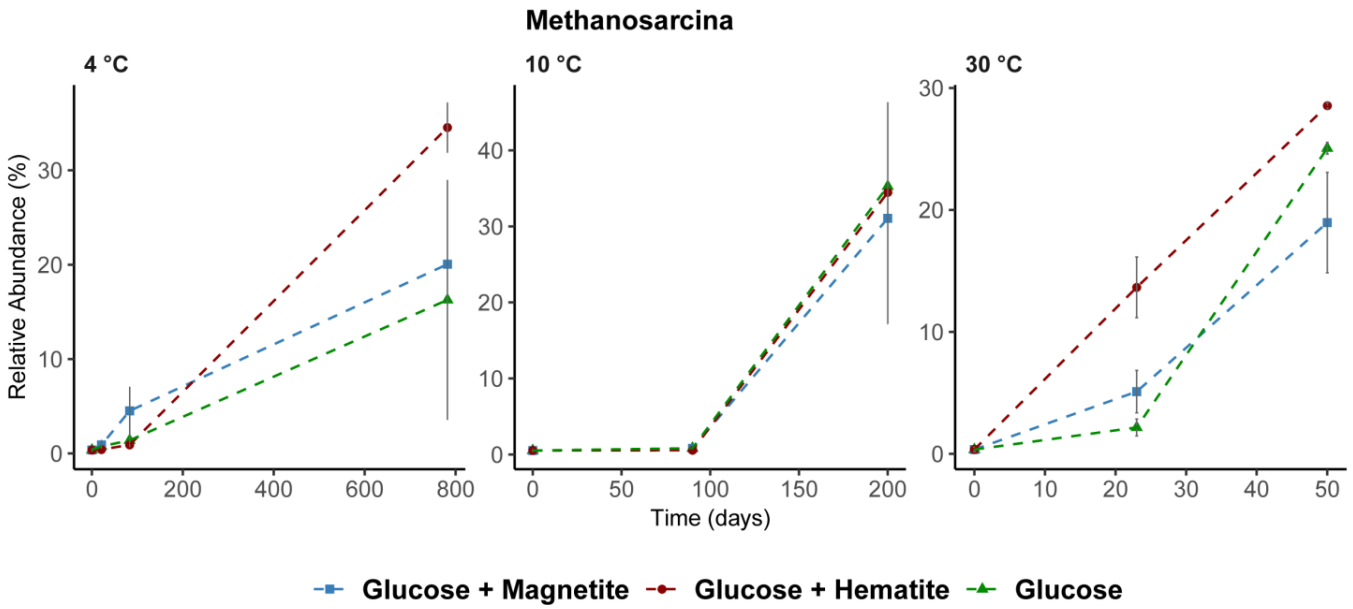

Figure 6: Relative abundance of *Methanosarcina* spp. across all temperatures determined by archaea 16S rRNA gene analysis. *Methanosarcina* was the only known methanogen that increased in relative abundance during methane formation regardless of incubation temperature.

Supplementary Information

Temperature Controls Crystalline Iron Oxide Utilization by Microbial Communities in Methanic Ferruginous Marine Sediment Incubations

David A. Aromokeye[1,2,3], Tim Richter-Heitmann[1], Oluwatobi E. Oni[1,2], Ajinkya Kulkarni[1,2,3], Xiuran Yin[1,2,3], Sabine Kasten[2,4,5] and Michael W. Friedrich[1,2,*].

[1]Microbial Ecophysiology Group, Faculty of Biology/Chemistry, University of Bremen, Bremen, Germany

[2]MARUM, Center for Marine Environmental Sciences, University of Bremen, Bremen, Germany

[3]International Max-Planck Research School for Marine Microbiology, Max-Planck-Institute for Marine Microbiology, Bremen, Germany

[4]Alfred Wegener Institute Helmholtz Centre for Polar and Marine Research, Bremerhaven, Germany

[5]University of Bremen, Faculty of Geosciences, Bremen, Germany

*Correspondence:

Michael W. Friedrich,

[1]Microbial Ecophysiology Group, Faculty of Biology/Chemistry & MARUM, University of Bremen, PO Box 33 04 40, D-28334 Bremen, Germany

Email: michael.friedrich@uni-bremen.de

Supplementary Figures

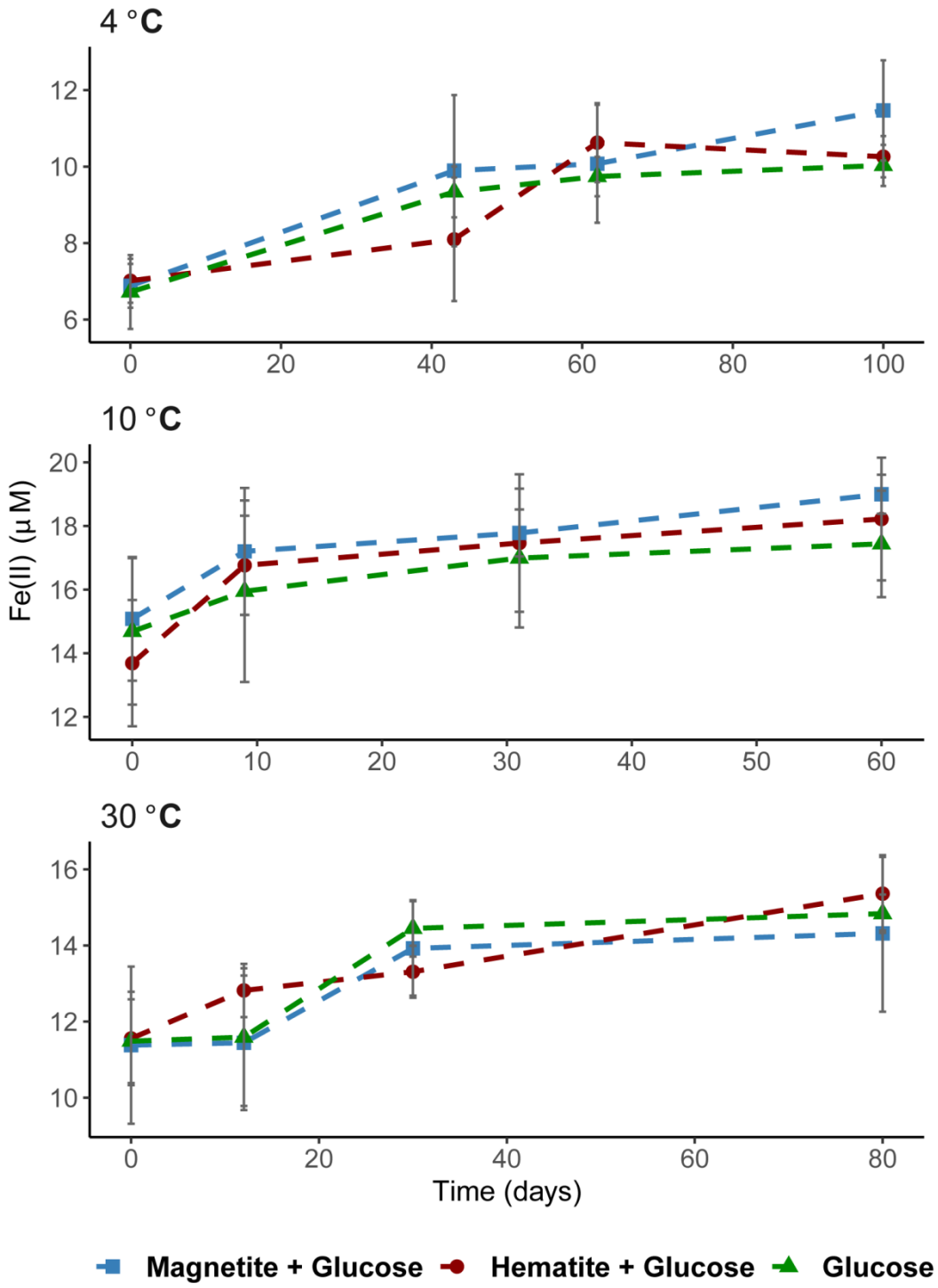

Figure S1: HCl extractable Fe(II) measured across selected time-points during the iron reduction experiments. The total Fe(II) measurements were done on whole slurry material (see methods) unlike the Fe^{2+} measurements from pore water (Fig. 1, main text).

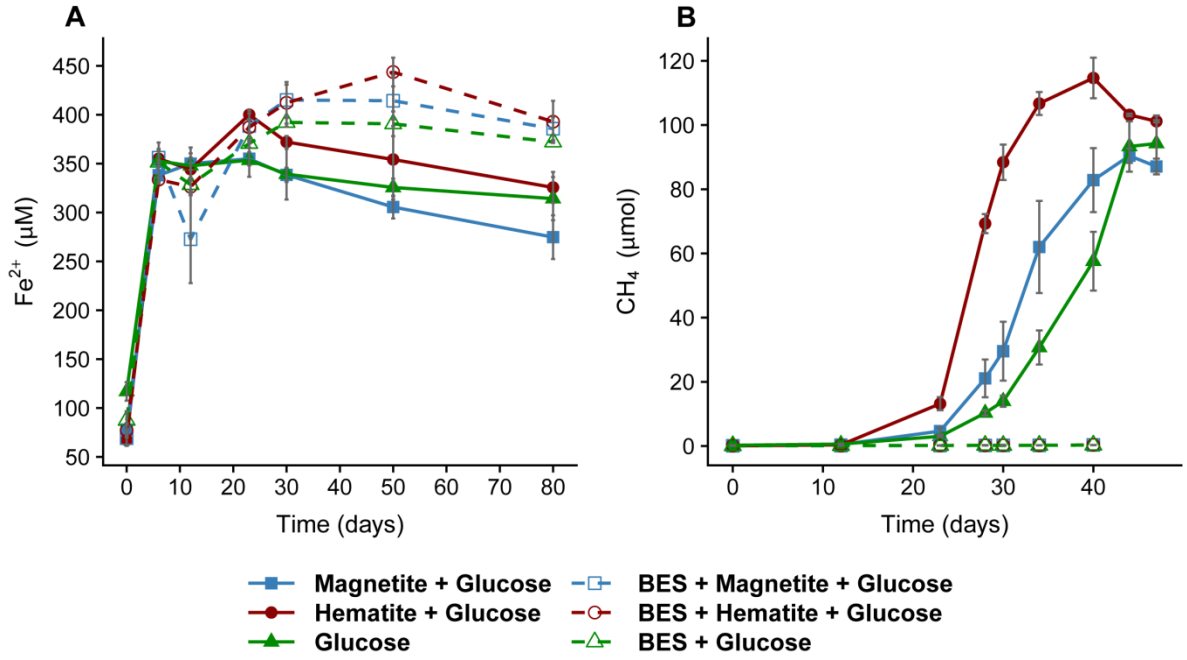

Figure S2: Effect of BES on iron reduction (A) and methanogenesis (B) in the presence of the crystalline iron minerals. Incubations were performed at 30 °C. Data presented for the non BES amended controls are presented in Figure 1 of the main text but are re-plotted here as controls for evaluating the effect of BES on iron reduction in comparison to the controls.

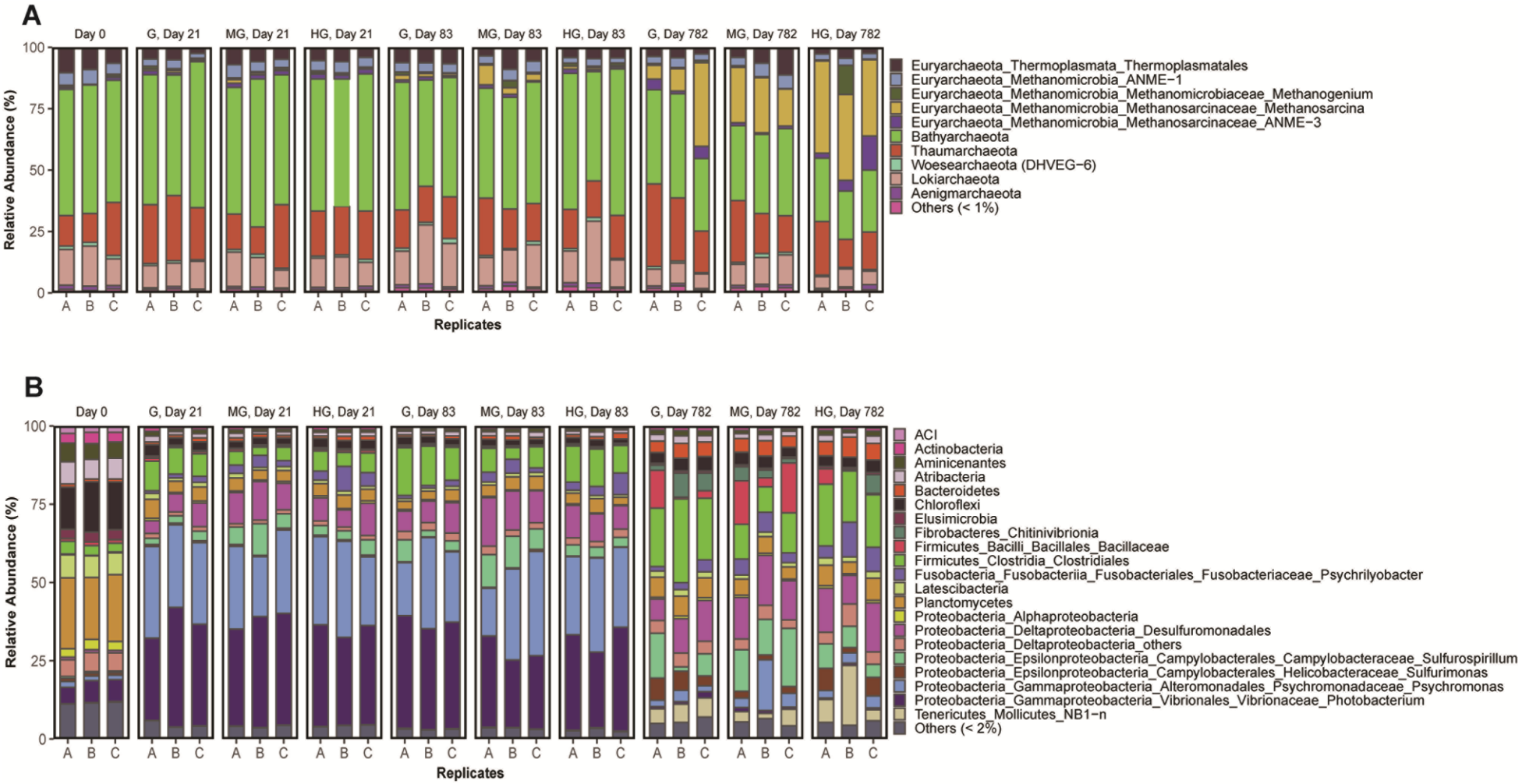

Figure S3: Total sum scaling of archaea (A) and bacteria (B) communities in incubations at 4 ºC between day 0, day 21 (intermediate iron reduction phase), day 83 (peak of iron reduction phase based on Fe^{2+} concentrations) and day 782 (methanogenesis phase). G, glucose amended incubation; MG, incubations amended with magnetite and glucose; HG, hematite and glucose amendments. Each triplicate sample was sequenced individually (see methods). Microbial communities were scaled in a mixed style such that the phyla with decreased relative abundance over time compared to day 0 were reported on the phylum level. Lower taxonomic classification was reported for orders, families and genera from other phyla with increased relative abundance compared to day 0.

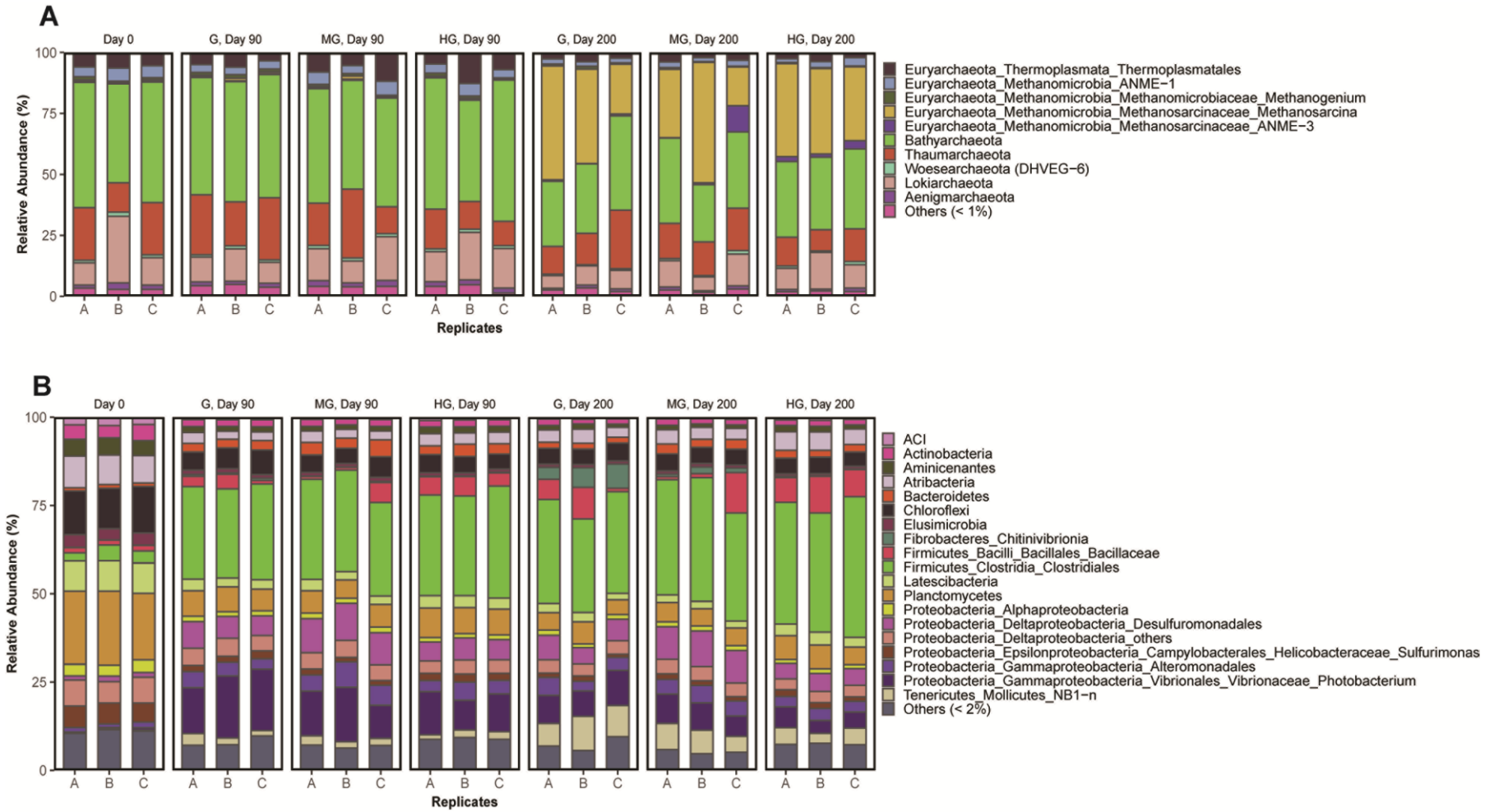

Figure S4: Total sum scaling of archaea (A) and bacteria (B) communities in the incubations at 10 ºC between day 0, day 90 (when aqueous Fe^{2+} concentrations reached a plateau) and day 200 (during active methanogenesis). G represents glucose amended incubation; MG represents incubations amended with magnetite and glucose while HG represents hematite and glucose amendments. Each triplicate sample was sequenced individually (see methods). Microbial communities were scaled in a mixed style such that the phyla with decreased relative abundance over time compared to day 0 were reported on the phylum level. Whereas, lower taxonomic classification was reported for orders, families and genera from other phyla with increased relative abundance compared to day 0.

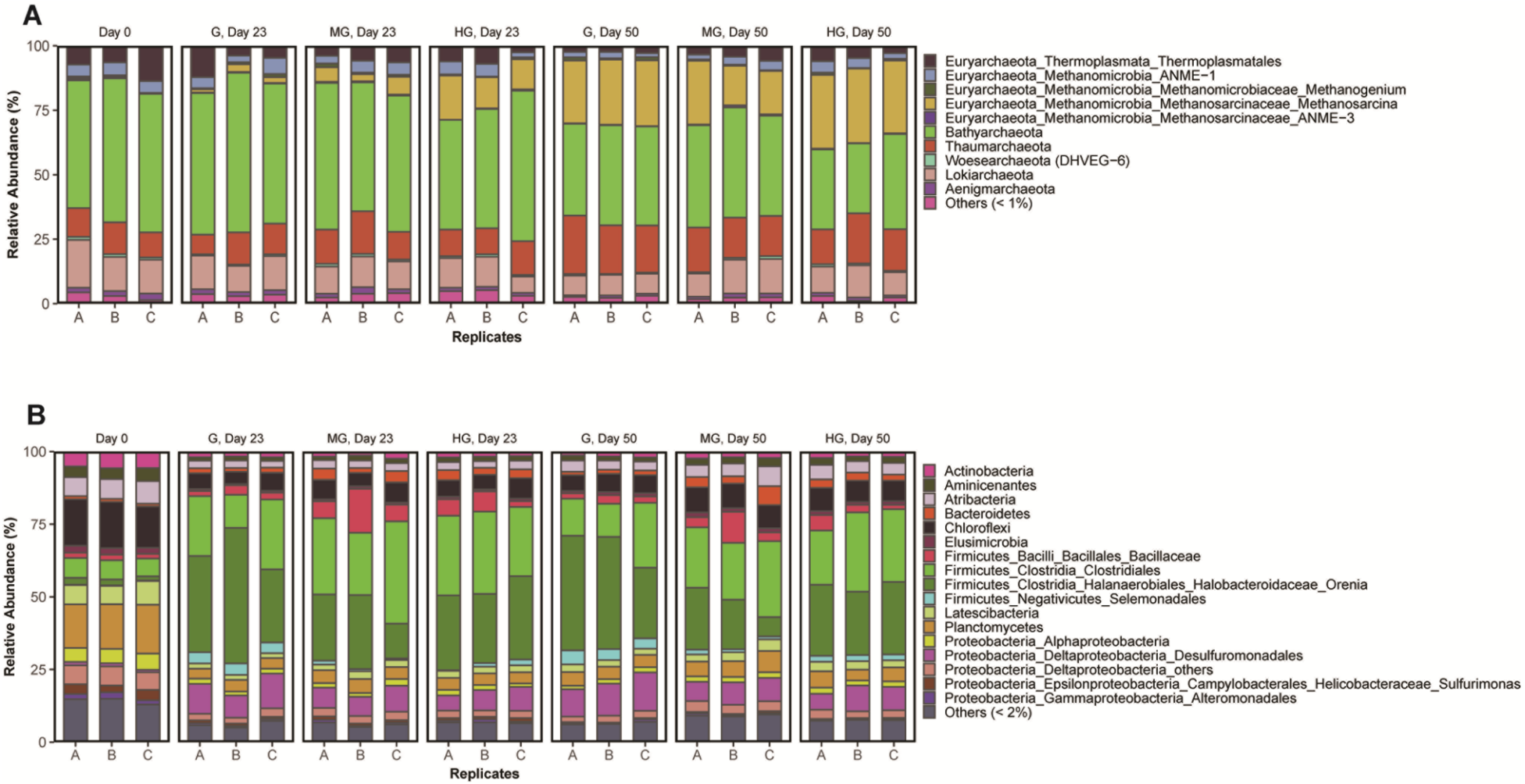

Figure S5: Total sum scaling of archaea (A) and bacteria (B) communities in the incubations at 30 ºC between day 0 day 23 when Fe^{2+} formation reached a plateau and at day 50, when methane concentrations levelled off. G represents glucose amended incubation; MG represents incubations amended with magnetite and glucose while HG represents hematite and glucose amendments. Each triplicate sample was sequenced individually (see methods). Microbial communities were scaled in a mixed style such that the phyla with decreased relative abundance over time compared to day 0 were reported on the phylum level. Whereas, lower taxonomic classification was reported for orders, families and genera from other phyla with increased relative abundance compared to day 0.

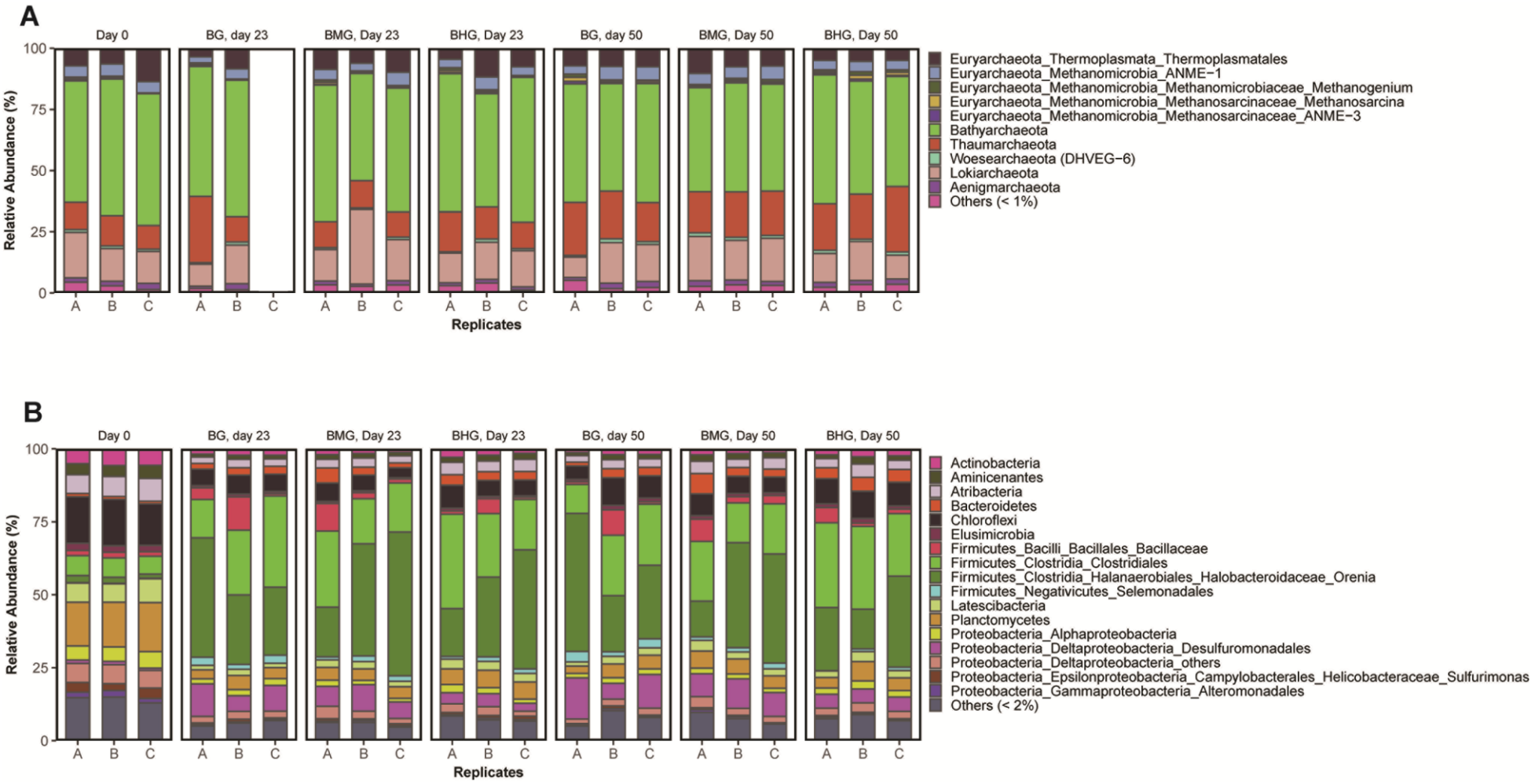

Figure S6: Total sum scaling of archaea (A) and bacteria (B) communities in the incubations amended with BES at 30 ºC. The archaea sample for BG.c at day 23 failed during the sequencing preparation, hence triplicates for that time point could not be shown.

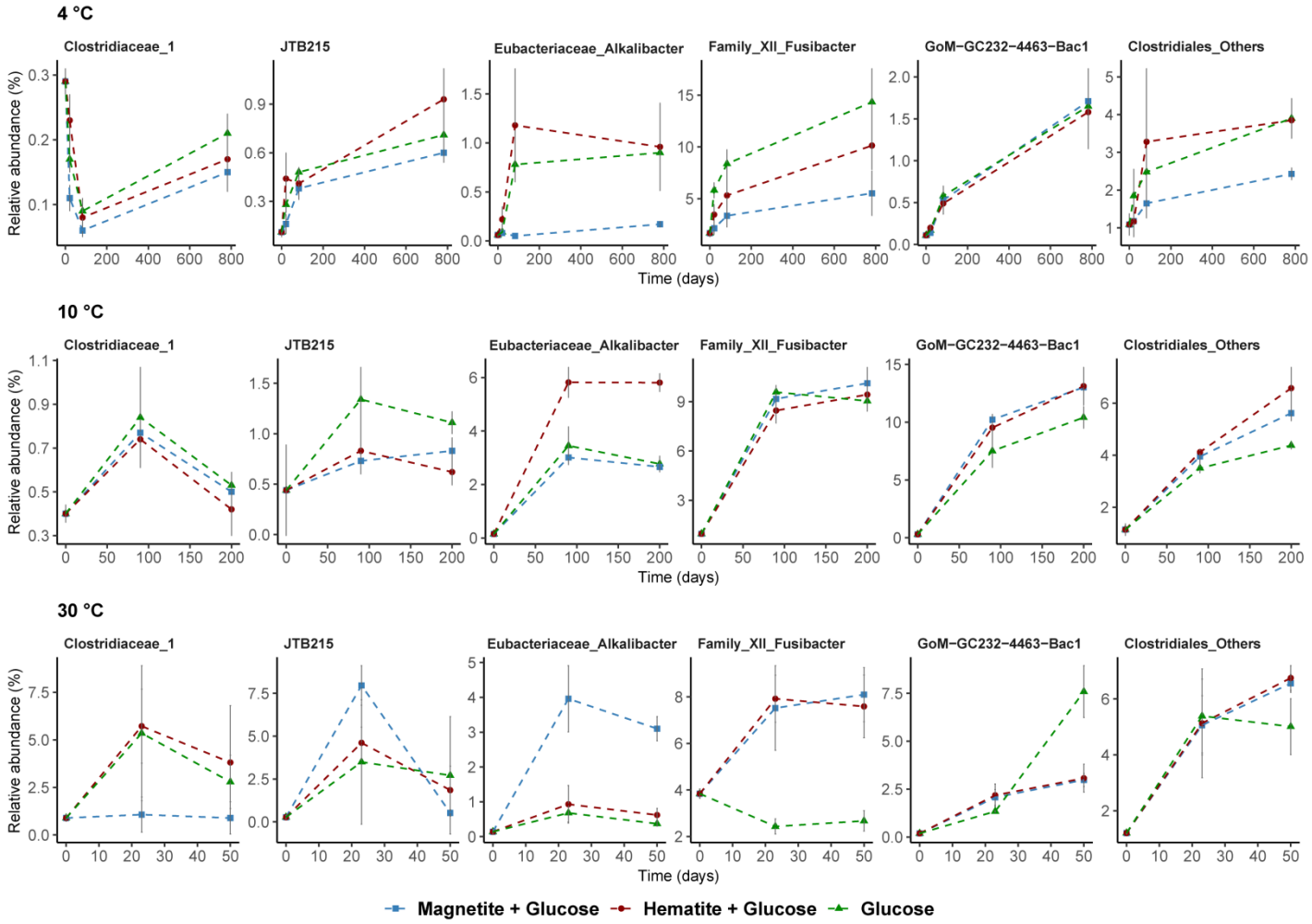

Figure S7: Relative abundance of genus or family belonging to the order Clostridiales that were identified at different temperatures demonstrating the versatility of the order Clostridiales at various temperatures**.**

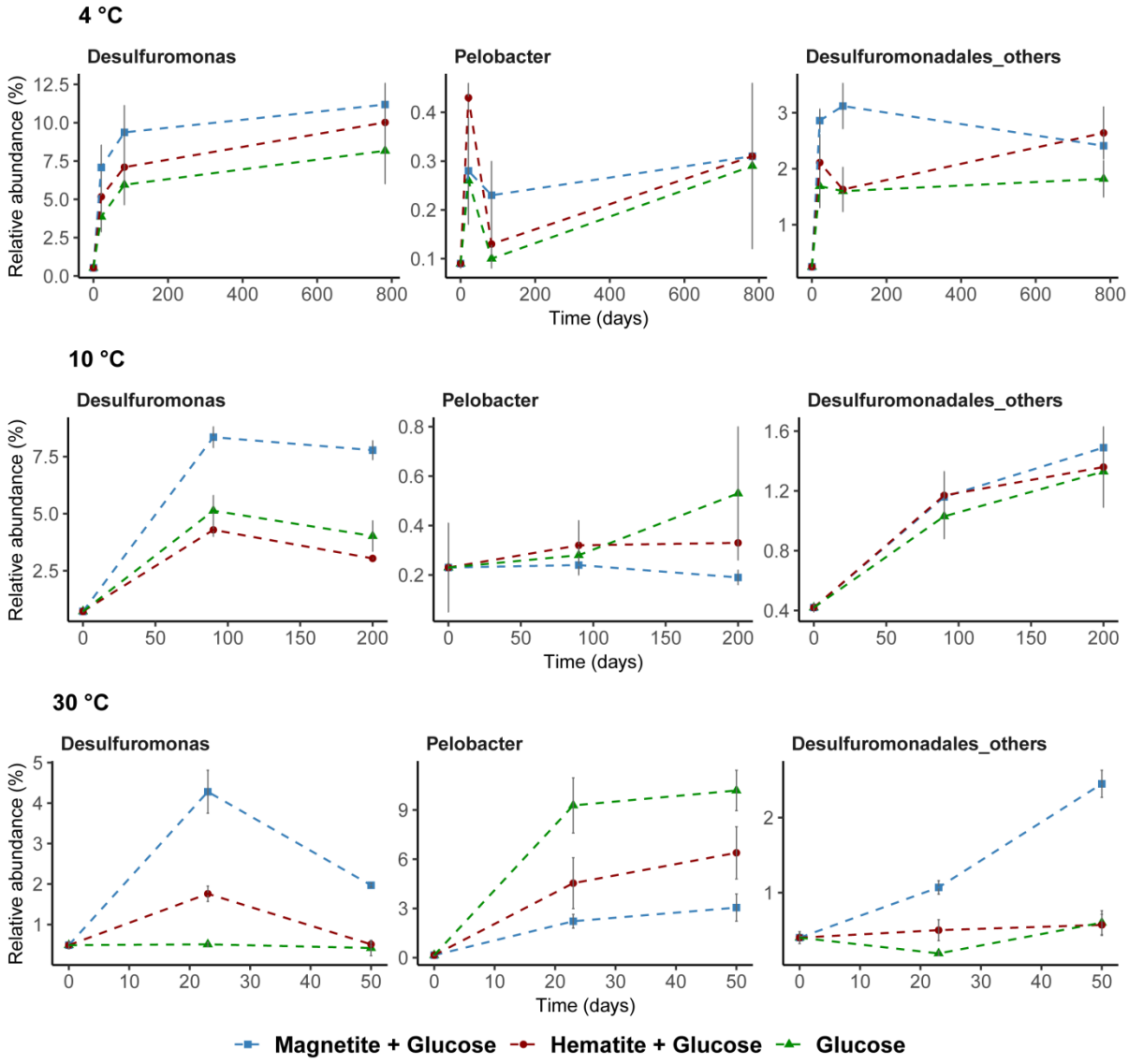

Figure S8: Relative abundance of dominant genus from the order Desulfuromonadales. *Desulfuromonas* was higher in relative abundance at 4 ºC and 10 ºC while *Pelobacter* was more enriched at 30 ºC.

Table S1. Summary of triplicate incubation experiment set up to study microbial iron reduction and methanogenesis.

Treatment (n=3)	Temperature (^{o}C)	Glucose (68 µmoles)	Magnetite (1020 µmoles)	Hematite (1020 µmoles)	Sodium 2-bromoethane sulfonate (BES, 15mM)	Sediment depth used (cm)	Incubation duration (days)
Magnetite + Glucose	4	+	+	-	-	441–466	900
Hematite + Glucose	4	+	-	+	-	441–466	900
Glucose	4	+	-	-	-	441–466	900
Magnetite + Glucose	10	+	+	-	-	441–466	216
Hematite + Glucose	10	+	-	+	-	441–466	216
Glucose	10	+	-	-	-	441–466	216
Magnetite + Glucose	30	+	+	-	-	416–441	80
Hematite + Glucose	30	+	-	+	-	416–441	80
Glucose	30	+	-	-	-	416–441	80
Magnetite + Glucose + BES	30	+	+	-	+	416–441	80
Hematite + Glucose + BES	30	+	-	+	+	416–441	80
Glucose + BES	30	+	-	-	+	416–441	80

Table S2. pH of incubations in duplicate supplementary set-ups to check the effect of glucose fermentation on the slurries.

Time (days)	Temperature	Magnetite + Glucose_ A	Magnetite + Glucose_ B	Hematite + Glucose_ A	Hematite + Glucose_ B	Glucose_ A	Glucose_ B	Unamended_A	Unamended_B
0	4 ºC	7.21	7.1	7.15	7.12	7.12	7.08	7.14	7.13
14		6.89	6.89	6.91	6.83	6.93	6.9	7.24	7.28
77		7	7.02	6.9	6.94	6.94	6.96	7.24	7.31
100		6.98	7.01	7.02	6.99	6.88	6.92	7.32	7.28
0	10 ºC	7.17	7.16	7.21	7.16	7.32	7.24	7.31	7.24
14		6.92	6.93	6.91	6.82	6.88	6.88	7.19	7.22
77		6.98	7.04	7.04	7.03	7.23	7.26	7.23	7.26
100		7.01	6.97	7.02	7	6.95	6.96	7.25	7.34
0	30 ºC	7.13	7.19	7.15	7.22	7.15	7.35	7.18	7.17
14		6.89	6.92	7.05	6.9	6.85	6.88	7.22	7.18
77		7.05	7.03	7.08	7.05	6.97	7.03	7.18	7.14
100		7.02	6.97	6.89	6.86	6.92	6.96	7.25	7.28

Data shows carbonate concentrations in the natural carbonate buffer system in the sediment is sufficient to keep the pH of the media stable over time as only slight changes were observed in incubations amended with glucose over time.

Table S3. Absolute numbers of sequence reads processed per sample after OTU classification. Archaea 16S rRNA reads in the bacteria sequences and vice versa was removed before arriving at absolute numbers.

Treatment	4 ºC			10 ºC			30 ºC		
	Time (days)	Bacteria	Archaea	Time (days)	Bacteria	Archaea	Time (days)	Bacteria	Archaea
day 0.a		28546	4318		25256	4180		11450	6591
day 0.b	0	19950	3646	0	26023	1891	0	19615	5083
day 0.c		13798	7386		27788	8592		17982	3385
G.a		28500	3077		33363	7242		26693	3489
G.b		17283	2392		32583	3222		17817	3348
G.c		13174	2550		27412	6563		16339	3175
MG.a		13931	1421		15186	4709		10184	2566
MG.b	21	24287	3118	90	21907	8333	23	26935	1492
MG.c		20235	4118		19129	4578		24041	3023
HG.a		19302	2809		17105	6143		23208	1789
HG.b		26092	3271		13894	7180		18273	1699
HG.c		19733	2227		26800	1781		21641	2466
G.a		57136	1429		41484	11515		25290	7277
G.b		61605	1336		53555	3319		52879	4740
G.c		98905	2255		40997	7809		29286	5558
MG.a		34489	3432		18151	4048		13546	5527
MG.b	83	32552	1883	200	34882	24628	50	8267	5549
MG.c		295843	2912		29285	7773		11893	6112
HG.a		50565	1243		20338	8554		13910	6807
HG.b		41664	1262		14696	11564		25312	4846
HG.c		45562	1826		42890	3132		18841	6589
G.a		24800	8057						
G.b		19682	3141						
G.c		18115	8980						
MG.a		13884	2791						
MG.b	782	6395	4769						
MG.c		11906	6057						
HG.a		12216	9376						
HG.b		19020	9437						
HG.c		18309	11681						

Absolute numbers used to determine relative abundance (%) of individual members of the community (see methods). MG represents incubations amended with magnetite and glucose; HG represents hematite and glucose amendments while G represents glucose amended incubation.

Table S4. Absolute numbers of sequence reads processed per sample after OTU classification in the BES incubations at 30 ºC. Day 0 treatments for the BES incubations are the same day 0 samples used for the 30 ºC incubations without BES (See Table S2).

Treatment	BES incubations at 30 ºC		
	Time (days)	Bacteria	Archaea
BG.a		40742	3650
BG.b		25851	1673
BG.c		21701	NA
BMG.a		42359	3794
BMG.b	23	30696	2072
BMG.c		35359	2053
BHG.a		21998	3427
BHG.b		35357	5001
BHG.c		32684	3132
BG.a		15660	1680
BG.b		7478	1815
BG.c		28052	3104
BMG.a		27804	3678
BMG.b	50	19719	2829
BMG.c		37051	3354
BHG.a		11310	5684
BHG.b		27417	4753
BHG.c		24534	3016

NA represents the BG.c archaea sample at day 23 that failed during sequencing preparation. The unavailability of that sample however had no effect on the overall result as the other two replicates looked similar and the archaea community remained undisturbed over time across all BES amended incubations**.**

Chapter Five

General Discussion and Perspectives

Mechanisms driving iron reduction in methanic sediments of Helgoland Mud Area

The subject of deep iron reduction below the sulfate methane transition (SMT) of marine sediments and responsible mechanisms fuelling the process currently generates intense debate in sub-surface geo-microbiology research. Potentially novel microbial interactions fuelled by iron oxides in the deep biosphere have important implications for both the iron and carbon cycle and could improve our understanding of microbial life in the energy limited deep biosphere. Within the scope of the debate regarding the mechanisms that fuel iron oxide reduction in the methanic zone, two hypothesis are more prevalently discussed: (I) the cryptic sulfur cycle propagated by Holmkvist and colleagues (2011) and (II) the iron oxide driven anaerobic oxidation of methane (Fe-AOM) hypothesis which has only been supported by geochemical arguments and modeling approaches so far (Riedinger et al., 2014; Egger et al., 2015; Egger et al., 2016a; Egger et al., 2016b; Rooze et al., 2016; Egger et al., 2017).

A major requirement for cryptic sulfur cycling to fuel dissolved iron (Fe^{2+}) dissolution into porewater is the availability of a sulfidization front shown for Aarhus bay methanic zone sediments where downward diffusing sulfide from the sulfate zone reacts with deeply buried iron oxides (Holmkvist et al., 2011) (see also Figure 2, Chapter one). This sort of sulfidization front is not present in the many other sites with elevated Fe^{2+} concentrations in the methanic zone, including the Helgoland Mud Area. Besides, for the Helgoland Mud Area methanic zone, distinct microbial communities were shown to be tightly linked to Fe^{2+} concentrations (Oni et al., 2015b). Therefore, abiotic cryptic sulfur cycling as a potential mechanism fuelling iron reduction in the methanic zone of Helgoland Mud Area can be

completely eliminated (Oni, 2015). A similar conclusion was made for sediments of the methanic zone in the Argentine Basin (Riedinger et al., 2014).

Since abiotic sulfur cycling mechanism is ruled out, this study intensively sought out further evidence supporting the potential biotic mechanisms driving iron oxide reduction in the methanic zone (Oni, 2015) including Fe-AOM. The following sections highlights the main findings from Chapters two, three and four of this thesis and provides my perspective, based on these findings, regarding the mechanisms that result in Fe^{2+} dissolution into porewater of Helgoland Mud Area and potentially into similar iron oxide rich marine sediments.

Direct evidence for Fe-AOM obtained in the Helgoland Mud Area methanic zone

Previous knowledge regarding AOM was focused on the activities in the interface called the SMT where upward diffusing methane from the methanic zone gets in contact with sulfate and is consequently oxidized coupled to sulfate reduction (Iversen and Jørgensen, 1985). Therefore, sulfate dependent AOM in SMT was the only recognized biological filter preventing the escape of about 90 % of produced methane in marine sediments into the water column (Hinrichs and Boetius, 2003; Knittel and Boetius, 2009). Recently, the juxtaposition of bioavailable iron oxides evidenced by ongoing iron reduction, low to undetectable sulfate concentrations and the availability of methane have led to geochemical arguments that Fe-AOM occurs in the methanic zone (see section 3.2, Chapter one and references therein). However, unlike with sulfate coupled AOM, a direct environmental signature for Fe-AOM is so far lacking beyond the Fe^{2+} concentrations in the sites where the process was proposed to be responsible for apparent iron reduction occurring *in situ*. Regardless, the existence of an iron oxide dependent methane sink in the methanic zone could have significant implications for calculations regarding estimates of methane flux from marine environments and for climate change. The geochemical pre-conditions for Fe-AOM to occur are present in

Helgoland Mud Area making this study site a good site to study the occurrence of this process.

Using short-term radiotracer ($^{14}CH_4$) experiments, we obtained direct evidence for Fe-AOM in the methanic zone and could clearly distinguish the process from sulfate coupled AOM (See Figure 1c, Chapter two). At 0.095 ± 0.03 nmol cm^{-3} d^{-1}, Fe-AOM in the methanic zone is clearly occurring at 2 % the rate of sulfate coupled AOM in the SMT, but given the larger volumes of the methanic zone (Bowles et al., 2014), substantial amounts of methane could be consumed locally in the methanic zone. Similar activity rates was detected in methanic sediments of the Alaskan Beaufort Sea, but minimal sulfate concentrations were detected in the sediment which might still fuel sulfate dependent AOM *in situ* (Treude et al., 2014). In the hydrothermal vent sediments of Chowder Hill, sulfate reduction was not detectable at lower depths and Fe-AOM rates were an order of magnitude higher than what was observed in the Helgoland Mud Area (Wankel et al., 2012; Table 1). However the sediment evaluated was shallow (16 cm) and doesn't qualify as deep biosphere sedimentary environment (Jørgensen and Boetius, 2007). Other Fe-AOM rates from marine sediments are either based on $^{13}CH_4$ enrichment studies in sulfate rich sediments or geochemical modeling (Table 1). Therefore, the findings from Helgoland Mud Area presents the first AOM rates attributable to iron oxide reduction under close to *in situ* conditions in a deep biosphere environment bearing geochemical preconditions for Fe-AOM. Generally, Fe-AOM rates, not just in marine sediments, are low perhaps owing to the difficulty in accessing iron oxides as an electron acceptor by microbes involved in the process (Table 1). These Fe-AOM rates, which were obtained either by geochemical modeling, radiotracer based activity measurements or enrichment studies, however indicate that Fe-AOM can be an additional sink for methane turnover in these ferruginous sediments.

Table 1: Estimated Fe-AOM rates in sediments from various freshwater and marine environments. Process rates were presented as annual rates for comparability between the different environments.

Ecosystem	Environment	Sediment zone	Fe-AOM Rates	Data collection source		Reference
				Method	Fe Oxide	
Marine	North Sea	Methanic	34.7 nmol CH_4 cm^{-3} yr^{-1}	$^{14}CH_4$ incubations	N.A.	Aromokeye et al., submitted
	Eel River Basin seep[§]	Surface	6 µmol CO_2 cm^{-3} yr^{-1}	$^{13}CH_4$ incubations	Ferrihydrite	Beal et al., 2009
	Chowder Hill hydrothermal vent	Surface	59 µmol CH_4 cm^{-3} yr^{-1}	$^{14}CH_4$ incubations	N.A.	Wankel et al., 2012
	Black Sea	Methanic	14.6 pmol CH_4 cm^{-3} yr^{-1}	Geochemical modelling estimates	N.A.	Egger et al., 2016
	Baltic Sea	Methanic	1.1 nmol CH_4 cm^{-3} yr^{-1}	Geochemical modelling estimates	N.A.	Egger et al., 2017
	Bothnian Sea	Surface	1.3 µmol CO_2 cm^{-3} yr^{-1}	$^{13}CH_4$ incubations	Ferrihydrite	Egger et al., 2015
	Santa Monica Basin seep[§]	Surface	292 µmol CO_2 cm^{-3} yr^{-1}	$^{13}CH_4$ incubations	Ferric citrate	Scheller et al., 2016
			36.5 µmol CO_2 cm^{-3} yr^{-1}	$^{13}CH_4$ incubations	Ferric EDTA	Scheller et al., 2016
Freshwater	Lake Kinneret	Surface	1.3 µmol CH_4 cm^{-3} yr^{-1}	$^{13}CH_4$ incubations	Amorphous Fe(III) oxide	Sivan et al., 2011
	Danish Lake Ørn	Surface	13 µmol CH_4 cm^{-3} yr^{-1}	$^{14}CH_4$ incubations	N.A.	Norði et al., 2011
	Dover Bluff salt marsh	Surface	1.4 µmol CH_4 cm^{-3} yr^{-1}	$^{14}CH_4$ incubations	Ferrihydrite	Segarra et al., 2013
	Hammersmith Creek river	Surface	4.5 µmol CH_4 cm^{-3} yr^{-1}	$^{14}CH_4$ incubations	Ferrihydrite	Segarra et al., 2013

The rates presented above are from iron-oxide rich geochemical zones of marine or freshwater sediments unless otherwise stated. [§] represents studies obtained from sulfate rich geochemical zones. So far, activity based Fe-AOM rates obtained from deep sedimentary biosphere i.e. at 1 meter below the seafloor based on the definition of Jørgensen and Boetius (2007) is only available from the Helgoland Mud Area. Other environments where Fe-AOM was previously demonstrated were therefore referred to as surface sediments in the table above as the sediment depth evaluated are below 1 meter. N.A.: Not available

Previously published Gibbs free energy calculated for metal dependent AOM at standard and *in situ* (experimental) conditions indicate that Fe-AOM is indeed thermodynamically feasible (Table 2). These numbers are however high considering the extremely low solubility of iron(III) oxides at neutral pH (Schwertmann, 1991). Solubility of ferric iron increases greatly at lower pH (especially below pH 2), leading to suggestions that Fe-AOM will be more favourable at lower pH (He et al., 2018). Fe-AOM activity, detected or proposed in the studies summarized in Table 1 above was obtained at neutral pH which constrains metal oxide reduction. However, other environmental factors such as absence of other electron

acceptors (e.g. sulfate), temperature and salinity may favour Fe-AOM activity at *in situ* conditions (He et al., 2018).

Table 2: Standard and *in situ* (experimental) Gibbs free energy of metal dependent AOM.

Process	Reaction	$\Delta G^{0'}$ (kJ mol^{-1} CH_4)	*In situ* (experimental) ΔG(kJ mol^{-1} CH_4)	Reference
Sulfate dependent AOM (S-AOM)	$CH_4 + SO_4^{2-} \rightarrow HCO_3^- + HS^- + H_2O$	N.A.	-14	Beal et al., 2009
	$CH_4 + SO_4^{2-} \rightarrow HCO_3^- + HS^- + H_2O$	-16.6	-33.0	Caldwell et al., 2008
	$CH_4 + SO_4^{2-} \rightarrow HCO_3^- + HS^- + H_2O$	-92.8	-109.2	Caldwell et al., 2008
Iron dependent AOM (Fe-AOM)	$CH_4 + 8Fe^{3+} + 3H_2O \rightarrow HCO_3^- + 8Fe^{2+} + 9H^+$	-418.3	-434.7	Caldwell et al., 2008
	$CH_4 + 8Fe^{3+} + 2H_2O \rightarrow CO_2 + 8Fe^{2+} + 8H^+$	-454.6	-434.7	Caldwell et al., 2008
	$CH_4 + 8Fe(OH)_3 + 15H^+ \rightarrow HCO_3^- + 8Fe^{2+} + 21H_2O$	N.A.	-270.3	Beal et al., 2009
	$CH_4 + 8FeOOH + 15H^+ \rightarrow 8Fe^{2+} + HCO_3^- + 13H_2O$	N.A.	-462 to -488.6	Norði et al., 2013
	$CH_4 + 8Fe(OH)_3 + 15H^+ \rightarrow HCO_3^- + 8Fe^{2+} + 21H_2O$	N.A.	-571	Segarra et al., 2013
	$CH_4 + 8Fe(OH)_3 + 15H^+ \rightarrow HCO_3^- + 8Fe^{2+} + 21H_2O$	N.A.	-150 to -170	Riedinger et al., 2014
	$CH_4 + 8Fe(OH)_3 + 15H^+ \rightarrow HCO_3^- + 8Fe^{2+} + 21H_2O$	N.A.	-572	Bar-or et al., 2017
	$CH_4 + 8Fe^{3+} + 2H_2O \rightarrow CO_2 + 8Fe^{2+} + 8H^+$	N.A.	-454	Ettwig et al., 2016
	$CH_4 + 8Fe(OH)_3 + 16H^+ \rightarrow CO_2 + 8Fe^{2+} + 22H_2O$	-571.2	N.A.	Timmers et al., 2017
	$CH_4 + 8Fe(OH)_3 + 15H^+ \rightarrow HCO_3^- + 8Fe^{2+} + 21H_2O$	-81.6	N.A.	He et al., 2018
Manganese dependent AOM (Mn-AOM)	$5CH_4 + 8MnO_4^- + 19H^+ \rightarrow 5HCO_3^- + 8Mn^{2+} + 17H_2O$	-991.7	-1008.1	Caldwell et al., 2008
	$5CH_4 + 8MnO_4^- + 24H^+ \rightarrow 5CO_2 + 8Mn^{2+} + 22H_2O$	-1028.1	-1044.5	Caldwell et al., 2008
	$CH_4 + 4MnO_2 + 7H^+ \rightarrow HCO_3^- + 4Mn^{2+} + 5H_2O$	N.A.	-556	Beal et al., 2009
	$CH_4 + 4MnO_2 + 7H^+ \rightarrow HCO_3^- + 4Mn^{2+} + 5H_2O$	N.A.	-790	Segarra et al., 2013
	$CH_4 + 4MnO_2 + 8H^+ \rightarrow CO_2 + 4Mn^{2+} + 6H_2O$	-763.2	N.A	Timmers et al., 2016
	$CH_4 + 4MnO_2 + 7H^+ \rightarrow HCO_3^- + 4Mn^{2+} + 5H_2O$	-494	N.A.	He et al., 2018

Standard and *in situ* free energy for sulfate dependent AOM inserted into the table for comparison. N.A.: Not available.

In long-term experiments, we could demonstrate that under the inhibition of sulfate reduction, crystalline iron oxides (lepidocrocite, hematite and magnetite) can facilitate Fe-AOM (Figure 3, Chapter two). Similar stimulation of faster Fe-AOM rates with hematite and magnetite amendment was shown in slurry incubations from iron-oxide rich sediments of Lake Kinneret (Bar-Or et al., 2017).

While anaerobic methane oxidizing archaea (ANME) clades: ANME-1, ANME-2 and ANME-3 perform S-AOM (Boetius et al., 2000; Orphan et al., 2001, 2002; Niemann et al.,

2006), knowledge on microbial key players involved in Fe-AOM is limited. Recently, two studies showed *Candidatus* 'Methanoperedens' (ANME-2d) are able to couple anaerobic methane oxidation to iron reduction via the reverse methanogenesis pathway while employing multi-heme cytochromes to reduce iron(III) (Ettwig et al., 2016; Cai et al., 2018). Until now, it is a long-held dogma that gammaproteobacterial methanotrophic bacteria such as members of the genus *Methylobacter* are strict aerobes (Kalyuzhnaya et al., 2013; Chistoserdova, 2015). DNA and lipid stable isotope probing approaches were recently used to identify these methylotrophic bacteria as key microbial players involved during Fe-AOM in lake sediments (Bar-Or et al., 2017; Martinez-Cruz et al., 2017). Molecular adaptations and underlying mechanisms that allows methanotrophic bacteria to perform Fe-AOM still requires further research. Only a few studies have demonstrated Fe-AOM in marine sediments and in some of these studies, either the microbial key players were not shown (Egger et al., 2015) or the geochemical preconditions for Fe-AOM do not exist in the environment where the sediments were obtained (Beal et al., 2009; Scheller et al., 2016). Therefore, our successful enrichment of ANME-2a with magnetite as electron acceptor (Figure 4, Chapter 2) represents a substantial advancement in Fe-AOM research as we identify for the first time ANME-2a as a microbial key player for Fe-AOM in marine environments. A clear indication for partner organisms was not obtained. In terrestrial mud volcanoes where Fe-AOM is also suggested to occur, high correlation between gene copies of Desulfuromonadales and ANME-2a was taken as indication for ANME-2a to oxidize methane with Desulfuromonadales as iron reducing partners (Chang et al., 2012; Tu et al., 2017). While dissimilatory iron reducers (e.g., Desulfuromonadales) have not been clearly shown to act as partners for ANMEs yet, they amounted to less than 1 % of bacteria populations based on 16S rRNA genes at day 0 and increased in relative abundance up to 6.5 % in Fe-AOM performing incubations (Figure 5, Chapter 2). There also exists the

possibility that ANME-2a completely oxidized CH_4 to CO_2 without a partner. A previous study showed that ANME-2a just as ANME-2d use reverse methanogenesis pathway for methane oxidation and possess multi-heme cytochromes in their genome (Wang et al., 2014). In fact, Wang and colleagues (2014) argued based on their metatranscriptome dataset that ANME-2a exist alone without bacteria partners in their highly active marine sediment derived AOM enrichment. Therefore they also could analogously perform Fe-AOM like their freshwater derived ANME-2d relatives (Ettwig et al., 2016; Cai et al., 2018). This hypothesis however should be a focus of future studies. In general, we could unequivocally show Fe-AOM, but given the low process rates, it seems plausible that other processes might contribute to the dissolved Fe pool in the methanic zone. These other processes, as discussed in Chapter one could involve fermentative or dissimilatory iron reduction. Key findings supporting these other hypothesis are discussed below.

Organic matter degradation linked microbial iron reduction

An additional but less intensively discussed explanation for the biotic mechanism of dissolved Fe formation is via the activity of fermentative and dissimilatory iron reducers during organic matter degradation. Some studies have suggested that crystalline iron oxides phases such as hematite or magnetite in the sediments (Figure. S1, Chapter 2) could facilitate both organic matter fermentation and methanogenesis, coupled to concurrent iron reduction (Riedinger et al., 2014; Egger et al., 2017). A key question in my PhD was to obtain evidence to improve the previous findings from Helgoland Mud Area that distinct communities of fermentative bacteria are tightly linked to Fe^{2+} concentrations and these fermentative bacteria could be degrading aromatic compounds in the methanic zone (Oni et al., 2015b; Oni et al., 2015a). We therefore set out to enrich microbial communities, with benzoate because it is often the central intermediate during aromatic compound degradation (Carmona et al., 2009), to be able to study methanogenic aromatic compound degradation and how iron oxides could

drive this process. In the initial sediment incubations, we immediately observed that amending slurries with benzoate and crystalline iron oxides (hematite and magnetite) stimulated concurrent iron reduction and methanogenesis (Figure 1, Chapter 3). Because crystalline iron oxides were thought to be less bioavailable (Lovley and Phillips, 1986), they were previously overlooked in the body of literature studying iron reduction and this might be why such an importance process that could be environmentally relevant was hidden prior to recent findings, including this thesis. If we assume that aromatic compounds clearly fuel methanogenic organic matter degradation in the iron-oxide rich methanic zone of Helgoland Mud Area, then our sediment incubation might have just recreated the environmental scenario that led to the dissolution of Fe^{2+} into porewater. We investigated this further by enriching the active communities in the slurry incubations over several transfers in synthetic enrichment medium to get rid of sediment matrix and glean a better understanding into the underlying mechanisms. Yet, after 5 successive transfers, the initial observation of concurrent iron reduction and methanogenesis persisted (Figures 2, 3, 4; Chapter 3). We could also show that the presence and concurrent reduction of magnetite facilitated complete benzoate degradation to CH_4 by ensuring acetate concentrations did not accumulate to such levels that methanogenesis becomes inhibited (Figures 2 and 3, Chapter 3). Thus, our enrichment efforts with a substrate which is likely degraded *in situ* revealed that fermentative iron reduction might also be in play and that crystalline iron oxides are potentially supporting the degradation of complex recalcitrant organic matter in the methanic zone. Considering the amounts of reducing equivalents that could be generated during fermentation, one might conclude that fermentative iron reduction contributes substantially to the Fe^{2+} pool in the methanic zone of iron-oxide rich marine sediments.

A limitation of this study however is the lack of comparative quantitative data of aromatic hydrocarbon (e.g., benzoate) degradation rates with that of Fe-AOM. This would have

facilitated direct evaluation of the relative importance and contribution of both processes to the Fe^{2+} pool. Therefore, the potential for organoclastic iron reduction to contribute to iron reduction *in situ* requires more studies. One could also argue that the key fermenting bacteria such as Atribacteria that correlate to the Fe^{2+} concentration profile in sediments of Helgoland Mud Area (Oni et al., 2015b) were not enriched with the targeted substrate benzoate. Instead, the enriched bacteria communities as discussed below were less than 1 % in the un-incubated sediment (Figure 1d, Chapter 3). By following the community shifts in each successive transfer while cultivating the highly enriched cultures, we enriched bacterial families Peptococcaceae and Syntrophomonadaceae (Figure 2–4, S1–S3; Chapter 3) known to perform syntrophic benzoate degradation from other environments (McInerney et al., 2008; Carmona et al., 2009; Sieber et al., 2010). Other bacteria phyla which hitherto have not been linked to benzoate degradation were uncovered. Halophilic spore forming clostridial family Halobacteroidaceae for example amounted to over 50 % of bacteria 16S rRNA genes in the enrichment with benzoate only. The family Synergistaceae from phylum Synergistetes and unclassified order NJ-1n from the phylum Tenericutes were also observed among the enriched bacteria pointing to their involvement in benzoate or aromatic compound degradation in the environment (Figure S1–S3).

The study with benzoate and iron oxides was done at 30 ºC. This was necessary because methanogenic benzoate degradation was not stimulated in sediment incubations at near *in situ* temperature of 10 ºC within conceivable timelines (250 days) in previous experiments (Oni, 2015). Therefore we set out in Chapter 4 to investigate how temperature controls both iron reduction and methanogenic organic matter degradation in ferruginous methanic marine sediments with an easily fermentable substrate (glucose). Here, concurrent reduction of iron oxides (hematite and magnetite) in the methanogenic phase was not observed (Figure 1, Chapter 4). This supports the conclusions with benzoate: concomitant occurrence of iron

reduction and methanogenesis in Helgoland Mud Area is linked to degradation of organic compounds of aromatic origin. This study however opened a new window into the dynamics of mineral mediated electron transfer under temperature control. Iron reduction was more pronounced with decreasing temperature (Figure 2, Chapter 4). To the best of my knowledge, such a phenomenon was only recently demonstrated in sub-glacial sediments (Nixon et al., 2017). Additionally, we could show that mineral enhanced methanogenesis is feasible at low temperatures down to 4 ºC: hematite amendment enhanced methanogenesis (Figure 3, Chapter 4). Magnetite on the other hand was more reduced at 4 ºC, hence the mode of microbial utilization of magnetite tended towards serving as an electron acceptor than as a conduit for electron transfer (Figure 3, Chapter 4). Molecular adaptations into either conduit or reduction use with temperature should be a subject of future studies.

Dissimilatory iron reducers (mostly Desulfuromonadales) were stimulated during iron reduction across all temperatures (Figure 5, Chapter 4). Dissimilatory iron reduction occurs in marine surface sediments and is known to preclude methanogenesis competitively especially as similar substrates (acetate and hydrogen) are required by the respective microbes (Lovley, 1991; Roden and Wetzel, 1996). However, dissimilatory iron reduction occurs favourably in the presence of substantial amounts of reactive organic matter (Lovley and Phillips, 1987; Roden and Wetzel, 2003), but the organic matter in methanic sediments is mostly recalcitrant (Riedinger et al., 2014; Oni et al., 2015b; Egger et al., 2017). Therefore, dissimilatory iron reduction as a potential mechanism fuelling deep iron reduction in methanic zones was often presumptuously overlooked (Riedinger et al., 2014; Egger et al., 2017). In another study which I was involved in during the course of my PhD, we could show using DNA-Stable isotope probing (DNA-SIP) that although few in relative abundance, known dissimilatory iron reducers i.e. Desulfuromonadales are also actively reducing iron oxides in the methanic zone (Kulkarni et al., 2018). Our DNA-SIP approach also revealed majority of these active

Desulfuromonadales clades were unclassified (previously unknown). Whether dissimilatory iron reduction quantitatively important to the overall iron reduction in the methanic zone is a subject for future studies.

Conclusion and outlook

The findings from the body of work presented in this thesis have profound implications for the discussions around the role of buried iron oxides below the SMT: we could clearly show that iron oxides can drive both methanogenic organic matter degradation and anaerobic oxidation of methane in the methanic zone of Helgoland Mud Area (Figure 1). Previous geochemical suggestions that Fe-AOM possibly drives Fe^{2+} dissolution into pore water were confirmed with activity rates measurements and the finding that ANME-2a is involved in the process. We also provided data for the first time supporting an additional but less vigorously mentioned process i.e. organoclastic iron reduction could also fuel deep iron reduction. In addition, enrichment of dissimilatory iron reducers can be stimulated in slurry incubations with sediment from the methanic zone pointing towards the possibility that dissimilatory iron reduction also contributes to the Fe^{2+} pool. We have shown that there are hitherto unknown aromatic compound degraders in marine sediments and that fermentative degradation of recalcitrant organic matter is enhanced in the presence of crystalline iron oxides. We also showed that the enhancement of methanogenesis by crystalline iron oxides can occur at cold temperatures which predominate in marine sediments and is thus environmentally relevant.

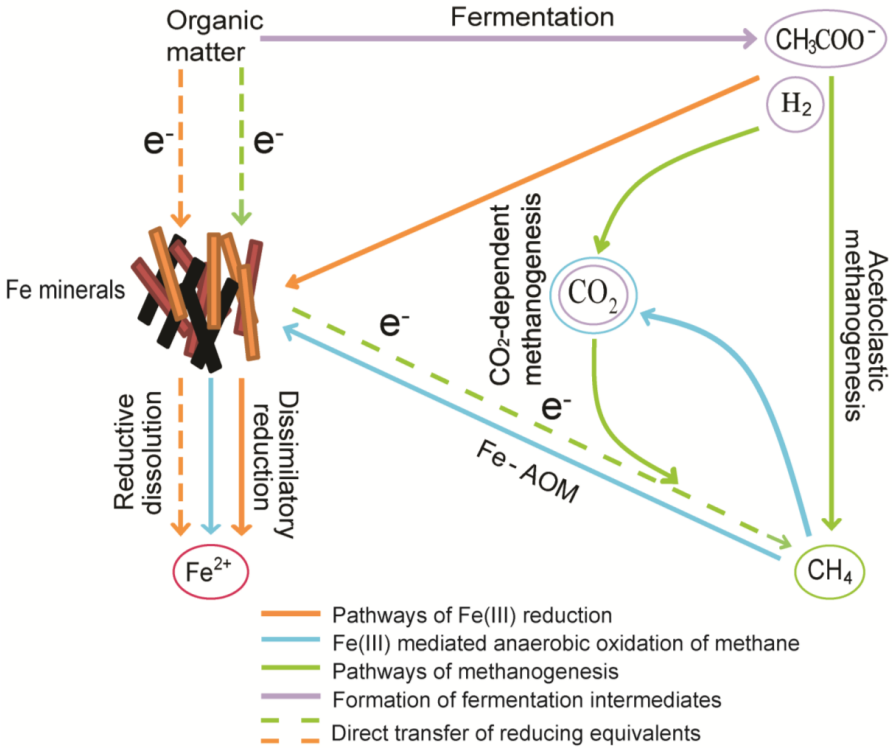

Figure 1: Potential biotic mechanisms that lead to Fe^{2+} dissolution into porewater in methanic zones of marine sediments based on findings from the Helgoland Mud Area. Figure taken from Chapter 3.

Certainly, new questions emerged from this study. A global scale determination of Fe-AOM rates from other sites bearing the geochemical preconditions for the process is now required. This will help quantify the contribution of Fe-AOM to methane fluxes from marine sediments. Future Fe-AOM studies should also attempt to uncover the mechanistic details of how ANME archaea perform Fe-AOM i.e. whether they completely perform the process without the help of syntrophic iron reducing bacteria partners or whether these bacteria partners are necessary just as in sulfate dependent AOM. Initial findings that iron reduction is favorable at cold temperatures require further exploration. Finally, the big open question remains as to what process majorly drives biotic iron reduction in the methanic zone. A systematic quantification of the process rates of methanogenic degradation of relevant organic carbon substrates and direct comparison with Fe-AOM rates should be done in future studies. This will help clarify the individual contribution of organoclastic iron reduction and Fe-AOM to the iron cycle in the methanic zone of marine sediments.

References

Aromokeye, D.A., Kulkarni, A.C., Elvert, M., Wegener, G., Henkel, S., Coffinet, S. et al. (2018) Rates and microbial players of iron-driven anaerobic methane oxidation in methanic marine sediments. Submitted.

Bar-Or, I., Elvert, M., Eckert, W., Kushmaro, A., Vigderovich, H., Zhu, Q. et al. (2017) Iron-coupled anaerobic oxidation of methane performed by a mixed bacterial-archaeal community based on poorly reactive minerals. *Environ Sci Technol* **51**: 12293-12301.

Beal, E.J., House, C.H., and Orphan, V.J. (2009) Manganese- and iron-dependent marine methane oxidation. *Science* **325**: 184-187.

Boetius, A., Ravenschlag, K., Schubert, C.J., Rickert, D., Widdel, F., Gieseke, A. et al. (2000) A marine microbial consortium apparently mediating anaerobic oxidation of methane. *Nature* **407**: 623-626.

Bowles, M.W., Mogollón, J.M., Kasten, S., Zabel, M., and Hinrichs, K.-U. (2014) Global rates of marine sulfate reduction and implications for sub–sea-floor metabolic activities. *Science* **344**: 889-891.

Cai, C., Leu, A.O., Xie, G.-J., Guo, J., Feng, Y., Zhao, J.-X. et al. (2018) A methanotrophic archaeon couples anaerobic oxidation of methane to Fe(III) reduction. *ISME J* **12**: 1929-1939.

Caldwell, S.L., Laidler, J.R., Brewer, E.A., Eberly, J.O., Sandborgh, S.C., and Colwell, F.S. (2008) Anaerobic oxidation of methane: Mechanisms, bioenergetics, and the ecology of associated microorganisms. *Environ Sci Technol* **42**: 6791-6799.

Carmona, M., Zamarro, M.T., Blázquez, B., Durante-Rodríguez, G., Juárez, J.F., Valderrama, J.A. et al. (2009) Anaerobic catabolism of aromatic compounds: A genetic and genomic view. *Microbiol Mol Biol Rev* **73**: 71-133.

Chang, Y.-H., Cheng, T.-W., Lai, W.-J., Tsai, W.-Y., Sun, C.-H., Lin, L.-H., and Wang, P.-L. (2012) Microbial methane cycling in a terrestrial mud volcano in eastern Taiwan. *Environ Microbiol* **14**: 895-908.

Chistoserdova, L. (2015) Methylotrophs in natural habitats: Current insights through metagenomics. *Appl Microbiol Biotechnol* **99**: 5763-5779.

Egger, M., Kraal, P., Jilbert, T., Sulu-Gambari, F., Sapart, C.J., Röckmann, T., and Slomp, C.P. (2016a) Anaerobic oxidation of methane alters sediment records of sulfur, iron and phosphorus in the Black Sea. *Biogeosciences* **13**: 5333-5355.

Egger, M., Lenstra, W., Jong, D., Meysman, F.J., Sapart, C.J., van der Veen, C. et al. (2016b) Rapid sediment accumulation results in high methane effluxes from coastal sediments. *PloS One* **11**: e0161609.

Egger, M., Rasigraf, O., Sapart, C.l.J., Jilbert, T., Jetten, M.S., Röckmann, T. et al. (2015) Iron-mediated anaerobic oxidation of methane in brackish coastal sediments. *Environ Sci Technol* **49**: 277-283.

Egger, M., Hagens, M., Sapart, C.J., Dijkstra, N., van Helmond, N.A., Mogollón, J.M. et al. (2017) Iron oxide reduction in methane-rich deep Baltic Sea sediments. *Geochim Cosmochim Acta* **207**: 256-276.

Ettwig, K.F., Zhu, B., Speth, D., Keltjens, J.T., Jetten, M.S.M., and Kartal, B. (2016) Archaea catalyze iron-dependent anaerobic oxidation of methane. *Proc Nat Acad Sci* **113**: 12792-12796.

He, Z., Zhang, Q., Feng, Y., Luo, H., Pan, X., and Gadd, G.M. (2018) Microbiological and environmental significance of metal-dependent anaerobic oxidation of methane. *Sci Total Environ* **610**: 759-768.

Hinrichs, K.-U., and Boetius, A. (2003) The anaerobic oxidation of methane: New insights in microbial ecology and biogeochemistry. In *Ocean Margin Systems*. Wefer, G., Billett, D., Hebbeln, D., Jørgensen, B.B., Schlüter, M., and van Weering, T.C.E. (eds). Berlin, Heidelberg: Springer Berlin Heidelberg, pp. 457-477.

Holmkvist, L., Ferdelman, T.G., and Jørgensen, B.B. (2011) A cryptic sulfur cycle driven by iron in the methane zone of marine sediment (Aarhus Bay, Denmark). *Geochim Cosmochim Acta* **75**: 3581-3599.

Iversen, N., and Jørgensen, B. (1985) Anaerobic methane oxidation rates at the sulfate-methane transition in marine sediments from Kattegat and Skagerrak (Denmark). *Limnol Oceanogr* **30**: 944-955.

Jørgensen, B.B., and Boetius, A. (2007) Feast and famine — microbial life in the deep-sea bed. *Nat Rev Microbiol* **5**: 770-781.

Kalyuzhnaya, M.G., Yang, S., Rozova, O.N., Smalley, N.E., Clubb, J., Lamb, A. et al. (2013) Highly efficient methane biocatalysis revealed in a methanotrophic bacterium. *Nat Commun* **4**: 2785.

Knittel, K., and Boetius, A. (2009) Anaerobic oxidation of methane: Progress with an unknown process. *Annu Rev Microbiol* **63**: 311-334.

Kulkarni, A.C., Aromokeye, D.A., Maier, L., Yin, X., Elvert, M., Richter-Heitmann, T., and Friedrich, M.W. (2018) DNA-SIP reveals active iron reducing populations in methanic sediment incubations of Helgoland Mud Area, North Sea. In Preparation.

Lovley, D.R. (1991) Dissimilatory Fe(III) and Mn(IV) reduction. *Microbiol Rev* **55**: 259-287.

Lovley, D.R., and Phillips, E.J. (1986) Organic matter mineralization with reduction of ferric iron in anaerobic sediments. *Appl Environ Microbiol* **51**: 683-689.

Lovley, D.R., and Phillips, E.J. (1987) Rapid assay for microbially reducible ferric iron in aquatic sediments. *Appl Environ Microbiol* **53**: 1536-1540.

Martinez-Cruz, K., Leewis, M.-C., Herriott, I.C., Sepulveda-Jauregui, A., Anthony, K.W., Thalasso, F., and Leigh, M.B. (2017) Anaerobic oxidation of methane by aerobic methanotrophs in sub-Arctic lake sediments. *Sci Total Environ* **607-608**: 23-31.

McInerney, M.J., Struchtemeyer, C.G., Sieber, J., Mouttaki, H., Stams, A.J., Schink, B. et al. (2008) Physiology, ecology, phylogeny, and genomics of microorganisms capable of syntrophic metabolism. *Annals New York Acad Sci* **1125**: 58-72.

Niemann, H., Lösekann, T., De Beer, D., Elvert, M., Nadalig, T., Knittel, K. et al. (2006) Novel microbial communities of the Haakon Mosby mud volcano and their role as a methane sink. *Nature* **443**: 854-858.

Nixon, S.L., Telling, J.P., Wadham, J.L., and Cockell, C.S. (2017) Viable cold-tolerant iron-reducing microorganisms in geographically diverse subglacial environments. *Biogeosciences* **14**: 1445-1455.

Norði, K.a., Thamdrup, B., and Schubert, C.J. (2013) Anaerobic oxidation of methane in an iron-rich Danish freshwater lake sediment. *Limnol Oceanogr* **58**: 546-554.

Oni, O.E. (2015) Structure and function of microorganisms in the methanic sediments of the Helgoland Mud Area, North Sea, Germany. Bremen, Germany: University of Bremen.

Oni, O.E., Schmidt, F., Miyatake, T., Kasten, S., Witt, M., Hinrichs, K.-U., and Friedrich, M.W. (2015a) Microbial communities and organic matter composition in surface and subsurface sediments of the Helgoland Mud Area, North Sea. *Front Microbiol* **6**: 1290.

Oni, O.E., Miyatake, T., Kasten, S., Richter-Heitmann, T., Fischer, D., Wagenknecht, L. et al. (2015b) Distinct microbial populations are tightly linked to the profile of dissolved iron in the methanic sediments of the Helgoland Mud Area, North Sea. *Front Microbiol* **6**: 365.

Orphan, V.J., House, C.H., Hinrichs, K.-U., McKeegan, K.D., and DeLong, E.F. (2001) Methane-consuming archaea revealed by directly coupled isotopic and phylogenetic analysis. *Science* **293**: 484-487.

Orphan, V.J., House, C.H., Hinrichs, K.-U., McKeegan, K.D., and DeLong, E.F. (2002) Multiple archaeal groups mediate methane oxidation in anoxic cold seep sediments. *Proc Nat Acad Sci* **99**: 7663-7668.

Riedinger, N., Formolo, M.J., Lyons, T.W., Henkel, S., Beck, A., and Kasten, S. (2014) An inorganic geochemical argument for coupled anaerobic oxidation of methane and iron reduction in marine sediments. *Geobiology* **12**: 172-181.

Roden, E.E., and Wetzel, R.G. (1996) Organic carbon oxidation and suppression of methane production by microbial Fe(III) oxide reduction in vegetated and unvegetated freshwater wetland sediments. *Limnol Oceanogr* **41**: 1733-1748.

Roden, E.E., and Wetzel, R.G. (2003) Competition between Fe(III)-reducing and methanogenic bacteria for acetate in iron-rich freshwater sediments. *Microb Ecol* **45**: 252-258.

Rooze, J., Egger, M., Tsandev, I., and Slomp, C.P. (2016) Iron-dependent anaerobic oxidation of methane in coastal surface sediments: Potential controls and impact. *Limnol Oceanogr* **61**: S267-S282.

Scheller, S., Yu, H., Chadwick, G.L., McGlynn, S.E., and Orphan, V.J. (2016) Artificial electron acceptors decouple archaeal methane oxidation from sulfate reduction. *Science* **351**: 703-707.

Schwertmann, U. (1991) Solubility and dissolution of iron oxides. *Plant Soil* **130**: 1-25.

Segarra, K.E.A., Comerford, C., Slaughter, J., and Joye, S.B. (2013) Impact of electron acceptor availability on the anaerobic oxidation of methane in coastal freshwater and brackish wetland sediments. *Geochim Cosmochim Acta* **115**: 15-30.

Sieber, J., McInerney, M., Plugge, C., Schink, B., and Gunsalus, R. (2010) Methanogenesis: Syntrophic metabolism. In *Handbook of Hydrocarbon and Lipid Microbiology*: Springer, pp. 337-355.

Sivan, O., Adler, M., Pearson, A., Gelman, F., Bar-Or, I., John, S.G., and Eckert, W. (2011) Geochemical evidence for iron-mediated anaerobic oxidation of methane. *Limnol Oceanogr* **56**: 1536-1544.

Timmers, P.H.A., Suarez-Zuluaga, D.A., van Rossem, M., Diender, M., Stams, A.J.M., and Plugge, C.M. (2016) Anaerobic oxidation of methane associated with sulfate reduction in a natural freshwater gas source. *ISME J* **10**: 1400-1412.

Treude, T., Krause, S., Maltby, J., Dale, A.W., Coffin, R., and Hamdan, L.J. (2014) Sulfate reduction and methane oxidation activity below the sulfate-methane transition zone in Alaskan Beaufort Sea continental margin sediments: Implications for deep sulfur cycling. *Geochim Cosmochim Acta* **144**: 217-237.

Tu, T.-H., Wu, L.-W., Lin, Y.-S., Imachi, H., Lin, L.-H., and Wang, P.-L. (2017) Microbial community composition and functional capacity in a terrestrial ferruginous, sulfate-depleted mud volcano. *Front Microbiol* **8**: 2137.

Wang, F.-P., Zhang, Y., Chen, Y., He, Y., Qi, J., Hinrichs, K.-U. et al. (2014) Methanotrophic archaea possessing diverging methane-oxidizing and electron-transporting pathways. *ISME J* **8**: 1069-1078.

Wankel, S.D., Adams, M.M., Johnston, D.T., Hansel, C.M., Joye, S.B., and Girguis, P.R. (2012) Anaerobic methane oxidation in metalliferous hydrothermal sediments: Influence on carbon flux and decoupling from sulfate reduction. *Environ Microbiol* **14**: 2726-2740.

Acknowledgements

To be able to get this far and realize a lifelong ambition of getting a PhD, I owe a considerably large number of people a life time of gratitude. Firstly, I would like to specially thank Prof Dr. Michael W. Friedrich for giving me this opportunity. Not just for securing the research funding, the fatherly mentorship, and excellent professional guidance that allowed me to complete my research within three years. Your absolute confidence in me, right from the beginning when you waited for me to finish my Masters for about six months before starting the project was a huge springboard for me to go through the rigours of PhD. I owe you a huge debt of gratitude.

I am very grateful to my second reviewer, Prof. Dr. Jens Harder as well as the scientists, students, and employees, who were willing to evaluate my performance in the public defense.

I thank the senior scientists that helped co-supervise me and gave me support in one form or the other which enabled me answer some of the research questions in my PhD. Prof. Dr. Sabine Kasten, Dr. Marcus Elvert, Prof. Dr. Kai-Uwe Hinrichs, Dr. Gunter Wegener and Prof. Dr. Tillmann Harder. I also thank key collaborators and co-workers Dr. Oluwatobi Oni, Dr. Tim Richter-Heitmann, Ajinkya Kulkarni, Dr. Susann Henkel, Dr. Sarah Coffinet, Dr. Heidi Taubner, Dr. Rolf Nimzyk, Dr. Jan Tebben, Dr. Thilo Eickhorst, Sten Littmann, Qingzeng Zhu and Jenny Wendt.

I thank Dr. Christiane Glöckner and the entire team in charge of the MarMic graduate school from the MPI-MM for admitting me into the MarMic programme and the opportunities I was afforded as a Marmic student during the last three years.

Members of the Microbial Ecophysiology group are highly appreciated for accepting me as one of them and giving me a ‘home’ where I could carry out my research. Prof Dr. Karl-Heinz Blotevogel, Tina Stickan, Xiuran Yin, Annika Schnakenberg, Charlotte Holz, Celina Schreiber and Nico Binnemann, I appreciate you all. I also acknowledge other students who worked with me during their Master or Bachelors studies: Shreya Tilve, Lea Wunder, Lisa Maier, Andreas Castillejos, and Sebastian Miksch. The technical support I received from technicians (Ingrid Dohrmann, Xavier Pareto and Mirja Meiners) in other departments I carried out research and obtained data is acknowledged.

I also thank my previous professional mentors and supervisors, Dr. Folakemi Omojasola, Dr. Femi Owolabi, Dr. Olufunke Adeyeye and Dr. Casten Vogt. Their tutelage and encouragement gave me the confidence to do a PhD. I recognize and appreciate all my

friends and thank them immensely for their moral support and encouragement especially Dr. Oluwatobi Oni (Tobi as I call him). Tobi, then a PhD student, got an email from a random Nigerian in 2012 who was interested in coming to Germany to study Environmental Microbiology for Masters and PhD. That person was me. I sought help with proof reading and correcting my motivation letter to boost my chances of getting admitted into a German University. He subsequently encouraged me to apply for the MarMic PhD programme during my masters and as fate will have it, it turned out that Tobi's Professor would be interested in working with me; the rest is history as I eventually continued the project he started. Thank you for your mentorship, Tobi and your invaluable contribution to my research. I am also grateful to Dr. Tim Richter-Heitmann for his friendship, encouragement and most especially for his help with writing the German translation of my thesis summary.

I thank the Ishola family, for their enormous financial and moral contribution to my life. I appreciate my life-long friend Adedoyin whom I simply call brother, for introducing me to his parents. I am grateful to his parents Mr Ambali Ishola and Mrs Funke Ishola for adopting me as a member of their family, funding my University education and helping me achieve the goal of coming to Germany to study. Perhaps I would not get here without their timely contribution. Words don't do justice to the debt of gratitude I owe your family.

Lastly but very importantly, I appreciate greatly the emotional and moral support I received from my family. It would have been nice to have my wonderful parents alive today to share this moment with but I'm glad that the rest of my family did their best to fill the gap they left over the years. Special acknowledgement goes to my late eldest sister Serah. She was my biggest fan but unfortunately her illness and eventual passing during the last months of PhD was very difficult to accept. May her gentle soul continue to rest in peace. My other siblings Bosede, Oyeniyi, Modupe and Titilayo together with their spouses are acknowledged as well for their equally supportive role. Finally, I thank God for putting all these beautiful people in my life and helping me get this far with my life's journey.

Versicherung an Eides Statt

Ich, **Adeyemi David, Aromokeye**, Ostendorpstraße 23, 28203, Bremen, Matr.-Nr. 3062782

(Vorname, Name, Anschrift, Matr.-Nr.)

versichere an Eides Statt durch meine Unterschrift, dass ich die vorstehende Arbeit selbständig und ohne fremde Hilfe angefertigt und alle Stellen, die ich wörtlich dem Sinne nach aus Veröffentlichungen entnommen habe, als solche kenntlich gemacht habe, mich auch keiner anderen als der angegebenen Literatur oder sonstiger Hilfsmittel bedient habe.

Ich versichere an Eides Statt, dass ich die vorgenannten Angaben nach bestem Wissen und Gewissen gemacht habe und dass die Angaben der Wahrheit entsprechen und ich nichts verschwiegen habe.

Die Strafbarkeit einer falschen eidesstattlichen Versicherung ist mir bekannt, namentlich die Strafandrohung gemäß § 156 StGB bis zu drei Jahren Freiheitsstrafe oder Geldstrafe bei vorsätzlicher Begehung der Tat bzw. gemäß § 161 Abs. 1 StGB bis zu einem Jahr Freiheitsstrafe oder Geldstrafe bei fahrlässiger Begehung.

_____ _____

Ort, Datum Unterschrift